Universitat Autònoma de Barcelona

Computational Study of Iron Carbenes and their Reactivity with Olefins

Égil de Brito Sá

Computational Study of Iron Carbenes and their Reactivity with Olefins

Égil de Brito Sá

Ph.D. Thesis
Ph.D. program in Chemistry

Supervisors:
Xavier Solans Monfort
Luis Rodríguez Santiago

Departament de Química
Facultat de Ciències

2018

Memòria presentada per aspirar al Grau de Doctor per

Égil de Brito Sá

Vist i plau,

Xavier Solans Monfort

Luis Rodríguez Santiago

Bellaterra
11 de Gener de 2018

Contents

Preface

The advent of an organometallic chemistry based on the first-row transition metals has been gaining attention within the propose of transform chemistry in a more environmentally friendly discipline. This movement sheds light on the Olefin Metathesis reaction, which is one of the most powerful reactions in organic synthesis as it allows the formation of new C=C double bonds. The reaction is catalyzed either by ruthenium or molybdenum metal carbenes whose cost and toxicity partially prevents their industrial applications. Therefore, the Olefin Metathesis reaction is a paradigmatic example in which the achievement of the long desired Fe-based catalyst can potentially have breakthrough consequences.

This Thesis is a theoretical exploration, using DFT methods, aiming to understand which parameters can be followed for such goal. To do so, we present here a study about the electronic structure of iron-complexes, its reactivity with olefins, and a *in-silico* design search about possible ancillary ligands that can be used to produce such catalyst. Forthcoming Chapters are overviewed in the next paragraphs.

Chapter 1 is an introductory background about some principles of the classical organometallic chemistry, and, within this field, we present the main aspects of olefin metathesis reaction. We still discuss the characteristics of this new emerging field of the organometallic chemistry, based on complexes of earth-based metals. Distinct kinds of iron-carbenes reported in the literature are presented, specially concerning the reactivity with olefins to metathesis and the cyclopropanation, which can act as a deactivation path.

A step forward, in Chapter 2, we discuss the foundations of the main methodology we use to approach the problem that we have suggested: the main pillars of Computational Chemistry are presented, in particular, the Density Functional Theory, that is the computational methodology we have applied. In this Chapter, we demonstrate the

reliability of the level of theory we have use, as well.

Moving to the presentation of the results and discussions, Chapter 3 offers hints to understand the reasons why iron-carbenes so far presented in the literature fails to catalyze olefin metathesis, but instead drives to cyclopropanation, focusing the electronic structure and the energetics of the above-mentioned reactions. This is done comparing with the effective ruthenium-carbene belonging to the family of the 2^{nd} Generation Grubbs catalysts.

We have also done a large analysis of which characteristics the ancillary ligands should fulfil in order to achieve as much as possible the thermodynamics and kinetics of a feasible metathesis catalyst. In Chapter 4, is dedicated to discussing the electronic structure of ML_4 iron-catalysts, as well as the reactivity of them with olefins, comparing olefin metathesis with cyclopropanation. In the Chapter 5, handling the same approach of the previous chapter, we study of pentacoordinated complexes bearing iron-carbenes.

Finally, General Conclusions gathers the main conclusion drafted from our research. After all, Appendices provide some additional data necessary to a better understanding of the main text.

1
Background

Olefin Metathesis is a remarkable reaction catalyzed by compounds belonging to the field of organometallic chemistry: corresponds to the breaking of two carbon–carbon double bonds and the subsequent formation of two new ones. Its importance has been growing in the past decades with a wide range of applications. Although since the very beginning his importance was recognized, the enlightenment of the mechanism and the development of well-defined catalysts allowed it to became one of the most important machinery to perform carbon-carbon coupling.[1] Obviously, this was not ignored in the scientific world, which awarded the chemistry Nobel prize of 2005, *"for the development of the metathesis method in organic synthesis"*,[2] to Yves Chauvin,[3] for the elucidation of the mechanism, and Richard R. Schrock[4] and Robert H. Grubbs[5] for the synthesis of the so-called well-defined catalysts.

On the other hand, nowadays, organometallic chemistry is witnessing a bold change in the attempt to move the chemistry performed with the elements in the center of the periodic table, mostly the precious metals, to the first-row transition metals. This attempt is motivated because the latter have a huge natural availability and are biocompatible. Within this effort, to continue the successful history of olefin metathesis, one step further is to try transform, as much as possi-

ble, into an environmentally friendly and more affordable process. One path for such task would be the use earth-abundant metals to make the catalyst system. In the case of olefin metathesis, iron systems can be an interesting alternative to be explored, since it belongs to the same family as ruthenium, which is the metal that one of the most effective catalysts families is made with.

We dedicated this Chapter to provide a background vision over the chemistry related to the problem we discuss in this thesis, from the most wide envisage until the most specific matter. To begin with, we discuss general organometallic chemistry. After that the olefin metathesis reaction, regarding the development, mechanism, catalysts, application, together with cyclopropanation reaction, which is one possible deactivation path. Another part is dedicated to present the iron-carbene chemistry, as part of a new chemistry based on earth abundant metals, regarding the structure, electronic states and reactivity, especially with olefins. After all, based on the points we have discussed, we present the goals that this work should address.

1.1 Traditional Organometallic Chemistry

The successful history of organometallic homogeneous catalysis lies in the use of metal complexes to catalyze reactions. During the nearly last 50 years, that catalyst technology has principally relied on the 4d and 5d transition metals in groups 8, 9, and 10 of the periodic table, as highlighted in the Figure 1.1. These are the so-called *precious metals* such as Palladium (Pd), Platinum (Pt), Rhodium (Rh), Iridium (Ir), and Ruthenium (Ru), which have been the pillars not only of homogeneous but also heterogeneous catalysis. The popularity of these metals was established by the research in the last five decades, carrying out a predictable chemistry, based on the relative stability of their complexes, low ligand lability and ability to characterize diamagnetic complexes in solution using NMR spectroscopy.[6–9] The high activity, predictable selectivity, availability of reliable synthetic precursors and general ease of handling has raised these metals catalysts among the most widely deployed in synthetic contexts.[10]

Complexes synthesized with those metals have been proven to be efficient for a large number of applications, showing a broad scope, high efficiencies, and ample tolerance to functional groups, playing a

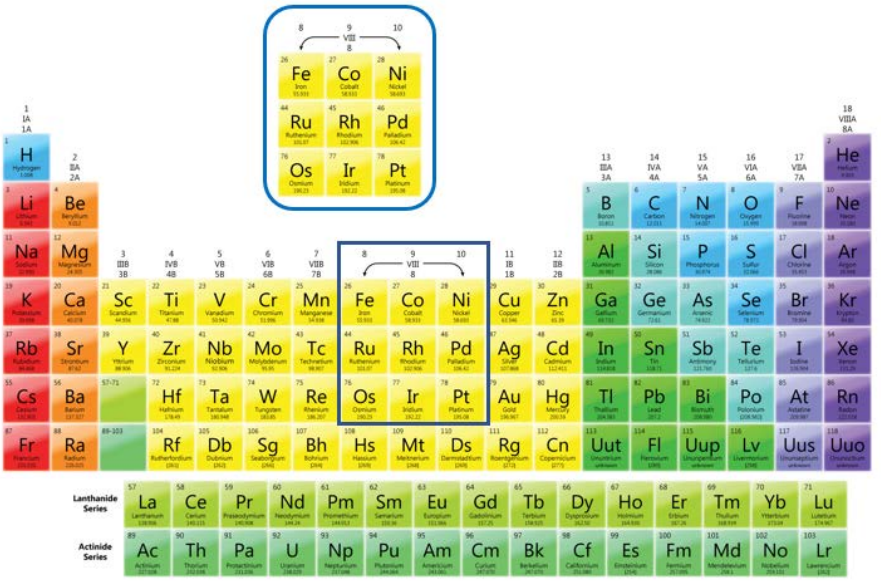

Figure 1.1: Periodic Table, featuring the *precious metals*.

important role in organometallic chemistry. They usually act in hydrocarbon transformations and strong bond activation, in many cases performing the most difficult part, such as breaking H–H bonds, forming C–H or C–C bonds, etc.[6,11] Prominent examples include cross-coupling reactions with palladium catalysts,[12–14] C–H activation reactions with iridium and rhodium catalysts,[15] hydrosilylation with platinum catalysts,[16] hydrogenation with the Rh-based Wilkinson's catalyst[17] and asymmetric hydrogenation with rhodium or iridium complexes[18,19] among others. Another important reaction belonging to this field, which is the focus of our study is alkene metathesis catalysed ruthenium catalysts, within others.[1,20]

The importance of this organometallic reactivity based on the precious metals is also illustrated by the widespread practical applications in the production of commodities where hydroformylation (Rh),[21] hydrosilylation (Pt), Wacker-oxidation (Pd)[22] are remarkable cases. They also increasingly expand their reach beyond specialty, like fine chemicals: palladium cross-coupling chemistry, for instance, is intensively used in the pharmaceutical and electronic materials manufacturing. Furthermore, asymmetric hydrogenation (Ru, Rh), olefin metathesis (Ru) are also broadly used in pharmacy.[23]

1.2 Olefin Metathesis

Olefin metathesis is one of most remarkable reactions in organometallic chemistry. It is an elegant reaction to promote the formation of unsaturated compounds by forming two new C=C bonds from the breaking of any two-else former double bonds, as the general transformation shown in the Scheme 1.1.[3–5,24,25]

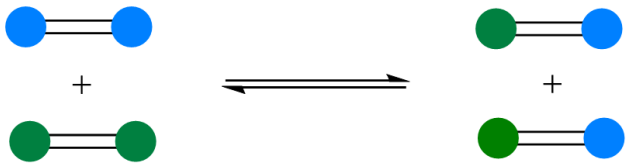

Scheme 1.1: Olefin Metathesis reaction

The word metathesis comes from the greek $\mu\varepsilon\tau\alpha\theta\varepsilon\sigma\iota\varsigma$, originally used in phonology, meaning a sound change that alters the order of phonemes in a word. In chemistry it resembles the interchange of atoms between molecules, as we have just defined for this olefin case.[26] Olefin metathesis is generally a reversible reaction and requires a proper catalyst to achieve the equilibrium in a useful time. Frequently it is unproductive and competitive with other reactions, resulting in a complex process depending on relative rates, and releasing of volatiles or insoluble products that change the equilibrium.[27]

Olefin metathesis was observed for the first time in 1931, reported as metathesis of propene to form butene and ethene at high temperatures, by Schneider and Frolich.[28] In the early 60s many reports (H. S. Eleuterio, E. F. Peters, B. L. Evering, R. L. Banks and G. C. Bailey) from chemical industry described again the formation of 2-butene and ethene from propene, catalysed by heterogeneous systems of molybdenum supported on alumina. This reaction was named olefin disproportionation.[29,30] Meanwhile, H. S. Eleuterio and Truett reported independently, in 1964, the polymerization of norbonene with $WCl_6/AlEt_2Cl$.[29] Using the same system, in 1964 Giulio Natta observed polymerization of cyclopentene and norbonene.[31] However, it was only in 1967 that Nissim Calderon and colleagues realized that olefin disproportionation and polymerization of cyclic olefins are the same reaction, which he termed olefin metathesis, a name that stands so far.[32]

1.2.1 Types and Practical Applications

Olefin metathesis shows a wide range of applications that is a consequence of the large number of different olefins able to react or be formed, for instance terminal olefins, inner olefins, cyclic, macrocyclics and polymers. Scheme 1.2 shows the versatility of most used processes involving olefin metathesis, either in laboratory or industry.

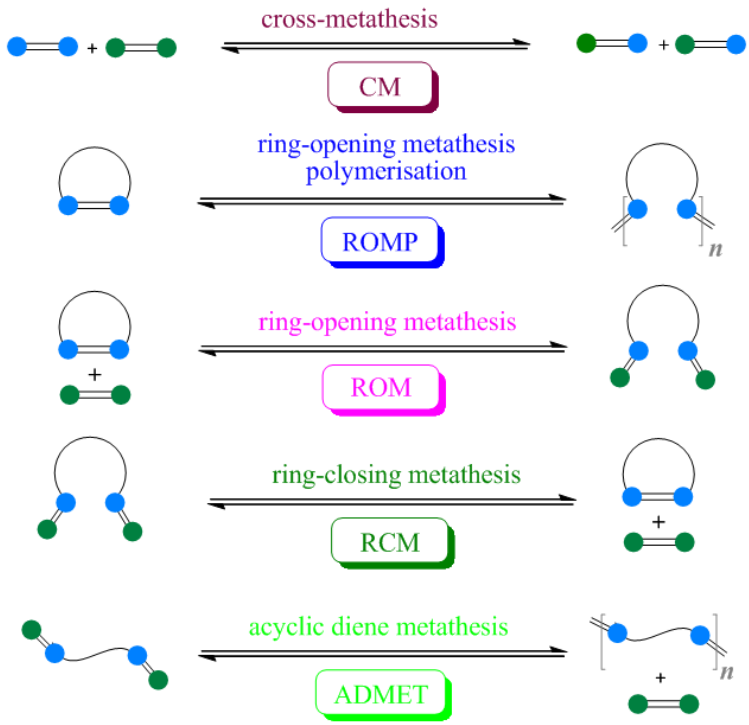

Scheme 1.2: Types of Olefin Metathesis Reaction

The first reaction is the *cross-metathesis-CM*, which refers the reaction between two acyclic olefins. Such reaction is essentially degenerate and an equilibrium is easily reached, but the equilibrium can be displaced towards products by releasing gaseous ethene produced during the reaction, if the reactants are terminal olefins. The olefin product can have E or Z conformation, although in general, thermodynamic control drives the reaction to produce the more stable E conformer, which is sometimes the only product. If the reacting olefins are equals, the process is called self-metathesis.[1,33–35]

The second reaction is *Ring-Opening Metathesis Polymerization-ROMP* that forms polymers by metathesis from cyclic olefins. Historically, is the most common application of olefin metathesis for preparation of new materials. It is particularly important in the chemical industry of polymer production. The driving force for this reaction is the loss of ring strain in the cyclic olefins.[26,36,37] If instead the olefins just opens, without form a polymer, we have the *Ring-Opening Metathesis-ROM*, shown in the third entry.[38] The fourth entry corresponds to the opposite reaction of ROM: intra-molecular coupling of two olefins, giving a cyclic olefin, called *Ring-Closing Metathesis-RCM*. This reaction is usually energetically unfavourable due to the ring strain of the products, but it can be favoured by the formation of volatile ethene.[39] The last kind is *Acyclic Diene Metathesis-ADMET*, which is the intermolecular reaction of a diolefin to form polymers or oligomers. ADMET is also driven by the release of volatile ethylene gas.[40]

This variety of metathesis reaction has been applied to the synthesis of a wide range of organic products such as polymers, petrochemical products and in advanced organic synthesis with pharmaceutical and biological implications.[41–45] Cross-metathesis, for instance, is the base of *Phillips Triolefin Process*, to produce ethene and 2-butene from propene with an heterogeneous catalyst. This process was used in 1966-72. Afterwords, propene demand forced the usage of the opposite reaction, called *Olefins Conversion Technology*: the last process can still be used to 1-hexene production from butene and propene. *Shell Higher Olefin Process (SHOP)* produces linear higher olefins from ethene, in a total of 1.2 million of ton per year as the trade name Neodene®. Regarding the fine chemicals, Neohexene (3,3-dimethyl-1-butene) can be produced by cross-metathesis using 2,4,4-trimethyl-1-pentene and ethene. It is an important intermediate for synthesis of Tonalide®, a synthetic musk perfume and also used to make Terbinafine®, an antifungal agent.[41] Insect pheromones, which are useful as environment friendly pest-control agents can be obtained with standard metathesis reaction from commodity starting materials.[46]

ROMP is definitely an important process for polymers production: the first commercial metathesis polymer was polynorbornene, under the trade name Norsorex®, obtained by polymerization of Norbonene, with $RuCl_3$/HCl in butanol. This compound is used for oil spill recovery, as sound barrier or for damping. ROMP of cyclooctene

form a polymer commercially known as Vestenamer®, performed in hexane as solvent in the presence of a WCl_6-based catalyst. The polymer is used for improving the properties of rubber compounds and for use in rubberised asphalt. There is innumerate other examples of polymers produced by means of ROMP, like polydicyclopentadiene. Hydrogenated analogues of some of these polymers are available as well; Zeonex® (suitable for optical applications) is a saturated ROMP polymer of substituted polynorbornene.[41]

The applications of olefin metathesis in the pharmaceutical field are intrinsically correlated to RCM, and in a less extend to the opposite reaction, ROM, remarkably for preparation of macrocycles, although it does have some limitations such as high dilution, selectivity and unwanted isomerization, which prevent in less extend their commercial use. Scheme 1.3 shows some examples of macrocycles synthesized using olefin metathesis.

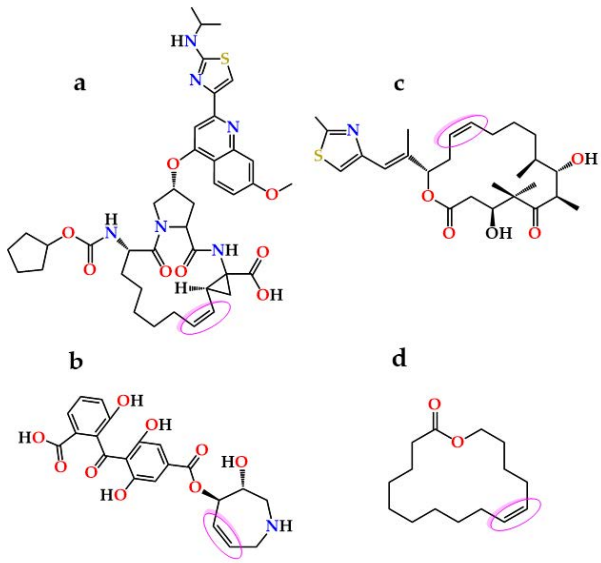

Scheme 1.3: Olefin-containing macrocycles obtained with olefin metathesis.

Some examples, among many, is the use of RCM to prepare multi-kilogram quantities of a complex molecule (BILN 2061 ZW) that is precursor of a potent anti-hepatitis C, for instance (**a**).[42] Fürstner and Thiel, using RCM, shortened the total synthesis of a 7-membered azepin compound (balanol), which is a drug used as anticancer agent

and in controlling inflammation, cardiovascular disorders, central nervous system dysfunction and even HIV infection(**b**).[47] Another anticancer drug, epothilone, and its derivatives were also prepared using ring closing metathesis(**c**).[48] It was found as well that with metathesis is possible to selectively cyclize musk-odored lactone, improving the industrial process(**d**).[49]

1.2.2 The Reaction Mechanism

After Calderon[32] craft the term olefin metathesis, the step forward was the understanding of the reaction mechanism. In the late 60s and early 70s, different suggestions for mechanisms and intermediates were brought froward.[50,51] Within this effort, in 1971, two chemists at the French Petroleum Institute, Yves Chauvin and his student Jean-Louis Hérisson[52] suggested that olefin metathesis is initiated by a transition metal carbene. The general mechanism for two different olefins reacting through olefin metathesis is summarized in Scheme 1.4

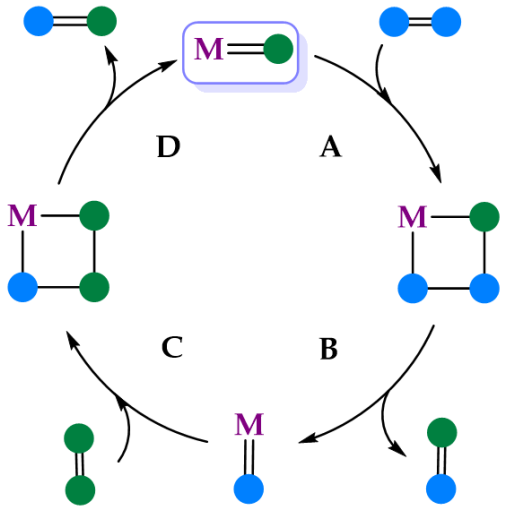

Scheme 1.4: Mechanism of Olefin Metathesis.

In this propose, the active species to catalyse the reaction is a metallic carbene, that interacts with an olefin to form a metallacyclobutane intermediate (step **A**), which subsequently breaks apart into a new olefin and a new carbene (step **B**). This new carbene interacts

with the second olefin to form another intermediate metallacyclobutane (step **C**), which breaks to form the the second new olefin and regenerate the initial carbene, starting over the cycle (step **D**). At this point, it is obvious that besides the metal-carbene, the intermediate metallacyclobutane is key stage in the reaction.

The formation of the metallacyclobutane (step **A**) is a [2+2] cycloaddition and the subsequent opening (step **B**) is a [2+2] cycloreversion. Those two processes are the main barriers (transition states, in the computational chemistry language) of the reaction. Usually direct [2+2] cycloaddition of main group elements is orbital-symmetry forbidden thus has a high activation energy.[53] However, in this case, interaction of the olefin molecule with the metal orbitals breakdowns the orbital-symmetry control and allows a formally forbidden process.[54]

Nowadays everyone agrees that the seminal paper of Chauvin & Hérisson was the first to envisage correctly the key role of metal carbenes in olefin metathesis and the events that lead to exchange of groups around carbon-carbon double bonds, but it took several years before the mechanism was experimentally supported and widely accepted, a task mostly achieved due to the efforts of Katz.[55,56]

It is clear the importance of the intermediate metallacyclebutane for olefin metathesis. Apart of cycloreversion to metathesis products, metallacyclebutanes of Pt, Ir, Rh, Ru can drive to alkanes, olefins, carbene–olefin complexes and allyl complexes (see Figure 1.2).[57]

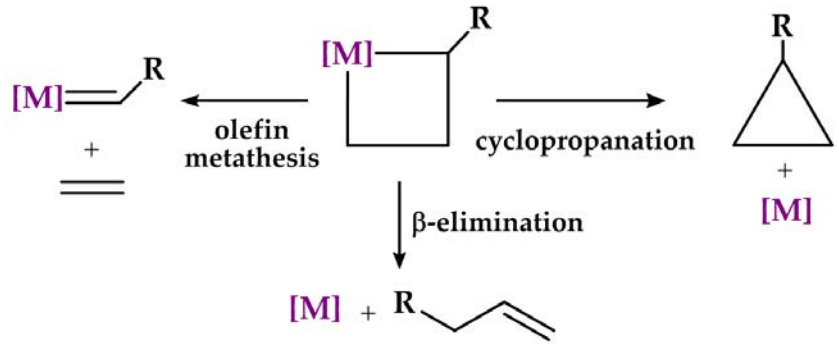

Figure 1.2: Representative examples of evolution paths from metallacyclebutane intermediate.

In our case, another deactivation process should be a matter of attention: cyclopropanation, since for iron-carbenes, which is our focus,

this process is often observed. Metallacyclebutane structures relevant for cyclopropanation are not well documented, possibly because reductive elimination is a fast process. This is more important in the case of Fischer-type carbenes.[29,58] However, in some cases, the intermediacy of metallacyclebutanes is clearly established, especially in reactions catalysed by Cu and Pd.[58]

In this way, the relevance of metallacyclebutanes as intermediates in cyclopropanation from olefins and diazocompounds may be under doubt, since in many cases it is not generated. Some evidences point to the direct reaction of metal-carbenes with olefins, whose gmechanism is detailed in Section 1.5. Therefore, it seems that there is no a single general mechanism for cyclopropanation. A further question is why some metallacycles yield cyclopropanes, whereas others olefin metathesis.

1.2.3 Olefin Metathesis Efficient Catalysts

The first catalysts used were multicomponent homogeneous and heterogeneous catalyst systems, poorly defined, usually composed by transition metal salts combined with main group alkylating agents or deposited on solid supports. Classical examples are WCl_6/Bu_4Sn, $WOCl_4/EtAlCl_2$, Mo_3/SiO_2, Re_2O_7/Al_2O_3. Because of their low cost and simplicity, these systems still have an important place in commercial applications. However the usage of those catalyst is limited due to the harsh condition and strong Lewis acid they require, which are incompatible with many functional groups. Besides, the existence of only few active species made hard the initiation process and reactivity control.[20]

The big step for enlightening the mechanism (Scheme 1.4) demonstrated that the active species are metal-carbenes, and metallacyclobutane is an important intermediate. This gave a chance to move further in the improvement of the reaction, influencing the development, by a rational design, of an alkylidene or metallacyclobutane catalyst. Katz showed, then, that isolated metal-carbenes initiate olefin metathesis,[55,56] which turned this structure the main focus of research. In this way, before going further in the discussion of the modern olefin metathesis catalyst, we want to discuss about the nature of metal-carbenes itself.

Metal-Carbenes

The first report of transition metal-carbene double bond was provided by Ernst Otto Fischer, in 1964 and it is shown in Figure 1.3.[59] Noteworthy this carbene gave to Chauvin some insights about the mechanism, since it proves that metal-carbene species exist. Carbenes similar to this are defined as Fischer carbenes. This family of complexes usually has a metal from the groups 6 to 8 with a low oxidation state.

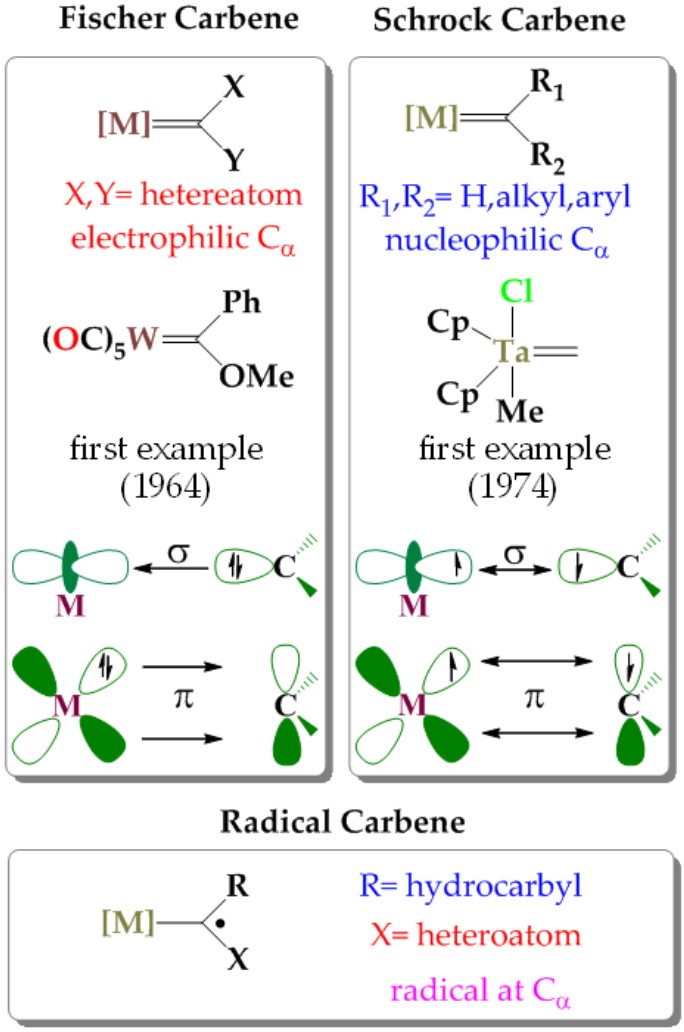

Figure 1.3: Types of metal-carbene and their orbital interaction

The orbital interaction, also depicted in Figure 1.3, shows that the [M]=CR_2 bond is made by the σ-donation of the carbon of the carbene ligand (C_α) and the π-retrodonation from the metal to the ligand. Overall, the electronic density on C_α is diminished, resulting in polarization of the metal-carbon double-bond, with the carbon carbenic becoming electrophilic.[60]

Another important family of metal-carbenes was introduced for the first time by Schrock in 1974,[61] then called Schrock carbenes. In this group, unlike the previous ones, the [M]=CR_2 bond is covalent-like, with the metal usually in a high-oxidation state. Each metal-carbene bond is polarized towards the carbene, reason why the C_α is nucleophylic. Orbital interaction and the first report Schrock carbene are shown in Figure 1.3.

At the fundamental level, the distinction between the two type of carbenes is based on the nature of the [M]=CR_2 bond, inferred from its cleavage, which can be seen as the reverse of the metal-carbene formation. The cleavage products of Fischer carbenes, both carbene and metal fragment, are singlets. For Schrock type, on the other hand, they are triplets.[60,62] Recently a new class of carbenes has emerged, where the carbene bears a significant radical character. The carbene radical (Figure 1.3) is formed by one-electron reduction of metallic center during the formation of [M]=CR_2, at an open-shell transition metal complex (in particular low-spin cobalt(II) complexes), using diazo compounds and related carbene precursors.[63]

Well-defined Catalyst

The successful history of metathesis in the field of organic synthesis is due to the development of the active, selective and efficient catalysts based on metal-carbene. The first result of this kind was published by Casey and Burkhardt[64] showing that $W(CO)_5(=CPh_2)$ reacts with isobutene to form 1,1′-diphenylethylene (1974) and Chauvin (1976)[65] using the same system reported metathesis as well. However, this complexes were not well determined.

Well-defined catalyst metal-carbene are said so because they are characterized by spectroscopic techniques and their composition is well established. These systems were developed only in the 80-90s. They are the catalyst commonly used today and can be divided in two families: the Schrock type metal-alkylidenes which present d^0 centers (Ta,

Mo, W, Re), and the Grubbs type metal-carbenes that are based on ruthenium. Both type of complexes present high catalytic activities and selectivities, and are commercially available.

Schrock catalysts are those metal-alkylidenes complexes of d^0 metals, but this history started one decade before with a Ta carbene ($[Ta(=CH–t\text{-}Bu)Cl(PMe_3)(O–t\text{-}Bu)_2$), which catalyses the metathesis of *cis*-2-pentene.[66] The first properly defined carbene of this kind was reported in 1990, made of a Mo atom with two alcoxide ligands, an imide and the carbene(Figure 1.4).[67]

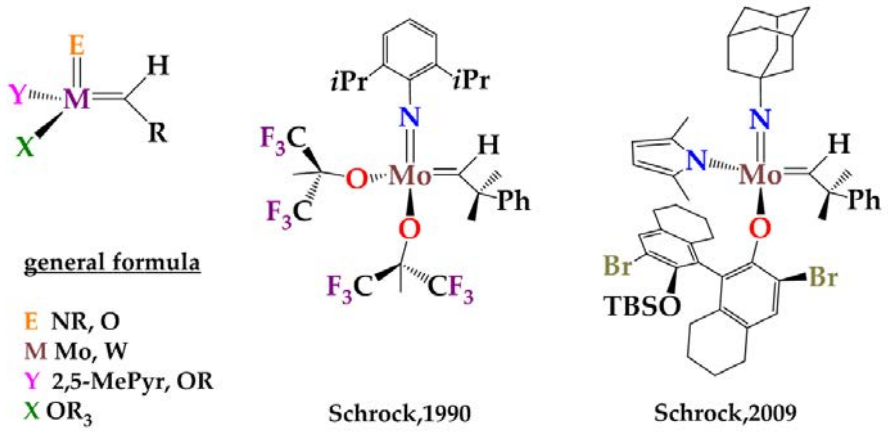

Figure 1.4: Schrock's Catalysts

Further studies culminated in a group of catalysts that exhibited better initiation and unique levels of reactivity under milder conditions than ever before.[4,68] They allow reaction of diverse substrates such as terminal and internal olefins, and also challenging olefins like ROMP low-strain monomers, or ring-close of sterically demanding and electron-poor substrates. On top of that, they also made possible deeper studies on the structure-reactivity relationship and mechanism, and provide a commercial catalyst.[20] However, those complexes showed some disaadvantages, basically deriving from the oxophilicity of the metal center, making them to be extremely sensitive to oxygen and moisture, limiting their usage. They are also intolerant to alcohol and aldehydes, which are present in many biological/natural substances.

More recently, in 2005, Schrock noticed that changing one of the alcoxy ligands by a pyrrol generates a very active catalyst. This was later explained by theoretical calculations,[69] analysing the role of the

ligands, which drove Schrock and Hoveyda (2008-2009) to produce a large number of similar catalysts, which are more stable and active, and at the same time Z-selective because of the large alcoxy group.[70]

Ruthenium complexes are an interesting element because it shows tolerance to air, moisture, nitrogen and oxygen containing functional groups, and at the same time reacts preferentially with C–C double bonds over other species. Indeed, at the very beginning of olefin metathesis history, $RuCl_3$ was used for ROMP of cyclobutene (1965).[71] The group of Grubbs studied for many years polymerization with these ruthenium salts. In 1992, in a great breakthrough, they reported the first well-define carbene of ruthenium able to catalyse ROMP of norbonene (Figure 1.5).[72]

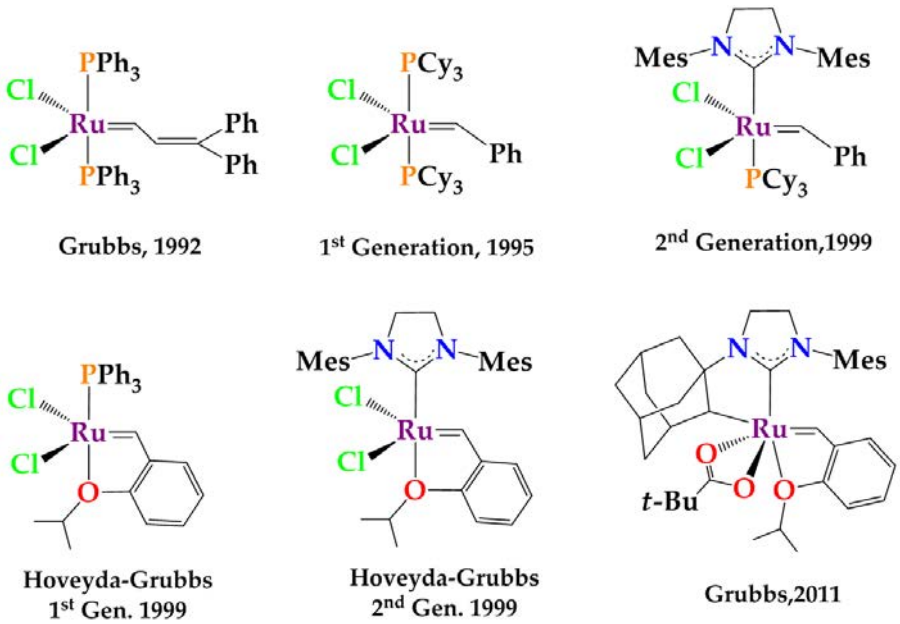

Figure 1.5: Grubbs's Catalysts

Three years later, in 1995, Grubbs prepared a new well-defined ruthenium-carbene, whose structure is closely similar to the vinyldene ones previously reported.[73] Those complexes were immediately commercialized, and even today are within the most used catalysts in organic synthesis because of their stability to air and compatibility with functional groups. This is known as *First Generation Grubbs Catalyst*. Please note that this complex is highly coordinated ($16e^-$) and the interaction with olefins is difficult. Mechanistic studies have shown

that the carbene active species is formed by dissociation of a phosphine forming a $14e^-$ reactive species.[74]

The groups of Fürstner and Herrmann,[75] Grubbs and[76,77] Nolan[78] figured out that replacing a phosphine with an Arduengo's cyclic bis-amino carbene ligand, the NHC, works to accelerate the activation process. These ligands are excellent σ-donors but show no π-acceptor properties, which increases electron density at the ruthenium center. This is called Second Generation Grubbs Catalyst, and is used for cross-metathesis and is commercially available. It is more thermally stable and active than the previous one, although it is not tolerant to amines and nitriles.[20,29]

Meanwhile, in 1999, Hoveyda[79] prepared a related ruthenium catalyst derived from the Grubbs' First generation catalyst, bearing one phosphine and a internal and chelating metal−oxygen carbene ligand, very reactive, stable and functional-group tolerant. Subsequently in 2000, Hoveyda[80] and Blechert[81] simultaneously reported a new catalyst bearing an Arduengo's carbene instead of the phosphine. Both catalysts are now commercially available, although expensive, and show better activities for electron-deficient olefins.[29] They are named Hoveyda-Grubbs catalyst of First and Second Generation, respectively. In 2011 Grubbs reported a catalyst with a adamantyl-containing NHC chelating ligand that is effective for Z-selectivity of products.[33]

Overall molybdenum and ruthenium catalysts offer complementary degrees of efficiency. The superior activity of a Mo catalyst in one case does not mean that such activity is true in all cases. Mo an W complexes are sensitive to moisture and air, and should be handled in inert atmosphere and used in anhydrous solvents. Alike another early-transition-metal complexes, they are incompatible with carboxylic acids, ketones, aldehydes, most alcohols and primary amines, but are effective in the presence of phosphanes and thioethers, which decompose Ru-complexes. Regarding the activity, some reactions, for instance, occurs within minutes with 5 mol% of Hoveyda catalysts, but others do not proceed, even at 70 °C, in the presence of catalytic or stoichiometric amounts of second generation Ru catalysts.[68]

1.3 Organometallic of Earth Abundant Metals

For nearly 50 years organometallic chemistry was supported, in a large extend, on the precious metals. However their use can become outdated and provide some inconveniences due to the nowadays fundamental emphasis on the sustainable matter, the environmental impact and associated carbon dioxide footprint derived from the extraction of scarce elements from the earth's crust, can somehow become outdated and provide some inconveniences on their usage.[10] Moreover, precious metals present precarious toxicological properties. Some of them, such as platinum and rhodium, are more toxic than Fe by two or more orders of magnitude[7,82] In fact, because of the toxicity of these metals, their levels in pharmaceuticals is limited to 10 ppm.[11] The ionic forms of ruthenium show toxicity as well, therefore, when used as a part of a catalytic process, they should be removed from the product, which can be difficult, depending of their nature.[83]

A second problem to be faced is that those precious transition metals are among the least abundant and subsequently most valuable in the Earth's lithosphere. Although in some cases the metals may be recycled, some lost is inevitably. In polymerizations based on alkene metathesis or hydrosilylation, the catalyst is typically left in the reaction product, especially if it is an organic product. On the other hand, substantial costs are involved when recovery and recycling of the metal is required.[11,16,84,85] Besides, a potentially non-sustained supply can be a consequence of 'political' price fixing due to a massively imbalanced global distribution.[86]

Such factors can be less relevant in the academic world or in processes carried out in relatively small scale, but it can be an important bottleneck for industrial applications in a global scale. For instance, if the wishful change of cars based on fossil fuels to hydrogen fuel cells comes true, the demand of Pt will be far bigger than the known ores, but such a change could be achieved with the development of efficient fuel cells that use Fe catalysts.[6]

Precious metals often cost more than 100 or 1000 times the cost of base metals, typically >50$/g, whereas the price of Fe, for instance, is often quoted per kilogram or ton. Ruthenium is somewhat less expensive than the other precious metals, but the inability of recovering the catalyst imply in high cost processes. The price comparison be-

comes even more favourable for Fe if is consider the much higher atomic weight of the precious relative to Fe. Figure 1.6 shows the comparison, in prices per mol, of the precious metals we have been discussing about.

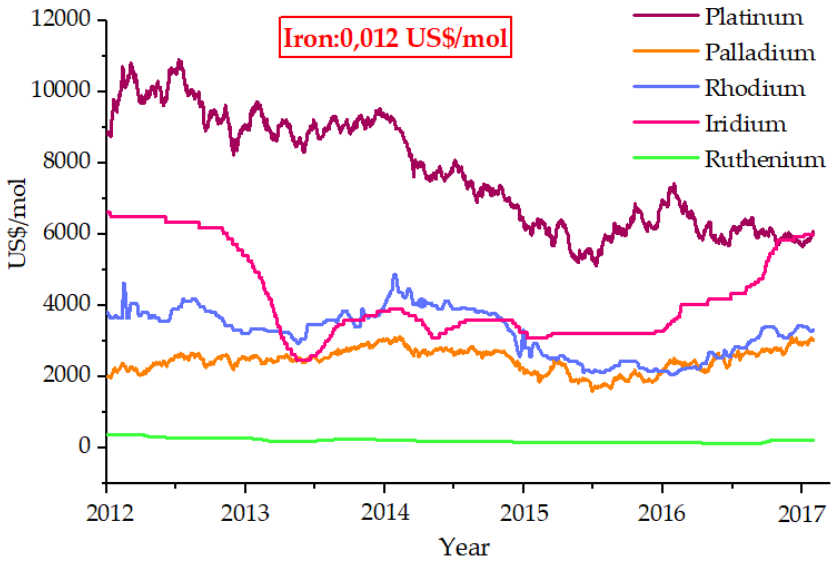

Figure 1.6: Market prices of transition metals. By the middle of 2017 the values are 6046 for platinum, 3018 palladium, 3308 rhodium, 5994 iridium and 215 for ruthenium, in US$/mol.[85] Iron's price is based on scrap iron quotation in August 2017.[87]

These considerations have motivated chemists to work on alternatives to this chemistry. One interesting solution came out: replace precious metals with base first-row transition metals on the basis of periodic similarities (Figure 1.1). Apart from the attempts at substituting for their precious-metal analogues, the wide use of less-explored metals coupled with the contemporary knowledge of homogeneous catalysis can often lead to new reactivities that have not been achieved with precious-metal catalysts.

Is not surprising, then, that in recent years, increasing efforts have been devoted to the design and discovery of homogeneous catalysts that incorporate base first-row metals, for chemical transformations, such as iron (Fe) and cobalt (Co), managing to offer sustainable alternatives to the conventional catalysts that now face diminishing

supply.[88,89] Comparably, the first-row transition metals, such as Fe, Co, and Ni, are much more abundant on earth, inexpensive, and more environmentally friendly. For example, the natural abundance of Fe, Ni, and Co on earth is about 32%, 1.8% and 0.88%, respectively as a consequence, production and separation of Fe, Co, and Ni is less energy-consuming than for precious metals.[11,82,90,91]

With regard to the biocompatibility, *ergo* the toxicity to living beings, the earth-abundant metals show an advantage, since, exactly because they are abundant in Earth crust, in the evolution of live they were incorporated in various biological processes. Enzymes activated by vanadium, manganese, cobalt, iron, and copper are ubiquitous and provide inspiration to catalytic chemists. Metals supported by porphyrin and other macrocyclic ligands are common in nature. Cobalamin is the very important vitamin B_{12}, which is a porphyrin complex with cobalt. Chlorophyll is another very important biological complex made of porphyrin and magnesium, and hydrolases are complexes of zinc (Zn).[11,92,93] Table 1.1 summarizes some life processes where those metals take part in.

Table 1.1: Functional roles of inorganic elements found in biology[92,93]

Function	**Metal**	**Representative Examples**
Acid-Base Catalysis	Zn, Fe, Ni, Mn, Mg	Hydrolysis reactions carried out by carboxypeptidase, urease, arginase, etc.
Atom or Group Transfer	V, Fe, Co, Ni, Cu,Mo, W	Dioxygen transport (hemoglobin); alkyl group transfer (cobalamin)
Electron Transfer	Fe, Cu, Mo	Iron-sulfur proteins, cytochromes, blue copper proteins
Redox Catalysis	V, Mn, Fe, Co, Ni,Cu, W	Enzymes involved in oxygen metabolism; nitrogen fixation; radical formation

1.3.1 Open-Shell Behaviour

The chemistry undergone by the precious metals is usually based on a even number of electrons and are redox-neutral. Olefin Metathesis is a example of this. Elements of the same group in the periodic table are expected to present similar chemical behaviour. However, the principles of the precious metal chemistry may be not present in their first-row counterparts that often form complexes with a tendency to generate paramagnetic species ($S > 0$) or preferring one-electron pathways. Additionally, is observed that high-spin systems as 'metalloradicals' lead to free radicals and decomposition. This can be one of the biggest challenges for the earth-based metals chemistry.[11,84]

Iron complexes, for instance, are undoubtedly able to promote two-electrons chemistry processes, but single electron processes are certainly competitive and, in many cases, preferred. Of course, this open-shell behaviour can favour new reactions, but if the wish is to emulate the chemical behaviour of noble metals, as is ours, regarding olefin metathesis, we have to face it.[94,95]

The electronic behavior of transition metals is governed by the spin state generated by the partially filled d-orbitals of the metallic center. The metals alone have high-spin configuration, but when forming complexes, the degeneracy of the d-orbitals is lost into a split that can lead to a low-spin configuration or, if the d-orbital splitting is not big enough, the high-spin configurations remains feasible. For example, in Figure 1.7 we can see how different coordination numbers and geometries influence the d-orbital splitting for iron complexes.

The logical way to solve this spin matter is to address the splitting of the d-orbital, controlling the electron occupancy. The determinant issues are the coordination geometry and the nature of the chosen ligands: strong field ligands lead to larger splitting, in particular, in the octahedral ligand field, and hence favour electron pairing and the formation of low-spin complexes.[93,94] In a given coordination number, changing the nature from independent ligands to chelating can provide a big change in the relative energies of the orbitals.[96]

The oxidation state also plays an important role, since a higher positive charge density contracts the metal orbitals and it costs more energy to pair electrons in a smaller orbital, leading preferably to higher spin-state. In the same sense, more electron donating ligands will reduce the pairing energy and more electron withdrawing ones will

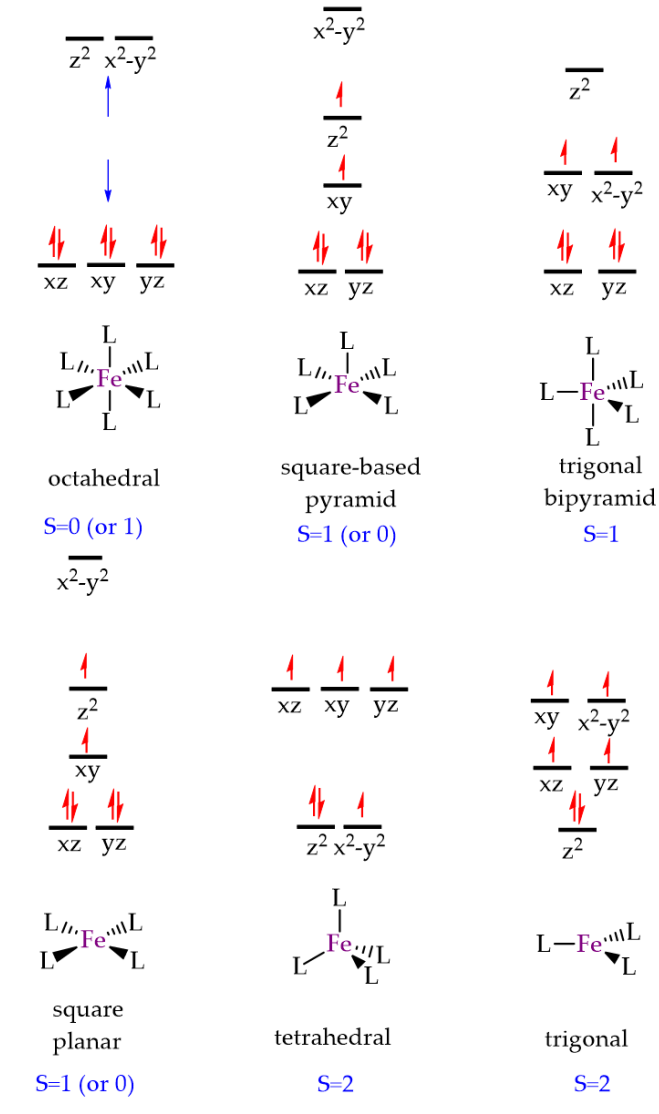

Figure 1.7: Most common open-shell configurations for Fe(II) complexes in different valence numbers.[96,97]

increase it.[98] A large number of ligands also forces a large value of the splitting of the d-orbitals. If the charge of the metal and the coordination sphere is constant, the pairing energy decreases from the first row to the two lower rows, because with a small covalent radius the 3d orbitals are less diffuse than the 4d and 5d orbitals, resulting in higher exchange interactions between compact 3d-orbitals, giving

more easily medium or high spin systems.[98–100]

Although is not the wished trend for this thesis, iron has been employed to generate radicals by an large numbers of reactions, and in another cases radical behaviour was observed as well. However, as expected, radical species are challenging to control the reactivity and stereoselectivity. Some examples of this open-shell reactivity catalysed by iron salts are C–H bond oxidations,[101] cyclizations, formation of few C−X Bonds (X=O, S, N, F, Cl),[102] different kinds of C–C cross-couplings by different approachs.[103] Another kind of C−C bond formation is previously convert olefins to radicals, promoted by iron salts as well.[104] High-valent non-heme iron complexes shows a versatility in radical-alike dioxygen binding.[105]

In comparing the chemistry of earth based and precious metals, Chirick says that the latter ones *"when surrounded by strong field ligands such as phosphines, carbenes, carbon monoxide, alkyls, and hydrides typically used in catalysis, predictable two-electron chemistry is observed. As such, fundamental transformations such as oxidative addition and reductive elimination are enabled and constitute the key bond breaking and making steps in many catalytic cycles. Strong field organometallic compounds of the first row transition metals are by no means rare and in fact, compounds such as ferrocene and $Fe(CO)_5$ launched the field of organometallic chemistry. These early organometallic complexes often contained saturated, 18-electron configurations that limited their utility in catalytic reactions. Nevertheless, many successful catalytic reactions, such as alkene hydroformylation, have been reported where the base metal catalyst operates in the traditional, strong field limit."*[10]

A general trend for replacing precious metals with first-row transition metals in homogeneous catalysis is to identify ligands that, binding properly to the metals, promote a reactivity similar to the precious metal, as decreases the focus on the metal. Along the control of the steric and electronic properties by manipulating the ligands and coordination geometry, some features have been useful for the recent success of the organometallic chemistry of first-row metals:[7]

(i) Strong chelation to metals increases the stability of the metal complexes and potentially minimizes the degradation of the catalysts;

(ii) Ligands such as hydride, alkyl or aryl, and CO provide a strong

ligand field that favours low-spin states, which are more commonly observed for precious metal-based complexes;

(iii) Redox-active ligands store and release electrons readily, thus obviating the need to change the oxidation states of the metals;

(iv) Ligands capable of activating a substrate via secondary coordination sphere interactions diminish the reactivity difference among the metals in the same group.

1.4 New Iron Organometallic Chemistry

Iron is one of most ubiquitous elements in the Earth crust, indeed is the second most common metal, after aluminium, constituting around $\frac{1}{3}$ of it, making availability and price not a problem. In contrast to man-made precious-metal catalysts, iron shows an interesting biocompatibility, since it is part of large number of fundamental molecules involved in biological process, most of them also organometallic complexes with prophyrins: hemoglobin in the oxygen transportation, cytochrome involved in the electron transportation process in the oxidation of carbohydrates for generating energy, etc. (see Table 1.1).[89,93,106]

This metal has a neutral electronic configuration of $[Ar]3d^6 4s^2$ located in the center of the d-block in the periodic table (Figure 1.1), just above the ruthenium, and is at the same time an early and late metal, and therefore should be able to embrace a wide range of chemistries. The oxidation states range from -2 to +6, being useful in reductive and oxidative processes[89,107] For iron(II) complexes ($[Ar]3d^6$) a coordination number of six with an octahedral ligand sphere is preferred. Iron in low oxidation state is more interesting for organometallic chemistry and in particular for iron-catalyzed reactions because it can form more reactive complexes than its iron(II) and iron(III) counterparts. Therefore, iron(0) and iron(–II) compounds are favoured for iron catalysis.[108] Iron also binds well with N and O-based ligands, as well as N-heterocyclic carbenes or similar donors. This allows phosphines and similar to be avoided, thus limiting cost, labour and environmental impacts. This characteristics suggests that iron complexes are able to cover almost the entire range of the organic synthesis.[89,107,109]

1.4.1 Reactivity

These characteristics allow iron complexes to be involved in a broad range of reactions, for instance, additions, substitutions, cycloadditions, hydrogenations, reductions, oxidations, coupling reactions, isomerizations, rearrangements, and polymerizations. Figure 1.8 summarizes some representative reactions carried out by iron catalysts.

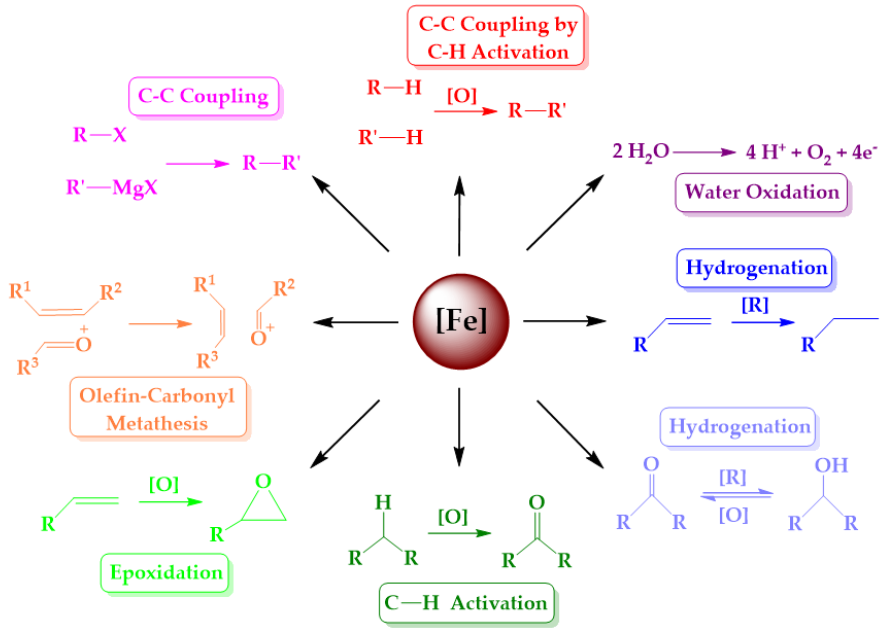

Figure 1.8: Representative examples of Fe-Reactivity

Recently, important discoveries have been accomplished in the field of iron-catalyzed cross-coupling chemistry, which classically is catalysed by nickel and palladium. Iron-catalyzed protocols do not merely benefit from economic advantages but entertain a rich manifold of reactivity patterns and tolerate various functional groups. The past years have witnessed a rapid development of more efficient protocols for the cross-coupling between alkyl, alkenyl, alkynyl, aryl, and acyl moieties becoming available to organic chemists. The practical aspects of this technologies was proved to be efficient to several synthesis of natural products.[110–117] Efforts to clarify the rather unclear mechanism, should unfold new opportunities to develop new reactions and improve turnover numbers, space–time yields and selectivity profiles of existing transformations. Although the mechanism is not completely

clarified it probably takes place through a radical mechanism. The catalysts are usually three-coordinate iron-salts,[118–121] but not exclusively,[122] presenting high spin states, such as quintuplet. The high-spin iron complex originates the radical species in the catalytic cycle.[123] Those same iron complexes are used, as well, in living polymerizations based on radical mechanisms.[124–126]

Another important subject that has been gaining attention is the activation of unreactive C–H bonds, such as the ones found in aliphatic and aromatic hydrocarbons, by means of iron complexes. This is a field of major interest in current organic chemistry, because is a window to new reactions and for the synthesis of new organometallic compounds. C-H bond activation is a fundamental step in the C-C and C-heteroatoms coupling.[127,128] Recently controlled radical polymerization of styrene and others olefins with an high-spin Fe(II) complex were reported.[129]

Reduction is also studied in the emerging iron chemistry, especially regarding the hydrogenation and hydrosilylation of alkenes, alkynes, imines and carbonyl groups.[7,130,131] It has been shown that low covalent iron complexes catalyse the hydrogenation of doubles and triple bonds.[10,132,133] Recently, iron catalysts have been used with efficiency, in such a way that they can compete with noble metal catalysts for carbonyl reductions.[134] The opposite reaction, oxidation, also can be catalysed by iron. Examples are the oxidation of $C(sp^3)$–H bonds resulting in ketones or alcohols and $C(sp^2)$–H bonds giving in epoxidation or alcohols.[135–140]Carbonyl-olefin metathesis also has been reported to be catalysed by an iron salt that acts as lewis acid polarizing the carbonyl bond.[141,142] Finally, water oxidation can provide a cheap source of electrons for the reduction of water to H_2. Some iron complexes also have been used to this transformation.[143–146]

1.5 Iron Carbenes

As shown in Section 1.2.2, in order to carry out olefin metathesis, a $[M]{=}CR_2$ species is needed. In this way, if we want to achieve olefin metathesis using iron as base metal of the catalyst, it is necessary to understand the nature and possible reactivity of iron carbenes. Historically, studies of $[Fe]{=}CR_2$ are intimately related with the carbene transfer reaction (cyclopropanation), usually carried out from a diazo

compound to an alkene, which can be catalysed by iron complexes generally bearing different nitrogen- and phosphorus-containing ligands.[147] In this case, the iron-carbene complex is actually a stable intermediate of the stoichiometric carbene transfer reaction from a diazocompound to an olefin.

In Scheme 1.5 we show the $Fe{=}CR_2$ complexes reported in literature, for which the structure was characterized mainly by X-ray and NMR techniques. Among these carbenes we can envisage two broad families: the first one, is composed of "free carbenes" in which the substituents in the carbon are not linked with the ancillary ligands or with another molecules (cases a-f). Unlike, in carbenes g-1 the substituents of the carbenic carbon are chelated with a ancillary ligands and thus can be seen as "bridge carbenes".

The first of the $[Fe]{=}CR_2$(**a** in the Scheme 1.5) corresponds to the family called *Piano-Stool* complexes with the general formula $Cp(CO)(L)Fe{=}CHR^+$ ($L{=}CO,PPh_3$;$R{=}Me,Et,CHM_2$). These catalysts are positively charged complexes synthesized by convenient procedures *via* hydride or alkyl anion reagents. They were developed to access stable iron-carbene or complexes for *in situ* generation of the carbene.[148,149] The first studies of this complexes reported cyclopropanation with stoichiometric amounts of the iron complex mainly by the groups of Brookhart, Lapinte and Casey.[150–160] It is worth noticing that in some of these complexes the groups X and CO are replaced by a bidentate chelate diphenylphosphine ligand.[159,160]

Afterwards, in the 1990s several other iron complexes, have subsequently been developed as efficient catalysts for cyclopropanation, which conserve the ancillary ligands of **a**, but without the carbene: Hossain and co-workers reported the use of the $CpFe(CO)_2^+$ fragment in the cyclopropanation of alkenes by utilizing diazo esters as the carbene source.[161–164] Cyclopropane products of this reactions usually present the least stable *cis*-isomer. Figure 1.9 shows the general mechanism for $[Fe]{=}CR_2$ formation from the iron complex plus the diazocompound - part A - and subsequent cyclopropanation - part B. In these cases, the metal-carbene complex is normally not characterized. Please note that this process is not catalytic regarding the diazo compound, which means that the carbene is generate at each turnover cycle, unlike the olefin metathesis reaction, where the carbene is generate only once.

An extensive study of iron carbenes having porphyrin as ancillary ligand has already been presented by various groups. This is the family

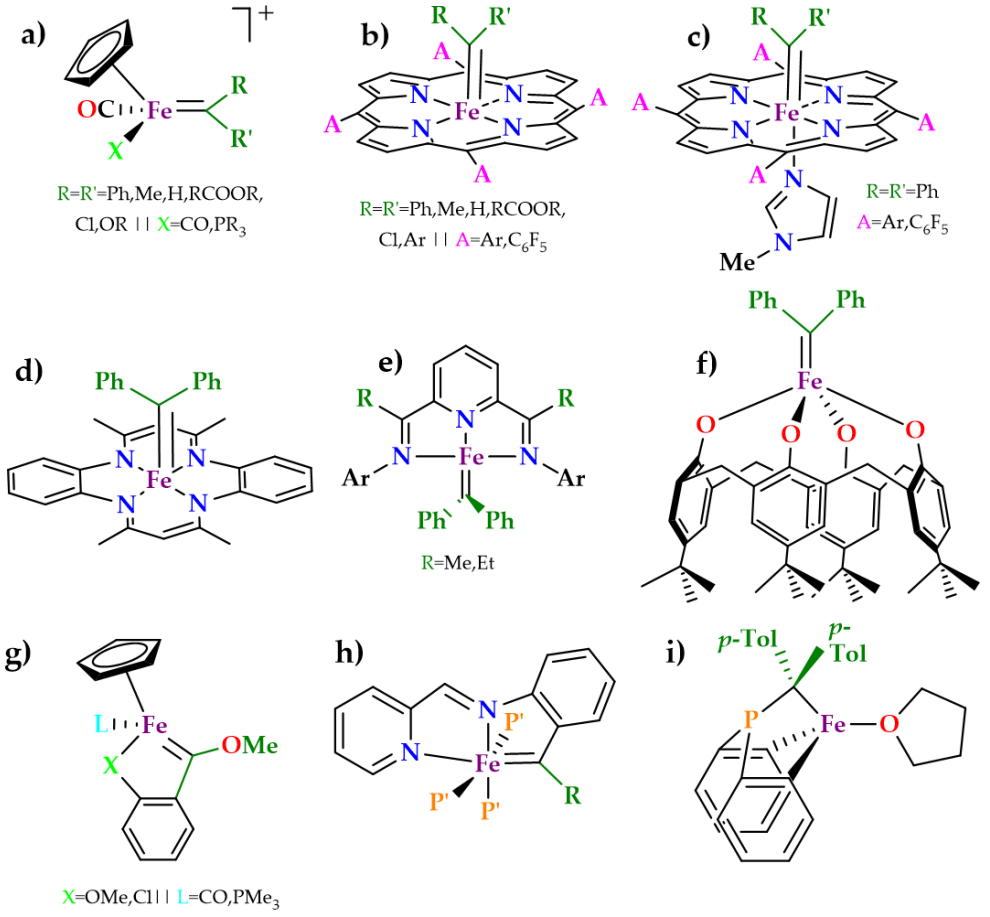

Scheme 1.5: Fe=CR_2 reported as characterized in the literature.

of iron-carbenes with the largest number of examples, represented by system **b** in Scheme 1.5.[165–173] The porphyrins of these complexes are usually the tetraphenylporphyrin (TPP) or its derivatives, such as the complex with an N-methylimidazole (**c**),.[174] Another type of tetracoordinate planar ligands has also been used to synthesize different Fe=CR_2, for instance the TMTAA- tetramethyldibenzotetraazaannulene (**d**).[175]

This class of iron complexes are also capable of carbene transfer to olefins, following the general scheme showed in the Figure 1.9, with a stoichiometric usage of diazo compounds to generate the [Fe]=CR_2. In fact, they have been reported as more effective for cyclopropana-

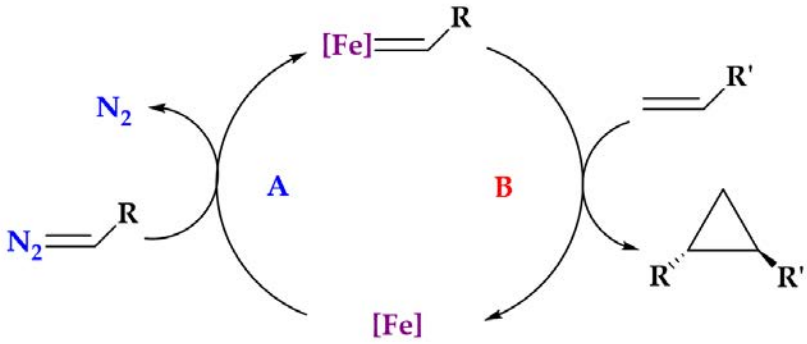

Figure 1.9: General reaction of the stoichiometric transfer reaction of carbenes from a diazocompound to a olefin, catalysed by an iron complex.

tion than others metal complexes.[172] Unlike the previous group of iron complex, it is rather common to determine the structure of these [Fe]=CR_2 by many techniques, like NMR and X-ray. These characterizations found those complexes to be low-spin (singlet) iron(II) species.[168,171,174] The resulting cyclopropanes of this reaction are the most stable *trans*-isomer.

Complex **e** in Scheme 1.5 is a low-coordinate iron carbene synthesized by the group of Chirik.[176] It is a remarkable system, due to its low-coordination environment, in opposite to the previous ones. This complex shows a S=1 behaviour and is a carbene radical. Regarding the reactivity, the complex is able to promote intramolecular C-H activation and carbene transfer to nitrenes or carbon monoxide, but no cyclopropanation was observed. Iron-carbene **f** was done in Floriani's group. The characterization showed that this is high-spin (S=2) complex, with no reactivity observed.[177,178]

Although some [Fe]=CR_2 catalyst were not isolated, their existence is sure due to the observed reactivity: besides some porphyrin iron complexes, μ-oxo-bis[(salen)iron(III)] complexes have been described as giving olefin cyclopropanation with diazoacetates, probably based on a mechanism similar to that of Figure 1.9.[179,180] Similarly, cyclopropanation with diazoacetates were reported in the presence of iron complexes with terpyridines as ancillary ligands.[181]

So far we have discussed the free-carbenes. In the group of the bridge-carbenes, one of them is similar to the piano-stool family that

was characterized by X-ray diffraction, but no reactivity was observed (**g**).[182] Complex **h** is a six-coordinate bearing chelating alkylidene ligands, characterized as high-spin. It was synthesized in a unfruitful attempt to catalyse olefin metathesis. In fact no reactivity was not observed, and even cyclopropanation was not observed either.[183–185] Very recently another high-spin (S=2) chelate iron carbene (**i**) supported by a tripodal amido-phosphine-amido was reported giving cyclopropanation when reacting with olefins.[186]

Besides cyclopropanation, iron porphyrin carbenes have been reported to mediate other reactions including, C–H insertion, carbonyl olefination, O–H insertion and remarkably, N–H insertion.[187–191] Also non-heme carbenes are able to promote $C(sp_2)$−H bonds activation.[192] In the next section we will discuss more precisely the mechanism of the cyclopropanation reaction.

1.5.1 Cyclopropanation Mechanism

As mentioned at the previous section one of the most common reactions of iron-carbenes is cyclopropanation, which would be a key deactivation process of olefin metathesis. That is, the reaction implies the transfer of the carbene to the olefin, and the first one is regenerated with a diazocompound, starting a new turnover cycle. The generation of the carbene is that in the part A of Figure 1.9 and its mechanism is already clarified as happening by a radical mechanism, but this is not the focus of this text.[191,193]

In Section **??** we have shown that cyclopropanation can be a feasible process from the intermediate metallacyclebutane through a reductive elimination mechanism. Since some of this complexes are high coordinated, the formation of the intermediate metallacyclebutane can be difficult, and cyclopropanation can happen in a direct interaction resulting in the transfer of the carbene to the olefin.

Within the efforts of enlarging the toolbox of the earth based metals reactivity, a extensive work about cyclopropanation with $[Co^{II}]{=}CR_2$ have been done, where the compounds are similar to the cyclopropanation with iron carbenes porphyrins that we have discussed. In the Figure 1.10 the general mechanism for this path is shown. This is a stepwise mechanism elucidated by experimental and computational efforts. Here, there is no previous interaction of the olefin with the metallic center to form the metallacyclebutane, as in the olefin metathesis

mechanism. Cyclopropanation occurs through a nucleophilic attack of the olefin to the carbon of the metal-carbene, or better said, an electrophilic attack of the carbon carbenic to the olefin. The attack is followed by an intermediate structure of the catalytic cycle, in which the metal carbene interaction has a single bond character, likewise, the olefin loses the double bond characteristics. Subsequently the ring-closing reaction lead to the cyclopropanation product and the metal fragment.[63,194,195]

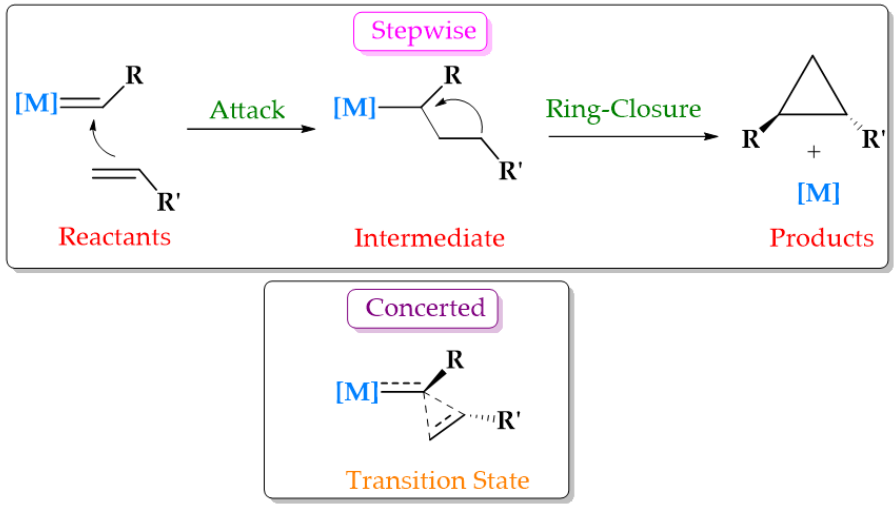

Figure 1.10: Cyclopropanation by a carbene transfer mechanism.

For the case of the cobalt-carbenes, the mechanism is said to be radical-alike: the cobalt has an odd number of electrons and when the carbene is formed the metallic center is oxidized by a unit and the electron density is concentrated over the carbenic carbon. In the intermediate, the unpaired electron is on the carbon-γ, and promotes the cyclization by attacking the α-carbon and the unpaired electron returns to the metallic center.[63,196,197]

Despite the existence of a fair number of experimental results of cyclopropanation with iron-carbenes, to the best of our knowledgement there is no conclusive study about the mechanism of this reaction. It is accepted that the reaction occurs through the carbene transfer mechanism, which starts by the electrophilic attack of the olefin by the carbene. In the case of [Fe]=CR_2 with porphyrin (**b**) Woo claimed that instead of the stepwise mechanism, rather a correspondent concerted

mechanism exists with a barrier corresponding to the transition state represented in the bottom of Figure 1.10.[166,167]

For this very same iron carbenes, however, a stepwise mechanism similar to the cobalt-carbene was also proposed.[169] For the [Fe]=CR_2 bearing porphyrin as ancillary ligands (**a**) the existence of a carbocation or radical species was suggested, which is formed in a non-concerted insertion of the carbene into the olefin.

In the case of iron carbenes of piano-stool family (**b**), the existence of a zwitterionic intermediate has been proposed (Figure 1.10), after the attack step, with a partial positive charge on the carbon-γ and the negative over the metal.[148,155] However concerted mechanism was also claimed to take place based in theoretical works.[198,199]

Very recently, Deng showed by theoretical approach that the cyclopropanation of styrene by the high-spin catalyst **i** proceeds by a radical mechanism similar to that one of the cobalt porphyrins.[186]

Overall, two different paths can be envisaged for cyclopropanation reaction:

(i) Reductive elimination from the metallacyclebutane;

(ii) Carbene transfer to the olefin.

The later can be divided in three different processes depending on the formation or not of a intermediate and the nature of this species be biradical or a zwitterionic.

(ii.a) Concerted;

(ii.b) Radical stepwise;

(ii.c) Cationic stepwise.

1.6 Fe-Carbenes for Olefin Metathesis?

To the best of our knowledge, there are very few existing examples of first row transition metal carbene complexes able to perform the olefin metathesis reaction. Only Tebbe's titanium complex[200] or V[201,202] have been reported and the scope of reactions in which they have been applied is still rather limited. However, iron could be the preferred choice, since it is the earth most abundant transition metal and

the main focus of this work is to explore possibilities of iron-carbenes catalyse olefin metathesis.

Unfortunately, several difficulties can be easily identified when thinking in an iron carbene able to perform olefin metathesis. First, early-transition-metal complexes are incompatible with carboxylic acids, ketones, aldehydes, most alcohols and primary amines.[68] The synthesis of the iron carbene is challenging and this is probably due to the usual low stability of first row transition metal carbenes: Grubbs, for instance, tried to synthesize [Fe]=CR_2 analogue to the First Generation Grubbs Catalyst (PCy_3Cl_2Ru=CHPh), without success.[203] Dixon and co-workers also arrived to similar conclusion when they performed CCSD(T) calculations on model systems of Ru, Os and Fe carbene complexes derived from the 2nd generation Grubbs catalysts. They found that while the metal carbene bond dissociation energy is large in the case of Ru and Os, the BDE for the [Fe]=CR_2 species is much smaller.[204] A second problem, probably related to the previous, is that the existing first row transition metal carbenes most commonly undergo cyclopropanation and/or free radical reactions when reacting with olefins, as we have shown above.

These two evidences can be associated to two aspects: a) the [M]=CR_2 carbene bond tends to be weaker for 3d metal containing complexes than when the metal belongs to the second or third row. This decreases the metal carbene stability and favours alkene cyclopropanation and other carbene transfer reactions; b) while 4d and 5d metal complexes usually present a singlet ground state, several spin states may be close in energy in first row transition metal carbenes. This includes open shell systems that would more easily proceed through radical reactions.

In this context, there are few works explicitly dealing with olefin metathesis with iron-carbenes. Experimentally Wolczanski and colleagues synthesized a carbene like (**h**) (of Scheme 1.5) with no much success, concluding that "*while it is easy to be discouraged by these and previous findings with regard to base metal catalysis of olefin metathesis, it is clear that stronger fields must be entrained in lower coordinate environments, and the pursuit of an [Fe]=CR_2 functionality must be realized, in order for the desired reactivity to have a chance at being observed.*" They also pointed out that the fail could be because the complex is high-valent and cationic, and an interesting catalyst must be neutral or anionic.[183–185]

Some theoretical contributions in the literature also evaluate the potential of the iron-carbenes for metathesis: Hoffmann and co-workers performed extended Hückel calculations on $ML_4{=}CH_2$ and $Cp_2M{=}CH_2$ carbene species with the aim of determining the electronic structures that would favour the olefin metathesis reaction. One of their main conclusions is that cyclopropanation should be forbidden for complexes with d^0 to d^4 metal centers, but favoured for d^6 systems (counting the carbene as a neutral ligand).[205]

More recently, Poater, Cavallo and co-workers studied the reaction mechanism for olefin metathesis of an iron carbene complex generated by substituting the ruthenium metal center of the 2^{nd} Generation Grubbs catalyst by iron.[206,207] Also, it was reported that a complex based on the 2^{nd} Generation Grubbs catalyst, where the chlorines were replaced by carbonyls, allegedly favours olefin metathesis over cyclopropanation, but the ligand NHC was chosen as model, with the mesityls substituted by hydrogen.[208]

1.7 Goals

Within the efforts for build a new chemistry based on earth-abundant metals, the general objective of this thesis is to rationalize how the nature of the ancillary ligands, coordination geometry around the metal center and the iron formal oxidation state control the spin multiplicity of the metal carbene ground state, the $[M]{=}CR_2$ bond strength and the reactivity of the resulting species over olefins, especially targeting metathesis. Such understanding can pave the way to define suitable routes for designing iron carbenes with potential catalytic activities in olefin metathesis that ultimately could guide experimental efforts and turn in the synthesis of iron-based olefin metathesis.

In view of the difficulties to obtain the desired catalyst, computational chemistry can be a powerful tool to clarify the mechanism involved in the reactivity of iron-carbenes with olefins, usually prevailing cyclopropanation over olefin metathesis, and compare with the reactivity of the ruthenium-carbenes which gives metathesis. Such effort aims at offer insights about the nature of the two families of complexes.

Computational efforts also can be used to explore the properties of potential iron complexes. For the particular aim at design a potentially active olefin metathesis catalyst based on iron, it can be used to

rationalize how the coordination sphere around the metal center and the nature of the ligands and the metal modify the electronic properties of iron carbenes as well as their reactivity towards olefins, thereby giving us insights on the key factors that such complex should fulfil to perform the olefin metathesis reaction.

Due to the complexity of the general objective of the work, the following specific objectives have been established.

(i) Determine the most plausible alkene cyclopropanation reaction mechanism when catalyzed by iron carbenes;

(ii) Understand the role of ancillary ligands and iron coordination sphere in stabilizing singlet state $L_3M{=}CH_2$ tetracoordinated metal carbenes and the metallacyclebutane resulting of its reaction with ethene;

(iii) Analyse how the nature of the ancillary ligands and iron formal oxidation state tunes the metal-carbene ground state and its reactivity facing olefins in $L_4M{=}CH_2$ pentacoordinated complexes.

2

Theoretical Foundations

As previously said, this thesis addresses the electronic structure of different iron carbenes complexes and their reactivity with olefins. With that, we want to provide some insights to help designing [Fe]=CR_2 complexes able to catalyze the olefin metathesis reaction, instead of transferring the carbene from the iron center to the olefin, which is a process that deactivates this potential catalyst.

The methodology used to address this problem is an approach based on computational quantum chemistry. Since the late 70s this field has grown exponentially, mainly because of the enlargement of computational power, allowing more and more applications to solve chemical problems with increasing complexity. Many times these theoretical efforts have helped or even totally enlightened some avoiding waste of chemical products saving resources and environmental aggressions. Our present work is within this idea, where we have been able to access a large number of complexes and analyze their behavior that could have been difficult to perform experimentally.

This Chapter aims at provide a general description about the theoretical basis of the methods used to perform the calculations in this thesis. Although most electronic structure methods we used are based on the Density Functional Theory, we start discussing some steps before, in order to comprehend the underlying support of this method.

2.1 The Schrödinger Equation

At the beginning of the 20th Century one of the most important breakthroughs in the history of science took place: the rising of Quantum Mechanics replacing Classical Physics in the field of atomic world. As such, it is a remarkable tool to understand chemical phenomena. Hence, one of the most important fields of Theoretical Chemistry, the Quantum Chemistry methods, are based on Quantum Mechanics and their goal is to relate the important macroscopic properties of chemical systems to their electronic structure.

The most important pillar of Quantum Mechanics is the Schrödinger Equation. Often, discussions of quantum chemistry start from this point, since after all, the goal of most of the approaches is to find, at least, an approximate solution for it. The non-relativistic time-dependent form of this is the Equation 2.1:

$$\left(-\frac{\hbar^2}{2m}\nabla^2 + V(q)\right)\psi(q,t) = i\hbar\frac{\partial}{\partial t}\psi(q,t) \tag{2.1}$$

This is a differential Equation. The left part is the Hamiltonian operator, also represented as $\widehat{H}$, that contains the kinetic and potential energy terms. In a many-particle system, like a molecule, this terms are mostly related with the position of the nuclei and electrons regarding each other.

If the potential term, $V(q)$, in the Hamiltonian does not change over the time, the wavefunction can be written as the product of the spatial part and the temporal part. The experimentally observable quantity is the probability distribution function - $|\psi(q,t)|^2$ - and the states where the probability density is constant over the time are called stationary states.

Most computational methods deal with situations where the potential can be considered time-independent and, therefore, are stationary states. In this way we can derive from Equation 2.1 the time-independent form:

$$\widehat{H}\psi(q) = E\psi(q) \tag{2.2}$$

With a given set of spatial coordinates, the solution of the time-independent Schrödinger Equation produces the wavefunction, $\psi(q)$ and gives the energy E of the stationary states of the system. However, the analytical solution of this Equation is only known for hydrogen-like systems, which demands the use of approximations.

2.1.1 The Born-Oppenheimer Approximation

An important step to solve the Schrödinger Equation is based in the large mass difference between the nuclei and the electrons. It is a good assumption that this mass difference makes the nuclear velocities much smaller than the electron velocities and the electron cloud can easily adjust to the nuclear change.

The time-independent Schrödinger Equation depends on the electronic and nuclear coordinates. The Hamiltonian $\widehat{H}$ of a molecular system can be written as Equation 2.3

$$\widehat{H} = -\frac{\hbar^2}{2}\sum_\alpha \frac{1}{m_\alpha}\nabla^2 - \frac{\hbar^2}{2m_e}\sum_i \nabla_i^2 + \sum_\alpha \sum_{\beta>\alpha} \frac{Z_\alpha Z_\beta e'^2}{r_{\alpha\beta}} - \sum_\alpha \sum_i \frac{Z_\alpha e'^2}{r_{i\alpha}} + \sum_i \sum_{i>j} \frac{e'^2}{r_{ij}} \tag{2.3}$$

where α and β refer to the nuclei and i and j are the electrons. The first term is the kinetic energy operator for the nuclei and the second is referred to the kinetic energy term of the electrons. The third is the potential energy of the nuclei repulsion and the fourth is the electronic-nuclear interaction. The last term is the potential energy due to the repulsion between the electrons.

As suggested above, if $m_\alpha \gg m_e$, the movement of electrons and nuclei can be decoupled, and the electrons can assumed to be moving in a fixed nuclei geometry. In this situation, for a given geometry, the third term of Equation 2.3, which is the nucleus-nucleus interaction, is a constant and the kinetics energy of the nucleus, in the first term, is nullified. Therefore, we can define the *electronic Hamiltonian* ($\widehat{H}_{el}$) with the remaining terms.

Schrödinger Equation can be written with the $\widehat{H}_{el}$ along with the nuclear interaction energy potential, $V_{\alpha\alpha}$, which is constant, giving Equation 2.4, where U is the potential energy including the repulsion energy of the nuclei. In this approach, energy and wavefunctions are parametrically dependent on the nuclear coordinates. This means that for a given geometry there is one energy and one wavefunction.[209]

$$(\widehat{H}_{el} + V_{\alpha\alpha})\psi_{el}(q_i, q_\alpha) = U(q_\alpha)\psi_{el}(q_i, q_\alpha) \tag{2.4}$$

In the last Equation, as nuclear interaction $V_{\alpha\alpha}$ is a constant for a given geometry, it can be dropped of the Hamiltonian giving the Equation below:

$$\widehat{H}_{el}\psi_{el} = E_{el}\psi_{el} \tag{2.5}$$

that provides the purely electronic energy (E_{el}), parametrically dependent on the nuclear coordinates. It is worth mentioning that U, also referred as the *adiabatic potential*, is a consequence of the resolution of Equation 2.4 constituted by the summation of the purely electronic energy plus the internuclear energy potential for a fixed geometry. Obviously, many different geometries can be experimented. This different interdependent positions arising from the movement of the nuclei provide the *Potential Energy Surface (PES)*, discussed properly in Section 2.3.

Regarding the wavefunction, this approximation implies that it can be treated as a separation of the nucleus wave-function and the electron wave-function:

$$\psi(q_i, q_\alpha) = \psi_{el}(q_i; q_\alpha)\psi_\alpha(q_\alpha) \tag{2.6}$$

2.1.2 Variational Principle

The terms needed for setting up the specific electronic Hamiltonian operator for a molecule are dependent on molecular geometry of the target system. What follows is to determine the eigenfunction ψ and the eigenvalue E correspondent to the Hamiltonian. Once we obtain ψ, it is possible to obtain others eigenvalues of others properties, applying the proper operator. The problem is that only for very few and trivial systems this strategy can be applied.

To solve this problem there is an approach that systematically drives to the best approximated wavefunction of a electronic state. This is the *variational principle*, which stands in a very important place for the quantum mechanics/quantum chemistry applications.

If any arbitrary wavefunction, called trial wavefunction (φ), but the real one, is considered, then we have:

$$\frac{\langle\ \varphi\ |\ \widehat{H}\ |\ \varphi\ \rangle}{\langle\ \varphi\ |\ \varphi\ \rangle} = \xi \geq E \tag{2.7}$$

This Equation states that the energy computed by $\langle\varphi|\widehat{H}|\varphi\rangle$ is an upper bound to the true energy of the ground state. To be eligible, the wavefunction should be well behaved and meet the boundary conditions, such as be continuous everywhere and quadratically integrable.[210]

The majority of machineries that look for the exact wavefunction in computational methods minimizes $\langle\varphi|\widehat{H}|\varphi\rangle$ until the $\Delta\xi$ is zero

within a pre-setted threshold, when the exact wavefunction is, then, considered as found. Although it is not the only condition to achieve the exact wavefunction, it works well for the most of the situations.

2.1.3 Hartree-Fock Method

The simplest method applying the variational principle to obtain an approximated wavefunction is the Hartree-Fock. In this case, the trial multielectronic wavefunction must be antisymmetric regarding the interchange of two electrons coordinates and the simplest approximation to accomplish that requirement is the *Slater Determinant*:

$$\Phi_{SD} = \frac{1}{\sqrt{N!}} \begin{vmatrix} \phi_1(1) & \phi_2(1) & \cdots & \phi_N(1) \\ \phi_1(2) & \phi_2(2) & \cdots & \phi_N(2) \\ \vdots & \vdots & \ddots & \vdots \\ \phi_1(N) & \phi_2(N) & \cdots & \phi_N(N) \end{vmatrix} \tag{2.8}$$

where the columns ϕ_i are the single-electron wavefunctions (*molecular orbitals*) composed by the product of a spatial orbital(χ) and a spin function (α or β), also known as spin-orbitals, while the rows are the electron coordinates.[211]

The expectation value of the Hamiltonian (H_{el}) with a Slater determinant provides the Hartree-Fock energy (E_{HF}) of the system, given by:

$$E_{HF} = \sum_{i}^{N_e} \langle \phi_i | \widehat{h}_i | \phi_i \rangle + \frac{1}{2} \sum_{ij}^{N_e} (\langle \phi_j | \widehat{J}_i | \phi_j \rangle - \langle \phi_j | \widehat{K}_i | \phi_j \rangle) \tag{2.9}$$

In this Equation $\widehat{h}_i$ is the one electron operator which gives the contribution from the kinetic energy and the electron-nucleus attraction.

$$\widehat{h}_i = -\frac{1}{2}\nabla_i^2 - \sum_{\alpha}^{N_n} \frac{Z_\alpha}{r_{i\alpha}} \tag{2.10}$$

The term $\widehat{J}_i$ is the so-called *Coulomb operator* that involves the "multiplication" of a matrix element with the same orbital on both sides and represents the classical repulsion between charges, while $\widehat{K}_i$ the *Exchange operator* "exchanges" the two functions on the right hand side of the $\frac{1}{r_{ij}}$ operator. The latter has no physical analogy and arises

from the antisymmetric character from the Slater determinant.[211] The two last terms of Equation 2.9 represents an average potential felt by each electron due to the rest of the electrons.

$$\widehat{J}_i|\phi_j(2)\rangle = \langle\phi_i(1)|\frac{1}{r_{ij}}|\phi_i(1)\rangle|\phi_j(2)\rangle \tag{2.11}$$

$$\widehat{K}_i|\phi_j(2)\rangle = \langle\phi_i(1)|\frac{1}{r_{ij}}|\phi_j(1)\rangle|\phi_i(2)\rangle \tag{2.12}$$

The task now is to find the best set of spin-orbitals that make the energy a minimum through the variational principle. The variation of the trial wavefunction composed by those spin-orbitals, however, shall maintain them orthogonal and normalized, condition that can be handled by using the *Lagrange multipliers*. This gives the *Hartree-Fock equation* 2.13,

$$\widehat{F}_i\phi_i = \varepsilon_i\phi_i \tag{2.13}$$

where F_i is the *Fock operator*:

$$\widehat{F}_i = \widehat{h}_i + \sum_{j}^{N_e}(\widehat{J}_j - \widehat{K}_j) \tag{2.14}$$

The Hartree-Fock equation is a pseudo-eigenvalue equation as the Fock operator needs all the spin-orbitals to define the Coulomb and Exchange operators. Because of this restriction, a procedure based on the variational principle, the so-called *Self-Consistent Field* (SCF) method is used. This method works iteratively: first, a guessed set of spin-orbitals forms the initial trial wavefunction, after the Fock operator is constructed, and then the Hartree-Fock equations are solved, providing a second set of spin-orbitals, that are used in the next iteration. This process runs until the the convergence of the energy and the wavefunction.[212]

Restricted and Unrestricted Hartree-Fock

In the building of the Slater determinant each electron occupies a different spin-orbital. Those spin-orbitals are expressed as the product of a spatial orbital and a spin function (α and β). In the case of the *closed-shell* systems, the same spatial orbital is used to describe two electrons with different spin functions, implying doubly occupancies of the spatial orbital. This procedure is called Restricted Hartree-Fock

(RHF). This solution is very useful because the vast majority of the ground state species are those with a paired even number of electrons, which gives, overall, a singlet electronic state.

For *open-shell* systems, two different treatment are possible: one of them is the Unrestricted Hartree-Fock (UHF), where different orbitals are used for electrons with different spin functions. Here, all the spatial orbitals (χ) are mono-occupied. The other method is the Restricted Open-Shell Hartree-Fock, where the closed-shell are described by doubly occupied orbitals and the open-shells by mono-occupied orbitals. These open-shell procedures can be applied to systems with an odd numbers of electrons or, even so, to that ones with even number of electrons, but with open-shells behaviour, such as the triplet ground states of many molecules.

One problem of the UHF technique is that the Slater determinant does not describe an eigenfunction of the total spin operator $\widehat{S}_2$. The more the expectation value of the total spin operator $\langle \widehat{S}_2 \rangle$ of a Slater determinant deviates from the correct value, more the unrestricted determinant is contaminated by functions related to states of higher spin multiplicities and has less physical meaning.[210]

2.1.4 Basis set

In the Hartree-Fock method the wavefunction is described by the Slater determinant, which is a combination of molecular orbitals. A covenient way to construct those wavefunctions to be easily optimized is expand each spatial orbital (χ_i) as a linear combination of basis functions (φ_a), which are called atomic orbitals. This is the *Linear Combination of Atomic Orbitals (LCAO)*.[211]

$$\chi_i = \sum_{a=1}^{k} c_{ai}\varphi_a \tag{2.15}$$

where the c_{ai} are yet unknown coefficients. From a set of basis functions we can obtain linearly independent wavefunctions, and the problem lies on calculating the coefficients.

In principle, the use of a complete set of basis functions would represent exactly the single-electron wavefunctions. However, a complete basis set means that an infinite number of functions must be used, which is impossible in actual calculations. Then, a finite number of ba-

sis set is usually applied, obviously at the price of the incompleteness of the basis, leading to the *basis-set truncation error.*[213]

There are two types of basis functions often used in electronic calculations: *Slater Type Orbitals (STO)* and *Gaussian Type Orbitals (GTO)*. The Slater type orbitals have the functional form below:

$$\varphi(r,\theta,\eta) = NY_{l,m}(\theta,\eta)r^{n-l}e^{-\zeta r} \tag{2.16}$$

However, resolution of the bielectronic integrals is easier using Gaussian functions(GTOs):

$$\varphi(r,\theta,\eta) = NY_{l,m}(\theta,\eta)r^{2n-2-l}e^{-\zeta r^2} \tag{2.17}$$

Despite GTOs being better than STOs regarding the computational solution, they have some disadvantages, such as give a poor representation of the atomic nuclei. To alleviate the problem, several GTOs are often grouped together to form what are known as *contracted Gaussian functions* (Equation 2.18).

$$\theta_j = \sum_i d_{ji} g_i \tag{2.18}$$

In particular, each contracted Gaussian (θ_j) is taken to be a fixed linear combination of the *primitive Gaussian functions* (g) centred on the same atomic nucleus. The spatial orbitals (χ_i) are then expressed as a linear combination of contracted Gaussians, similar to Equation 2.15.

The smallest number of basis functions corresponds to the so-called *minimal basis set* in which one function is used to represent each orbital. An improvement is to use two basis functions to describe each orbital: the *double zeta (DZ)*. The next up is the *triple zeta (TZ)* with three functions per orbital.

Obviously, the use of a large basis set increases the computational cost. As usually the chemistry takes place with the electrons of the valence shell, and thus, those are the ones that should be better treated. In a *split-valence basis set* the valence orbitals are described with more orbitals than the inner orbitals.

Sometimes the orbitals during a chemical process become distorted (polarized) and can be described more properly if basis functions representing orbitals with higher angular momentum are included. Those are the *polarization basis* functions.

Anions, highly excited electronic states and molecular complexes tend to be much more spatially diffuse than regular orbitals. When a basis set does not have the flexibility necessary to allow a weakly bound electron to localize far from the remaining density, standard basis sets are often augmented with *diffuse basis* functions.

One of the most used types of basis set was developed by Pople and co-workers. In this model, the minimal basis set is *STO-nG*. STO-3G basis is a widely used minimum basis. Pople's split-valence double-ζ basis set is called **6-31+G(d)**; the core orbital is a contracted Gaussian function made of 6 primitives, and the valence is described by two orbitals: one contracted made of 3 primitives and one single primitive. It has also one set of diffuse sp-functions on heavy atoms only and a single d-type polarization function on heavy atoms.

6-311++G(d,p) is a triple-ζ split-valence basis, where the core orbitals are described by one function that are a contraction of six primitives and the valence orbital are described by three functions, represented by three, one and one primitives, respectively. Furthermore, the basis set is augmented with a set of diffuse s- and p-functions on heavy atoms, and a diffuse s-function on hydrogen. Finally, a polarization d-function is added on heavy atoms and one p-function on hydrogen atoms.

Effective Core Potential

When elements from the lower part of the periodic table are part of the system, there will be a large number of core electrons that demands basis functions to be described. Those electrons in the core of the atoms are less relevant for chemical interests, such as reactivity or bonding analysis, not consider them can impoverish the description of the valence electrons, due to a poor calculation of the electron-electron interactions. Furthermore, an implicit description of relativistic effects, essentially arising in the core region, is routinely necessary, so that a formally non-relativistic Hamiltonian can be used in valence-only calculations, even for heavy-atom compounds.

These two problems can be avoided at once by modelling the core electrons with an appropriate function and treating the valence electrons explicitly. This function is the *Effective Core Potential-ECP*. In this work we do calculations of some ruthenium complexes that are treated with this procedure.

2.1.5 Electron Correlation

In the Hartree-Fock method, the real electron-electron interaction is replaced by an average interaction generated by a mean field of the rest of the electrons. Therefore, even enlarging the basis set to infinite, the real energy can not be achieved. The energy difference between the Hartree-Fock limit and the exact energy is called *correlation energy* and, although it accounts only for a small amount of the total energy, it is fundamental for discussing properly many systems and properties.

This energy is usually split in two components: the *dynamical correlation* caused by not taking into account the instantaneous relative movement of the electrons. The second component, the *static correlation*, is due to the monodeterminatal nature of the Hartree-Fock method, which can not give a good description the electronic state in cases where exist another Slater determinant with similar energy than the ground state.[210]

Find a method to solve the electron correlation problem was, and still is, one of the main goals of computational quantum chemistry. A large variety of schemes have been developed in the scope of *ab initio* methods: they are the so-called *post*-Hartree-Fock methods. Among these methods, the most important ones are the Configuration Interaction, that is based on the variational method, the Many Body Perturbation Theory and the Coupled Cluster method.

The principal advantage of this methods is that they allow a systematic improvement of the accuracy of the computational results. However, they are, generally, highly computationally demanding and this make them not suitable for large systems.

Because we have not used those methods in this work, we are not discussing their formalism any further. Instead, in the next sections, we describe another method to take into account the correlation energy.

2.2 Density Functional Theory

An alternative to wavefunctions based methods are the density functional methods. Those methods are based on the Density Functional Theory (DFT). Their success is due to the calculation of the electronic properties from the density instead of the wavefunctions. They are cheaper because while a wavefunction for n electrons has $4n$ variables, which are the three spatial variables plus the spin one, the

density electron density has only three spatial variables, regardless of the complexity of the molecule. Hence, these methods allow the study of medium to large size systems introducing the correlation energy at more affordable computational cost.

The electron density is the central entity in DFT. It is defined as the integral over the spin coordinates of all electrons and over all, but one of the spatial variables, as in the Equation:

$$\rho(\vec{r}) = N \int ... \int |\Psi(\vec{x}_1, \vec{x}_2, ..., \vec{x}_N|^2 ds_1 d\vec{x}_2 \vec{x}_N \tag{2.19}$$

$\rho(\vec{r})$ determines the probability of finding any of the N electrons within the volume element $d\vec{r}_1$ with an arbitrary spin, while the other N-1 electrons have arbitrary positions and spin, commonly known as electron density.[210]

It is easy to see that $\rho(\vec{r})$ is a non negative function of three spatial variables which vanishes at infinity ($\rho(\vec{r} \to \infty) = 0$) and integrates to the total number of electrons ($\int \rho(\vec{r}) d\vec{r}_1 = N$). Unlike the wave-function, which itself has no physical meaning, the electron density can be measured experimentally.

2.2.1 Hohenberg-Kohn Theorems

The nowadays DFT was born in 1964 when Hohenberg and Kohn provided[214] the needed foundations of DFT through two theorems. Within the Born-Oppenheimer approximation the nuclear positions are constant and we have the following Hamiltonian:

$$\widehat{H} = -\frac{\hbar^2}{2m_e} \sum_i \nabla_i^2 - \sum_\alpha \sum_i \frac{Z_\alpha e'^2}{r_{i\alpha}} + \sum_i \sum_{i>j} \frac{e'^2}{r_{ij}} \tag{2.20}$$

The second term is the potential energy of interaction between the electrons and the nuclei and depends on the coordinates of the nuclei, which are fixed. In DFT this quantity is called the external potential(V_{ext}).[209]

Quoting directly from the Hohenberg-Kohn paper,[214] this first theorem state that *"the external potential ($V_{ext}(\vec{r})$ is (to within a constant) a unique functional of $\rho(\vec{r})$; since, in turn $V_{ext}(\vec{r})$ fixes $\widehat{H}$ we see that the full many particle ground state is a unique functional of $\rho(\vec{r})$"*. This is the existence theorem. They demonstrated, via *reductio*

ad absurdum, that two diferrent V_{ext} cannot be determined by only one non-degenerate electron density, which is equal to say that the ground state electron density univocally generates the V_{ext}, and thereby the Hamiltonian and thus the wavefunction.[215]

The first theorem states the existence of the electron density, but says nothing about the form of this electron density. The second theorem of Hohemberg-Khon is the variational principle that provides a approach to achive the exact density. It is analogous to that in wavefunction based variation method (see Equation 2.7). Given an approximated electron density (ρ') that integrates the number of electrons, the energy derived from this density is an upper bound to the exact ground state energy, provided by the exact electron density.[211]

$$E_0(\rho') \geq E_0(\rho) \tag{2.21}$$

2.2.2 Kohn-Sham Methodology

Althoug the Hohemberg-Kohn theorems states us that is possible to find the properties from the electronic density, it does not show any form to calculate the energy from this density or even how to find the electronic density without finding the wavefunction in the first place. In this way, a breakthrough step for establishing the DFT as a functional theory was provided by the introduction of the Kohn-Sham equations.[216]

Khon-Shan approach is aimed at determining with good accuracy the major part of the kinetic energy by considering a fictitious reference system of n non-interacting electrons. This system is described by a set of orbitals ϕ_i that experiences the same external potential, in such a way as to make the ground state electron probability density of the reference system - $\rho_S(r)$ - equal to the exact ground state electron density of the molecule we are interested in -$\rho(r)$. Those orbitals of this system are given by the Kohn-Sham equations 2.22:

$$h^{KS}\phi_i = \varepsilon_i\phi_i \tag{2.22}$$

where h^{KS} is the Kohn-Sham Hamiltonian, which is going to be described later, and ϕ_i are the molecular orbital.

This is a similar approach to the Hartree-Fock theory, where the orbitals are described as spatial one-electron orbitals, which form the wavefunction of the reference system as an antysimmetrized product

of these orbitals, like the Slater determinant.[215] These orbitals are the denominated Kohn-Sham orbitals and with them we can yield the electron density:

$$\rho(r) = \sum_{i=1}^{N} \mid \phi_i(r) \mid^2 \tag{2.23}$$

The exact ground state electronic energy of the real system can be put as follows:

$$E(\rho) = T_s(\rho) + V_{\alpha e}(\rho) + J(\rho) + E_{XC}(\rho) \tag{2.24}$$

The first term is the kinetic energy of the non-interacting electron gas, calculated by Equation 2.25. This energy differs only slightly from the kinetic energy of the real system, but significantly improves the DFT energy value over Hartree-Fock one, being an important advantage of this method. In the second term is the nuclear-electron interaction, also referred as external potential, whose energy is determined by the Equation 2.26. The classical Coulomb electron-electron repulsion is the third term and its energy is given by the Equation 2.27.

$$T_s(\rho) = \sum_{i=1}^{N} \langle \phi_i(r) | -\frac{1}{2}\nabla^2 | \phi_i(r) \rangle \tag{2.25}$$

$$V_{ne}(\rho) = -\sum_{\alpha}^{M} \int \frac{Z_\alpha}{r_{1\alpha}} \rho(r_i) dr_i \tag{2.26}$$

$$V_{ee}(\rho) = \frac{1}{2} \int \int \frac{\rho(r_i)\rho(r_j)}{r_{ij}} dr_i dr_j \tag{2.27}$$

Still about the Equation 2.24, $E_{XC}(\rho(r))$ is the so-called exchange-correlation energy, which is the only one that has no explicit form. It includes all terms that remains unknown within the Kohn-Sham approach, and is defined by Equation 2.28

$$E_{XC}(\rho) = [T_0(\rho) - T_S(\rho)] + [E_{ee}(\rho) - J(\rho)] \tag{2.28}$$

where the first bracket counts for the residual part of the real true kinetic energy, $T_0(\rho)$, that is not covered by $T_S(\rho)$. The second part regards the non-classical electrostatic contributions corresponding to the difference between the real electron-electron interaction potential

and that of the reference system. This functional embraces also the correction for the classical self-interaction energy.

The Hamiltonian, or the Kohn-Sham one-electron operator, of the Equation 2.22 can be stated as

$$h^{KS} = -\frac{1}{2}\nabla^2 - \sum_{\alpha}^{M} \frac{Z_\alpha}{r_{1\alpha}} + \int \frac{\rho(r_j)}{r_{ij}} dr_j + V_{XC} \tag{2.29}$$

where the term V_{XC} is the potential due to the exchange-correlation energy. Because this energy is not known, also the explicit form for the corresponding potential is ignored, then it is simply defined as the functional derivative of E_{XC} with respect to the electronic density:

$$V_{XC} = \frac{\delta E_{XC}}{\delta \rho} \tag{2.30}$$

If E_{XC} is known, then V_{XC} can be obtained, and the Kohn-Sham strategy would lead to the exact energy.

The machinery of the Kohn-Sham scheme operates iteratively as in the flow of the figure Figure 2.1. To begin with, an electronic density is guessed, typically using a superposition of atomic densities. Using some approximated form for the exchange-correlation functional we can find the exchange-correlation potential and with that, it is possible to construct the Khon-Sham one-electron operator as well. The Kohn-Sham equations are, then, solved to obtain the Kohn-Sham orbitals, which are used to compute a new improved density, presumably. This process is repeated until the density and the exchange-correlation energy have converged within a threshold. Then the electronic energy is calculated by means of Equation 2.24.

The open-shell systems can also be treated by unrestricted DFT in a similar way as in UHF (section 2.1.3), but in this case the Slater determinant is constructed from the Kohn-Sham orbitals. Noteworthy for the unrestricted DFT, the spin-contamination is usually less significant, since the exchange-correlation functionals shows a local nature as opposed to the non-local Hartree-Fock exchange.[210]

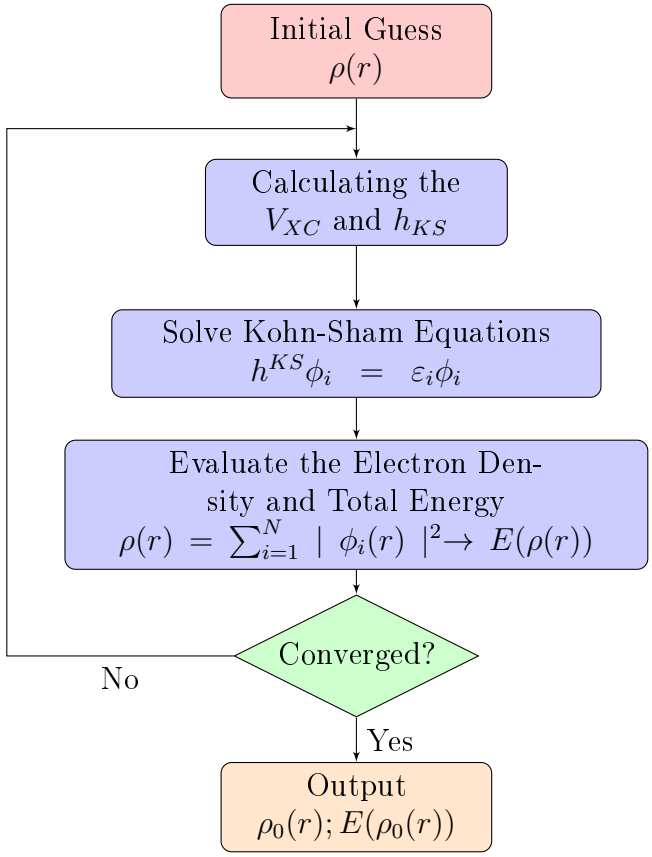

Figure 2.1: Flow of the Kohn-Sham method.

2.2.3 Exchange-Correlation Functionals

The Kohn-Sham formalism allows an exact treatment of the system if the E_{XC} is obtained. Unfortunately, E_{XC} remains unknown and the different functionals existing in the literature differ on how this unknown term is defined. Those are the exchange-correlation functionals - XC functionals. In many of these approaches is common to split the functionals in two parts: the exchange (E_X) and the correlation (E_C) terms. These two terms are themselves also functionals of the electron density and the corresponding functionals are known as exchange functionals and correlation functional, respectively.

$$E_{XC}(\rho) = E_X(\rho) + E_C(\rho) \tag{2.31}$$

There is no a sistematic way to improve the DFT method as it can be done in the post-HF methods. Enhance those DFT functionals

usually means splitting them in more terms, with some of these terms fitting to experimental values. Perdew[217,218] compares the enhancement of the density functionals to climb Jacob's ladder, leading the way from the Hartree world to the heaven of chemical accuracy, illustrated in Figure 2.2. Each rung of the ladder adds a refinement to the approximation of the exchange-correlation energy. This is an analogy about a biblical excerpt where Jacob had a dream about a stair from the earth to the heaven*.

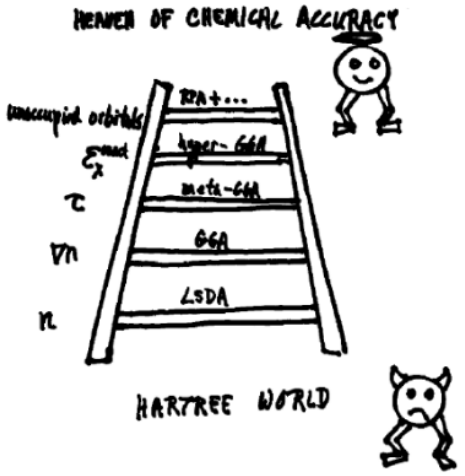

(a) Jacob's ladder of density functionals ascending to chemical accuracy.[217]

(b) Jacob's Dream by Gustave Dore

Figure 2.2: "Jacob's Ladder" proposed by Perdew

The first rung is the **Local Density Approximation** that is based on the idea of a hypothetical uniform electron gas, in such a way that the density varies slowly. The advantage of this approximation is that of the exchange functional is known, which is expressed by Equation 2.32, often called Slater exchange.

$$E_X^{LDA}(\rho) = -\frac{3}{4}\left(\frac{3}{\pi}\right)^{1/3}\int \rho^{4/3}(r)dr \tag{2.32}$$

Although the analytical form for the correlation functional part is not

* *"And he dreamed and behold a ladder resting on the earth, with its top reaching to heaven, and the angels of God were ascending and descending on it."* (Genesis 28:12)

known, Monte Carlo simulations and sophisticated interpolations allowed many authors to present expressions for the correlation functional. One of the most famous was developed by Vosko, Wilk and Nussair.[219]

In the more general case, where the α and β densities are not the same, LDA is replaced by the **Local Spin Density Approximation** which is composed by the sum of the individual spin densities:

$$E_X^{LSDA}(\rho) = -2^{1/3}\frac{3}{4}\left(\frac{3}{\pi}\right)^{1/3}\int(\rho_\alpha^{4/3}+\rho_\beta^{4/3})dr \qquad (2.33)$$

LDA performs reasonably well for metallic systems, but it presents important limitations when treating molecules as their electron density is typically far from being spatially uniform. So there is good reason to believe that the LDA approach can show limitations. An improvement can be obtained considering the changes of the density along the system. In this way, the next step climbing the Jacob's ladder can be achieved by considering the gradient of the density. In the **Generalized Gradient Methods** the first derivative of the density is included as a variable. One of the earliest and most common functionals was proposed by Beck (B88)[220] as a correction to the LDA exchange functional:

$$E_X^{B88}(\rho) = E_X^{LDA}(\rho) - \beta\sum_\sigma\int\rho_\sigma^{4/3}\frac{x_\sigma^2}{1+6\beta x_\sigma sinh^{-1}x_\sigma}dr \qquad (2.34)$$

where $x = \dfrac{|\nabla\rho|}{(\rho)^{4/3}}$ and β=0.0042 is an empirical parameter that was determined by fitting known Hartree-Fock exchange energies of several atoms. OPTX is another exchange functional that was proposed by Handy and Cohen:

$$E_X^{OPTX}(\rho) = a_1E_X^{LDA}(\rho) - a_2\sum_\sigma\int\frac{\rho^{4/3}(\gamma x_\sigma^2)^2}{(1+\gamma x_\sigma^2)^2}dr \qquad (2.35)$$

with the parameters a_1= 1.05151, a_2=1.43169 and γ =0.006 determined by fitting to the unrestricted HF energies of first and second-row atoms.[221,222]

Similarly, there have been many GGA correlation functional, most of them with intimidating forms. A popular one was proposed by

Lee, Yang and Parr (LYP).[223] The LYP correlation functional is often combined with the B88 or OPTX exchange functional to produce the BLYP and OLYP acronyms.[211]

Still within the GGA approach, Perdew, Burke and Ernzerhof have proposed an exchange and correlation functional (PBE) that is an enhancement Taylor-like expansion based on gradient corrections of the LDA exchange functionals. Likewise, the correlation functional is written as an enhancement factor added to the LSDA functional.[211,224] The OPBE functional uses the GGA parts of Handy and Cohen's OPTX exchange functional with the PBE correlation functional.[225,226]

A logical improvement to achieve the next rung is allow the exchange and correlation functionals to depend on higher order derivatives of the electron density, with the Laplacian ($\nabla^2\rho$) being the second-order term. As alternative, the functional can be taken to depend on the orbital kinetic energy density τ, according to the following Equation:

$$\tau = \frac{1}{2}\sum_{i}^{occ} \mid \nabla\phi_i(r) \mid^2 \tag{2.36}$$

The inclusion of these terms heads to this third rung, the so-called **meta-GGA** functionals. The TPSS(Tao–Perdew–Staroverov–Scuseria) exchange–correlation functional is non-empirical and can be considered as the next improvement over the PBE functional.[227]

The Adiabatic Connection Formula provides a link between a fictitious reference system with non-interacting electrons and the the actual fully interacting system. If is assumable that the wave function of the non-interacting system is a Slater determinant composed of KS orbitals, the exchange energy is exactly that given by Hartree–Fock theory, calculated by HF wave mechanics methods, which is the exact exchange energy.[211] Within this approximation, some models that includes in the formula the exact exchange are often denoted **hybrid** methods or **hiper-GGA**. One of the most popular DFT functional belongs to this kind: B3LYP.

$$E_{XC}^{B3LYP} = (1-a_o)E_X^{LSDA} + a_o E_X^{exact} + a_x \Delta E_X^{B88} + a_c E_C^{LYP} + (1-a_c)E_C^{VMW} \tag{2.37}$$

The a_o, a_x and a_c parameters are determined by fitting to experimental data and depend on the chosen forms for E_X GGA and E_C GGA, with

typical values being a_o around 0.2, a_x close to 0.7 and a_c close to 0.8.[228,229]

Likewise, for instance, the TPSS functional has been augmented with 1/10 ($a = 0.1$) of exact exchange to give the popular TPSSh method.[230]

$$E_{XC}^{TPSSh} = aE_X^{exact}(1-a)E_X^{TPSS} + E_C^{TPSS} \tag{2.38}$$

In the higher levels of Jacob's ladder, not only the occupied orbitals are employed in the calculation, but also the virtuals are used. Although inclusion of the virtual orbitals is expected to improve the results in areas that usually are a problem for the others functionals, such as dispersion, for instance, on which very little work have been done.[211]

2.2.4 Dispersion Correction

It has been known for a while that commonly used density functional methods do not describe the long-range dispersion interactions, like Van der Waals. Dispersion energies are due to phenomena that can be considered as instantaneous electron correlations processes, like, for instance, dipole moments that have its origin in 'charge fluctuations'. These phenomena are better described by methods that provide 'true' wave-function, which is not the case of DFT.[231]

A solution to this quest was assiduously developed by Grimme and co-workers.[231] The idea is to treat the (quantum mechanically) difficult dispersion interactions semi-classically and to combine the resulting potential with a quantum chemical approach. This can be said as a kind of quantum mechanical–molecular mechanical hybrid scheme. It is usually termed DFT-D.

The DFT-D2[232] variant takes the following explicit form:

$$\begin{aligned} E_{disp}^{D2} &= -S_6 \sum_{i,j>i} \frac{C_6^{ij}}{(R_{ij})^6} f_{dmp}(R_{ij}) \\ f_{dmp}(R_{ij}) &= \frac{1}{1+e^{-\alpha_6(R_{ij}/RvdW-1)}} \end{aligned} \tag{2.39}$$

Here, dispersion coefficients, C_6^{ij}, obtained from the geometric mean of tabulated elemental values, are summed over interatomic distances,

R_{ij}, modulated by a damping function, $f_{dmp}(R_{ij})$, that gradually activates the dispersion correction (at a rate characterized by α_6) over a distance characterized by the sum of the two atomic vdW radii, R_{vdW}, while an scaling factor, S_6, is optimized to be unique to adjust the repulsive behaviour of each E_{XC} functional.

2.3 Potential Energy Surface Exploration

The main part of this thesis is based in calculations to explore the Potential Energy Surfaces of the specific paths related to the reactivity of olefins with iron-carbenes. An exploration of a PES is based on the concept of the Born-Oppenheimer approximation, discussed on the Section 2.1.1: there, nuclei are fixed and the Schrödinger Equation is solved for this static electric potential arising from the nuclei in that particular arrangement. Then, different arrangements of nuclei may be adopted and the calculation repeated. The set of solutions so obtained composes the Potential Energy Surface (PES) of a polyatomic species.[213] The PES is a hypersurface defined by the potential energy of a collection of atoms over all possible atomic arrangements. It has 3N-6 dimensional coordinates, where N(number of atoms)$\geq$3.[215] Figure 2.3 is a schematic representation of a hypothetical hyperdimensional PES of a given system.

A particularly interesting matter in a PES are the stationary points. Those are the points where all the forces vanish - $\left(-\frac{\partial E}{\partial q_i} = 0\right)$- q_i is an arbitrary nuclear coordinate. In the Figure Figure 2.3, the points labelled with a,b,c and d are stationary, but they are not of the same kind. To distinguish the types of stationary points, it is necessary to consider the second derivatives of the energy with respect to the nuclear coordinates.

Second derivatives quantities $-\frac{\partial^2 E}{\partial q_i q_j}$ comprise the Hessian matrix. A minimum of a potential energy surface corresponds to all positive second derivative (points **a** and **b**). A maximum of a potential energy surface is characterized by the eigenvalues of the Hessian matrix all being negative(d). The minimum with the lowest value is called the global minimum (**b**) , while all the others are local minima (**a**).

First-order saddle points are characterized by one negative eigenvalue, whereas all the others are positive - points **c**. They are associ-

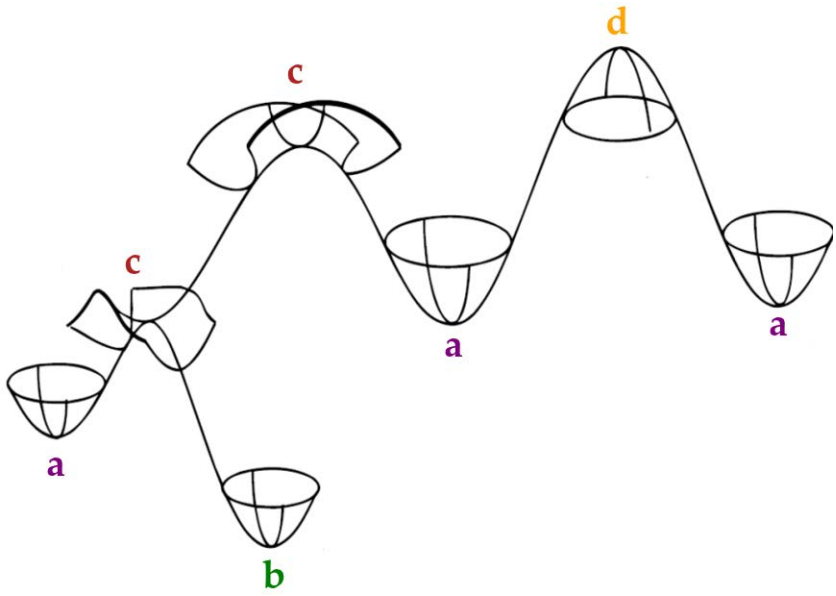

Figure 2.3: Hyperdimensional PES of an hypothetical system.

ated with the chemical concept of transition state that is the minimum energy that has to be overcome in order to go from a minimum to another. The minima in this case can represent, for instance, reactants, products or intermediates of a given reaction.[213]

The procedures to find the stationary points in the PES are called *geometry optimization*. Energy minimization optimization looks for the minima in the PES. Optimized structures are useful because often correspond to a substance as it is found in nature. On the other hand, one might desire optimize to a transition state in order to gain understanding about the mechanism of a reaction. In a general form, optimized geometries can be found by computing all the forces at a given molecular geometry and check if they vanish. If they do not, the geometry is varied, using an appropriated algorithm, until one is found that can be considered as corresponding to zero forces which is a gradient vector of zero length.[213]

2.3.1 Multiple-State Reactivity

Many chemical reactions of systems containing unpaired electrons can involve changes in the total spin of the system. This is called *Multiple-States Reactivity*. Such a reaction is referred as spin-

forbidden, since that in the absence of spin-orbit coupling, hopping from a potential energy surface of one spin to another of different spin is "forbidden" and does not happen. They are particularly common in the chemistry of compounds containing transition metals, especially those from the middle of the first transition series, such as iron or manganese, though they can also occur for species with unpaired electrons located on many other types of atom.[99,233,234]

An approach that describe spin-forbidden reactions is based on the properties of a much more limited number of points on the potential energy surfaces. The idea is to locate the regions in which the different potential energy surfaces cross one another, and more specifically to find minima on the crossing hypersurfaces: so-called minimum energy crossing points or MECPs.[235]

One of the most used methods in the literature to locate MECPs was proposed by Jeremy N. Harvey and co-workers[236] using gradients and energies at the same level of theory. The energies E_i on the two PESs and corresponding energy gradients $\partial E_i/\partial q$ with respect to the nuclear coordinates q are combined to yield two effective gradients, $\boldsymbol{f}$ and $\boldsymbol{g}$:

$$\begin{aligned} \boldsymbol{f} &= (E_i - E_2)\left[\left(\frac{\partial E_1}{\partial q}\right) - \left(\frac{\partial E_1}{\partial q}\right)\right] = (E_i - E_2)x_1 \\ \boldsymbol{g} &= \left(\frac{\partial E_1}{\partial q}\right) - \frac{x_1}{|x_1|}\left[\left(\frac{\partial E_1}{\partial q}\right).\frac{x_1}{|x_1|}\right] \end{aligned} \tag{2.40}$$

These vectors $\boldsymbol{f}$ and $\boldsymbol{g}$ are orthogonal, and go to zero at the MECP, where the energy gradients on the two surfaces are parallel. Around the MECP, $\boldsymbol{f}$ is orthogonal to the crossing hyperline, whereas $\boldsymbol{g}$ is parallel to the hyperline and points towards the minimum.

2.3.2 Thermodynamic Properties

So far, we have shown methods to calculate the energy of an individual atom or molecule. Nevertheless, the majority of chemical research does not concern individual molecules, but instead macroscopic quantities of matter that are made up of enormous number of molecules. The behavior of such aggregates of molecules are governed

by the laws of thermodynamics and most of the chemical properties and reactions are defined regarding some of the fundamental thermodynamics quantities.[215]

The connection between the microscopic energy obtained from electronic calculations and the macroscopic values that can be measured in the laboratory is provided by *statistical thermodynamics*, by formulations used to obtain zero-point energy, entropy, free energy, enthalpy and so on. The fundamental function that characterizes statistical thermodynamics is the *partition function*. Using the canonical ensemble- which is for a constant number of particles N, volume V, and temperature T- it is written as:

$$Q(N,V,T) = \sum_i e^{-E_i(N,V)/k_BT} \tag{2.41}$$

where i runs over all possible energy states of the system with energy E_i and k_B is the Boltzman's constant. For the canonical ensemble and using established thermodynamics definitions, the following is true:

$$\begin{aligned} U &= k_BT^2 \left(\frac{\partial lnQ}{\partial T}\right)_{N,V} \\ H &= U + PV \\ S &= k_BlnQ + k_BT \left(\frac{\partial lnQ}{\partial T}\right)_{N,V} \\ G &= H - TS \end{aligned} \tag{2.42}$$

The energy of the partition function E_i can be written as the sum of terms: the translational, rotational, electronic and vibrational energy. Handling the ideal gas and rigid-rotor approximation is possible determine the two first terms. Electronic energy is obtained with regular electronic calculations. Finally, the vibrational energy, can be provided through a vibrational frequency calculation using the harmonic oscillator approximation, in terms of the reduced mass and force constants, which are the same second derivatives of the energy with respect to the coordinates, $\left(-\frac{\partial^2 E}{\partial q_i q_j}\right)$. So, the frequency calculation provides the Hessian that gives information about the nature of the stationary points on the PES and also contributes for the calculation of

the thermodynamic properties. In practice it is fairly straightforward to convert the potential energy determined from an electronic structure calculation into thermodynamic data - all that is required is an optimized structure with its associated vibrational frequencies.[211,215]

Based on the *transition state theory*, the macroscopic rate constant can be expressed as in Equation 2.43

$$k_{rate} = \frac{kT}{h} e^{-\Delta G^{\ddagger}/RT}$$
$$\Delta G^{\ddagger} = \Delta G_{TS} - \Delta G_{reactant} \tag{2.43}$$

$\Delta G^{\ddagger}$ is the Gibbs free energy difference between the TS and the reactant and k is Boltzmann's constant. This equation allows to address the kinetics of the reaction that, together with the thermodynamic properties of the systems, can be very useful in the understanding the feasibility of a given processes.

2.4 Computational Details

We are going to present in this thesis a computational strategy based on density functional theory, to explore the potential energy surface of metal carbenes interacting with olefins as we have presented in our Goals, in the end of Background: Chapter 3 is dedicated to understand their different reactivity, while in Chapters 4 and 5 we discuss how different ancillary ligands tunes such reactivity in favour of olefin metathesis. Because the computational details we use are basically the same in the three Chapters of results, we decide present them at once.

In the methodology of that computational strategy, all structures were performed with the OPBE density functional.[221,222,224] Geometry optimizations were done in gas phase without any geometrical constraint. Main group elements were represented with the valence double-plus polarization 6-31G(d,p)[237,238] basis set. For iron and cobalt were treated with the Wachters-Hay valence triple-plus polarization basis set enlarged with diffuse functions, 6-311+G(d,p).[238,239] For ruthenium, the small-core quasi-relativistic Stuttgart/Dresden effective core potential was used, which replaces the 28 inner electrons by a non-local effective potential. The remaining electrons were described with the associated (8s7p6d)/[6s5p3d] basis set.[240]

Frequency calculations were done to ensure the nature of the stationary points in the potential energy surface: whether they were minima (absence of imaginary frequencies) or transition states (possessing one imaginary frequency). Connectivity of the transition states to the correspondent minima was confirmed by Intrinsic Reaction Coordinate (IRC) calculations. These calculations also provide the thermal corrections, whose the free-energy corrections were obtained at 298.15 K and 1 atm.

Afterwards, in order to refine the energies, single point calculations were done with the same functional OPBE and a large basis set 6-311++G(d,p)[238,241] for all atoms of the systems, except for ruthenium atoms, which were again treated with the SDD pseudopotential. These calculations were executed with Gaussian 09 suite of programs.[242]

Calculations for open-shell systems were carried out considering the spin-unrestricted formalism. Moreover, for all pre-catalyst carbene species complexes with a singlet ground state, we performed unrestricted calculations to also explore the possible existence of a more stable open-shell singlet state. However, in all cases, the optimization collapsed to the closed shell solution. The nature of all stationary points was verified by vibrational analysis, ensuring that all frequencies are real for minima and that transition structures only present one imaginary frequency. All calculations described so far were performed with Gaussian 09 package.[242]

Grimme's correction for dispersion forces were evaluated at the optimized geometry using the S_6 scaling factor of OPBE functional (0.75),[232] calculated with Moldraw visualization code.?? All reported values along the text are based on the total energy obtained with the larger basis, summed with Free Gibbs Energies thermal corrections aforementioned obtained at 298.15 K and 1 atm with the smallest basis set, and the Grimme's corrections.

Minimum energy crossing points were calculated using a code developed by J. N. Harvey and co-workers,[236] which acts as a wrappen program working with Gaussian 09. Thermal corrections to the MECP structures were obtained by performing frequency calculations (*freq = projected* keyword in Gaussian 09) for the two states and taking the average values of the corrections. This protocol was proposed by Maseras and co-workers.[243]

In the beginning of 3, aiming at analyzing the structure of the metal carbenes, orbital localization based on maximally localized Wan-

nier functions,[244,245] was done with the CP2K code.[246,247] The Quickstep algorithm was used to solve the electronic structure problem based on DFT calculations using the PBE exchange correlation functional,[224] where only valence electrons were included in the calculations, representing the valence-core interactions by means of the GTH-type pseudopotentials.[248,249] A double-zeta plus polarization (DZVP) basis set was used to represent the orbitals and plane waves (up to 300 Ry) for the electron density. Wave function optimization was achieved through an orbital transformation method.[250] The results of these calculations are discussed in terms of the centroids of the localized orbitals, as suggested by Lledós and Vidossich,[251] authors of an extensive work where this approach is applied to understand chemical bonding in organometallics systems.

2.4.1 The level of theory

The OPBE density functional[225,226] has been proposed as one of the best functional to properly describe spin states of iron complexes specially in formal iron(II)species: Swart and co-workers demonstrated that this functional reproduce the S=2 spin state of classical well stabilised $Fe(H_2O)_6^{2+}$ and $Fe(NH_3)_6^{2+}$ complexes.[252] Corroborating this paper, works of benchmarking with different functional for calculate spin state of many kinds of iron complexes, have pointed OPBE as a good choice.[253,254] OPBE also has been used to study reactivity[97,255–257] and spin-crossover[258] of iron compounds. Even so, we decide test the chosen DFT functional to analyze the spin state for three the most recurrent iron carbenes in the literature, which we have introduced in Section 1.5. These complexes, bearing the methylene carbene, are defined in the Scheme 2.1.

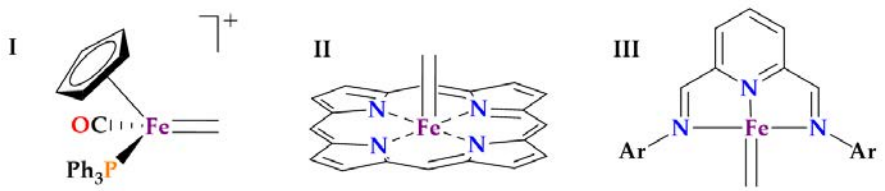

Scheme 2.1: Fe-methylidenes based on known Fe-carbenes.

At this point, it is worth mentioning that Complex **I** has a singlet ground state and it has been reported to undertake alkene cyclopropanation. Similar behaviour is reported to Complex **II**. Finally Complex III has a triplet ground state and according to Chirik and co-workers does not react with olefins. The results for these three complexes we summarize in Table 2.1 which reports the relative stabilities of the different spin states of the metal-carbene, metallacyclebutane and cyclopropanation products. Optimized structures of the stationary points are in Appendix A.1

Table 2.1: Relative Gibbs (G_{gp} + D2) energies with respect to the singlet state metal carbene and ethene (in kcal mol^{-1}) of the different spin states of the metal carbene, the metallacyclobutane intermediate and cyclopropanation products for complexes **1** to **3**.

complex	carbene			metallacyclebutane			cyclopropanation		
	S=0	S=1	S=2	S=0	S=1	S=2	S=0	S=1	S=2
I	0.0	n/a[a]	n/a[a]	-4.8	n/a[a]	n/a[a]	-16.4	-22.0	3.3
II	0.0	16.3	18.3	0.2	n/a[a]	-1.9	-0.5	-35.8	-28.0
III	0.0	-8.8	10.5	-29.6	-26.4	n/a[a]	-23.8	-28.7	-32.0

[a] Optimizations lead to structures that do not correspond to carbene or metallacyclobutene species.

Complex **I** is stable only as singlet, while singlet and triplet decompose through the carbene coupling to the carbonyl ligand. Complex **II** presents a singlet ground state, as the most stable form, with triplet and quintet states lying 16.3 and 18.3 kcal mol^{-1} above the singlet respectively. Finally, Complex **III** is a triplet with the singlet state being 8.8 kcal mol^{-1} higher in energy and the quintet state even less stable.

Moreover, alkene cyclopropanation is predicted to be strongly exergonic for **I**, **II** and **III**, regardless of the spin multiplicity. It is worth pointing out that the metal fragment in which the carbene has been lost to form cyclopropane presents both in **I** and **II** has a triplet ground state. Consequently, cyclopropanation is the thermodynamically favoured process.

Overall, these results suggest that the combination of OPBE and Grimme's Dispersion (D2) along with 6-311^{++}G(d,p) basis sets, re-

garding the ground spin of carbene methylidene state and cyclopropanation shows an agreement with the experimental results, supporting our model approach, and thus it will be used in the rest of the thesis.

3

Reactivity of Existing Metal Carbenes with Olefins

The Background Chapter shows that ruthenium-carbenes are one of the best catalysts for olefin metathesis. On the other hand iron-carbenes frequently catalyze cyclopropanation reactions. In particularly, Piano-Stool and Heme iron-carbenes are oftenly studied iron carbenes reporting as cyclopropanation catalyst.

This Chapter aims at providing insights to understand which factors are involved in some metal carbenes that determines their reactivity with olefins, particularly regarding the electronic structure of those carbenes and their activity towards cyclopropanation and olefin metathesis. Since iron compounds were reported as presenting non-low-spin behavior for various systems, an important part of this study considers medium-spin states and compares them with singlet states of the catalysts to observe the role played by different spin state electronic surfaces. The carbenes studied in this Chapter are drawn in Scheme 3.1

The first catalyst is the very effective Grubbs Second Generation olefin metathesis catalyst (**1**), for which we want to compare olefin metathesis with possible cyclopropanation paths. Complex **2** is the same as the one before, but the ruthenium atom was replaced by an

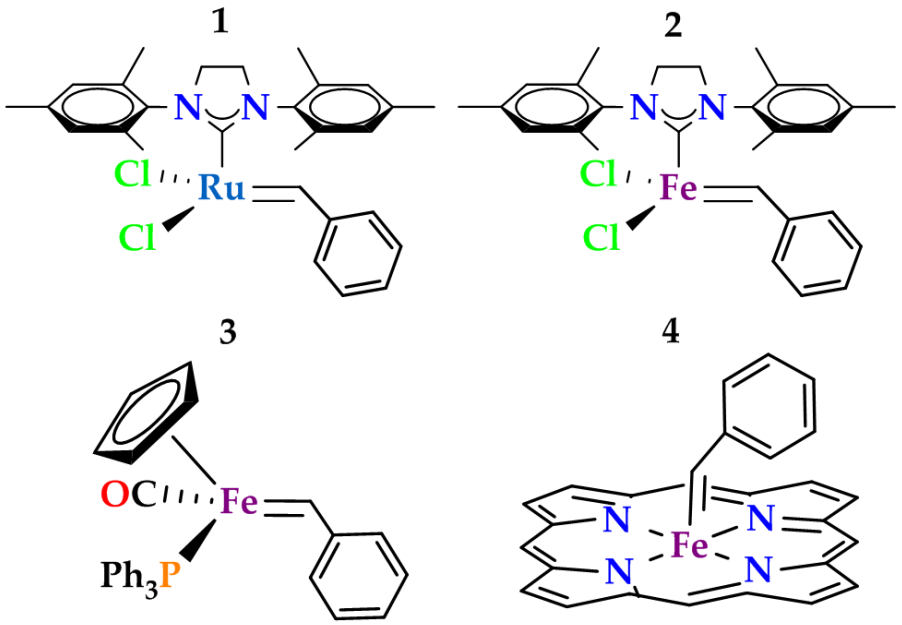

Scheme 3.1: Fe-methylidenes based on known Fe-carbenes.

iron atom, seeking to see how this changes the electronic behavior and the reactivity with olefins. The others complexes were reported as synthesized, characterized, and with a well-determined reactivity : **3** is the so-called piano stool $[Cp(CO)_2Fe^{II}{=}CHPh]^+$ that has been reported as giving cyclopropanation products when reacting with olefins. Complex **4** has an heme group as ancillary ligand, which is a model of the original tetraphenylporphine bearing carbene – $(TPP)Fe^{II}{=}CHPh$, and shows similar reactivity as the previous one described.

Results are presented in the following order: first we analyze the electronic structure of the four complexes shown in Scheme 3.1, focusing on the metal-carbene bond. Afterwards we discuss their reactivity with olefins with the aim of determine the preferred cyclopropanation mechanism and compare with olefin metathesis. But before entering properly in the discussion of our problem, aiming at doing a comparison, we discuss the case of a cobalt-carbene, which the reactivity and electronic structure was well clarified.

3.1 Metal-Carbenes Electronic Structure

As already mentioned, first row transition metal complexes are more prone to present open shell ground states and, for the particular case of metal carbenes this can turn in species in which the carbon of the carbene shows a significant radical character. This is, for instance, observed for the iron-carbene (**e** in **??**) synthetized by Chirik and co-workers or the cobalt-carbenes with porphyrins as ancillary ligand (similar to **4** in Scheme 3.1). For the cobalt carbene this implies that alkene cyclopropanation occurs through a radical mechanism. It is for this reason that we start with an analysis of the iron-carbene electronic structure. We wonder whether the iron-complexes studied here can show a similar behavior to that of the cobalt open-shell carbene, with a possible radical chemistry, when they show a non-low spin electronic state.

The metal center of these species has a d^6 electronic configuration and thus, they can exhibit a singlet low-spin (S=0), a triplet intermediate-spin (S=1) state or a quintet (S=2) high-spin electronic state, this one being usually much higher in energy than the other two and will not be discussed further. Table 3.1 reports the Gibbs energy difference between the singlet and triplet state as well as Mulliken spin densities.

Table 3.1: Mulliken spin densities over the metallic center and carbon of the metal-carbene bond for the the triplet state of complexes **1-4**, and relative energy of the triplet state relative to the singlet state (in kcal mol^{-1}).

Complex	Metal	Carbon	ΔG_{S-T}
1	1.61	-0.07	22.0
2	2.38	-0.52	-4.2
3	1.18	0.27	-
4	1.22	0.54	18.2

Complexes **1**, **3** and **4** show a singlet ground state while **2** is a triplet. Noteworthy, for Complex **3**, and despite many efforts, we were not able to optimize a minimum for the triplet electronic state. Instead, a triplet structure with the carbon of the carbene bound to the carbonyl ligand was located (see Section 3.5 for further discussion).

Apart of the values in the previous Table, the spin densities of the triplet states are also pictorially in Figure 3.1.

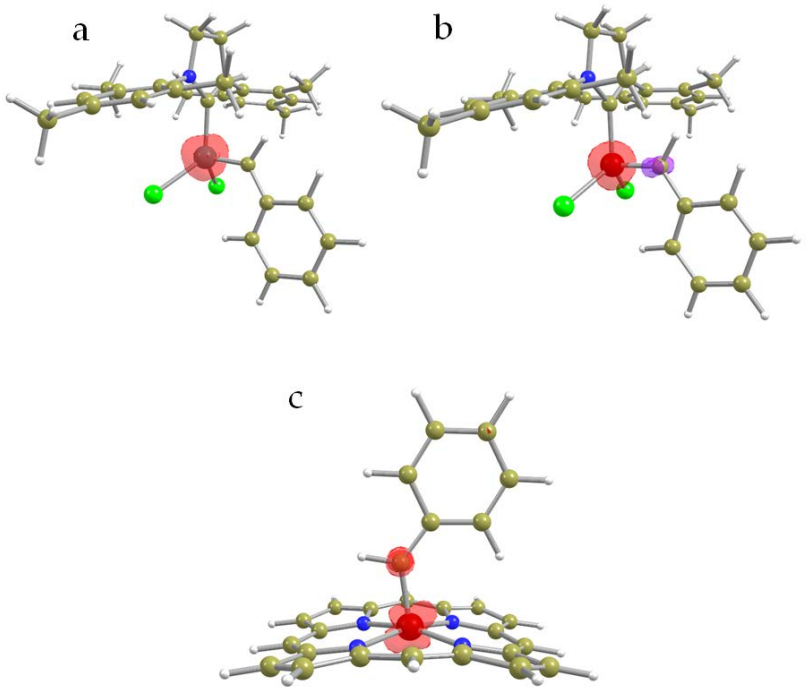

Figure 3.1: Calculated isosurfaces of α (red) and β (violet) spin-density of the triplet state (0.03 a.u. m^3) for Complexes **1** (a), **2** (b) and **4** (c).

It can be observed that the Ruthenium carbene, Complex **1**, has the spin density located mainly at the metal, the Mulliken spin density values being 1.61 at ruthenium and virtually 0 at carbon. Thus, even if the complex is in its triplet state, one would not expect a radical carbene-based chemistry.

In the case of catalyst **2**, the iron analogue of Complex **1**, the spin density distribution in the triplet ground state shows important differences as compared to **1**. That is, the metal shows positive spin density values (red contours), and the carbene negative values (violet contours), thereby indicating that the π bond is not completely formed, probably due to the smaller overlap between iron d orbitals and those of the carbene fragment in **2**. This is confirmed by the spin density at iron and the carbene (Table 3.1), which are 2.38 and -0.52, respectively. These values are indicative that in this triplet state there is not only

two unpaired alpha electrons, as expected, but instead we have three unpaired alpha electrons and one unpaired beta electron, resulting in an overall triplet state. These observations suggest that catalyst **2** could be prone for a non-closed shell chemistry behavior. Such behavior has been defined as hyper open-shell states, and has been reported theoretically[254] and experimentally[183] for different Fe-systems.

For complex **4**, the spin density of the triplet state is delocalized between the metal and the carbene, with spin density values being 0.54 at the carbon atom and 1.22 over the metallic center, which can be visualized in Figure 3.1 and suggest that the triplet state of **4** can also present radical based reactivity, if in the triplet was the ground state.

Figure 3.2 shows the centroids of the localized molecular orbitals in the singlet and triplet states, respectively. These calculations have been done with the CP2K code which only explicitly considers 14 outer electrons of the formally 2+ metal cation center (ns^2 np^6 nd^6). Thus, the number of electrons around the metal in all cases have to account for these 14 electrons. For Complex **1**, the blue dots represent an electron pair, since in the restricted DFT (PBE) approach, alpha and beta orbitals are identical and as such they have the same centroid. It can be observed that it is possible to count 6 dots around the ruthenium center, corresponding to 12 electrons. The other 2 electrons, along with 2 electrons from the carbene, are involved in the double bond M=C and thus, there are two dots in the middle of this bond. This is in agreement with a Schrock carbene like behavior, the M=C bond arising from the interaction of the metallic fragment and the CR_2 carbene both in the triplet state.[62] Note that the centroids over the other M–L bonds can be viewed as two electrons from the ligands. A similar behavior can be inferred for the others complexes in the singlet state.

Complexes show a different behavior in the triplet state. In the unrestricted DFT treatment, used for calculating open shell species, each orbital holds one electron, instead of two (as it happens in the restricted DFT). In this way, instead of one blue dot corresponding to the centroid of the doubly occupied orbital, we have two dots: a red one corresponding to the centroid of an occupied α orbital and one yellow dot corresponding to a β orbital.

For Complex **1**, there are 5 red-yellow dots pairs around the ruthenium, resulting in 10 electrons, and two red dots indicative of two unpaired electrons, as expected for the triplet state. The unpaired

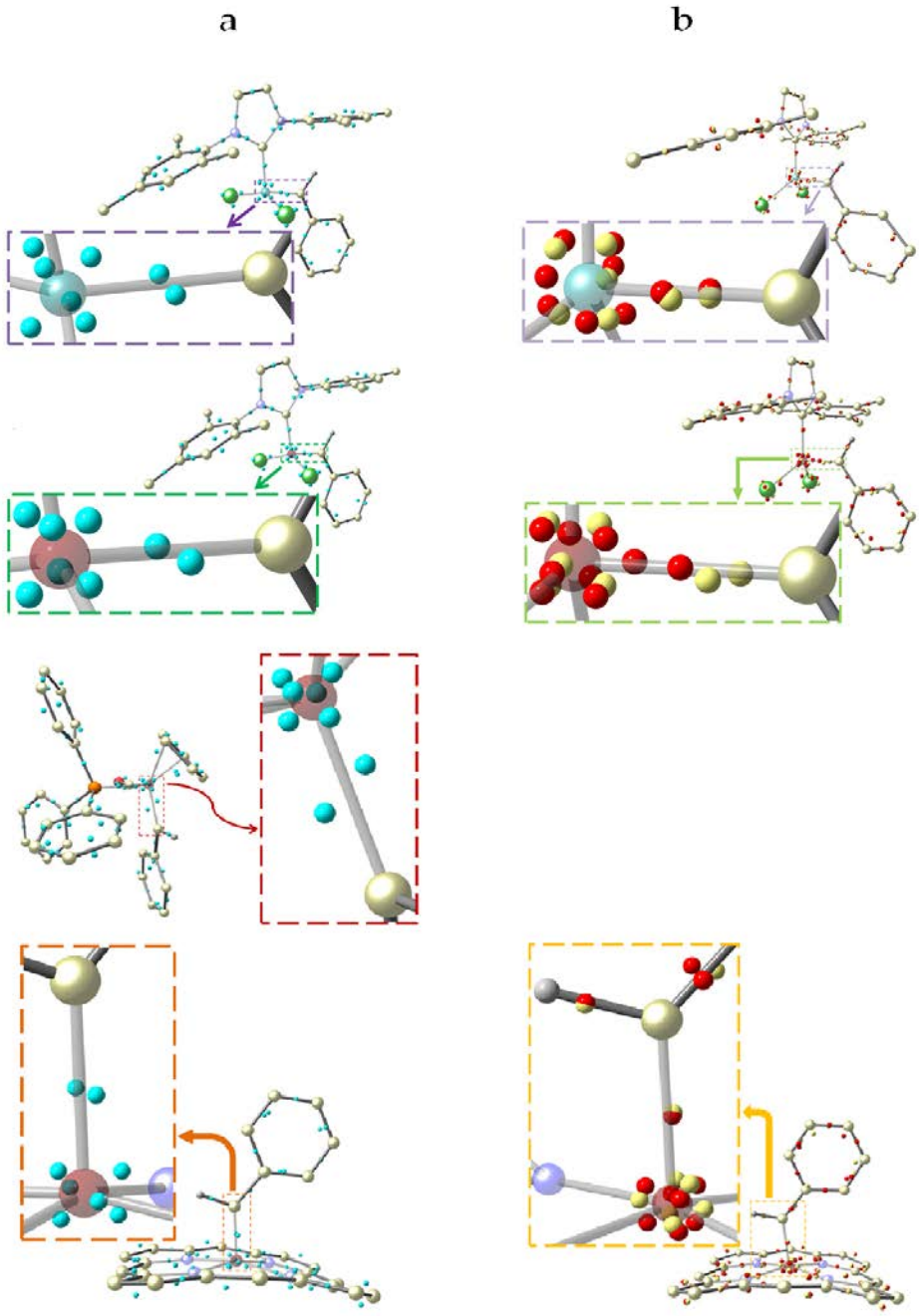

Figure 3.2: Wannier functions of the (a) singlet and (b) triplet states. Blue spots corresponds to a electron pair, red ball means a α and yellow ball β.

electrons are mainly localized at the ruthenium center. Finally, the other two electrons needed to complete the 14 electrons considered explicitly for the metal in the calculation are involved in the M=C bond.

Regarding Complex **2**, there are also 5 pairs of red-yellow dots, and two red dots corresponding to two unpaired a orbitals. However, there is only one electron pair corresponding to the M=C bond. The other pair is split in two, in such a way that the centroid of the α orbital is close to the metal and that of the β orbital is closer to the carbon atom. Therefore, triplet is formed by three alpha electrons at the iron atom and one beta at the carbon, which would explain the spin density values with opposed sign observed for this compound and suggest that the double bond is not completely formed.

Complex **4**, in the triplet state, has 6 pairs on the metal, one additional pair corresponding to the M=C bond and two unpaired α electrons, one over the metal and the other located at the carbon atom of the M=C.

(TPP)Co^{II}=CHPh is a cobalt-porphyrin whose radical behaviour driving to cyclopropanation is known. Using our methodology on this carbene, we analyze its electronic structure for comparison. Results are shown in Figure 3.3.

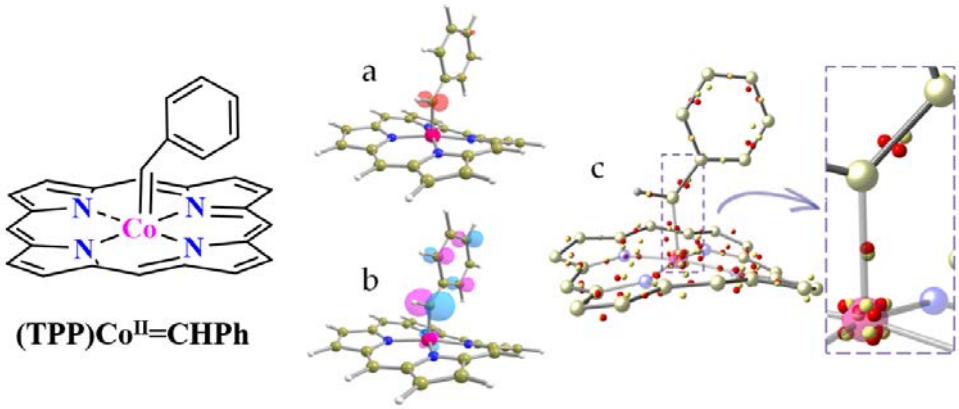

Figure 3.3: Electronic structure of (TPP)Co^{II}=CHPh: (a) spin-density (0.03 a.u. m^3), (b) HOMO , and (c) Wanier functions of the doublet ground state.

Our calculations clearly show that the spin-density of this complex in the doublet spin ground state is indeed concentrated over the

carbon of the carbene (Figure 3.3-a). This spin density is concentrated on the HOMO orbital, since the surface of the spin density has a topological similarity with this orbital (Figure 3.3-b). Actually, Mulliken spin density values are of 0.73 for the carbon of the metal-carbene bond and 0.00 for the cobalt. This complex has a Co^{II} with a d^7 electronic configuration and is a low spin where the doublet state is 19.29 kcal mol^{-1} lower in energy than the quadruplet. The doublet state implies the presence of only one unpaired electron. The basis set of the Wannier functions calculations treats the valence shell of the Co with 17 electrons. As the complex is neutral, and the ligand TPP is doubly charged, then the cobalt atom in this calculation should have 15 electrons in its valence shells. However centroids of the localized orbitals provided by the Wannier functions (Figure 3.3-c) show 14 dots around the cobalt atom, showing it has only 14 electrons performing actually a Co^{III}. The other unpaired electron remains on the bond formed between the carbon of the carbene and the atom of the phenyl ring. This bond was supposed to bear only two electrons, one α (red dot) and the other β (yellow dot), but instead we can see one α electron more. This completely agrees with previous experimental and theoretical studies.[63,197]

Overall, the electronic structure analysis of these compounds indicates that if the iron-carbene complexes are in the triplet state, they could be involved in a radical chemistry, similarly to that observed for cobalt-carbenes that promote cyclopropanation, just above described. This is in contrast to that observed for the ruthenium Carbene **1**, since the two unpaired electrons are localized at ruthenium and thus, a two electron chemistry is expected.

3.2 Remarks on the Reactivity

Next sections are focused on understand possible mechanisms for the reactivity of the complexes **1**, **2**, **3** and **4** with *p*-methyl-styrene. We focus basically in paths that drive to cyclopropanation, although we also compare the Gibbs with olefin metathesis, since it is desirable to understand the competitiveness of these reactions. In particular, we explore the three possible cyclopropanation mechanisms as well as that of olefin metathesis, as shown in Scheme 3.2. Note that *Ph* stands for the phenyl group and *Tol* for the he *p*-toluyl substituent.

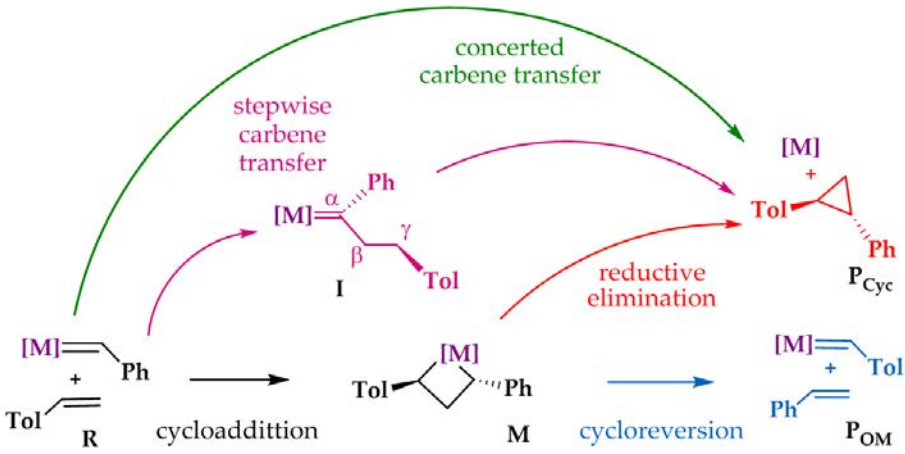

Scheme 3.2: Considered reactivity of metal-carbenes with olefins.

One of these pathwaysr refers to the olefin metathesis mechanism: **R** is the active carbene species, which by the *cycloaddition* step, passes through the metallacyclobutane intermediate (**M**), and gives olefin metathesis products ($\mathbf{P}_{OM}$) by *cycloreversion*. *Reductive elimination* drives to cyclopropanation (P_{Cyc}), from the metallacyclobutane intermediate. The others paths refers to cyclopropanation mechanisms that involve the nucleophilic attack of the olefin to metal carbene bond. They can proceed either through intermediate **I**, and we call *stepwise carbene transfer* or directly, in a *concerted carbene transfer* approach. This intermediate can have an open-shell biradical character with unpaired electrons at carbons α and γ if the reaction takes place in the triplet state, or it can be a zwitterion when the process proceeds in the singlet state.

3.3 Reactivity of Grubbs Catalyst

The catalytic activity for olefin metathesis of Complex **1**, and other related Ru-based catalysts have been widely studied computationally.[259–269] However, their capacity to undergo the cyclopropanation has been scarcely studied. In fact, it has been proposed that formation of cyclopropane can be in one pathway for its deactivation: Bernardi and co-workers reported the energetics of the reductive elimination from the metallacyclebutane and carbene transfer, but only in the singlet state.,[54] in general, considerations about the reactivity of

intermediate spin state states are missing, as well. In Figure 3.4 we present the already well-established mechanism for olefin metathesis of Complex **1** with *p*-methyl-styrene in singlet state and in the triplet state as well and the optimized geometries are shown in Figure 3.5 for cycloaddition and Figure 3.6 for cycloreversion.

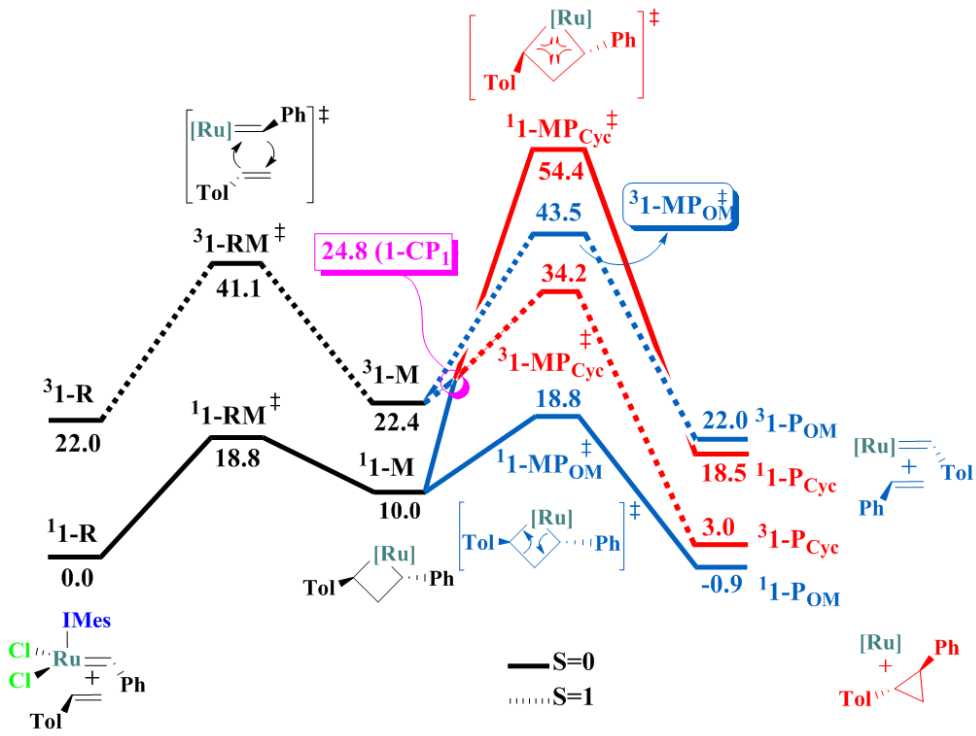

Figure 3.4: Gibbs energy profile (in kcal mol^{-1}) for olefin metathesis – *cycloaddition* (black) and *cycloreversion* (blue)– and alkene cyclopropanation by *reductive elimination* (red) processes involving **1** with styrene in both singlet and triplet states.

The pre-catalyst **1** is a singlet with the triplet resting 22.0 kcal mol^{-1} above. The black line is the Gibbs energy surface (PES) through which the incoming olefin coordinates to the ruthenium atom, and overcoming a transition state forms the intermediate metallacyclobutane: the so-called cycloaddition step of the olefin metathesis mechanism. This transition state singlet ($^1 1 - RM^{\ddagger}$) is 18.8 kcal mol^{-1} over reactants ($^1 1 - R$), while the triplet ($^3 1 - RM^{\ddagger}$) is around 22 kcal mol^{-1} over the singlet. Metallacyclobutane singlet ($^1 1 - M$) is 10.0 kcal mol^{-1}

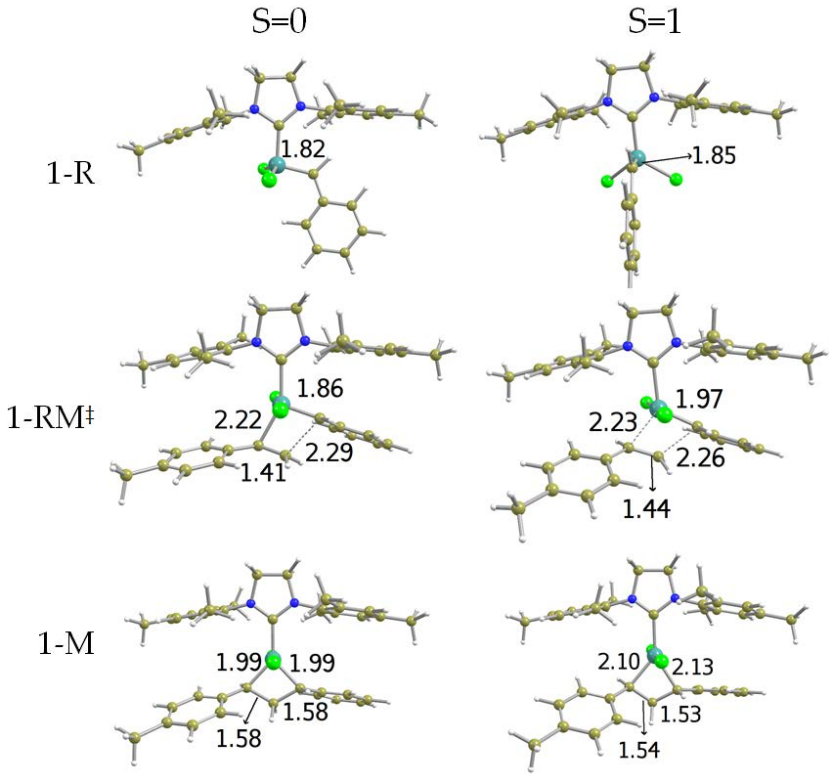

Figure 3.5: Optimized geometries of *cycloaddition* step in singlet and triplet states, for Complex **1** with styrene. All distances are in Å.

higher in energy than the reactants, while triplet (${}^3\mathbf{1}-M$) is 22.4 kcal mol^{-1}. From the metallacyclobutane the cycloreversion process (blue lines) gives the products, also crossing a barrier similar to the previous described: the singlet (${}^1\mathbf{1}-MP^{\ddagger}_{OM}$) is at 18.8 kcal mol^{-1} and the triplet (${}^3\mathbf{1}-MP^{\ddagger}_{OM}$) is around 25 kcal mol^{-1} over the singlet. Olefin metathesis products in the singlet state are almost isoenergetic with reactants, being 0.9 kcal mol^{-1}(${}^1\mathbf{1}-P_{OM}$) below them, and the triplet (${}^3\mathbf{1}-P_{OM}$) 22.0 kcal mol^{-1} higher. Since a methyl substituent is the only difference from the olefin reactant to the olefin product of metathesis, the energetics of the cycloaddition part is similar to the cycloreversion, as well as the products energies are similar to the reactants.

Until this point, the singlet state surface of the already largely studied mechanism for olefin metathesis is in a good agreement with previous works.[261,265] The triplet surfaces, on the other hand, provides

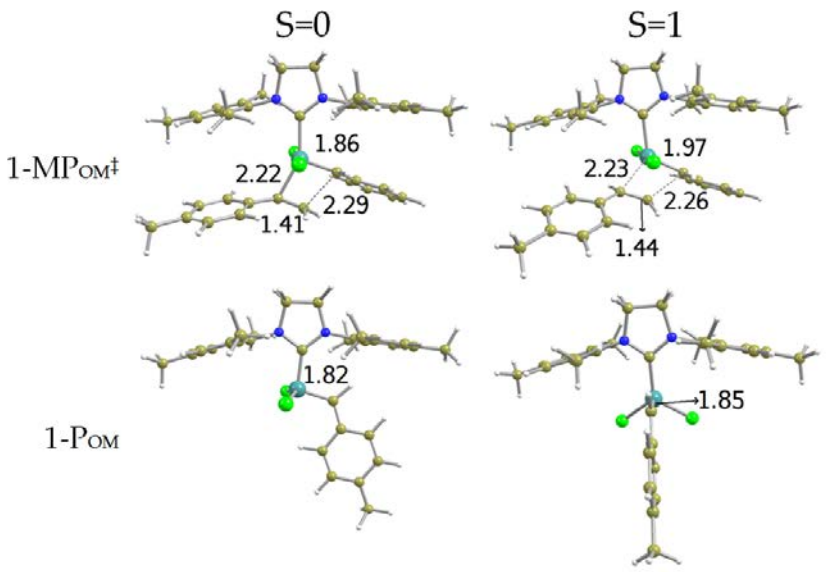

Figure 3.6: Optimized geometries of *cycloreversion* step in singlet and triplet states, for Complex **1** with styrene. All distances are in Å.

interesting hints: they are largely disfavored with the split between the two surfaces ranging from around 12.0 kcal mol^{-1}, in the metallacycle ($^1 1 - M$) until around 25 kcal mol^{-1} in the transition state of cycloreversion step. Ruthenium belongs to the fourth row of periodic table and is tetracoordinate, therefore it is unlike to go through a high-spin behavior, which can favor the singlet surface. Also, olefin metathesis is a two-electron reaction: for instance, in the cycloaddition through the transition state to form the metallacycle is somehow a concerted mechanism where an electron pair of the incoming olefin is donated to the metallic center and at the same time a bond is formed between the carbenic carbon and the other carbon of the olefin. In this way, the stationary points in the triplet surface with similar geometry to the points in the singlet surface are considerably high in energy.

A different behavior is observed for the cyclopropanation reaction by reductive elimination from metallacyclobutane intermediate, represented by the red lines in Figure 3.4 with optmized geometries in Figure 3.7. Products from this reaction ($^3 1 - P_{Cyc}$) exhibit a triplet ground state by 15.5 kcal mol^{-1} and thus a spin crossing is expected to occur. This pathway implies a barrier in the triplet state, $^3 1 - MP^{\ddagger}_{Cyc}$, of 11.8 kcal mol-1 (the transition state lies 34.2 kcal mol^{-1} over sepa-

rated reactants) whereas for the singlet state ${}^{1}1 - MP^{\ddagger}_{Cyc}$ the energy barrier is significantly higher. As expected, the metathesis process is more favorable than cyclopropanation both kinetically and thermodynamically and thus, the one expected to occur. Noteworthy, the lowest energy path towards cyclopropanation involves a spin crossing point $(1 - CP_1)$ between the ${}^{1}1 - M$ and the cyclopropanation transition state that is located 2.4 kcal mol^{-1} higher in energy than the triplet metallacyclobutane ${}^{3}1 - M$, and 6 kcal mol^{-1} higher than the ${}^{1}1 - MP^{\ddagger}_{OM}$ transition structure that leads to olefin metathesis products.

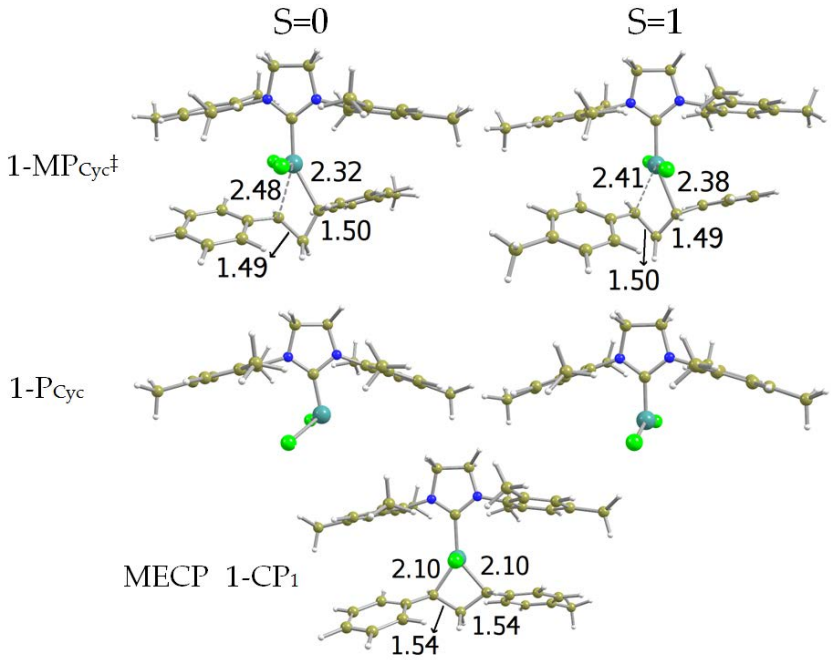

Figure 3.7: Optimized geometries for *cyclopropanation* path, in singlet and triplet states, and MECP $1 - CP_1$ for Complex **1** with styrene. All distances in Å.

Figure 3.8 shows the potential energy surface for the path of carbene transfer reaction, in the singlet and triplet spin states. In transition state $({}^{1}1 - RI^{\ddagger})$ one single carbon of the olefin molecule (carbon β) attacks the carbon of the carbene (carbon β), with a barrier of 40.6 kcal mol^{-1}. Subsequently, we have intermediate $({}^{1}A - I)$ consisting of a kind of toluil-propane that is single-bonded with the ruthenium,

with a relative energy of 29.5 kcal mol^{-1}. Next step involves another transition state ($1-IP^{\ddagger}_{Cyc}$) consisting in the cyclization by the carbene γ coupling with carbon α, forming the cyclopropane and a metallic tri-coordinate, fragment presenting energy of 45.7 kcal $^{-1}$ in the singlet state. 13.16 kcal mol^{-1} over the intermediate $^{1}1-I$ a spin-crossing ($1-CP_2$) exists, between the triplet and the singlet surface, and the last step of this path takes place on the triplet surface ($^{3}1-IP^{\ddagger}_{Cyc}$). Note that this crossing-point would not imply in additional barrier. Obviously the singlet surface rules out is not a radical mechanism, but instead a cationic/anionic path. Optimized geometries of the direct cyclopropanation path discussed above are shown in Figure 3.9.

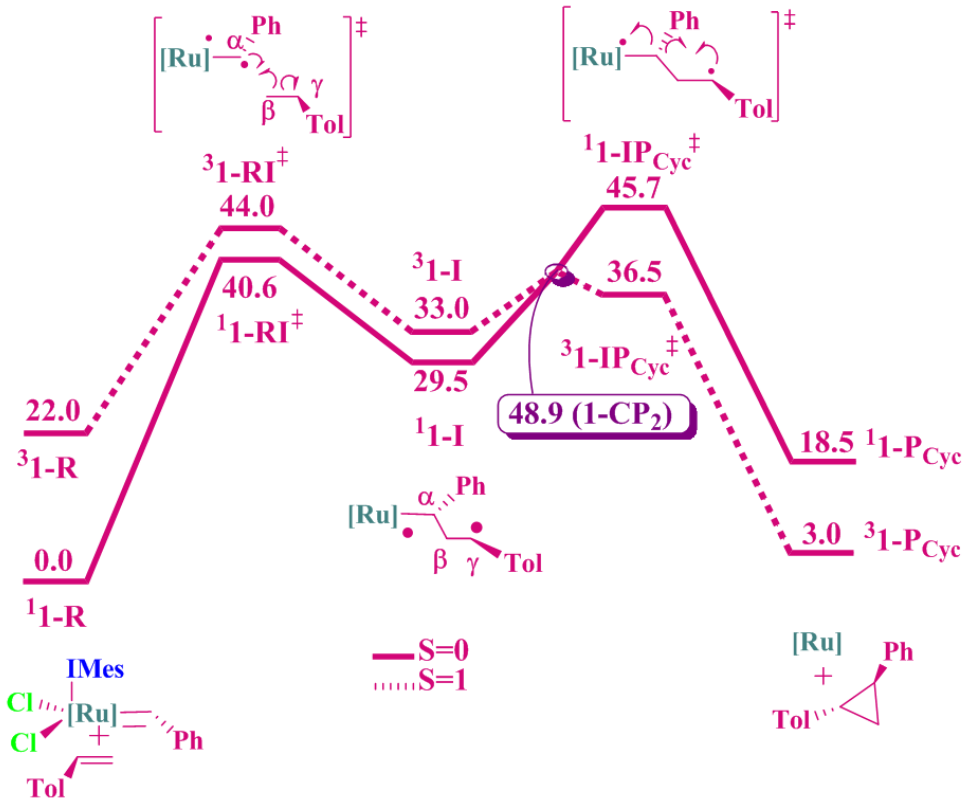

Figure 3.8: Gibbs energy profile (in kcal mol^{-1}) for *carben transfer* involving Complex **1** with styrene in both singlet and triplet states.

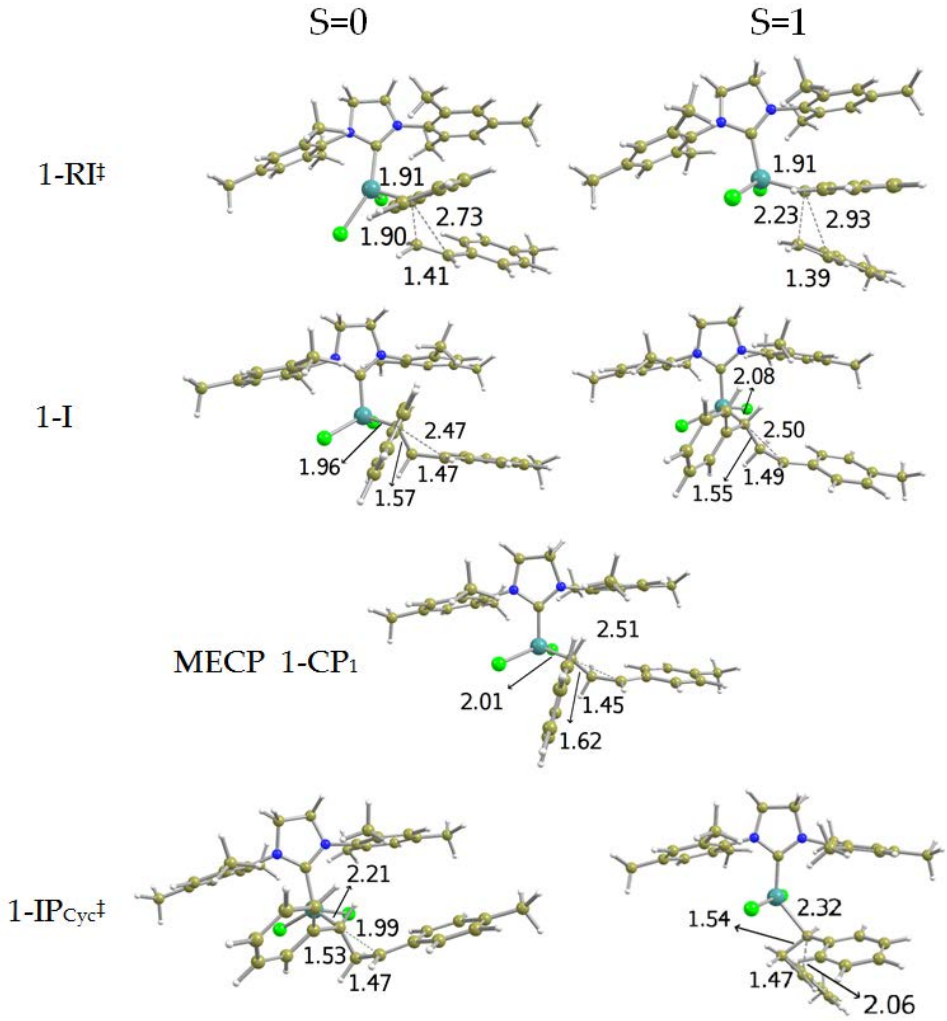

Figure 3.9: Optimized geometries for the *carben transfer* path, in singlet and triplet states, and MECP $1-CP_2$ for Complex **1** with styrene. All distances are in Å.

Figure 3.10 shows the spin density in the pathway of the cyclopropanation by carbon transfer mechanism, in the triplet state. Although in the species ${}^3 1 - R$ the spin density is concentrated on the metal, along the surface a significant part of the spin density is split also onto carbon α and β, suggesting a radical mechanism. However, this process is unlikely, because since the beginning, in the pre-catalyst stationary point, the singlet is less stable than the triplet. Also, triplet

surface is all over the singlet surface except for the TS $^{3}1 - IP^{\ddagger}_{Cyc}$, perhaps because this structure is more feasible as belonging to a radical mechanism. This destabilization compared to the triplet surface, regarding the singlet, that even being only of 3.4 kcal mol^{-1} in the first TS ($^{1}1 - RI^{\ddagger}$), shows the strongly low-spin nature of the Grubbs catalyst that contributes to it success as a catalyst for olefin metathesis.

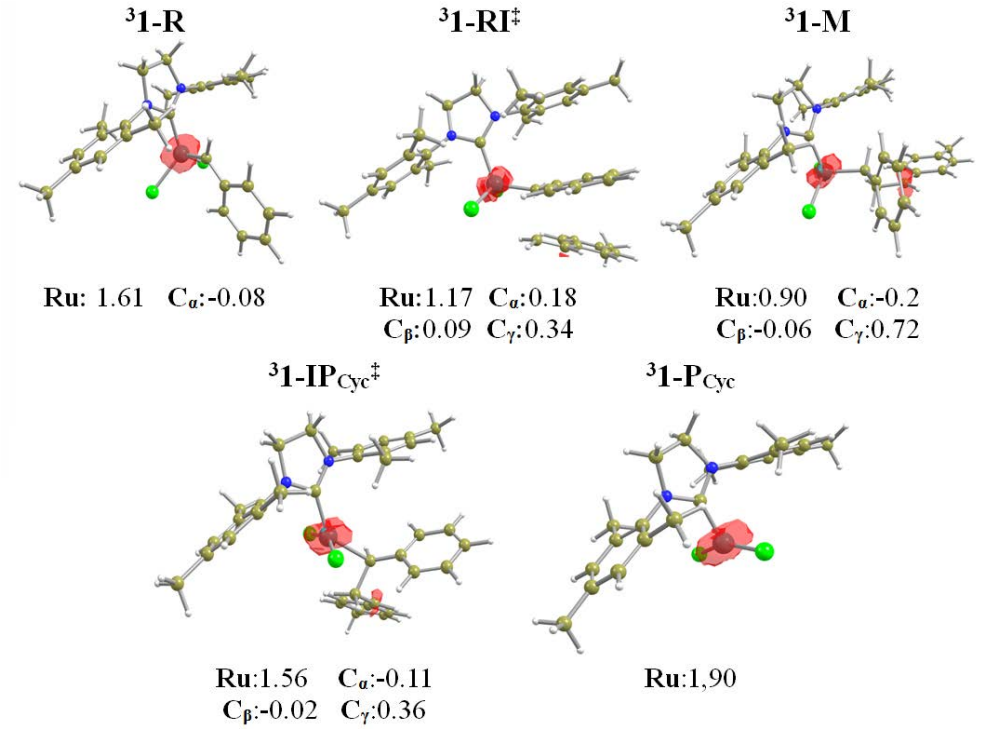

Figure 3.10: Spin-densities of triplet stationary species of *carbene transfer* of Catalyst **1** with styrene.

3.4 Reactivity of [Fe]=CH_2 bearing Grubbs Motifs

The energy profiles associated with the olefin metathesis and cyclopropanation by reductive elimination for Complex **B** are shown in Figure 3.11, while the optimized structures of the stationary points of these profiles are shown in Figure 3.12 to Figure 3.14.

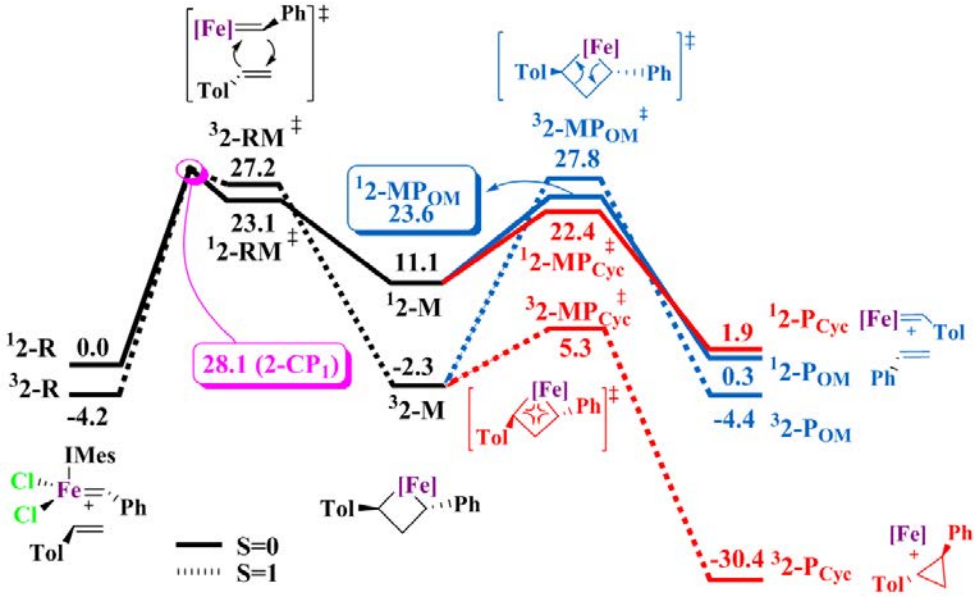

Figure 3.11: Gibbs energy profile (in kcal mol^{-1}) for olefin metathesis – *cycloaddition* (black) and *cycloreversion* (blue) – and alkene *cyclopropanation* by reductive elimination (red) processes of **2** with styrene in both singlet and triplet states.

Unlike Grubbs Catalyst **1**, the pre-catalyst **2** has a triplet state ground state, the Gibbs energy difference with the singlet being 4.2 kcal mol^{-1}. The metallacyclobutane intermediate also presents a triplet state, the singlet state being around 15 kcal mol^{-1} higher in energy. However, the energy barrier for the formation of the metallacyclobutane in the singlet state (23.1 kcal mol^{-1}) is smaller than in the triplet one (31.4 kcal mol^{-1}) and this turns in the fact that the transition structure ($^12 - RM^{\ddagger}$) is more stable than that in the triplet state ($^32 - RM^{\ddagger}$) by 4.1 kcal mol^{-1}. This suggests that the reaction could

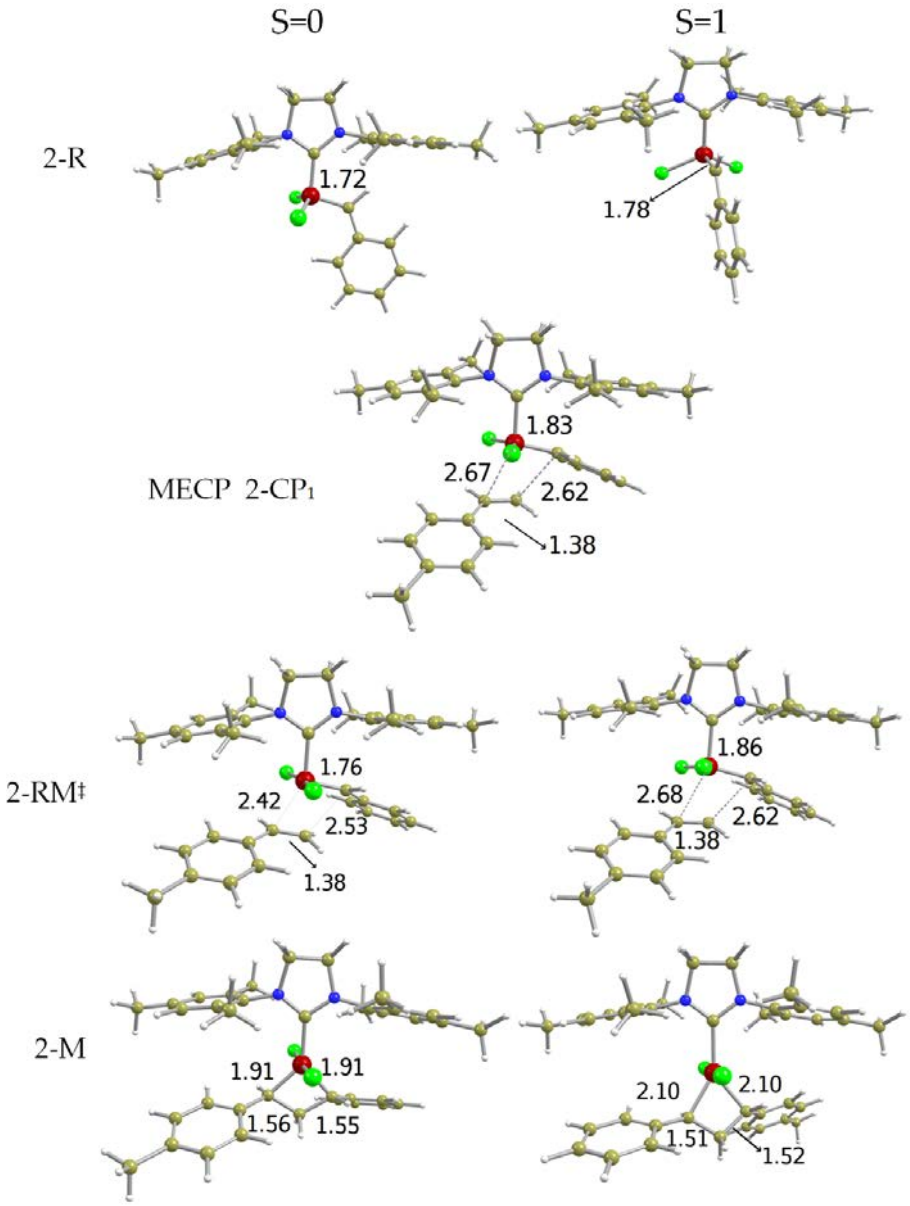

Figure 3.12: Optimized geometries of *cycloaddition* step in singlet and triplet states and and MECP $B-CP_1$ for complex **2** with styrene. All distances are in Å.

take place through spin crossing. The energy barrier of this process $(2-CP_1)$ is marginally higher in Gibbs energy than the $^3 2-RM^{\ddagger}$ transition state. This is probably due to the fact that the cycload-

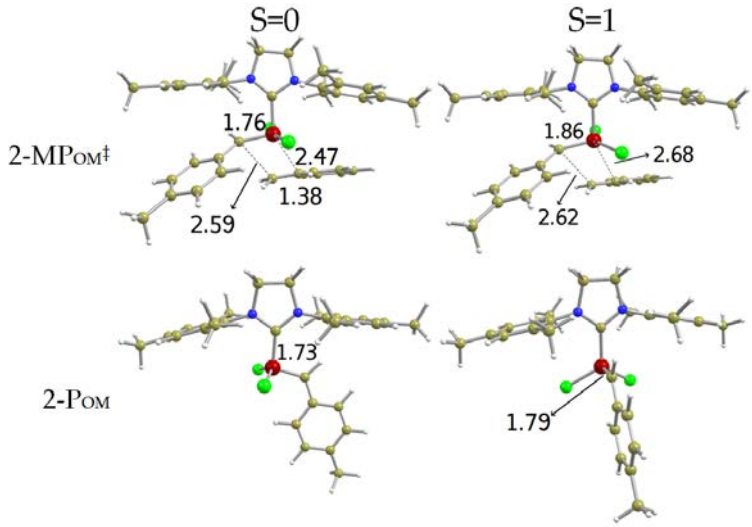

Figure 3.13: Optimized geometries of the *cycloreversion* step, singlet and triplet states, for complex **2** with styrene. All distances are in Å.

dition process is clearly a two-electron process and more feasible to occur in the singlet state. Therefore, crossing to the singlet surface is not expected. One can envisage another similar MECP between the transition structure ($(^12 - RM^‡)$) and the intermediate metallacyclobutane (2-M), that we have not located because a similar behavior to that of the first MECP is expected. Finally, the cycloreversion process is the mirror process of the cycloaddition with the only difference of the methyl substituent of the reacting olefin. Consequently, it shows essentially the same energetics with analogous spin-crossing points.

The path corresponding to the reductive elimination from the metallacycle is represented by the red lines in Figure 3.11. The associated energy barrier from the triplet ground state metallacyclobutane is 7.6 kcal mol^{-1} and thus, $^32 - MP^‡_{Cyc}$ transition state is around 17 kcal mol^{-1} smaller in energy than the barriers for cycloreversion. The hypothetical transition state singlet ($^1B - MP^‡_{Cyc}$) was not found. A relaxed potential energy scan shortening the distance between the two carbon-α of the metallacyclebutane shows a rapidly increasing of the energy (see Figure B.2 in Appendix).

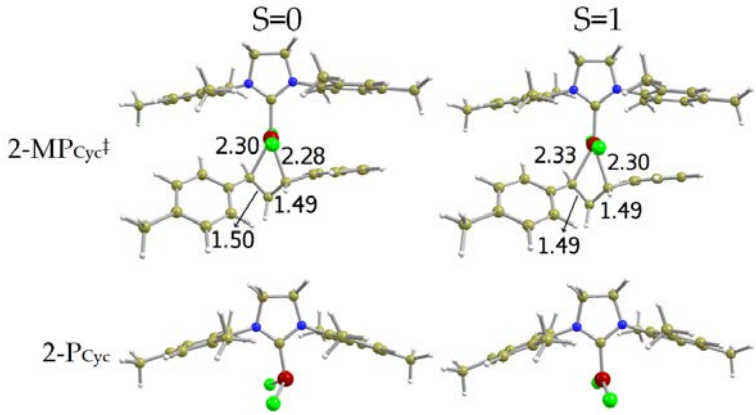

Figure 3.14: Optimized geometries of the cyclopropanation by *reductive elimination* step, singlet and triplet states, for complex **2** with styrene. All distances are in Å.

Direct cyclopropanation path for this complex has its potential energy profile reported in Figure 3.15 and the associated geometries in Figure 3.16.

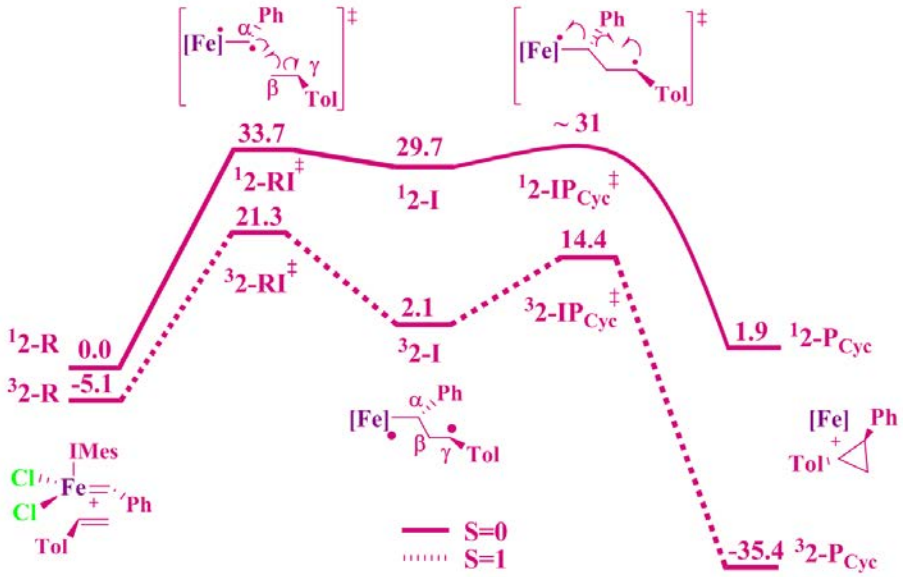

Figure 3.15: Gibbs energy profile (in kcal mol^{-1}) for *direct cyclopropanation* involving Complex **2** in both singlet and triplet states.

In this path, again, the behavior is very different if compared with the ruthenium Grubbs catalyst (Complex **A**). Triplet surface is always more stable, and the barriers are lower compared to those of ruthenium complex: the highest is 21.3 kcal mol^{-1} ($^3B - RI^{\ddagger}$), while for the Grubbs catalyst they are around 40.0 kcal mol^{-1}. Intermediate ($^3B - I$) is also lower in energy (2.1 kcal mol^{-1}), as well as the cyclization transition state ($^3B - IP^{\ddagger}_{Cyc}$), 14.1 kcal mol^{-1}. An interesting fact is that in the singlet surface, the hypothetical transition state $^1B - IP^{\ddagger}_{Cyc}$ was not located at this level of theory. A scan (see in Figure B.3 of Appendices) approaching the distance C_α—C_γ shows a small barrier of around 1 kcal mol^{-1}, in electronic total energy, which suggests virtually a barrierless process.

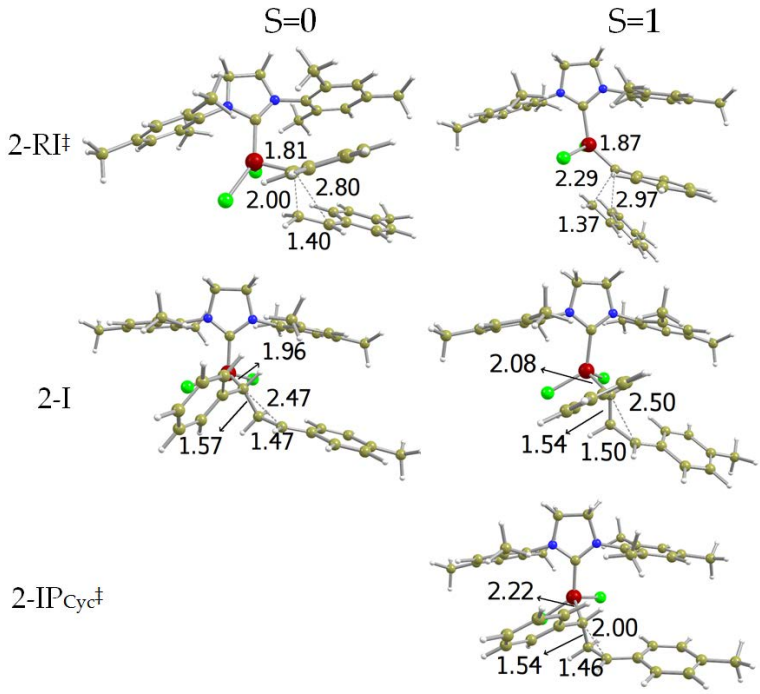

Figure 3.16: Optimized geometries for *carbene transfer* path for Complex **2** with styrene.

Figure 3.17 shows the spin density evolving along the stationary points of the direct cyclopropanation pathway. It can been see that the distance Fe=C_α increases in the following order: $^32 - RI^{\ddagger}$ (1.87) > $^32 - I$ (2.08) > $^32 - IP^{\ddagger}_{Cyc}$ (2.22). In this same order, the C_α—C_γ bond

distance decreases (2.97 Å, 2.50 Å, 2.00 Å), showing the formation of the cyclopropane product. The isosurfaces of the spin-density show a β-density in the pre-catalyst on carbon-α. Going further in the PES, in the transition state $^3 2-RI^{\ddagger}$ the β-density is partially transferred to the carbon γ. In the intermediate $2-I$ a large amount of β-density is over the carbons α and γ. The transition state $^3 2-IP^{\ddagger}_{Cyc}$ is associated with the coupling of the carbons α-γ and thus, there is almost no spin-density besides that at the metal, probably because the electrons are coupling to form the bond C_α—C_γ. This radical stepwise mechanism was already theoretically proposed for iron carbenes[186] and is similar to the cyclopropanation with cobalt carbenes above mentioned.[197]

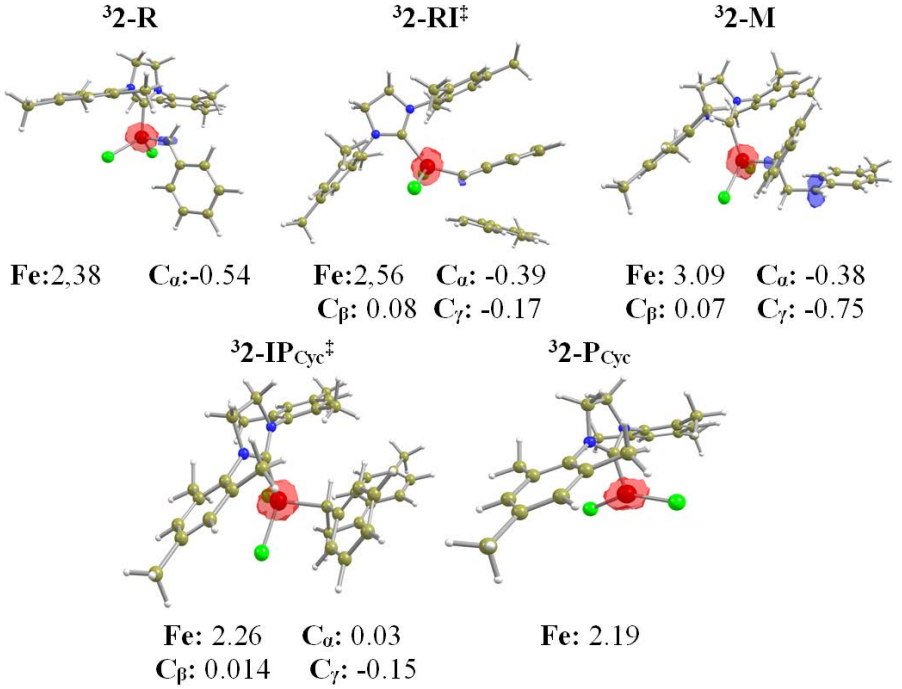

Figure 3.17: Spin-densities of triplet stationary species of *carbene transfer* of Catalyst **2** with styrene. Red surfaces correspond to α-spin density and blues isosurfaces correspond to β-spin density

3.5 High-Coordinate [Fe]=CH_2: Piano-Stool Complex

For olefin metathesis to occur an incoming olefin needs to coordinate to the metallic center, forming the intermediate metallacyclobutane that can break to olefin metathesis products or even for cyclopropanation products, as demonstrated for Complexes **1** and **2**. In a review Brookhart and co-workers[148] claim the absence of evidence of metallacyclobutane existence. The reason for this could be that formally Complex **3** has already 6 ligands, since cyclopentadienyl acts donating three electrons pairs. With such a coordination number, this complex has 18 electrons around the iron atom that might prevent the coordination of a new ligand. In spite of that, we have still been able to optimize the metallacyclobutane structure ($^1 3-M$) showed in Figure 3.18.

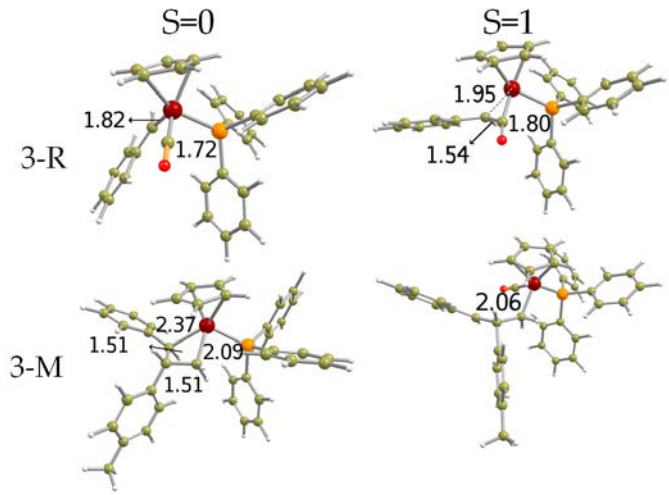

Figure 3.18: Optimized geometries of *cycloaddition* step, singlet and triplet states, for complex **3** with styrene. Distances in Å.

The values of the M-$C_{\alpha 1}$ and M-$C_{\beta 2}$ are 2.37 and 2.09 Å, respectively, that is larger than the analogous bonds in the metallacycle singlete for Complex **1**, which are both of 1.99 Å. This may be because of the large coordination number of this complex. At this level of theory, we did not found the metallacyclobutane in the triplet state though and hypothetical $^3 C-M$ decomposes. Neither have we been able to

locate the transition states of the cycloaddition step, which forms the metallacyclebutane, nor the transition state of cycloreversion leading to the olefin metathesis products. The cycloaddition step is an oxidative addition and the metallacycle is a hexacoordinate structure with four electrons, presenting 18 electrons around the metal, which can explain why we found the optimized structure for the metallacycle but not for the transitions state aforementioned.

Another possibility[199] would be the discoordination of one ligand, that could be either the carbonyl or the phosphine. Then the metallic center would become a 16 electrons species and be more prone to coordination by an olefin. We tested this hypothesis performing scans for the discoordination of those ligands and we found that it is very unfavorable and unlike happen, as showed in Figure 3.19.

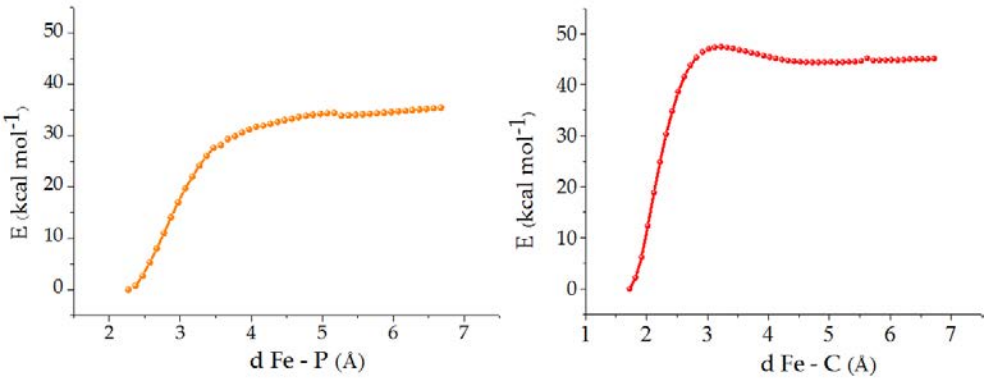

Figure 3.19: Scan for the decoordination of carbonyl and phosphine ligands in Complex **3**.

Overall, since we have neither been able to locate the transition state of the concerted cycloaddition nor the transition state of cycloreversion of the metallacycle, the experimentally observed cyclopropanation from this complex, would probably occur through carbene transfer. The computed energy profiles for these pathways both in the singlet and triplet states are shown in Figure 3.20 and the associated optimized geometries are given in Figure 3.21.

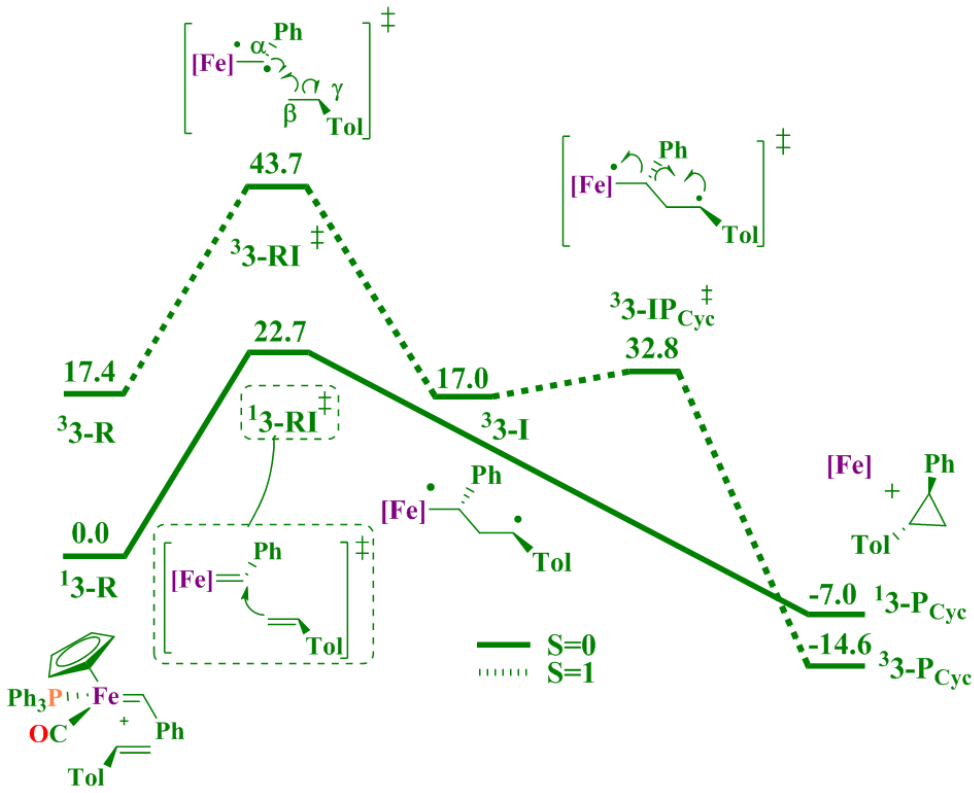

Figure 3.20: Gibbs energy profile (in kcal mol^{-1}) for *carbene transfer* involving **3** in both singlet and triplet states. $^3 3 - R$ does not correspond to an iron-carbene.

First of all, the triplet pre-catalyst $^3 3 - R$ does not exist, instead its optimization leads to a structure in which the carbon atom of the carbene binds to the carbon of the adjacent CO. (see Figure 3.18). For this spin state, cyclopropanation occurs in a step-wise mechanism: the transition state $^3 3 - RI^{\ddagger}$ lies very high in energy (43.7 kcal mol^{-1}) as compared to Catalyst **2** (21.3 kcal mol^{-1}), which may be attributed to the ancillary ligands favoring the singlet state, specially cyclopendienyl and the carbonyl. The next stationary point is the intermediate $^3 3 - I$ that is 26.7 kcal mol^{-1} below the previous barrier, followed by a barrier of 2.6 kcal mol^{-1} ($^3 3 - IP^{\ddagger}_{Cyc}$). Cyclopropanation products in the triplet state lye 1.8 kcal mol^{-1} above the reactants. Note that the profile is more similar to that of Complex **1** than to that of Complex **2**; remarkably, the pre-catalyst metal carbene is singlet in both cases.

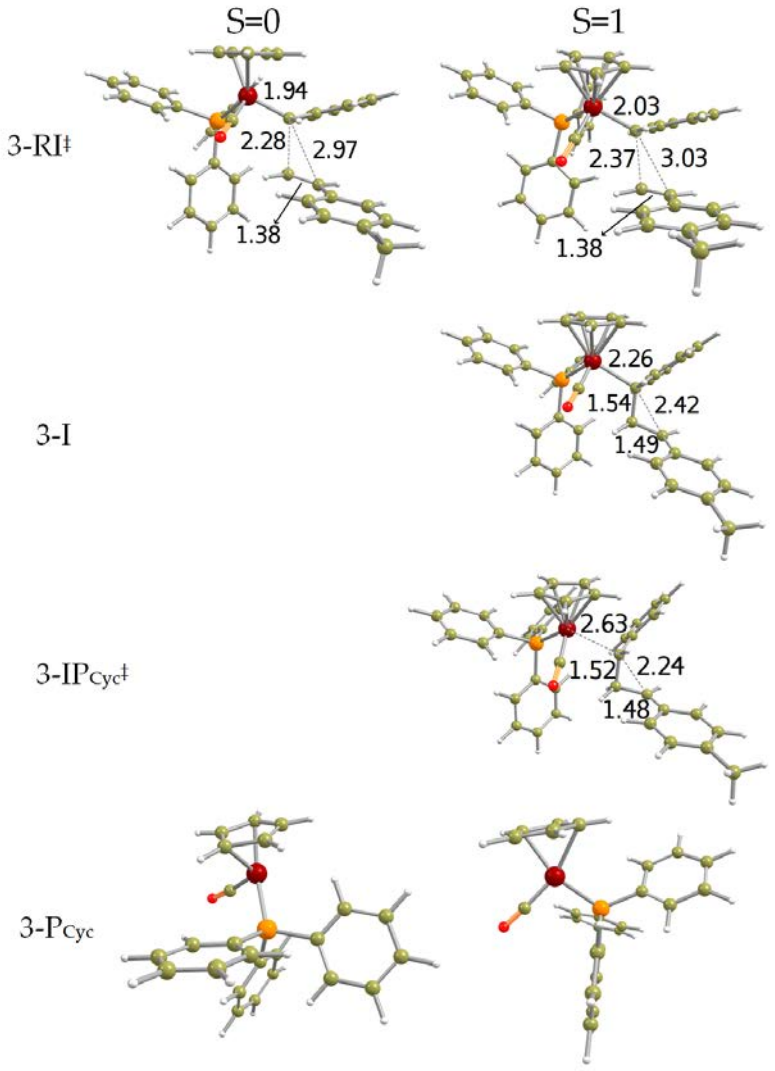

Figure 3.21: Optimized geometries for *carbene transfer* path, singlet and triplet, for Complex **3** with styrene. All distances in Å.

Evolution of the spin density along the path is exposed in Figure 3.22: in the TS $^3 3 - RI^{\ddagger}$ part of is on the carbon-α and carbon-γ. In the intermediate $^3 3 - I$ and in the TS $^3 3 - IPCyc^{\ddagger}$ it is more concentrated over the carbon-γ. This spin-density is now only α-density, unlike Catalyst **2**, where part of it was β-density. Apart from that, large part of the spin-density along the path is on the metal.

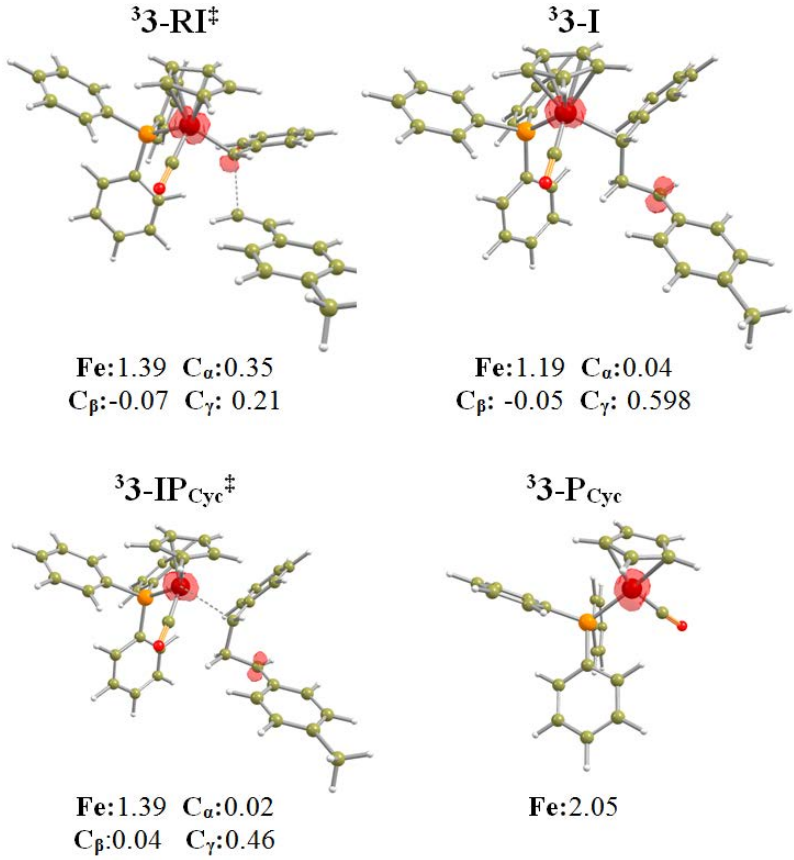

Figure 3.22: Spin-densities of triplet stationary species of *carbene transfer* of Catalyst **3** with styrene. Isosurfaces corresponds to α-spin density.

This stepwise mechanism in the triplet surface is similar to the case of Complex **1**. However, as in Complex **1**, it is more likely to not happen. Indeed, regarding the singlet 0surface, we have the $^1 3 - RI^‡$ transition state with a barrier of 22.7 kcal mol^{-1}, which is 21.0 kcal mol^{-1} smaller than $^3 3 - RI^‡$. The intrisic reaction coordinate of TS $^1 3 - RI^‡$ drives to a structure similar to what would be the $^1 3 - I$, but the free optimizations of this structure drives straight to the products of cyclopropanation. At this level of theory, we were not able to optimize any structure relative to a possible $^3 3 - IPCyc^‡$. Therefore, we believe the cyclopropanation occurs trough a single step concerted mechanism in the singlet state, in a two-electron process.

3.6 Pentacoordinated [Fe]=CH_2 bearing Heme Groups

Complex **4** also presents the common metallacyclobutane intermediate for olefin metathesis and cyclopropanation by reductive elimination, depicted in Figure 3.23.

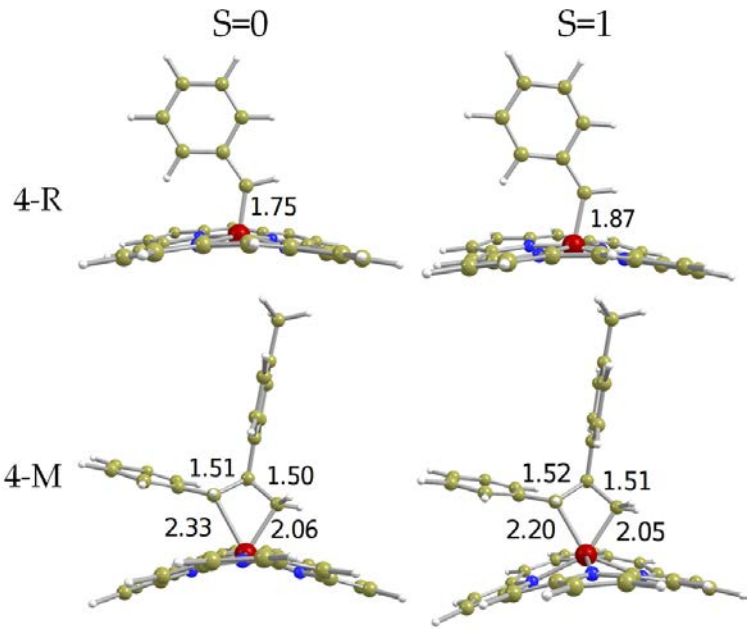

Figure 3.23: Optimized geometries of *cycloaddition* step, singlet and triplet states, for complex **4** with styrene. Distances in Å.

The metallacyclebutane singlet ($^1 4-M$) is 19.5 kcal mol^{-1} higher than the reactants, almost degenerate with the triplet ($^3 4-M$) which is only 3.3 kcal mol^{-1} higher in energy. This value is much higher in energy than the analogous with Grubbs catalysts $^1 1-M$ (10.0 kcal mol^{-1}). Moreover, we have not been able to find the transition states corresponding to the cycloaddition step neither. Obviously the cycloreversion transition state was not located either. Thus, neither metathesis nor cyclopropanation through this intermediate, are expected to occur with this catalyst.

Besides that, the carbene complex and the metallacyclobutane in the triplet state lye higher in energy than the corresponding singlet species, suggesting that they will not play a major role in the

cyclopropanation process. Consequently, from now on we will focus on the nucleophilic direct attack carbene transfer pathway. Computed Gibbs energy profiles in the singlet and triplet sates for such pathway are shown in Figure 3.24. The optimized structures are given in Figure 3.25.

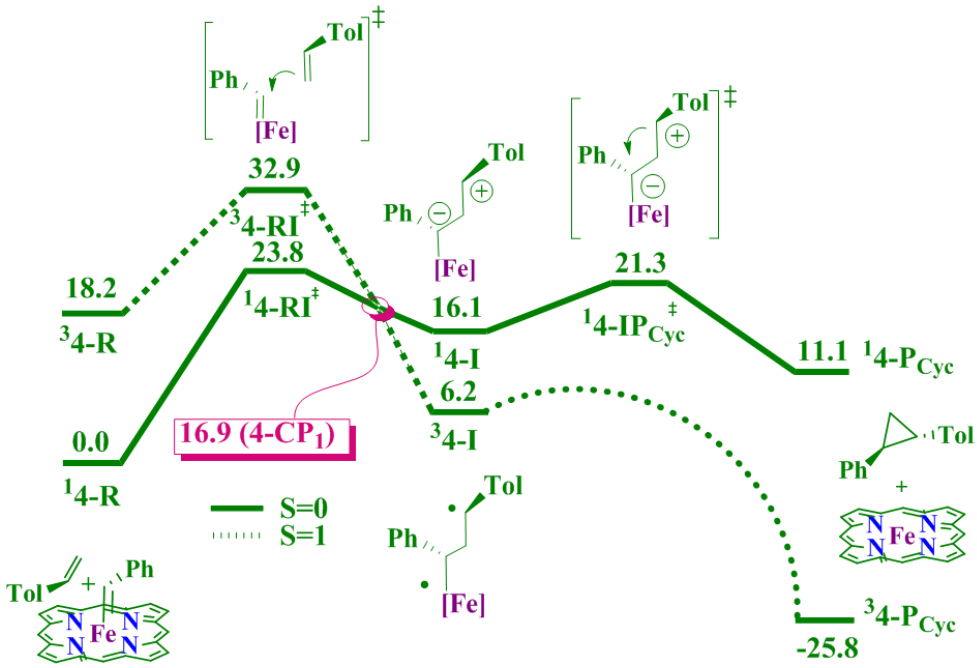

Figure 3.24: Gibbs energy profile (in kcal mol^{-1}) for *carbene transfer* involving **4** with styrene in both singlet and triplet states.

An overall analysis indicates that in the singlet state this path proceeds through an ionic-like intermediate, the energy barrier being 23.8 kcal mol^{-1}. Noteworthy, while the reactant ^3D-R and transition structure $^1D-RI^‡$ have a singlet ground state, the singlet-triplet relative stability changes in the intermediate, thereby indicating that a spin-crossing may occur upon formation of $D-I$. Indeed, a spin-crossing point at 16.9 kcal mol^{-1} above reactants has been localized (4-CP$_1$). This is different to that observed for Complex **3**, since in here the spin-crossing occurs previous to the formation of the intermediate.

Furtehrmore, from the triplet intermediate ^3D-I, cyclopropanation products are formed in an almost barrierless process: a relaxed potential energy scan covering the approach of carbons-α and β of

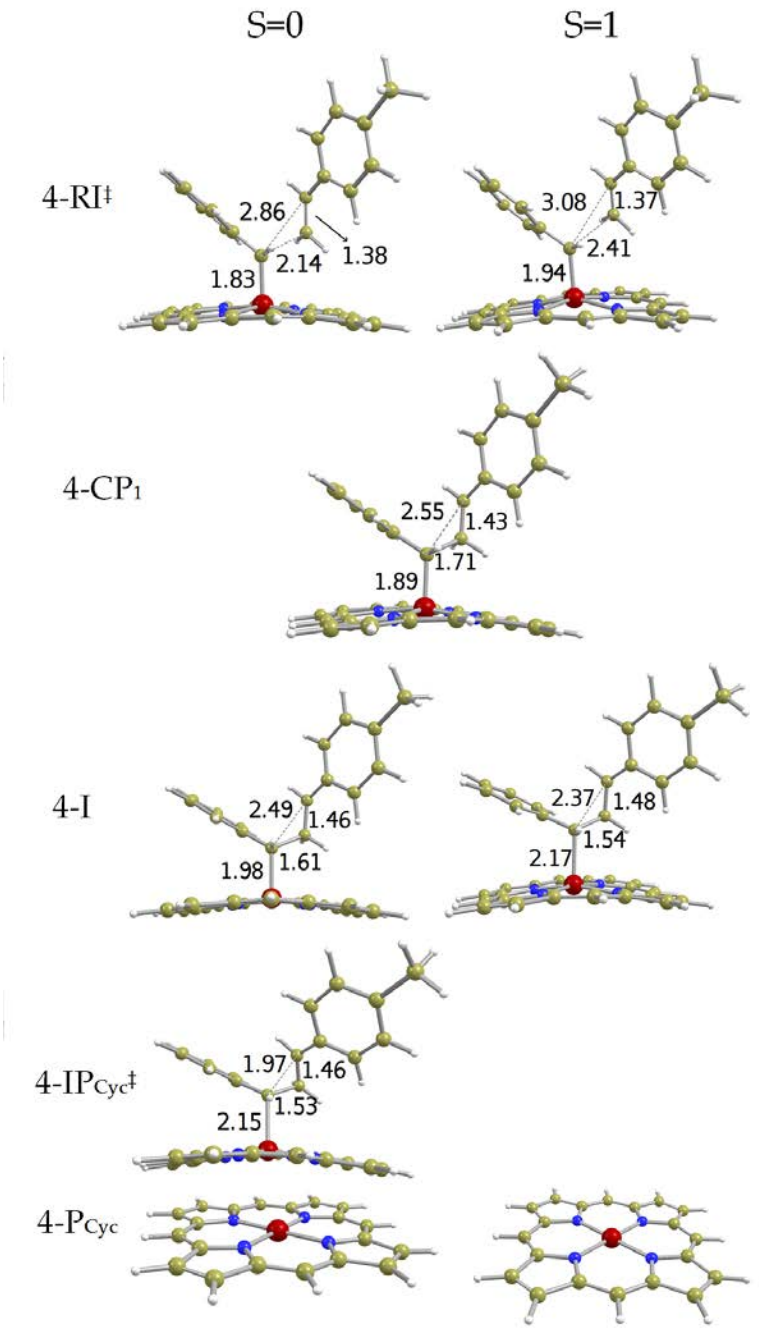

Figure 3.25: Optimized geometries for *carbene transfer* path, singlet and triplet, for Complex **4** with styrene. All distances in Å.

^3D-I yelds a virtually barrierless (0.3 kcal mol^{-1}) downhill curve culminating in the cyclopropane formation (see Figure B.4 of Appendices) In this way, this path can be faced as similar mechanism to the concerted one observed in the case of Catalyst **3**, but here it takes place in two different spin surface. The spin-density behavior (Figure 3.26) is similar to that of Complex **3** (Figure 3.22).

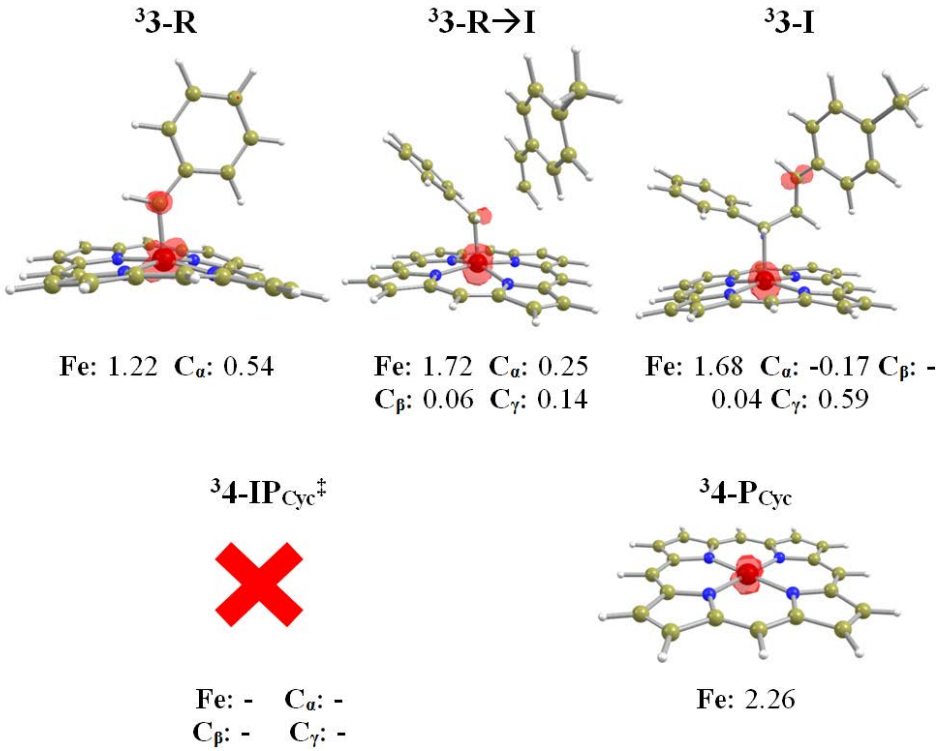

Figure 3.26: Spin-densities of triplet stationary species of *carbene transfer* of Catalyst **4** with styrene. Isosurfaces corresponds to α-spin density.

3.7 Stereoselectivity

In this chapter we are considering the *trans*-cyclopropane isomer of the cyclopropanation products that is 2.5 kcal mol^{-1} more stable than the *cis*-cyclopropane. Indeed, Catalyst **4** drive to major ratio of the trans-isomer.[167] However, experimental data show that in the case of the Catalyst **3** the principal product is *cis*-cyclopropane isomer.[148]

To conciliate these contrasting results, we calculate both *cis*- and *trans*-isomers for the rate determinant step for those mechanisms: $^1 3 - RI^{\ddagger}$ and $^1 4 - RI^{\ddagger}$, for cyclopropanation catalyzed by **3** and **4**, respectively. The results of such calculations are sumarized in Table 3.2.

Table 3.2: Relative stability and and Grimme's correction of the *cis*/*trans* isomers of the $^1 3 - RI^{\ddagger}$ and $^1 4 - RI^{\ddagger}$. Values in kcal mol^{-1}

	3		**4**	
Exp. Stereoselectivity	*cis*		*trans*	
	RI‡-*cis*	RI‡-*trans*	RI‡-*cis*	RI‡-*cis*
Grimme's Corr.	-73.6	-66.9	-59.1	-58.9
Relative Stability	0.0	7.9	0.0	-1.6

As expected, results show that $^1 4 - RI^{\ddagger}$-*cis* is less stable than $^1 4 - RI^{\ddagger}$-*trans*, by 1.6 kcal.mol^{-1}. However, for Catalyst **3**, the $^1 3 - RI^{\ddagger}$-*cis* is 7.9 kcal.mol^{-1} more stable than $^1 3 - RI^{\ddagger}$-*trans*. These data agrees with the experimental values regarding the stereoselectivity of cyclopropanation products, in both cases.

The unexpected large stability of species $^1 3 - RI^{\ddagger}$-*cis*, that implies in the *cis*-selectivity of the cyclopropanation products, can be attributed to larger non-covalent interactions in the transition structure. Non-covalente interactions can be measured by the Grimme's dispersion correction that are included in the total energy in the values used in this study. Such energies, for this especific case, are also shown in 3.7. As we can see, there is an important difference between the *cis*-*trans* pair for the case of complex **3**, which overcome the expected relative stability of the *trans* products. Whereas for complex **4**, the isomers *cis* and *trans* of $^1 4 - RI^{\ddagger}$ are virtually degenerated in energy, prevaling the *trans*-selectivity.

3.8 Final Remarks

The nature of metal-carbenes and their reactivity with olefins was studied in diferent spin states using a computational procedure by DFT means, with OPBE functional.

Results show that complexes **1**, **3** and **4** have a singlet ground state and **2** a triplet ground state. Furthermore, electronic structure analysis of the triplet state of the different catalysts shows that whereas for the Grubbs catalyst **1** the two unpaired electrons lye on the metal cation, for the iron carbene complexes there is an unpaired electron at the carbene, which may induce radical mechanisms.

As expected according to experimental data, the metathesis reaction is the preferred process with the Grubbs catalysts **1**, cyclopropanation by reductive elimination from the metallacyclobutane being kinetically less favorable. In contrast **2**, with a triplet ground state, is more prone to cyclopropanantion, through a two-step radical mechanism in which the two C-C bonds are sequentially formed (carbene transfer cyclopropanation).

Catalyst **3**, an 18 e^- complex, and Catalyst **4**, a porphirinic 16 e^- complex, have both a singlet ground state, and preferentially lead to cyclopropanation. For catalyst **3** cyclopropanation occurs through carbene transfer in a concerted mechanism in the singlet surface. For Complex **4** involves a birradical intermediate, in the triplet surface, has been located, albeit short lived considering that the cyclization process is essentially barrierless, resulting in a concerted-alike with singlet-triplet spin-crossing.

Overall, present results show that reactivity of iron-carbene complexes is very sensitive to the coordination around the metal center and the spin state of the metal-carbene complex.

4

Tetracoordinated Iron Carbenes

As already mentioned in previous Chapters, the main focus of this thesis is to advance in the design of iron-carbene able to perform olefin metathesis. Previously, in 3, we demonstrated the reactivities of the principal iron-carbenes experimentally reported with olefins, where we show that high-coordination of iron-carbene with piano-stool and porphyrin ancillary ligands prevents the formation of the intermediate metallacyclebutane, and the experimentally observed cyclopropanation takes place through electrophylic attack of the carbenic carbon to the olefin. We also saw that high spin iron-carbenes drive the reactivity towards cyclopropanation by a stepwise mechanism.

In this context, this Chapter and next aim at rationalizing how the nature of the ligands and geometries around the metal center, influence the ground state multiplicity, as well as the kinetics and thermodynamics of olefin metathesis and cyclopropanation products. The most promising set of ligands would favor the singlet state and disfavor alkene cyclopropanation in the singlet state.

4.1 Model and Approach

Cyclopropanation should be prevented when designing an iron carbene complex able to perform olefin metathesis. In this view, our computational strategy is similar to that of Rappé and Goddard when comparing alkene cyclopropanation *versus* olefin metathesis catalyzed by tungsten, molybdenum and chromium chlorine species.[270] However, we explored a larger combination of ancillary ligands as well as spin states for iron-carbenes.

In this Chapter we focus on tetracoordinated complexes with methylidene as carbene ($L_3M{=}CH_2$). Such a choice is based on the fact that the most active carbene in olefin metathesis are tetracoordinated. The use of methylidene as model carbene is to save computational resources and because methylidene carbene are active species of many olefin metathesis reactions.

For each complex, we computed the active form of the iron carbene, the metallacyclobutane resulting from the reaction with ethene , and the products of the cyclopropanation reaction, as represented in Scheme 4.1. In all cases, all potential spin states (S=0, S=1 and S=2) were considered. Noteworthy, although most of the iron carbenes considered in this work have not been reported before, we decided to use already reported ligands for constructing our models, or with small modifications.

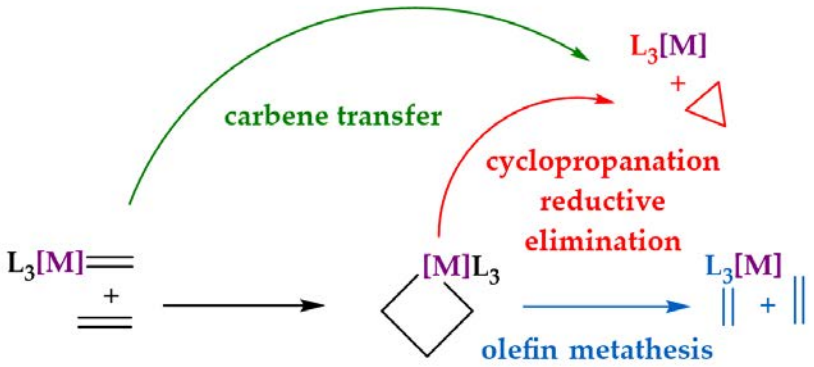

Scheme 4.1: Competing reactions Olefin Metathesis *versus* Cyclopropanation with a carbene methylene and ethene.

We localized the olefin metathesis reactants and products of olefin metathesis, as well as, the transition states for cycloaddition and cy-

cloreversion barrier for some selected systems. Please note that for this specific case of self-metathesis of methylidene with ethene, the transition states of cycloaddition and cycloreversion are the same. Based in the strategy of the previous Chapter, we considered two paths for cyclopropanation for those same selected systems: one path passing by the intermediate metallacyclebutane and subsequently reductive elimination, and the other by a electrophilic attack of the carbon carbenic to the olefin that for sake of clarity from now on we will call *carbene transfer* path. See in Scheme 4.1 the general scheme for these mechanisms.

4.2 Reference system

The purpose of this and next Chapter is the *in silico* design of iron carbenes aiming at make better the ratio olefin metathesis *versus* cyclopropanation. We want to reproduce, as much as possible, the characteristics and effectiveness of Grubbs catalyst. In this way, we report here the results of the reference system, which is a methylidene active species of the 2^{nd} Generation Grubbs catalyst, labelled as **5**.

In Chapter 3 we studied the reactivity for the singlet and the triplet for the Grubbs catalyst with usual phenyl substituent on the carbene and reactivity with *p*-methylstyrene. Now our model does not include any substituent as shown in Scheme 4.1, and thus we decided to re-address the study to take into account the effect of the carbene and ethene. Although the trends are kept, there are some several particularities of the smaller methylene carbene system that are worth to be mentioned.

The ability to undergo cyclopropanation and the non-low-spin states been more stable seems to be crucial in preventing the use of iron carbenes for metathesis, in this way our focus is on the energy difference between singlet and triplet state, as well as on the selectivity for alkene metathesis with respect to cyclopropanation.

Figure 4.1 shows the optimized geometries of the carbene, metallacyclobutane, and the metal fragment resulting from alkene cyclopropanation in the three spin states. The ground singlet state of carbene **5** shows a coordination around the metal center that lies between a tetrahedral and a butterfly structure.[271] This structure can be viewed as distorted octahedral with two vacant sites, as showed in Figure 4.2.

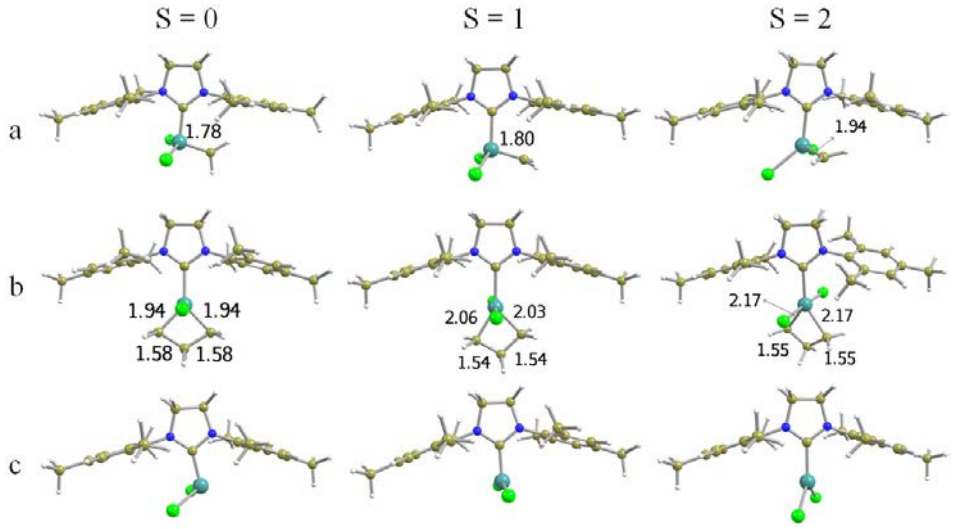

Figure 4.1: Optimized geometries of (a) 2^{nd} Generation Grubbs methylidene; (b) metallacyclobutane resulting from the cycloaddition of ethene; and (c) the metal fragment resulting from alkene cyclopropanation, in the three different spin states. All distances are in Å

The structure presents a wide Cl–Ru–Cl angle of 144.5°, while all other L-Ru-L angles are lesser than 103°. Interestingly, this coordination around the metal center changes significantly when changing the spin state. The triplet state lies 19.5 kcal mol^{-1} above the singlet state and shows a metal coordination intermediate between a tetrahedron and a trigonal pyramid with the carbene occupying the apical position. The C_{ene}–Ru–L angles are all smaller than 105°, and those involving the three basal ligands range from 111 to 123° degrees. The quintuplet state is even higher in energy and presents a pseudo-square planar geometry around the metal center (see Figure 4.1).

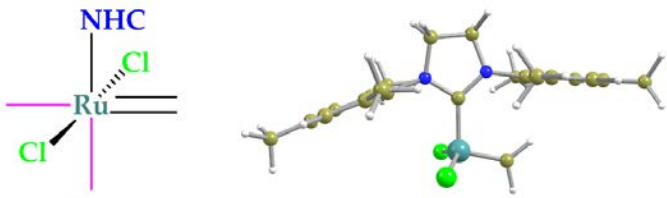

Figure 4.2: Octahedral-like distorted geometry of the carbene singlet of **5**. Pink sticks are the empty sites.

The singlet state metallacyclobutane arising from the reaction of the Grubbs complex with ethene is more stable than separated reactants ($\Delta G = -6.8$ kcal mol^{-1}). This value is in agreement with the experimental observation of this intermediate.[272,273] Moreover, the metallacyclobutane of **4** presents the well-described trigonal bipyramid (TBP) geometry around the metal center with long C_α–C_β bonds and a short Ru$\cdots C_\beta$ distance.[207,274,275] Again, the triplet state is significantly less stable (15.0 kcal mol^{-1} above the singlet state), and it presents a significantly different geometry. In this state, the coordination around the metal center is in between the TBP and the SBP with one of the C_α of the metallacyclobutane fragments being in a pseudo-apical position. This turns into a Ru$\cdots C_\beta$ distance that is significantly longer (2.57 *vs* 2.23 Å) and C_α–C_β bonds that are slightly shorter (1.54 *vs.* 1.58 Å) than those of the singlet state. Despite the puckered structure of the metallacyclobutane fragment found for the Mo and W species, these geometrical features recall those of the SBPs found for Mo and W catalysts, which have been proposed not to be involved in the metathesis pathway.[69,276] Finally, the quintet state is even less stable (54.3 kcal mol^{-1} over the singlet state) and presents a TBP structure with a metallacyclobutane fragment closer to that of the triplet state with large Ru$\cdots C_\alpha$ distance and normal C–C bonds.

For the Grubbs catalyst, the alkene cyclopropanation is endergonic if the singlet spin state is maintained along the reaction pathway ($\Delta G = +8.6$ kcal mol^{-1}), but it is significantly favorable if spin crossing occurs during the reaction and the triplet state is reached ($\Delta G = -7.4$ kcal mol^{-1}). This shows that although it is well-known that **4** catalyzes olefin metathesis reaction, cyclopropanation can be a competitive process, at least in the thermodynamic point of view.

Because this catalyst is our standard, we have also explored its reactivity regarding the paths that we similarly studied in 3. Transitions states for cycloaddition/cycloreversion were localised, as well as for cyclopropanation. For cyclopropanation two mechanisms were considered: by reductive elimination and carbene transfer. Figure 4.3 shows the energetics for the cycloaddition, forming metallacyclobutane, and subsequent cycloreversion to the olefin metathesis products, and also the competitive deactivation by reductive elimination yielding cyclopropanation products. Figure 4.4 shows the energetics for the carbene transfer path *via* olefin attack to the carbene. Optimized geometries are presented in Appendix C.2.

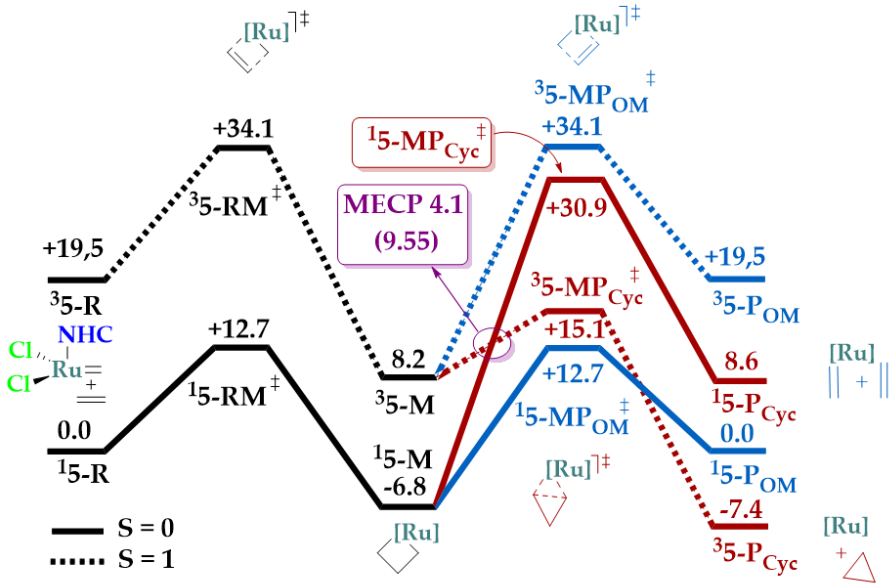

Figure 4.3: Gibbs energy profile (kcal mol^{-1}) for cycloaddition (black), cycloreversion to alkene metathesis (blue), and alkene cyclopropanation by reductive elimination (red), involving **5** with ethene.

In general, these profiles are similar to those discussed in the Section 3.3, however the values for barriers and intermediates are small, because here the substituents are smaller, thus less steric hindrance is present. In both mechanisms for cyclopropanation, in the singlet state, the higher barriers ($^1 5 - RM^{\ddagger}$ and $^1 5 - RI^{\ddagger}$) involve a transition state around 18 kcal mol^{-1}. In this context the cycloaddition ($^1 5 - RM^{\ddagger}$) and cycloreversion ($^1 5 - MP^{\ddagger}_{OM}$) transition states lies 12.7 kcal mol^{-1} above the reactants. This clearly shows that in spin state, metathesis is kinetically favoured. Such a kinetic preference for olefin metathesis was already highlighted by Bernardi and co-workers when performing DFT calculations with simplified models of first-generation Grubbs catalyst.[54]

Moreover, the transition state for cyclopropanation from the metallacyclobutane in the triplet state ($^3 5 - MP^{\ddagger}_{Cyc}$) is 2.4 kcal mol^{-1} higher in energy than that for metathesis in the singlet state. This value already suggests a preference for metathesis, but in addition to this, the cyclopropanation process imply a spin crossing, whose the MECP is located with a value of 9.6 kcal mol^{-1} over the reactants. As the exper-

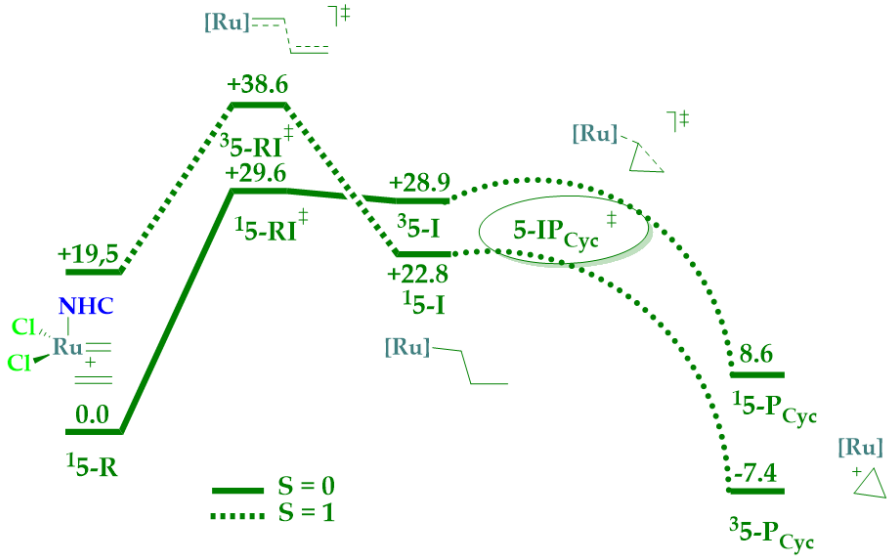

Figure 4.4: Gibbs energy profile (kcal mol^{-1}) for carbene transfer of **5** with the ethene.

imental results show that this complex is prone to olefin metathesis, the coupling to the crossing of the two potential energy surfaces must be difficult.

Regarding cyclopropanation by carbene transfer pathway, formation of the intermediate zwitterionic ($^1 5-I$) or biradical ($^3 5-I$) implies overcome a transition state ($^1 5-RI^{\ddagger}$) that are very high in energy: the singlet is 29.6 kcal mol^{-1} above the reactants, and the triplet ($^3 5-RI^{\ddagger}$) lies even higher. This suggests that this mechanism is less likelier to happen than the reductive elimination. Although we have been able to locate the intermediates, we did not find the transition states for cyclization (the hypothetical $5-IP^{\ddagger}_{Cyc}$), for neither singlet nor triplet spin state, suggesting that this is concerted carbene transfer.

Overall, a potentially active iron carbene should present a similar thermodynamics to that of **4**, that is, a singlet ground state for the metal carbene and the metallacyclobutane intermediate and barely favorable cyclopropanation process especially in the singlet state, in order to have a kinetic preference for alkene metathesis rather than cyclopropanation.

4.3 Stabilization of the singlet state in ML_4 Iron Carbenes

Once we established the reference energetics that our *in silico* designed iron carbene complex should have, we analyze the factors that determine the ground state multiplicity of iron carbene and iron-based metallacyclobutane species, as well as their tendency to undergo alkene cyclopropanation. Here we analyze the influence of the nature of the ancillary ligands that have been used experimentally in iron or other metal based complex. Rationalization of the key factors that need to be controlled and how ancillary ligands tune them will lead us to defining the most promising *in silico* designed carbenes with energetics similar to that of the Ru-based catalysts in the singlet state. For that, we first considered the complexes shown in Scheme 4.2.

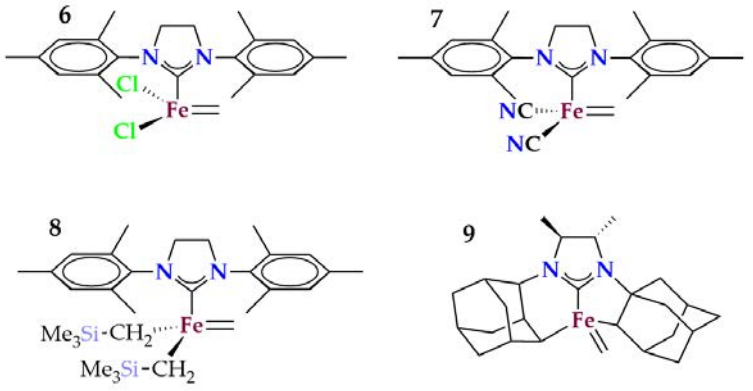

Scheme 4.2: *In-silico* studied $L_3Fe{=}CH_2$

Complex **6** is the obvious choice in which ruthenium is substituted by iron in the original 2^{nd} generation Grubbs complex. In complexes **7**–**9**, the two chlorine ligands of the original Grubbs catalyst have been substituted by two cyano, two neosilyl, or two adamantyl ligands. It is worth mentioning that the $(NHC)CH_2Si(CH_3)_3)Fe^{II}$ fragment of carbene **8** has already been described in the literature[277] and is representative of several complexes containing two alkyl groups and one N-heterocyclic carbene.[278,279] Moreover, ligands that are very similar to those used in complex **9** have also been synthesized,[280] and Grubbs

and co-workers have reported Ru-complexes bearing a chelating NHC-monoadamantyl ligand.[33,34] Table 4.1 summarizes the relative Gibbs energies of the singlet, triplet and quintuplet state of the carbene, metallacyclebutane and metal complex resulting from cyclopropanation for all considered species with respect to the carbene singlet state and ethene.

Table 4.1: Relative Gibbs (G_{gp} + D2) energies (in kcal mol^{-1}) of the species involved in the metathesis and cyclopropanation reactions of the Grubbs Ru complex **5**, and iron carbene complexes **6-9** with respect to the carbene singlet state and ethene.

complex	carbene			metallacyclebutane			cyclopropanation		
	S=0	S=1	S=2	S=0	S=1	S=2	S=0	S=1	S=2
5	0.0	19.5	49.1	-6.8	8.2	47.5	8.6	-7.4	9.7
6	0.0	-4.1	-5.2	-6.6	-13.2	-1.4	-9.8	-45.1	-57.9
7	0.0	4.5	n/a^a	-14.9	n/a^a	n/a^a	-1.6	-28.8	-35.0
8	0.0	5.5	9.9	16.1	6.7	3.6	-13.5	-28.2	-37.9
9	0.0	11.7	19.6	-0.3	-6.0	3.7	-6.0	-14.4	-9.0

[a] Optimizations leading to structures that do not correspond to carbene or metallacyclobutene species.

4.3.1 Complex based on 2nd Generation Grubbs Catalysts

Regarding complex **6**, the substitution of the ruthenium metal center by iron without modifying any of the ancillary ligands produces major effects on the relative stabilities of the different spin states both in the carbene and the metallacyclobutane. In contrast to what is obtained for ruthenium, the triplet and quintuplet spin states of the carbene are almost degenerate and are 4.1 and 5.2 kcal mol^{-1} lower in Gibbs energy than the singlet state. These values are close to the energies reported by Dixon and co-workers (0.0, −4.3, and −10.1 kcal mol^{-1} for the singlet, triplet, and quintuplet states, respectively) when performing CCSD(T) calculations with models including simplified ligands.[204]

The metallacyclobutane intermediate presents a triplet ground state that is 6.6 kcal mol^{-1} lower in Gibbs energy than the singlet. Finally, alkene cyclopropanation is thermodynamically much more favorable than for the analogous Ru-based Second Generation Grubbs catalysts, with values ranging from -9.8 to -57.9 kcal mol^{-1}, depending on the spin state. Optimized geometries of the carbene, metallacyclobutane, and the metal fragment resulting from alkene cyclopropanation in the three spin states are in the Figure 4.5.

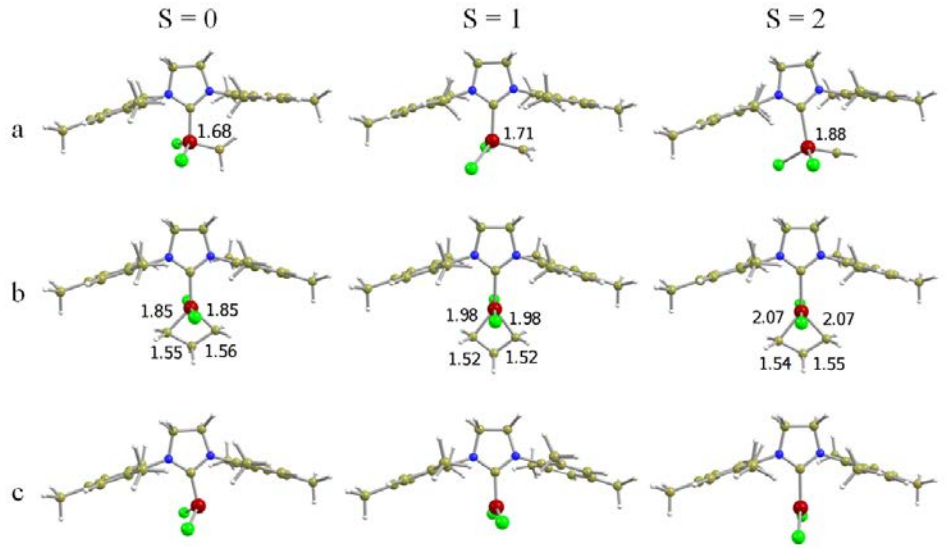

Figure 4.5: Optimized geometries of a) carbene; b) metallacyclobutane resulting from the addition of ethene and; c) the metal fragment resulting from alkene cyclopropanation in the three different spin states, for complex **6**.

Regarding the kinetics of olefin metathesis metathesis and cyclopropanation, showed in Figure 4.6, the trend showed in Section 3.4 appears also here: results show that cyclopropanation is kinetically favoured over metathesis, as evidenced by the energetics of the transitions structures in the ground triplet state, even considering the cyclopropanation through an intermediate metallacyclebutane, whose the transition state for the reductive elimination, in the triplet state ($^3 6 - MP^{\ddagger}_{Cyc}$), is almost 30 kcal mol^{-1} lower than olefin metathesis ($^1 6 - RM^{\ddagger}$). Indeed, this reductive elimination transition state is almost degenerate with the energy of the metallacyclebutane, in the triplet state, indicating a *quasi* barrierless process. The transition

state for reductive elimination in the singlet state was not found: a relaxed potential energy surface scan approaching the two carbon-α of the metallacyclebutane, shows a rapidly increasing of the energy (see Figure C.4 in Appendix)

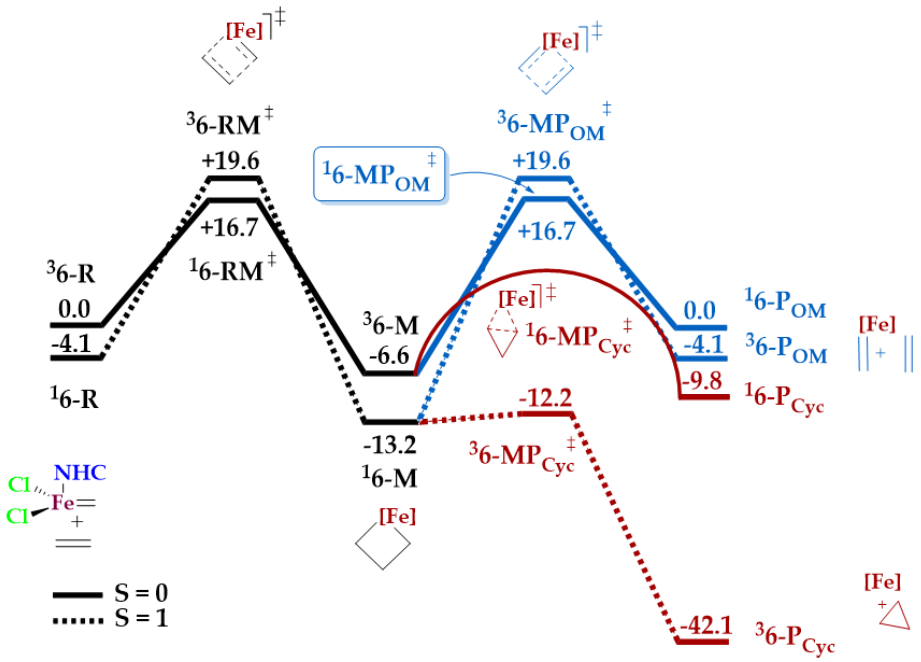

Figure 4.6: Gibbs energy profile (in kcal mol^{-1}) for metallacyclobutane formation (black), alkene metathesis (blue), and olefin cyclopropanation by reductive elimination (red) processes involving **6** and ethene.

Moreover, the cyclopropanation in this case is even easier through the carbene transfer mechanism, showed in Figure 4.7, as already observed in the previous Chapter. In this path, the higher barrier corresponds to the attack of the olefin to the iron-carbene, which lies at 14.9 kcal mol^{-1} ($^3 6 - RI^{\ddagger}_{Cyc}$), 2.0 kcal mol^{-1} lower than the transition state for cycloaddition that ranges from 16.7 ($^1 6 - RM^{\ddagger}$) to 19.6 kcal mol^{-1} ($^3 6 - RM^{\ddagger}$). This implies the no formation of the intermediate metallacyclebutane. Noteworthily, the singlet surface of this mechanism involves a concerted mechanism, since the IRC for the transition state $^1 6 - RI^{\ddagger}_{Cyc}$ evolves direct to cyclopropanation products. The geometries of the stationary points of these paths are pictured in the Figure 4.5 and Appendix C.2.

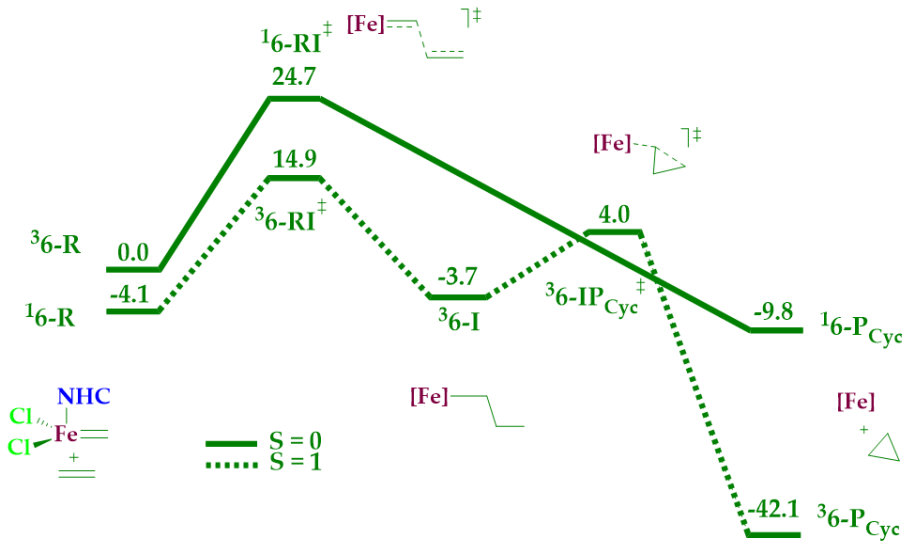

Figure 4.7: Gibbs energy profile (in kcal mol^{-1}) for alkene cyclopropanation by carbene transfer of **6** with ethene.

Overall, present calculations suggest that complex **6** would not catalyze alkene metathesis since the ground state of all intermediates are triplets, and alkene cyclopropanation is largely preferred, both thermodynamically and kinetically.

Replacing the two chlorines with strong field ligands is expected to stabilize the low spin state. Calculations were performed with chlorines substituted by cyano groups (complex **7**) and chlorines substituted by alkyl ligands complex **8**. The energetics of these complexes were presented in Table 4.1, and the geometries in Figure 4.8 and Figure 4.9, respectively.

According to those calculations, the ground spin states are singlet, 4.5 and 5.5 kcal mol^{-1} lower in Gibbs energy than the triplet, respectively. This indicates that strong donor ligands stabilize the singlet state enough to become the ground state for the carbene. Moreover, the fact that the cyano and alkyl ligands behave similarly suggest that this effect is mainly controlled by the σ-donation ability of the ligands and not by the back-donation to the π^* orbitals of the cyanide groups.

A similar effect should also be expected for the metallacyclobutane intermediate. However, this is not the case: in fact, the triplet and quintuplet states remain more stable than the singlet for **8**. For

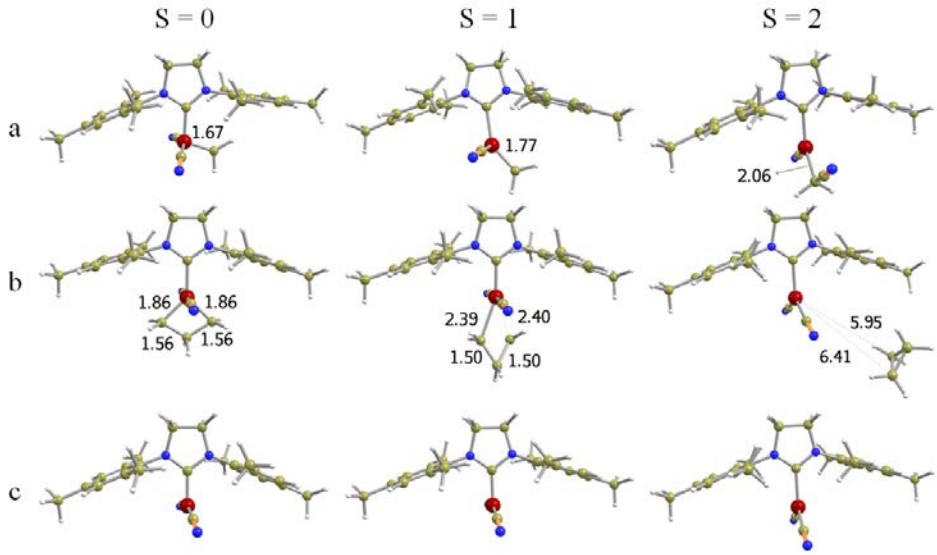

Figure 4.8: Optimized geometries of a) carbene; b) metallacyclobutane and; c) the metal fragment from alkene cyclopropanation in the three different spin states for complex **7**. All distances are in Å.

7 quintuplet state structures lead directly to cyclopropanation. Moreover, for the particular case of **8**, the metallacyclobutane in the singlet state is much higher in Gibbs energy than separated reactants (ΔG = 16.1 kcal mol^{-1}). This suggests that **8** would not undergo metathesis easily, since efficient catalysts are known to present reaction intermediates that are close in Gibbs energy to separated reactants.

It is worth mentioning that optimizations of the carbene and metallacyclebutane in the quintuplet state of Complex **7** lead to different structures: in the former, the carbene bound to the adjacent cyanide ligands, while in the later the metallacycle evolves to the cyclopropanation products, as can be seen in Figure 4.8.

Finally, although in general the addition of σ-donor ligand slightly destabilizes the thermodynamics for the alkene cyclopropanation, this process is still strongly favoured. These data, therefore, indicate that the inclusion of strong σ-donor ligands could be useful for obtaining singlet state carbenes, but does not seem to be sufficient to obtain a carbene potentially active for metathesis.

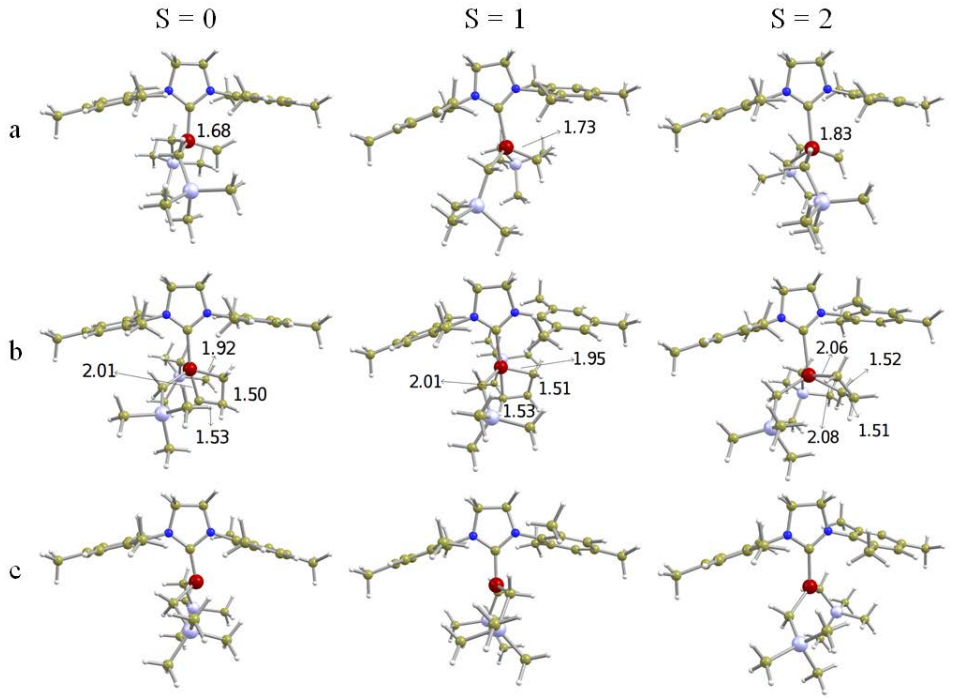

Figure 4.9: Optimized geometries of a) carbene; b) metallacyclobutane and; c) the metal fragment from alkene cyclopropanation in the three different spin states for complex **8**. All distances are in Å.

4.3.2 Chelating σ-donating ligands

The use of chelating ligands in alkene metathesis has been shown to highly influence the catalytic activity and selectivity of both Schrock and Grubbs type complexes.[33,34,281–284] Thus, starting from the previously obtained results, we would like to stabilize the metallacyclobutane intermediate and disfavor alkene cyclopropanation. Inspired in the findings of Veige and co-workers, who showed that the use of tridentate ligands can stabilize the metallacyclobutadiene intermediate in alkyne metathesis,[285] we explored the possibility of using strong σ-donor tridentate ligands such as those in complex **9**, whose optimized geometry are shown in Figure 4.10, and the energetic in Table 4.1.

We thought that this chelating ligand could stabilize the metallacyclobutane intermediate and eventually make cyclopropanation less favorable by destabilizing the metal fragment product. Results show that the methylidene species of **9** present a singlet ground state with

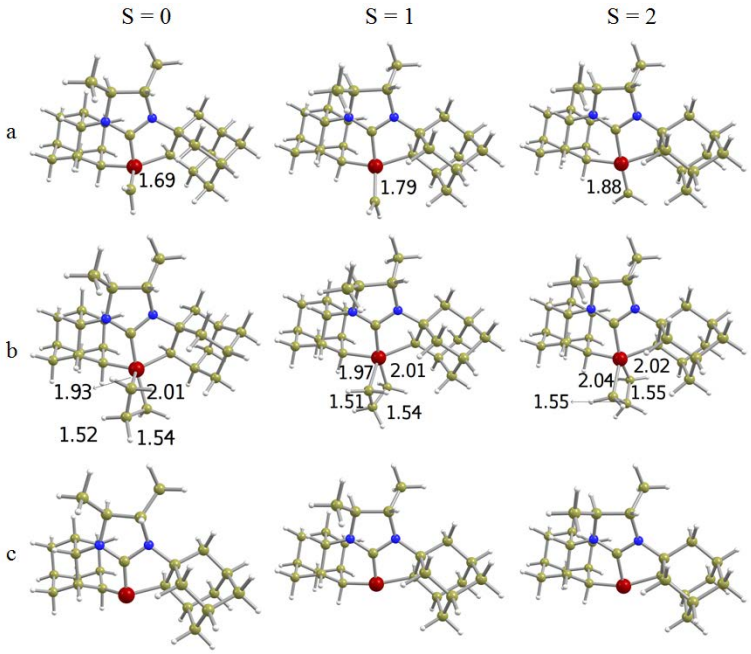

Figure 4.10: Optimized geometries of a) carbene; b) metallacyclobutane and; c) the metal fragment from cyclopropanation in three different spin states, for complex **9**. All distances are in Å

the same butterfly structure as all other complexes with donating σ-ligands (see geometries of **5-8**). In addition, the metallacyclobutane has essentially the same Gibbs energy than separated reactants (-0.3 kcal mol^{-1}), thus suggesting that this complex may be more prone to undergo metathesis than those discussed previously (**7** and **8**), even though the ground state for the metallacyclobutane is still the triplet.

Finally, the reaction energy for cyclopropanation in the singlet state is -6.0 kcal mol^{-1} and -14.4 kcal mol^{-1} in the triplet state, indicating a less favorable cyclopropanation process than that for **8**. Overall, **9** appear to exhibit better features for metathesis than the previous carbene complexes. It is for this reason that we decided to explore the kinetics for complex **9**, whose results are shown in Figure 4.11.

The transition state structure associated with the alkene metathesis in the singlet state ($^1 9 - RM^{\ddagger}$) lies 18.9 kcal mol^{-1} above the metallacyclobutane ($^1 9 - M$), indicating that the process may be feasible, but not as much as those involving Ru-based catalysts. In this cycload-

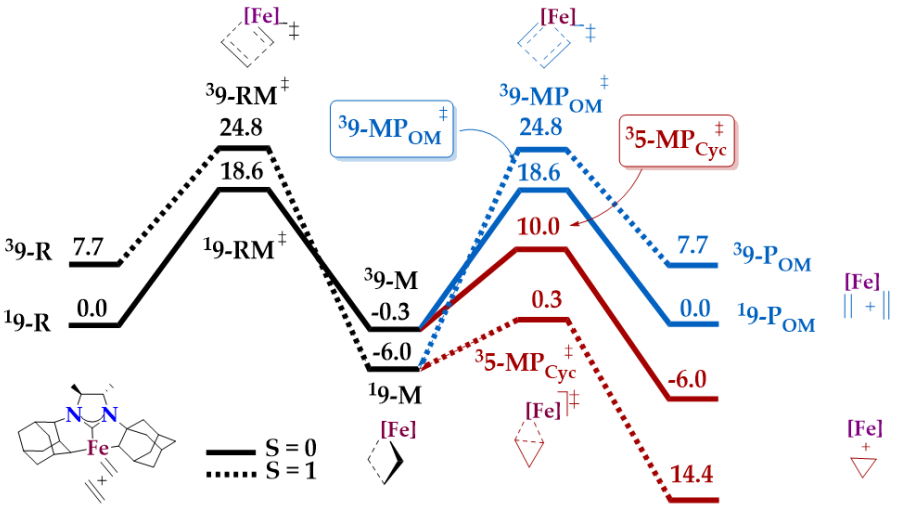

Figure 4.11: Gibbs energy profile (in kcal mol^{-1}) for metallacyclobutane formation (black), alkene metathesis (blue), and alkene cyclopropanation (red), involving **9** with ethene in both singlet and triplet states.

dition process, the transition state singlet ($^1 9 - RM^{\ddagger}$) is more stable than triplet ($^3 9 - RM^{\ddagger}$), but for the subsequent stationary point – metallacyclobutane – the triplet structure ($^3 9 - M$) is more stable. This suggests the presence of a spin crossing between the two surfaces, which we localized at 1.8 kcal mol^{-1} over the metallacyclobutane in the triplet state ($^3 9 - M$)–(**MECP 9.1**) Those geometries are shown in Figure 4.12.

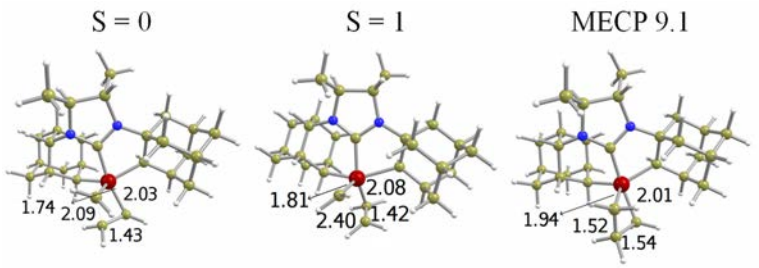

Figure 4.12: Optimized geometries of TS of cycloaddition, singlete and triplete, and the MECP 9.1, corresponding to the cycloaddition/cycloreversion of **9** with ethene. All distances are in Å.

However, the key point is that for **9**, alkene cyclopropanation presents low transition state structures both in the triplet and singlet states. In particular, the transition state structure for cyclopropanation by reductive elimination in the singlet state ($^1 9 - MP^{\ddagger}_{Cyc}$) is 8.6 kcal mol^{-1} lower than the transition state for metathesis, and the analogous transition state in the triplet state ($^3 9 - MP^{\ddagger}_{Cyc}$) is even lower. The optimized geometries for transition state for reductive elimination process are shown in Figure 4.13.

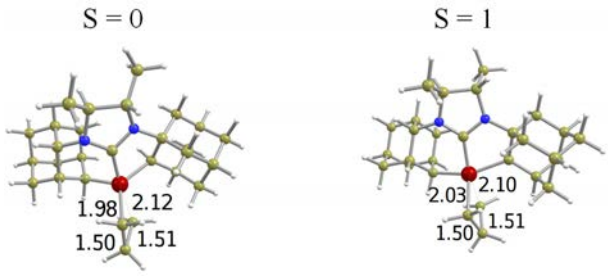

Figure 4.13: Optimized geometries of transition states, singlete and triplete, for cyclopropnation by reductive elimination from the metallacyclebutane formed with **9** and ethene. All distances are in Å.

Figure 4.14 shows the Gibbs energy profile for carbene transfer process with its associated optimized stationary points in Figure 4.15

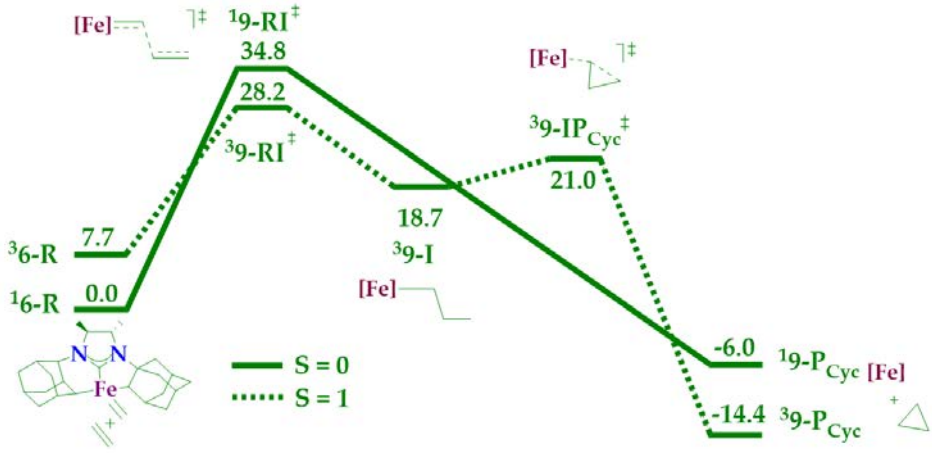

Figure 4.14: Gibbs energy profile (in kcal mol^{-1}) for carbene transfer mechanism of **9** with ethene.

Cyclopropanation following this path present the highest barrier around 10 kcal mol^{-1}($^3 9 - RI^{\ddagger}$) over the transition state for cycloaddition that forms the metallacycle, therefore implying in the feasibility of this intermediate. However the barriers in this path are larger of those for cyclopropanation by reductive elimination, that after all, is the preferred path. Noteworthy this path imply in a spin-crossing between the singlet and triplet surface prior the olefin attack transition state and, again, while the triplet state pathway is stepwise, in the singlet is concerted.

Overall, complex **9** is not suitable for alkene metathesis, where some main drawbacks can be identified:

(i) The metallacyclobutane intermediate has a triplet ground state;

(ii) alkene cyclopropanation is still favorable both in the singlet and triplet states.

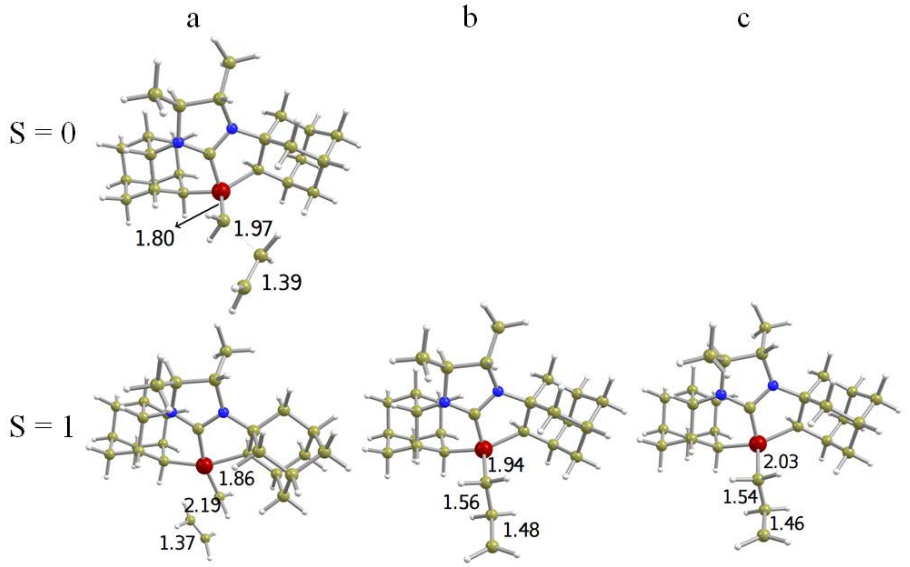

Figure 4.15: Optimized geometries of singlet (if exists) and triplet states for the stationary points (a) $9-RI^{\ddagger}$, (b) $9-I$, and (c) $9-IP^{\ddagger}_{Cyc}$, of the carbene transfer path of **9** with ethene.

Isomers of Adamantyl based Complexes

Complex **9** can present several different isomers depending on the size of the ring formed by the metal center, the NHC central ligand, and each of the adamantyl groups that act as terminal ligands. Before we discussed about non-symmetric tridentate ligand which contains one 5-membered ring and one 6-membered ring.

However we decided to study the relative stabilities of the singlet, triplet and quintuplet spin states for the probable isomers of **9** that contain either two 5-membered rings ($\mathbf{9}_{55}$) or two 6-membered rings ($\mathbf{9}_{66}$), to analyze if there is an important chelating effect related to the size of the ring. With the aim of separating, as much as possible, the electronic effects of each ring size from the sterics of the ligands, we also considered simplified models of **9** and their isomers $\mathbf{9}_{55}$ and $\mathbf{9}_{66}$ in which the steric constraints of the adamantyl are reduced by substituting them by methyl groups. These later complexes are referred as **9'** (5 and 6 membered ring), $\mathbf{9'}_{55}$ (two 5-membered rings) and $\mathbf{9'}_{66}$ (two 6-membered rings).

Table 4.2 reports the relative stabilities of the different spin states for all isomers of **9** and **9'** as well as the relative energies of isomer $\mathbf{9}_{55}$ and $\mathbf{9'}_{66}$ regarding the singlet **9**. Figure 4.16 shows the optimized geometries for all complexes except **9** that can be found in Figure 4.10. It is, obviously, pointless to compare the relative energy of the structures in the different spin states between **9** and **9'** because the models have a different number of atoms.

Table 4.2: Relative Gibbs (G_{gp}+D2) energies (in kcal mol^{-1}),with respect to the singlet, of the different spin states of the metal carbene for isomers $\mathbf{9}_{55}$ and $\mathbf{9}_{66}$ derived from **9**, as well as their simplified models derived of **9'**. Relative stabilities of the different spin states species regarding the most stable **9** isomer are given in parenthesis.

complex	singlet	triplet	quintuplet
9	0.0	7.8	19.6
9'	0.0	9.7	24.5
$\mathbf{9}_{55}$	0.0 (8.4)	-2.1 (6.3)	12.1 (20.5)
$\mathbf{9'}_{55}$	0.0	7.6	26.0
$\mathbf{9}_{66}$	0.0 (6.2)	9.8 (16.0)	22.5 (28.7)
$\mathbf{9'}_{66}$	0.0	10.2	20.5

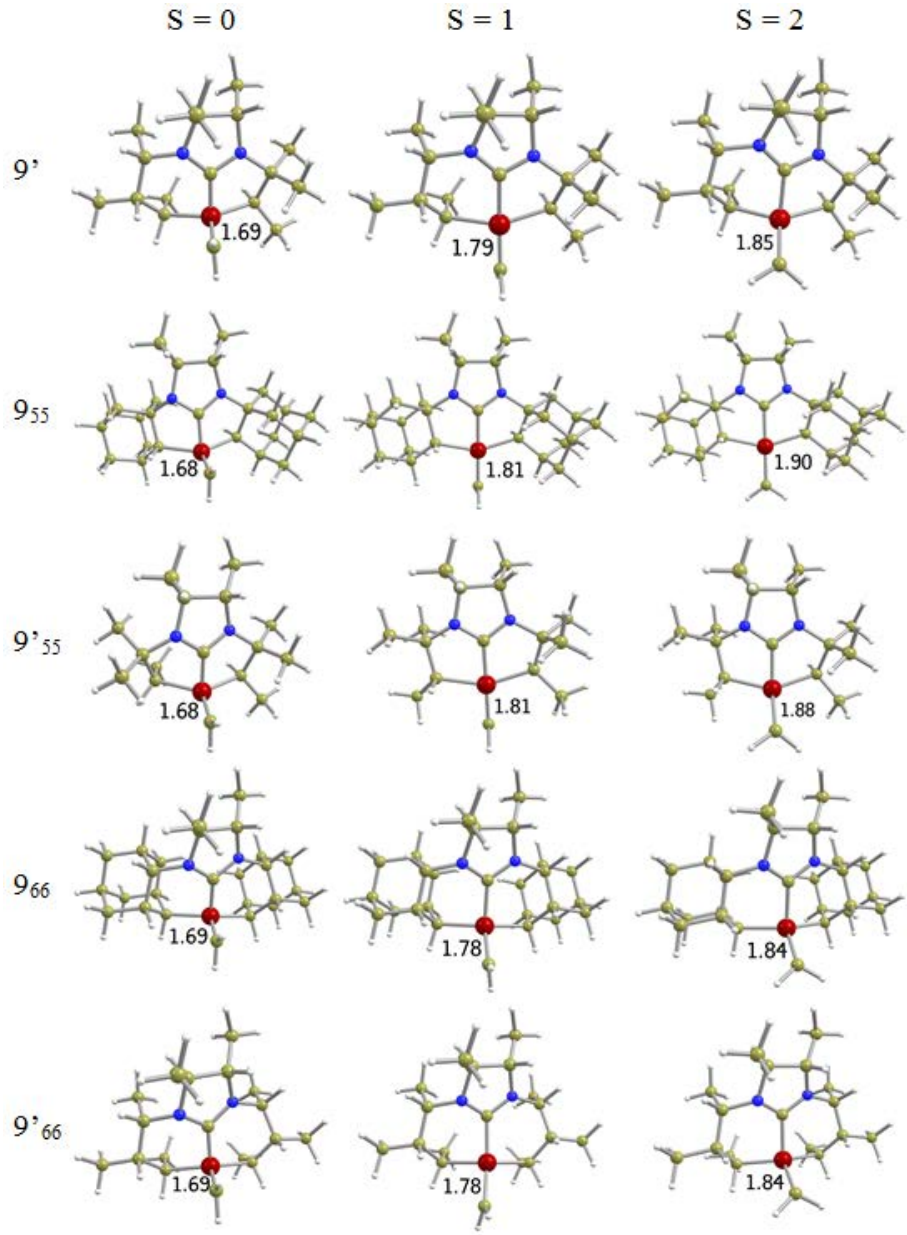

Figure 4.16: Optimized geometries of metal carbene complexes in the three different spin states for the isomers of **9** ($\mathbf{9}_{55}$ and $\mathbf{9}_{66}$) as well as those of the simplified models **9'**,$\mathbf{9'}_{55}$ and $\mathbf{9'}_{66}$. All distances are in Å.

Results show that isomer **9** is more stable than $\mathbf{9}_{55}$ and $\mathbf{9}_{66}$, the most stable singlet state of **9** being at least 6.2 kcal mol^{-1} more stable

than any of the spin states of the other isomers ($\mathbf{9}_{55}$ and $\mathbf{9}_{66}$). Moreover, the preference for the singlet state is very similar for **9** and $\mathbf{9}_{66}$, the Gibbs energy difference between the singlet and the triplet state being 7.8 and 9.8 kcal mol^{-1}, respectively. In contrast, the $\mathbf{9}_{55}$ isomer presents a triplet ground state, the energy difference between the triplet and quintuplet states indicating that this is more likely due to a destabilization of the singlet state rather than a stabilization of the triplet.

The results of the simplified models allow us to rationalize the discrepancy between **9**, $\mathbf{9}_{66}$ and $\mathbf{9}_{55}$ isomers. As it is shown in Table 4.2, once the steric influence of the adamantyl ligand is reduced, the **9'**, $\mathbf{9'}_{66}$ and $\mathbf{9'}_{55}$ isomers behave similarly and they all show an important preference for the singlet state of about 7.5 to 9.4 kcal mol^{-1}. This suggests that isomer $\mathbf{9}_{55}$ should be considered an exception.

Thorough analysis of the conformations of the two 5-membered ring in $\mathbf{9}_{55}$ and $\mathbf{9'}_{55}$ evidences that there is only a noticeable difference between the two models in the singlet state. In fact, while in the singlet state of $\mathbf{9'}_{55}$ the two rings are puckered towards the carbene, for the case of singlet state of $\mathbf{9}_{55}$ the two rings are puckered in opposite sides of the plane defined by the two rings. We associate this fact to the steric hindrance of the adamantyl groups that prevents the most stable conformation.

Further support for this interpretation is obtained when performing a constrained optimization of $\mathbf{9'}_{55}$ model, fixing the 5-membered ring conformations as those in the case of $\mathbf{9}_{55}$ species. Results show that even for the simplified model the conformation in $\mathbf{9}_{55}$ produces a significant destabilization of the singlet state of about 5.9 kcal mol^{-1}, which is in the range of the expected destabilization of the singlet state in $\mathbf{9}_{55}$.

Overall, the behaviour of tridentate ligands formed by one central NHC group and two terminal alkyl groups seems to be very similar and does not depend on the size of the ring, unless other steric factors play role as it is the case of $\mathbf{9}_{55}$.

4.4 Stabilization of the Metallacyclobutane Singlet State

Because σ-donating alkyl groups containing chelating groups stabilize the intermediate metallacyclebutane (**9**) more than the free alkyl groups (**8**), we decided to study this kind of ancillary ligand in order to favor the intermediate metallacyclebutane singlet.

Alkyl, chlorines and cyanides are negatively charged species, and carbene and NHC ligands are neutral. As the global charge in the complexes **5-10** is zero, the oxidised state of iron center of the active species carbene is 2+, while it is oxidate to 4+ in the metallacyclebutane. In this case, as the catalysts has formally six electrons around the iron in the carbene, in the metallacyclebutane it will have four electrons.

A molecular orbital analysis of the TBP and SBP structures of ML_5 metallacycle coordination environments (see Figure 4.17) shows that low spin complexes of d^4 metal ions with a TBP structure will present a singlet ground state, while those having a SBP coordination geometry would favor a triplet spin ground state. This agrees with the observation that most metallacyclobutane optimized geometries have a TBP structure for the singlet state and a distorted SBP one for the triplet state.

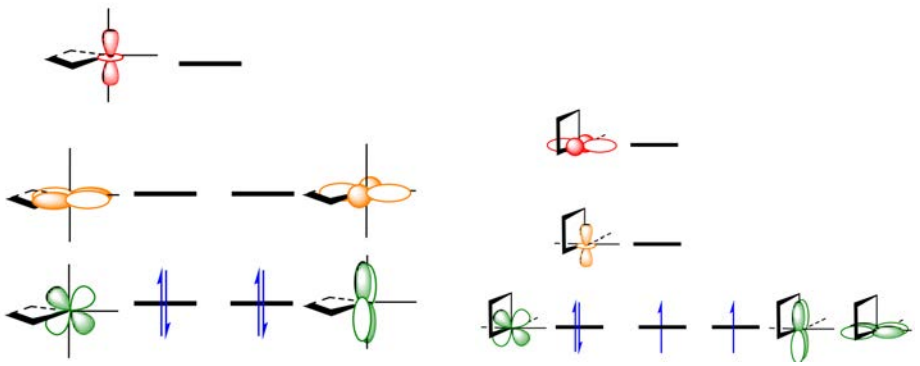

(a) Trigonal Bipyramidal (TBP) (b) Square Based Pyramid (SBP)

Figure 4.17: Molecular orbital diagrams of d^4 ML_5 TBP and SBP metallacyclobutane intermediates.

Therefore, in order to obtain a singlet state metallacyclebutane, one has to destabilize the SBP structures. This can be achieved by changing the nature of the chelating ligand. The two terminal coordinating groups of the tridentate ligand are in *trans*-arrangement in both the SBP and TBP structures. The central coordinating group is *trans* to one of the carbon atoms of the metallacycle in the SBP and has no ligand in trans in the TBP. Therefore, the proper chelating ligand that favours SBP geometry should have a strong donating central group to destabilize the SBP structure. This strong σ-donating ligand will exert a *trans*-influence on one of the alkyl groups of the metallacyclebutane in the SBP geometry, destabilizing it. In contrast, since there is not a ligand in the *trans*-position in the TBP geometry, the presence of the akyl ligand will not influence it as much as the SBP. In this view, we have explored the reactivity of complexes **10**–**13** defined in Scheme 4.3. All these carbenes have an alkyl ligand in the central position of the pincer ligand.

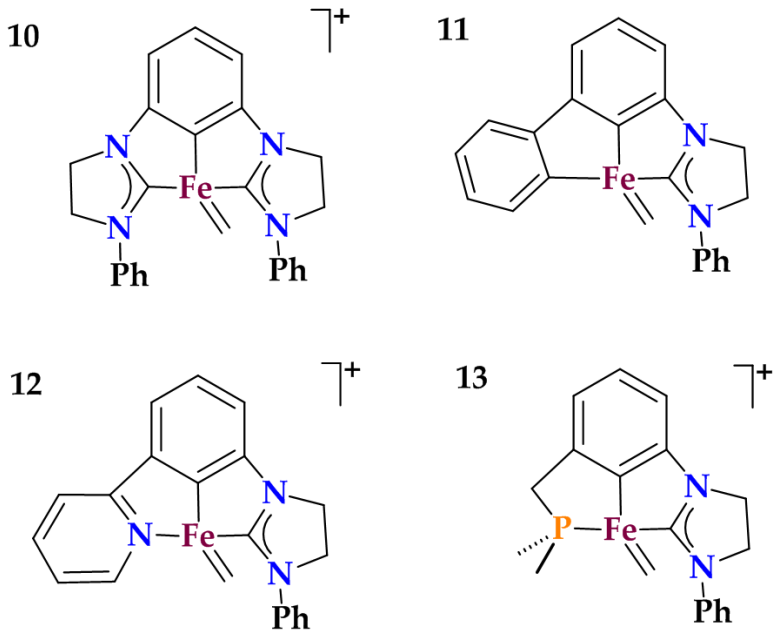

Scheme 4.3: *In silico* studied pincer-containing $L_3Fe{=}CH_2$

Complexes **10**, **12**, and **13** are positively charged and may not look appropriate as catalysts. However, it is worth mentioning that other charged catalysts have been reported for olefin metathesis, and

they show very good activities.[286] The ligand of complex **10** has been reported in the literature[287] for its use with other transition metals. The ligands of complexes **11-13** are variations explored with the aim of evaluating the role of the σ-donating ability of the terminal coordinating groups.

Table 4.3 shows the thermodynamics for alkene metathesis and alkene cyclopropanation for complexes **10-13** and includes the values of reference system **5**. The optimized geometries of the carbenes, intermediate metallacyclebutane and the iron fragment of cyclopropanation are shown in Figures 4.18-4.21.

Table 4.3: Relative Gibbs (G_{gp} + D2) energies, in kcal mol^{-1}, of the species involved in the metathesis and cyclopropanation reactions of the Grubbs Ru complex **5**, and iron carbene complexes **10-13** with respect to the carbene singlet state and ethene.

complex	carbene			metallacyclebutane			cyclopropanation		
	S=0	S=1	S=2	S=0	S=1	S=2	S=0	S=1	S=2
5	0.0	19.5	49.1	-6.8	8.2	47.5	8.6	-7.4	9.7
10	0.0	4.3	26.9	-13.5	-5.9	3.4	8.9	-20.2	-9.8
11	0.0	3.8	21.0	-11.3	-11.8	0.1	10.1	-22.3	-11.0
12	0.0	6.2	22.7	-18.6	-9.9	-0.6	8.3	-25.4	-11.7
13	0.0	2.7	24.1	-15.2	-10.5	-1.7	11.4	-22.5	-10.8

As for complexes **7;-9**, the strong σ-donating ability of the ligands in complexes **10-13** favors a ground singlet state for the carbene, with the energy difference between the singlet and the triplet lying between 2.7 and 6.2 kcal mol^{-1}. Besides that, the presence of an alkyl group *trans* to one of the carbon atoms of the metallacyclobutane in the SBP structure produces a general destabilization of the triplet state, thus leading also to a singlet ground state for the metallacyclobutane except for complex **11**, which is the only complex with two alkyl groups.

The largest preference for the singlet metallacyclobutane is found for complex **12**, the one presenting the weakest σ-donating ligand in one of the terminal positions. All singlet state metallacyclobutanes are between 11.3 and 18.6 kcal mol^{-1} lower in energy than the separated reactants, showing reasonable albeit slightly too negative energetics for being involved in a catalytic process.

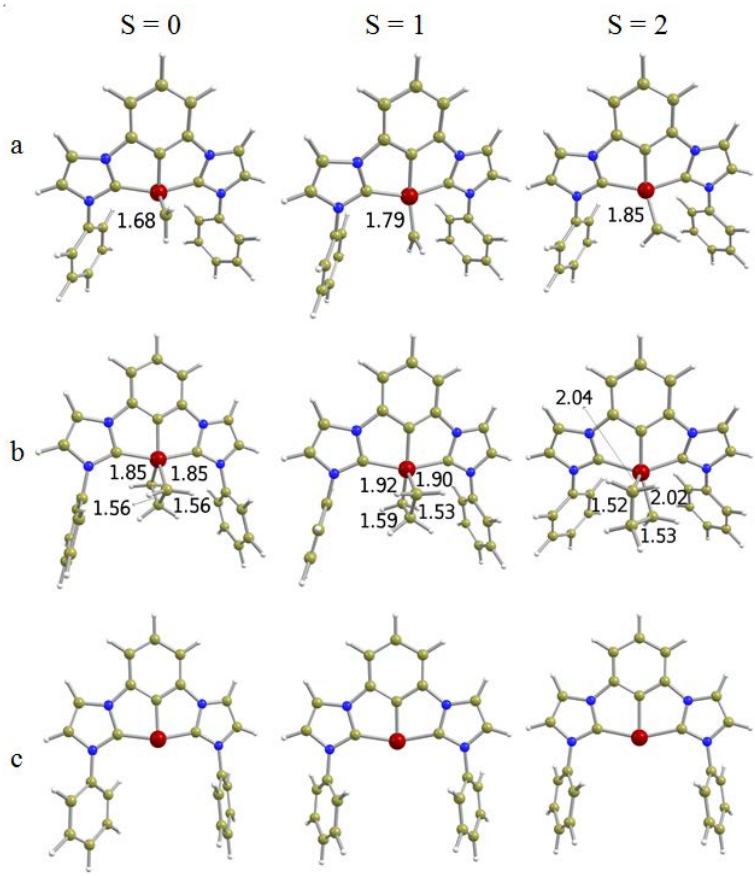

Figure 4.18: Optimized geometries of a) carbene; b) metallacyclobutane and; c) the metal fragment from alkene cyclopropanation in the three different spin states, for complex **10**. All distances are in Å

Overall, these complexes bearing pincer-type ligands are characterized by both a carbene and metallacyclobutane intermediate with a singlet ground state and the associated thermodynamics for the metallacyclobutane formation close to that of an efficient catalyst such as **5**.

Furthermore, alkene cyclopropanation in the singlet state is strongly disfavored when compared to that of the other iron complexes analyzed before, and becomes endergonic (ΔG ranging between 8.3 and 11.4 kcal mol^{-1}). These values are also close to that of the very efficient ruthenium Grubbs catalyst for which alkene cyclopropanation is computed to present a ΔG of 8.6 kcal mol^{-1}.

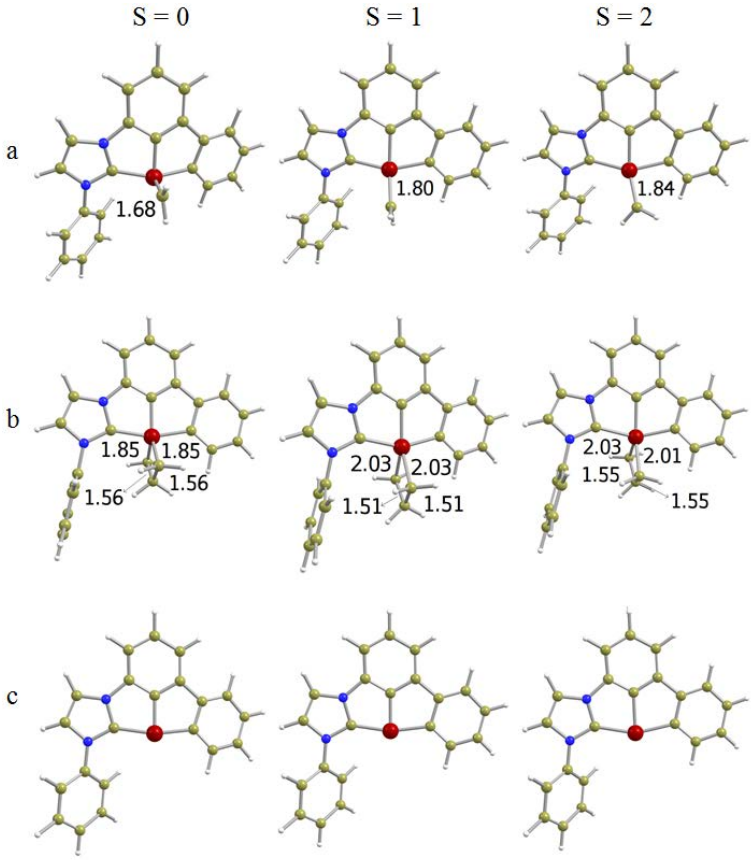

Figure 4.19: Optimized geometries of a) carbene; b) metallacyclobutane and; c) the metal fragment from alkene cyclopropanation in the three different spin states, for complex **11**. All distances are in Å

Alkene cyclopropanation is significantly favored thermodynamically in the triplet state, the energy differences between the cyclopropanation products and initial reactants ranging between −20.2 and −25.4 kcal mol^{-1}. These values are still between 12 and 17 kcal mol^{-1} lower than the values for the alkene cyclopropanation of the Grubbs ruthenium complex in the triplet state.

Present calculations suggest that changing one of the NHC terminal ligands by weaker σ-donor groups such as pyridine or phosphine would favor the metallacyclobutane singlet state without stabilizing the alkene cyclopropanation in the singlet state. Unfortunately, the same substitution does not seem to disfavor the cyclopropanation in

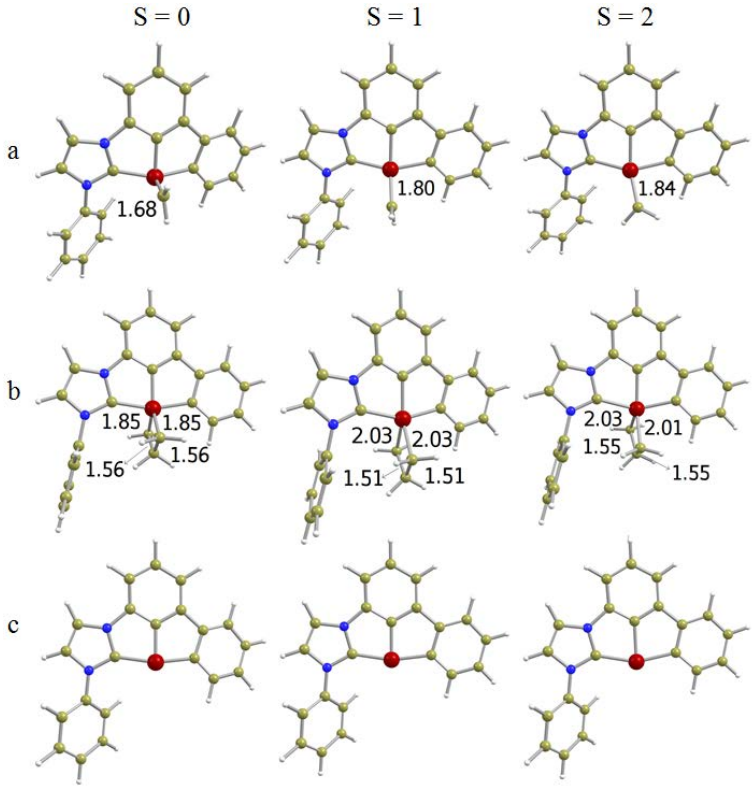

Figure 4.20: Optimized geometries of a) carbene; b) metallacyclobutane and; c) the metal fragment from alkene cyclopropanation in the three different spin states, for complex **12**. All distances are in Å

the triplet state. Therefore, the design of the proper catalyst would require a subtle control of how easy spin crossing is and how strong alkene cyclopropanation has to be destabilized in both spin states.

Complexes **10** to **13** accomplish several requirements that an iron carbene should fulfil for catalyse the alkene metathesis reaction. They present a singlet ground state for the carbene and metallacyclobutane species, with a reasonable energy preference for the latter, and an unfavorable alkene cyclopropanation in the singlet state. With the aim of analyzing if the reactivity in the triplet state could prevent olefin metathesis to occur, we localized the transition state structures for the two processes in the singlet and triplet states. Since complex **10** is the one with the more realistic ligand and presents thermodynamics closest to those of Grubbs complex **5**, it was taken as representative of this set

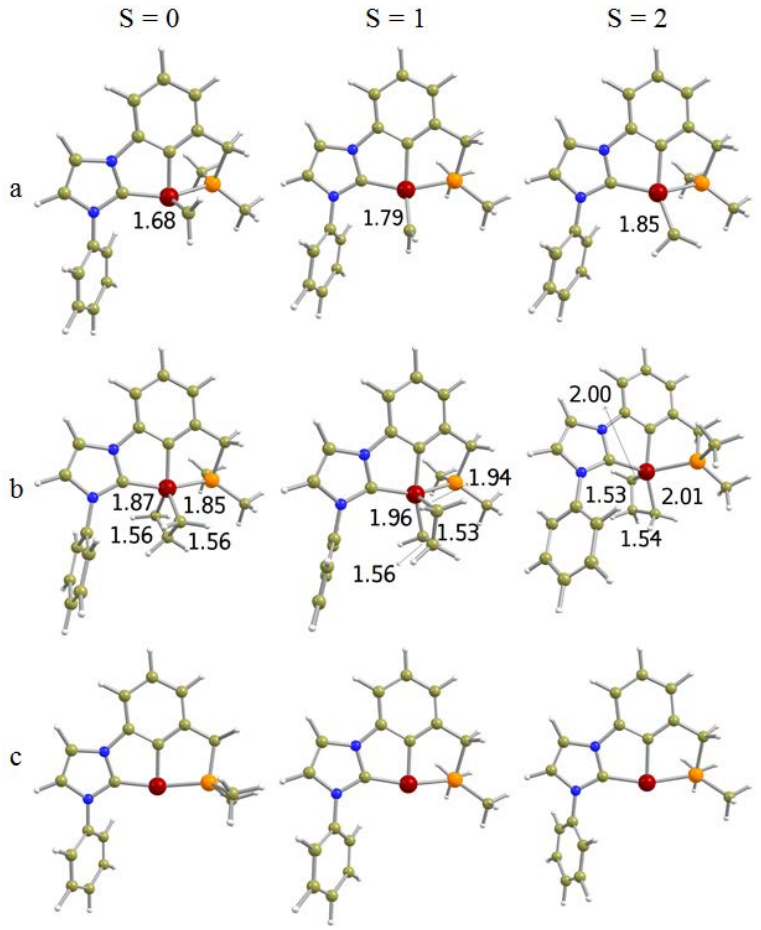

Figure 4.21: Optimized geometries of a) carbene; b) metallacyclobutane and; c) the metal fragment from alkene cyclopropanation in the three different spin states, for complex **13**. All distances are in Å

of complexes. Figure 4.22 shows the energy profile associated with the cycloaddition to form the metallacyclebutane and the two competitive process: cycloreversion to olefin metathesis and reductive elimination to cyclopropanation, and the associate geometries are in the **??**.

These these calculations show that alkene metathesis presents energy barriers that are in agreement with a feasible process, with the transition state structure for cycloaddition ($^1 10 - RM^{\ddagger}$) and cycloreversion ($^1 10 - MP^{\ddagger}_{OM}$) being 20.3 kcal mol^{-1} above that of metallacyclobutane and 6.8 kcal mol^{-1} higher in energy than that of separated reactants. These values are similar to those computed for the Ru-based

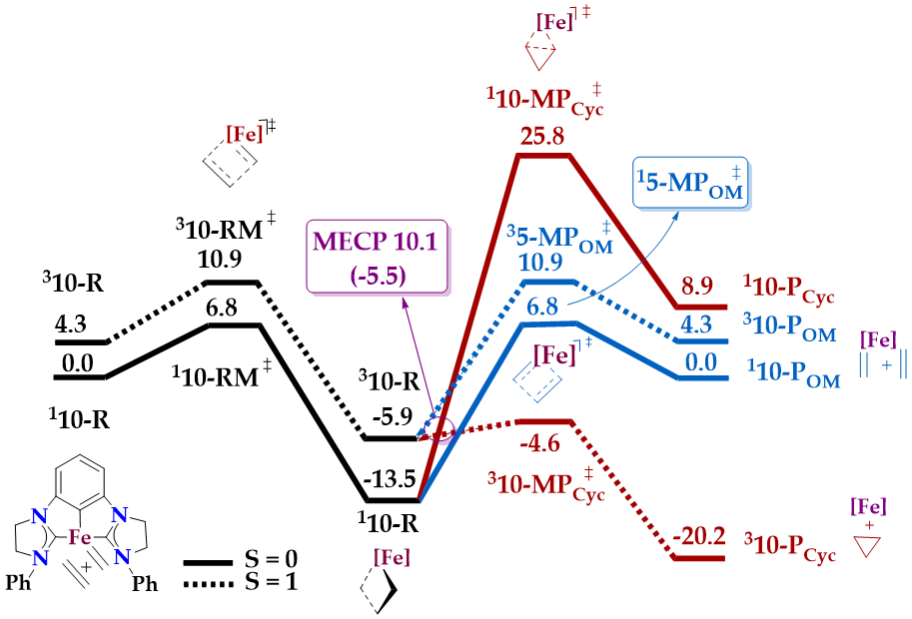

Figure 4.22: Gibbs energy profile (in kcal mol^{-1}) for metallacyclobutane formation (black), alkene metathesis (blue), and alkene cyclopropanation (red) processes involving **10** and ethene.

Grubbs catalyst, for which $\Delta G^{\ddagger}$ is 19.5 kcal mol^{-1} with respect to the metallacyclobutane and 12.7 kcal mol^{-1} with respect to the separated reactants (see Figure 4.3).

Cyclopropanation by reductive elimination in the singlet state is strongly disfavored from a kinetic point of view. It lies 19.0 kcal mol^{-1} ($^1 10 - MP^{\ddagger}_{Cyc}$) higher in energy than the productive transition state for metathesis, an energy difference that resembles that one computed for **5**. However, cyclopropanation by this path remains the preferred pathway in the triplet state, with the transition state ($^3 10 - MP^{\ddagger}_{Cyc}$) lying 1.3 kcal mol^{-1} above the metallacyclebutane ($^3 10 - M$). Besides, the access of the triplet state surface from the singlet surface occurs through a spin crossing point (**MECP 10.1**) that was located just 0.4 kcal mol^{-1} over the triplet state of the intermediate metallacyclebutane ($^3 10 - M$), suggesting that this is the preferred pathway.

Finally, cyclopropanation by carbene transfer, we found that the mechanism is concerted, without the formation of the intermediate zwitterionic or biradical. The transition state for the attack of the

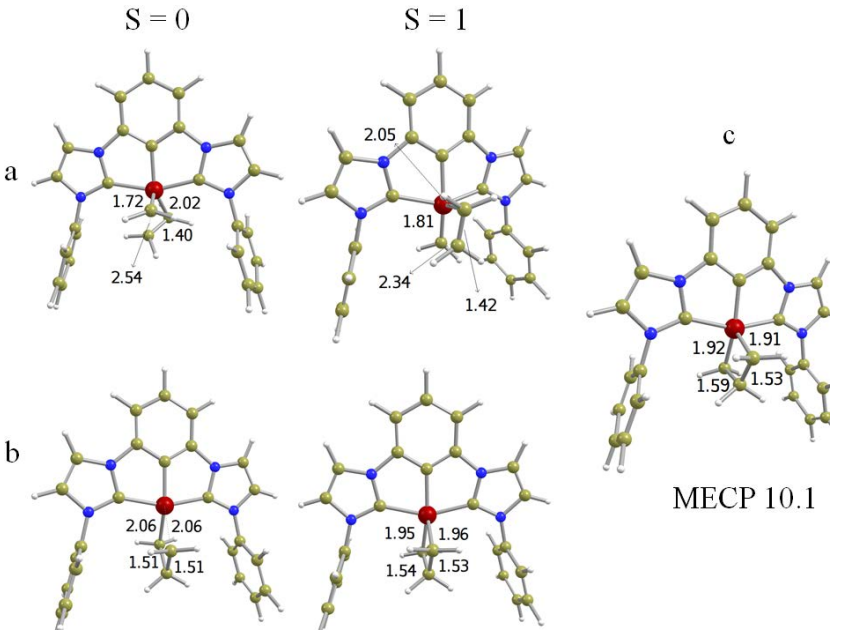

Figure 4.23: Optimized geometries evolved in the reactivity of complex **10** with ethene: (a) TS of cycloaddition and (b) TS for cyclopropanation by reductive elimination, in both singlet and triplet states, and (c) MECP 10.1.

olefin by the metal carbene in the singlet and triplet states are almost degenerate with energies of 22.6 and 22.9 kcal mol^{-1}, respectively, regarding the reactants. Those values are higher than the barrier for cycloaddition (^{1}10 – $RM^{\ddagger}$). This means that here the formation of the intermediate metallacyclebutane is more favorable than the direct transfer of the carbene to the ethene. Figure 4.24 shows the geometries of the transition states involved in this carbene transfer mechanism.

Overall, present calculations suggest that complexes **10** – **13** react in a manner similar to that of the Grubbs catalyst in the singlet state, showing a remarkable preference for metathesis not found for the other iron carbene complexes considered here. However, the viability of these complexes as alkene metathesis catalysts is strongly dependent on the energetics and feasibility associated with the spin crossing in the cyclopropanation pathway.

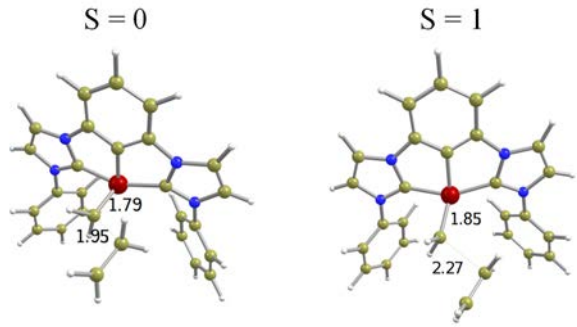

Figure 4.24: Geometries of the transition states for carbene transfer involving **10** and ethene.

4.5 Final Remarks

The nature of the ancillary ligands and geometry around the metal center that could favor the catalytic activity for olefin metathesis of a $L_3Fe{=}CH_2$ iron carbene were determined by means of DFT(OPBE)–D2 calculations.

We focused on the factors favoring a singlet ground state for the active carbene and metallacyclobutane intermediate as well as those disfavoring the alkene cyclopropanation. These requirements arise from the fact that according to the results alkene metathesis present lower energy barriers in the singlet state than the triplet, in contrast to the alkene cyclopropanation which always presents lower energy barriers in the triplet state. Therefore, precise control of the relative stabilities of the different spins states seems to be crucial. Results show that the addition of strong σ-donating ligands favors the carbene singlet state.

However, the use of σ-donating ligands alone is not sufficient for developing an efficient catalyst. The presence of alkyl ligands strongly destabilizes the metallacyclobutane (**8**), which becomes too high in energy to be involved in an efficient catalytic process. Moreover, these kinds of ligands are not able to favor a singlet ground state metallacyclobutane intermediate *per se*.

Remarkably, the coordination geometry around iron in the metallacyclobutane is significantly different depending on the spin state multiplicity. The singlet state favors a TBP similar to that reported to be active in metathesis, while the triplet state leads to a distorted SBP.

Therefore, the stabilization of the singlet state metallacyclobutane requires the destabilization of SBP structures. This can be achieved by using tricoordinated chelating ligands with the strongest σ-donor group in central position such as those of complex **10**–**13**. Moreover, the tricoordinating ligand also stabilizes the metallacyclobutane intermediate with respect to separated reactants due to a preorganization of the initial carbene that adopts a closer structure to that of the metallacycle than when using monodentate ligands.

Overall, the reactivity of complex **10** in the singlet state is very similar to that of the Grubbs catalyst, with a large kinetic preference for alkene metathesis when compared with alkene cyclopropanation. Although cyclopropanation in the triplet state is still strongly exergonic and presents a transition state that is lower than that of the olefin metathesis.

5

Pentacoordinate Iron Carbenes

In this Chapter, we expanded the efforts of last Chapter to pentacoordinated $L_4Fe{=}CH_2$ complexes. We focus on how the nature of the ligands, the geometry around the metal center and the formal oxidation state of iron can favor the formation of a singlet carbene and metallacycle, as well as disfavor alkene cyclopropanation. As in the previous Chapter we compute all potential spin states of the metal carbene, the metallacyclobutane intermediate and the metal fragment resulting from alkene cyclopropanation. For simplicity, the chosen carbene was $[Fe]{=}CH_2$ reacting with ethene. We expand the study to other *in-silico* designed ligand groups that represent borderline cases. Finally, we explore the possibility of metal reduction to formally Fe^0, keeping a selection of the ligands explored in the first two sets of complexes.

We first analyze the electronic structure of the carbene and in a second stage we discuss the thermodynamics of its reactivity towards olefins. A third part is dedicated to the energetics of the transition state structures for alkene metathesis and alkene cyclopropanation of a representative complex showing thermodynamics close to that of reference system are discussed. Afterwards, two sections are dedicated to address aspects of the metal-carbene bond and its relation with the cyclopropanation.

Results are compared to the reference values computed previously for the ruthenium based 2^{nd} Generation Grubbs active species (see Section 4.2).This reference system showed that a potentially active iron carbene should present a singlet ground state for the metal carbene and the metallacyclobutane intermediate and an unfavorable cyclopropanation process, especially in the singlet state, in order to have a kinetic preference for alkene metathesis rather than cyclopropanation reaction.

5.1 Complexes Based on Experimental Ligands

The first set of systems is composed of three complexes containing ligands already reported in the literature. The resulting complexes are schematically shown in Scheme 5.1.

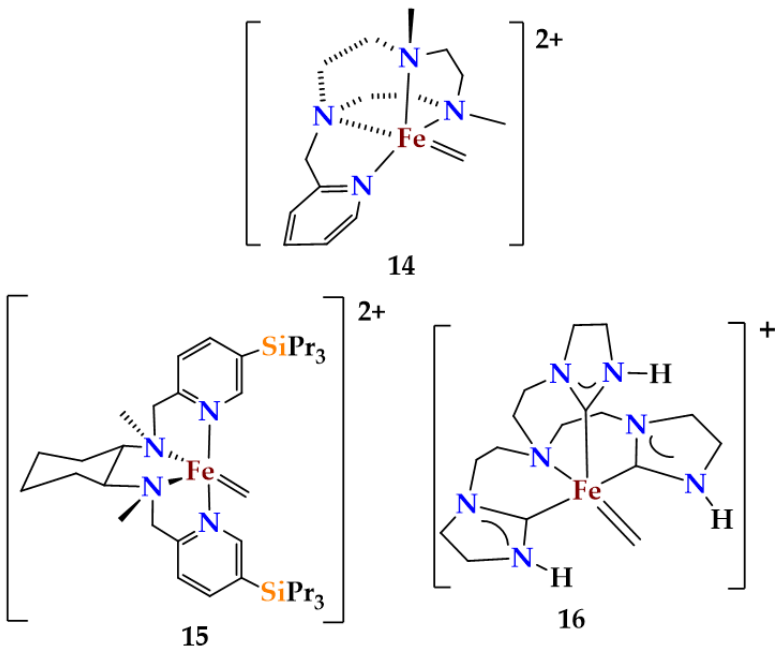

Scheme 5.1: Set of *in-silico* studied $L_4Fe{=}CH_2$ complexes.

The ligands of Complex **14**[288] and **15**,[289] were used by Costas and co-workers for the synthesis of high oxidation state iron oxo complexes.[138] Moreover, **14** has been proposed to be involved in the car-

bene insertion in C-H bonds of arenes using a derivative of **14** as precursor, as highlighted in the background Chapter.[192] On the other hand, the ligand of Complex **16** is a variation of the Scorpionato motive[290] in which the central boron is replaced by a triethyleneamine linker.[291,292] This ligand was used by Meyer and co-workers for the synthesis of a high oxidation state iron nitride complex.[291]

Figures 1.1-1.3 shows the optimized geometries of **14-16** and the complexes derived from the reactivity with ethene as representative example. Regarding the energetics, the results are reported in Table 5.1,a long with values for the well-known Ru-based 2^{nd} generation Grubbs catalyst (Complex **5** in Chapter 4), which were added for comparison.

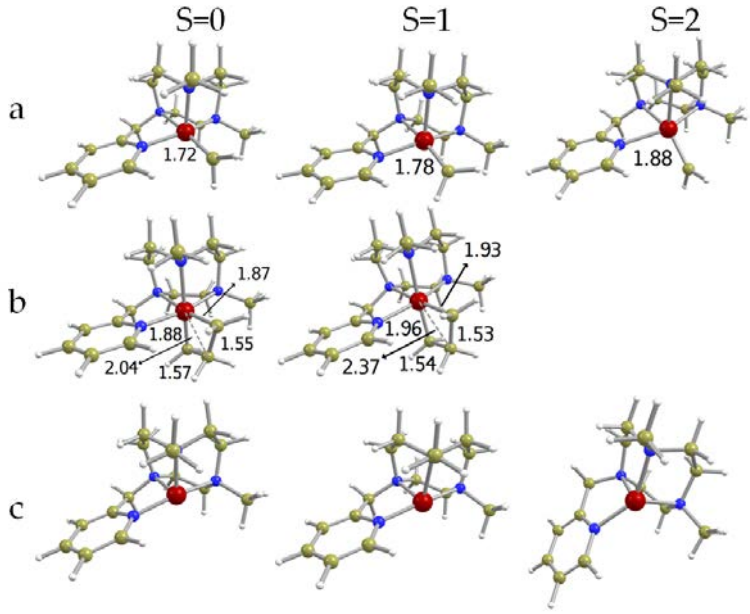

Figure 5.1: Optimized geometries of (a) carbene **14**; (b) metallacyclobutane resulting from its cycloaddition with ethene; and (c) the metal fragment resulting from alkene cyclopropanation, in the three different spin states. Attemps to obtain the quintet state metallacycle structure directly evolved to cyclopropanation products. Distances are in Å.

All singlet state carbenes present a square based pyramid (SBP) coordination around the metal center with the carbene occupying one of the basal positions. Moreover, carbene substituents are perpendicular to the basal plane, suggesting that the Fe=C π-bond is formed

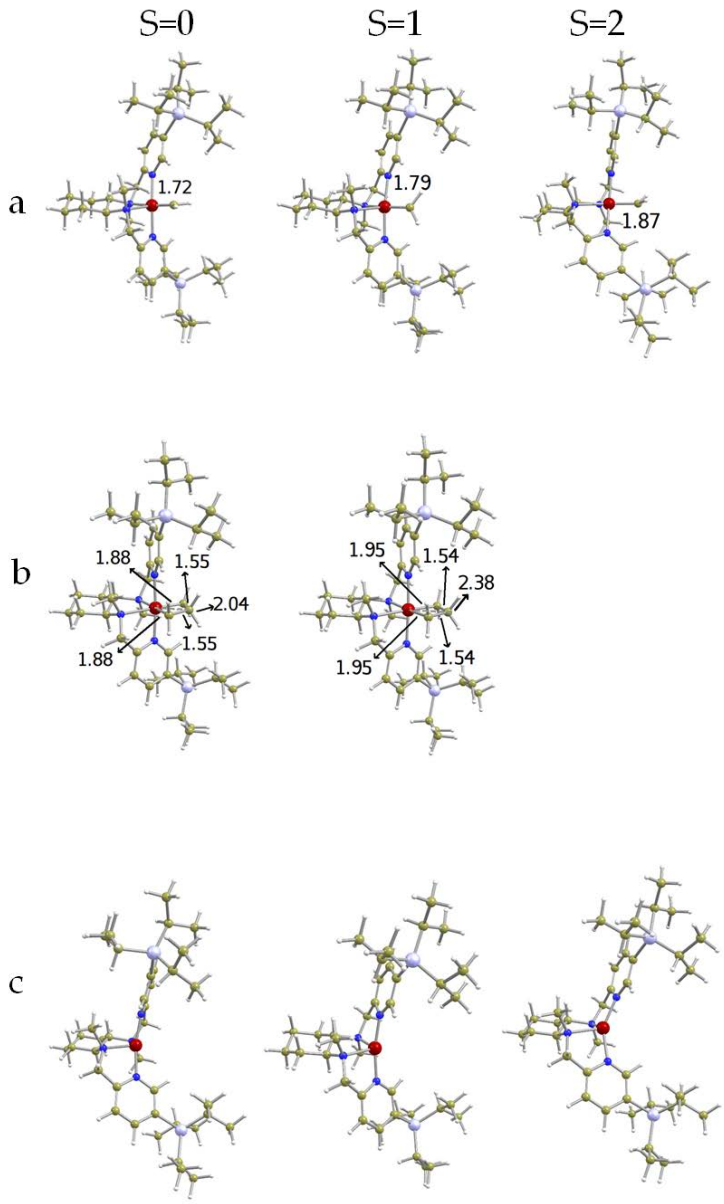

Figure 5.2: Optimized geometries regarding Complex **15**: a) carbene; (b) metallacyclobutane and (c) fragment of cyclopropanation. Attemps to obtain the quintet state metallacycle structure directly evolved to cyclopropanation products.

Table 5.1: Relative Gibbs (G_{gp} + D2) energies of the species involved in the metathesis and cyclopropanation reactions of Grubbs Ru Complex **4** and iron carbene complexes **14-16** with respect to the carbene singlet state and ethene. All values are in kcal mol^{-1}.

complex	carbene			metallacyclebutane			cyclopropanation		
	S=0	S=1	S=2	S=0	S=1	S=2	S=0	S=1	S=2
4	0.0	19.5	49.1	-6.8	8.2	47.5	8.6	-7.4	9.7
14	0.0	-2.3	3.8	-20.7	-23.1	-[b]	-22.3	-28.6	-43.8
15	0.0	-6.3	5.1	-23.4	-26.7	-[b]	-26.8	-33.2	-50.8
16	0.0	7.6	22.7	-4.5	-6.0	-[b]	-18.3	-23.1	-32.1

[a] The [Fe]=CH_2 carbene is not a minimum of the potential energy surface, optimization leads to carbene insertion into the NHC ligand.
[b] Optimizations spontaneously evolved to the formation of cyclopropane.

by the overlap between the iron d_{xy} orbital of the basal plane and the corresponding p_y carbon orbital. The Fe=C bond distance ranges from 1.708 Åto 1.724 Å, values that are similar to those found for $L_3Fe{=}CH_2$ carbenes and consistent with an important double bond character.

The triplet state structures of **14** and **15** also present a distorted SBP coordination around the metal center. In contrast, complex **16** presents a trigonal bipyramid (TBP) geometry with the carbene in apical position. Regardless the coordination around the metal center, in all these cases the [Fe]=CH_2 bond distance is larger than that of the singlet (between 1.756 and 1.792 Åand the carbene substituents are not fully perpendicular to the basal plane.

Finally, the quintet state of complex **14** presents a TBP coordination around the metal center with the carbene in the equatorial plane and showing a large [Fe]=CH_2 bond distance (1.881 Å). On the other hand, the quintet states of **15** and **16** present distorted SBP structures with a long [Fe]=CH_2 bond distance and a pyramidalized CH_2 fragment. In the three cases, the geometric features suggest that π-bond is even weaker than in the triplet state.

Complexes **14** and **15**, which only have N-based ligands except the carbene, present a triplet ground state. In contrast, complex **16**, with the strong donating N-Heterocyclic carbene (NHC) ligand,

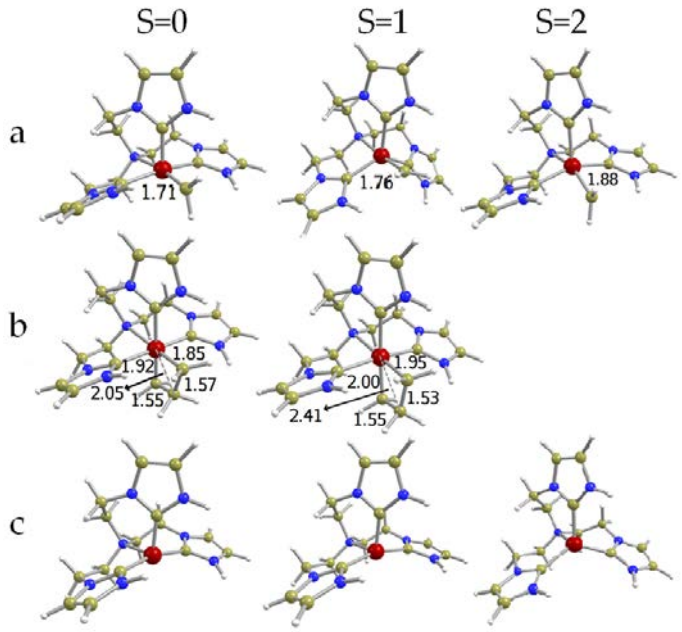

Figure 5.3: Optimized geometries regarding Complex **16**: a) carbene; (b) metallacyclobutane and (c) fragment of cyclopropanation. The quinted metallacycle attempt evolves to cyclopropanation.

present a singlet ground state. This singlet state lies 7.6 kcal mol^{-1} below the triplet state. Indeed, as already seen for $L_3Fe{=}CH_2$ carbenes, addition of stronger σ-donor ligands favors the complex to be low spin.

Singlet and triplet stable metallacyclobutanes resulting from the reaction of **14-16** methyledenes with ethene present octahedral geometry around the metal center, while quintuplet spontaneously evolves to cyclopropanation products. Significant differences in the geometrical features of the metallacyclobutane fragment are observed as function of the spin state. Singlet state metallacyclobutanes are characterized by relatively short M-C_α distances, relatively large C_α-C_β bonds and relatively large C_α-C_β-C_α angles. This is associate with in short M-C_α distances as already described for the d^0 and Ru-based TBP metallacyclobutanes involved in alkene metathesis.[275,276]

In contrast, triplet metallacyclobutanes present larger M-C_α distances, shorter C_α-C_β bonds and M-C_β distances that are at least 0.3 Å longer than those of the singlet state intermediates. Overall, the

open shell metallacycles are geometrically closer to those of the d^0 SBP metallacyclobutane that do not perform metathesis.[276] However these geometrical differences at the metallacycle do not arise from a change on the coordination around the metal center as it is the case of pentacoordinated metallacyclobutanes, but from a different occupation of the metal d orbitals, as it can be seen in Figure 5.4. Note that in the triplet state the orbital pointing towards the C_β is single occupied, whereas in the singlet state this orbitals is empty.

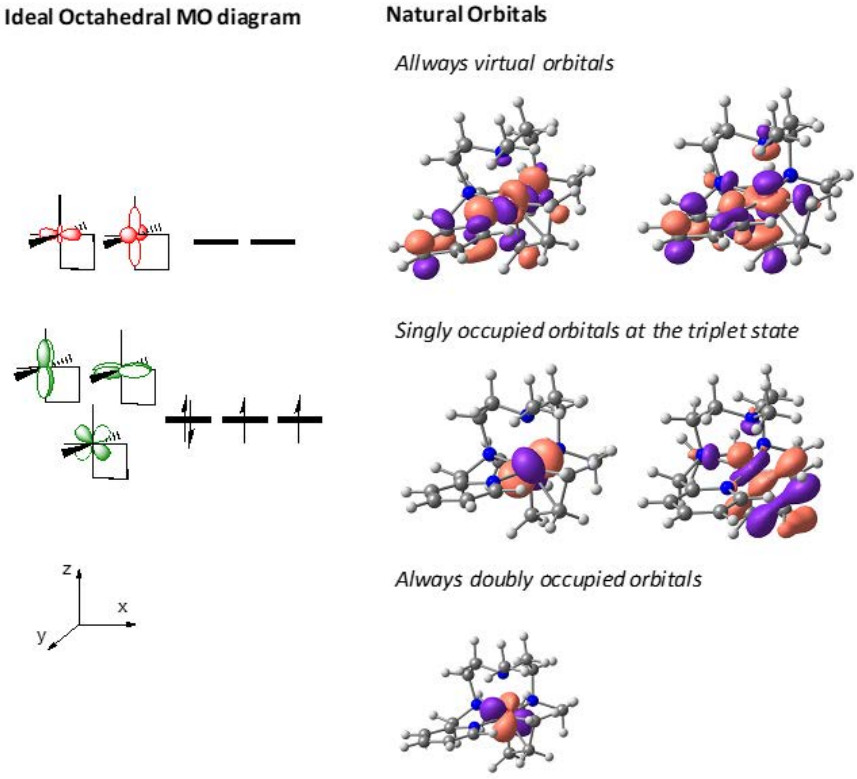

Figure 5.4: Schematic Molecular Orbitals diagram for an ideal high field d^4 octahedral metallacyclobutane intermediate with the associated Natural Orbitals of the metallacyclobutane S = 1 state arising from the reaction of **14** with ethene.

Overall, the $Fe(CH_2CH_2CH_2)$ geometrical features suggest that singlet state metallacyclobutane are more prone to undergo metathesis than the triplet ones as already found for tetracoordinated species and appears to be the spin state to favor, as shown in the previous chapter.

Metallacyclobutane formation from the methylidene and ethene is favorable for all singlet and triplet states, the $\Delta G°_{298K}$ of the reaction being between -26.7 and -4.5 kcal mol^{-1}. The addition of C-based ligands leads to the least stable metallacyclobutanes, although, in this case, this seems to be appropriate because, while values for **14** and **15** appear too negative for an efficient catalytic process, and those of **16** are closer to the values for the efficient 2^{nd} generation Grubbs catalyst.[293] Unfortunately, the metallacyclobutane intermediate presents always a triplet ground state, which should make it less prone to metathesis.

Finally, alkane cyclopropanation is strongly favorable for **14** to **16** complexes in all spin states. The reaction $\Delta G°_{298K}$ ranges from -50.8 to -18.3 kcal mol^{-1}. Complex **16** presents the least favorable cyclopropanation, which is consistent with the presence of stronger σ-donor ligands. The resulting metal fragment has a butterfly coordination around the metal center in most singlet and triplet states, while it presents a trigonal pyramid structure in the quintet states with flexible ligands. Regardless of the coordination around the metal center, the quintet ground state presents four unpaired electrons that, as in the case of the triplet state, are localized on the metal center. Overall, complexes **14** to **16** do not appear to be good candidates for alkene metathesis. Three main drawbacks can be identified: i) the singlet state is not always the ground state for metal carbene; ii) the metallacyclobutane intermediate presents a triplet ground state and iii) alkene cyclopropanation is largely favored.

5.2 Strong σ-Donors Ligands

According to our findings explained in the last Chapter for tetracordinated iron-complexes, addition of C–based ligands appears to favor the singlet state carbene, destabilize the metallacyclobutane intermediate and disfavorm alkene cyclopropanation. These three factors may favor alkene metathesis. Therefore, we decided to explore species in which N–based ligands of complexes **14** to **16** were substituted by C–based ones, the maximum number of substitutions resulting in the formation of a neutral complex, shown in Scheme 5.2. The optimized structures of these complexes are shown from Figure 5.5 to Figure 5.8 and Table 5.2 summarizes the energetics.

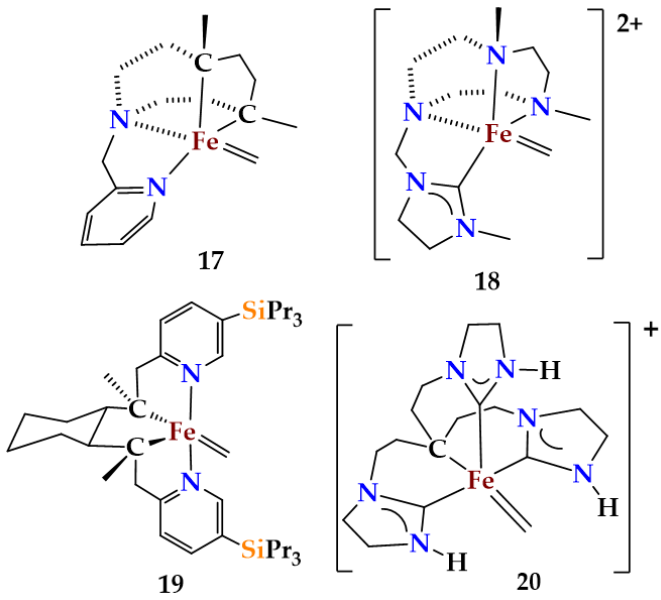

Scheme 5.2: Set of *in-silico* studied $L_4Fe{=}CH_2$ with C-based modifications.

Table 5.2: Relative Gibbs (G_{gp} + D2) energies of the species involved in the metathesis and cyclopropanation reactions of complexes **17-20** with respect to the carbene singlet state and ethene. All values are in kcal mol^{-1}

.

complex	carbene			metallacyclebutane			cyclopropanation		
	S=0	S=1	S=2	S=0	S=1	S=2	S=0	S=1	S=2
4	0.0	19.5	49.1	-6.8	8.2	47.5	8.6	-7.4	9.7
17	0.0	3.8	13.9	-3.4	-11.8	1.3	-18.7	-24.2	-25.6
18	0.0	-3.9	-[a]	-15.9	-19.0	-[b]	-17.8	-25.7	-37.3
19	0.0	11.8	23.3	-2.6	-1.3	3.7	-26.2	-21.9	-19.8
20	0.0	5.3	20.1	-8.9	-8.0	24.4	-36.2	-29.0	-29.4

[a] The [Fe]=CH_2 carbene is not a minimum of the potential energy surface, optimization leads to carbene insertion into the NHC ligand.
[b] Optimizations spontaneously evolved to the formation of cyclopropane.

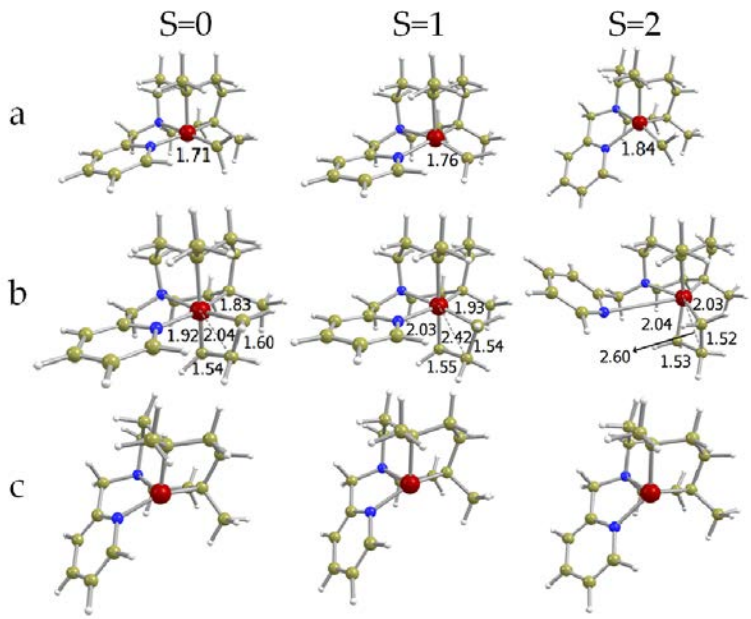

Figure 5.5: Optimized geometries of Complex **17**: a) carbene; (b) metallacyclobutane and (c) fragment of cyclopropanation.

These substitutions have little influence on the structure of the metallacyclobutanes as well as on that of the metal fragments resulting from cyclopropanation. In this way, the metallacycle present an octahedral geometry around Fe, regardless of the spin state and the unpaired electrons are located mainly on the metal center for the triplet and quintet states. In addition to this, the M···C_β metal distance becomes larger and the metallacyclobutane fragment turns more puckered as the multiplicity increases. Similarly upon cyclopropanation the metal fragment, presents the unpaired electrons in the triplet and quintet states at the metal center.

In contrast, the nature of the ligands has a larger influence on the carbene. In this way, C by N substitution does not usually change the coordination around the metal center for singlet state carbenes, which is always a SBP. However, it changes the preferred geometry and the spin distribution for several triplet states. While complexes **14** to **16** present a SBP coordination around the metal in the triplet state, the analogous **17** to **20** complexes mostly show a TBP coordination, the only exception being carbene **14**. Noteworthy, the quintet state carbenes present large [Fe]=CH_2 bonds. The energy trends already

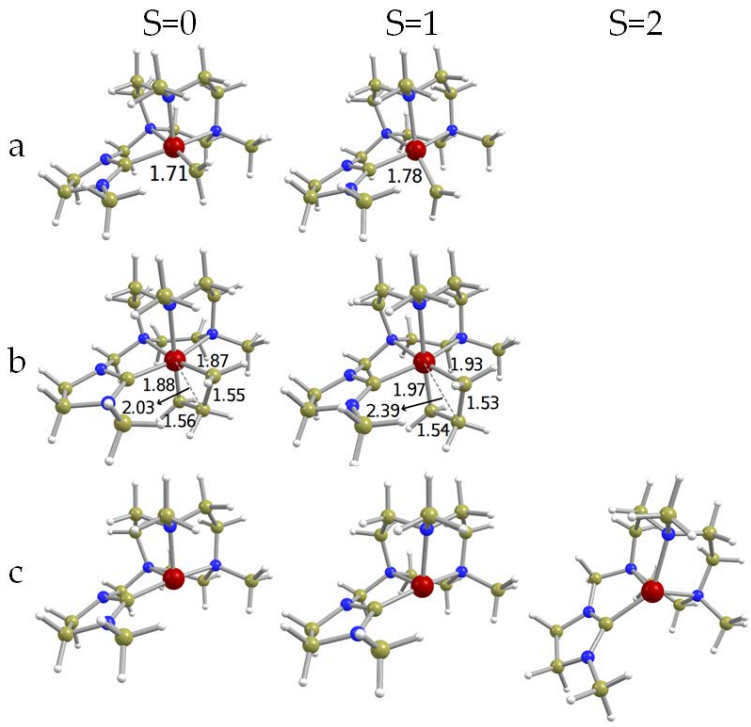

Figure 5.6: Optimized geometries of (a) carbene **18**; (b) metallacyclobutane resulting from its cycloaddition with ethene; and (c) the metal fragment resulting from alkene cyclopropanation, in the three different spin states. Distances are in Å. All attempts to obtain the quintet state carbene lead to an optimized structure in which the carbene is inserted in the Fe-NHC bond. Moreover, optimization of the quintet metallacycle structure directly evolved to cyclopropanation products.

found for **17** to **16** set of complexes are similar to those found for catalysts **14** to **16** present in Table 5.2.

The addition of C-based ligands favors the singlet state, destabilizes the metallacyclobutane intermediate and makes alkene cyclopropanation slightly less favorable. The latter can be associated with a [Fe]=CH_2 bond strengthening, the exception being complex **20** compared to **16**. This is related to the fact that the N to C substitution is performed in *trans* to the carbene, which weakens this bond despite the electron density on the metal increases. That is, the strong donating groups should be in *cis* to the carbene. Moreover, since the number of

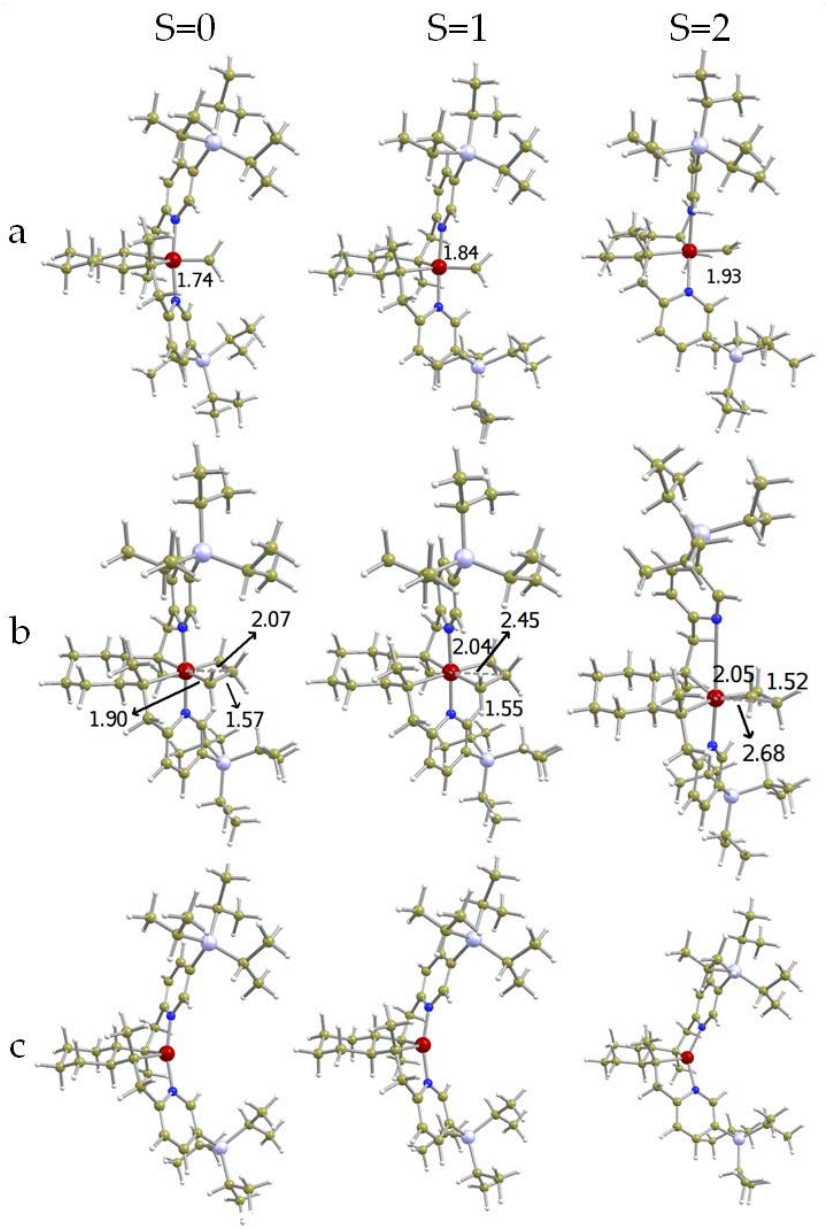

Figure 5.7: Optimized geometries regarding Complex **19**: a) carbene; (b) metallacyclobutane and (c) fragment of cyclopropanation.

C-based ligands is larger for complexes **17** to **20** compared with **14** to **16** species, the effects are in general more pronounced. This turns in the fact that all designed carbenes present the desirable singlet ground

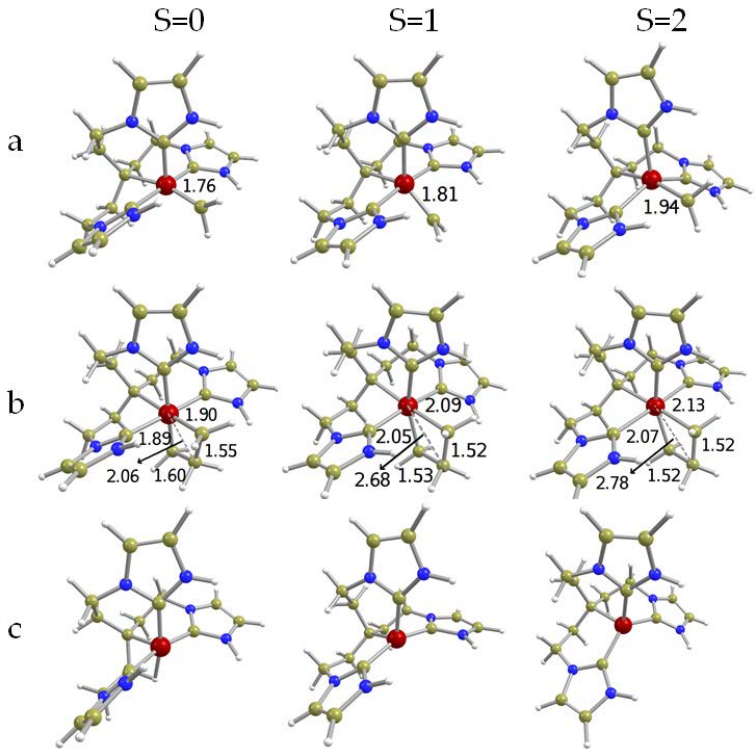

Figure 5.8: Optimized geometries regarding Complex **20**: a) carbene; (b) metallacyclobutane and (c) fragment of cyclopropanation.

state, with the exception of complex **18**, which has the weakest σ-donor ligands of this series. Unfortunately, several drawbacks persist. In this view, although the preference for cyclopropanation is reduced, this process is still by far more favorable than metathesis in all spin states.

Moreover, results suggest that the metallacyclobutane intermediate has still a triplet ground state in the majority of cases. In fact, for complexes **19** and **20**, the singlet state is more stable than the triplet but the associated energy difference is less than 1.3 kcal mol^{-1}. One would expect a triplet ground state in all cases as it is the ideal situation for a d^4 low spin octahedral complex. Therefore, the stabilization of the singlet state can only be understood by an important destabilization of the iron d orbital pointing toward the C_β of the metallacycle, due to the presence of strong donating groups *trans* to the metallacyclobutane fragment. Only when this destabilization is large

enough, the ground state becomes a singlet. This could eventually be a potential strategy to favor the metallacyclobutane singlet state. Noteworthy, the fact that the d orbital pointing towards the C_β of the metallacycle is empty in the singlet state is in agreement with the shorter M···C_β distance in this state.

5.3 Reduced Complex

Scheme 5.3 shows complexes **21-24** that were obtained by reducing the metal center of the doubly positively charged complexes **14-18**. Table 5.3 summarises the associated energetics of these complexes, and optimized geometries are depicted in Figure 5.9 to Figure 5.11.

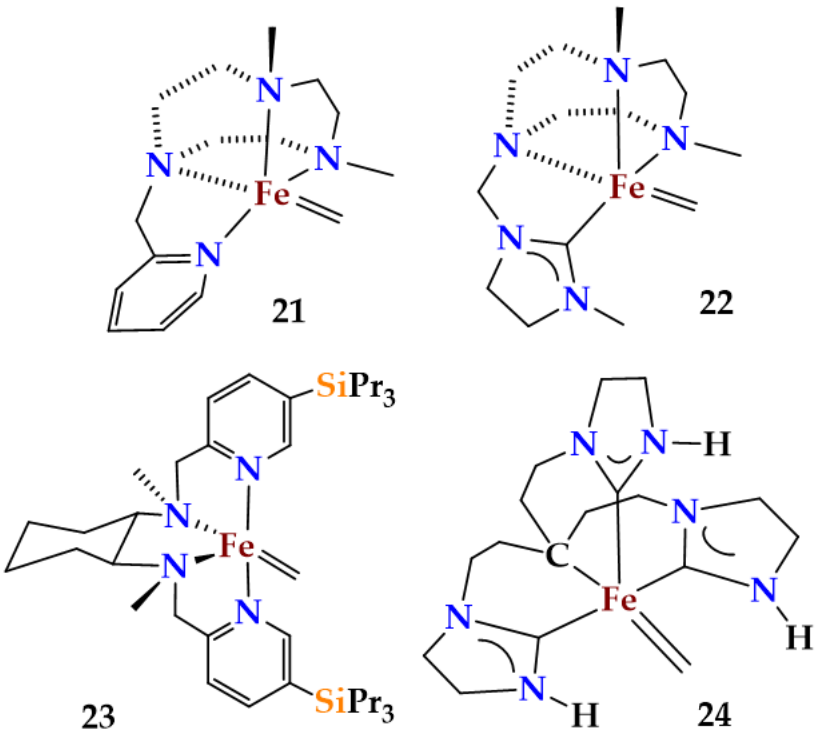

Scheme 5.3: Set of *in-silico* studied $L_4Fe^0{=}CH_2$

We have analyzed these systems, because we expected that metal reduction leading to formally Fe^0 carbenes (carbene considered as a neutral ligand) could favor the singlet state metallacyclobutanes. This

Table 5.3: Relative Gibbs (G_{gp} + D2) energies of the species involved in metathesis and cyclopropanation reactions of complexes **21-24** with respect to the carbene singlet state and ethene. All values are in kcal mol^{-1}

complex	carbene			metallacyclebutane			cyclopropanation		
	S=0	S=1	S=2	S=0	S=1	S=2	S=0	S=1	S=2
4	0.0	19.5	49.1	-6.8	8.2	47.5	8.6	-7.4	9.7
21	0.0	-0.4	0.2	-26.5	-21.9	-18.9	4.8	-17.1	-12.9
22	0.0	4.9	7.6	-23.3	-12.4	-10.2	8.9	-12.2	-3.1
23	0.0	2.9	12.3	-15.1	-12.3	-[b]	4.9	-29.7	-21.7
24	0.0	9.3	-[a]	-23.4	-0.9	23.3	-0.6	-16.6	0.9

[a] The [Fe]=CH_2 carbene is not a minimum of the potential energy surface, optimization leads to carbene insertion into the NHC ligand.
[b] Optimizations spontaneously evolved to the formation of cyclopropane.

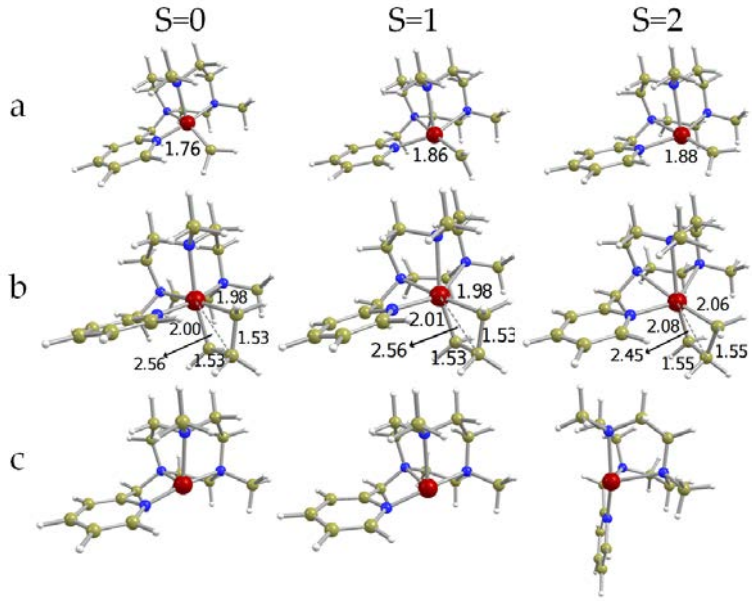

Figure 5.9: Optimized geometries of regarding Complex **21**: a) carbene; (b) metallacyclobutane and (c) fragment of cyclopropanation.

assumption arises from the fact that this intermediate would present a formal Fe^{2+} metal center and thus, with formally six d electrons in an octahedral environment. In this way, the singlet state would be the ground state of the low spin situation and this would not depend on the splitting between the ideal t_{2g} orbitals. Moreover, the additional electrons could reinforce the [Fe]=CH_2 bond and thus, disfavor alkene cyclopropanation.

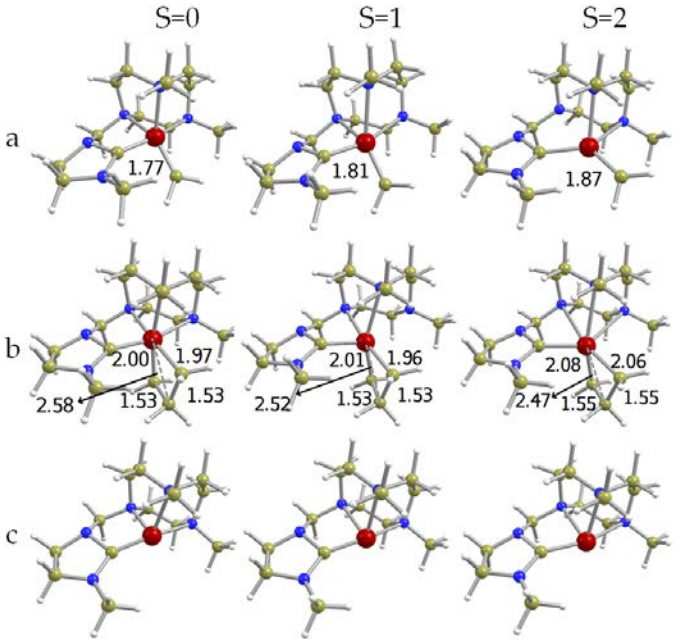

Figure 5.10: Optimized geometries regarding Complex **22**: a) carbene; (b) metallacyclobutane and (c) fragment of cyclopropanation.

Results show that reduction of the metal center on complexes **21** to **24** involves important geometrical modifications of the carbene and the metallacycle. Regarding the carbene, while **14** to **20** Fe^{2+} complexes present a SBP coordination in the singlet state, species **21** to **24** present a TBP one. This is accompanied by an elongation of the [Fe]=CH_2 bond, which ranges from 1.76 to 1.78 Å. Moreover, all triplet state carbenes present a SBP geometry around the metal center. These changes in the coordination environment around iron can be rationalized by the increase of d electrons of iron. Low spin pentacoordinated complexes with d^6 metal centers should present an SBP singlet state, while the low spin pentacoordinated d^8 ones are expected to be TBP.

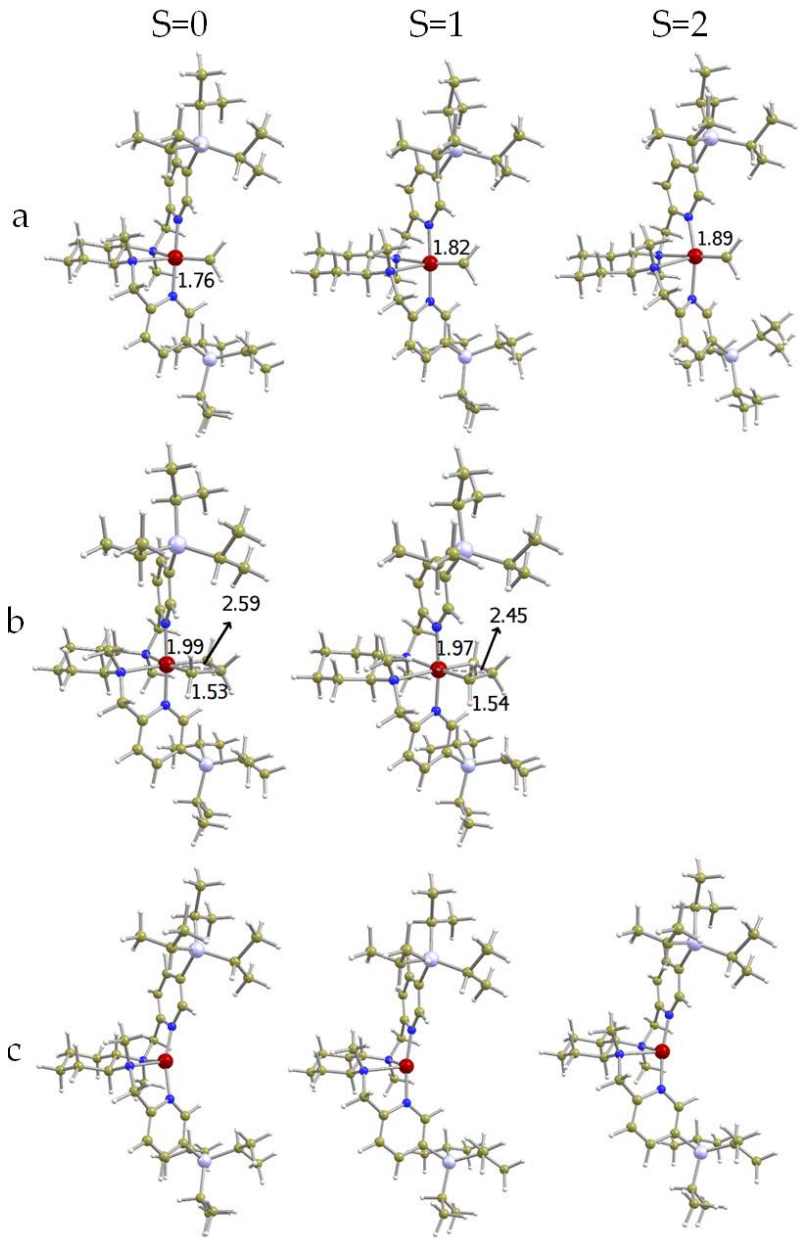

Figure 5.11: Optimized geometries regarding Complex **23**: a) carbene; (b) metallacyclobutane and (c) fragment of cyclopropanation.

The metallacyclobutane intermediate presents the expected octahedral coordination around the metal center, regardless of the spin

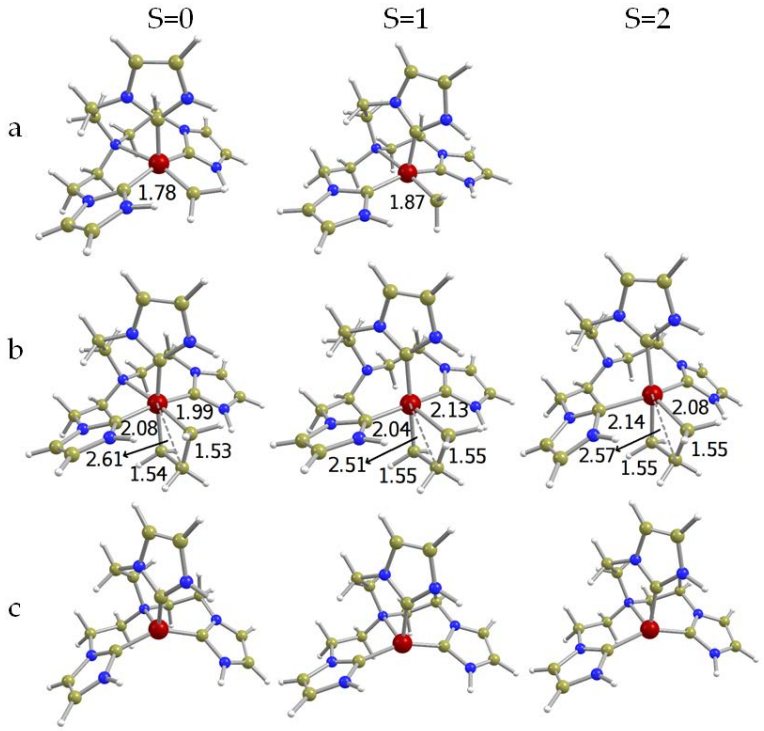

Figure 5.12: Optimized geometries regarding Complex **24**: a) carbene; (b) metallacyclobutane and (c) fragment of cyclopropanation. All attempts to obtain the quintet state carbene lead to an optimized structure in which the carbene is inserted in the Fe–NHC bond.

state, but the characteristic wide C_α-C_β-C_α angle and the short M···C_β distance of the metallacyclobutanes involved in metathesis is not observed in any of the spin states. This can be attributed again to the two additional d electrons of iron that in the case of the singlet state occupies the d orbital pointing to C_β. Consequently, since this orbital has a repulsive overlap with orbitals centered on the metallacycle fragment, the system evolves in such a way that the M and the C_β are as far away as possible.

The thermodynamics of the formally Fe^0 complexes is substantially different from that of the **14** to **20** Fe^{2+} complexes. First, species **21** to **24** generally present a singlet state metal carbene, which is not the case for the analogous Fe^{2+} complexes **14**, **15** and **18**. Moreover, the formation of the metallacyclobutane is largely favored and leads to a species with the desirable singlet state. The preference for the singlet

state ranges between 2.8 and 22.5 kcal mol^{-1}. Finally, alkene cyclopropanation becomes unfavorable in the singlet state and, although it remains exergonic for the triplet and most of the quintet states, the obtained values are closer to those computed for the second generation Grubbs catalyst. This is particularly the case of **22**, which is an *in-silico* modification of the ligands used by Costas and co-workers for the synthesis of iron oxo complexes. Overall, from a thermodynamic point of view complexes **21** to **24** appear as promising candidates, **22** being the most interesting one.

5.4 Reaction of complex 22 with Ethene

Complex **22** appears as a promising candidate as its thermodynamics resembles that of the second generation Grubbs catalyst. It is for this reason that we decided to explore the energetics of the transition states associated with cycloaddition, cycloreversion and other deactivation processes, mainly cyclopropanation. In the case of the deactivation process, two pathways have been explored: carbene extraction by ethene that mainly leads to cyclopropanation through carbene transfer or cyclopropanation from metallacyclobutane intermediate, by reductive elimination. Moreover, while we have only considered the singlet state in the alkene metathesis process, we explored both the singlet and triplet states in the deactivation pathways. Note that in the case of cyclopropanation, a spin crossing is expected as reactants have a singlet ground state, while cyclopropanation products have a triplet one. We start this mechanistic discussion with the cycloaddition process to form the intermediate metallacyclebutane, whose the energy profile is in Figure 5.13, with the geometries in Figure 5.14.

Metallacyclobutane formation from separated reactants (methylidene + ethene) takes place in two steps: first the formation of a Fe–C between one carbon of the olefin and the metal center ($^1 22 - RI^{\ddagger}_{OM1}$) and afterwards, the formation of the C–C bond between the carbene and the other end of the olefin ($^1 22 - I_{OM1}M^{\ddagger}$). These two steps are significantly different to those reported for the usual alkene metathesis reaction catalyzed by the Mo, W or Ru complexes.[259,260,262,264,265,271] Moreover, the intermediate resulting from the formation of the Fe-C bond formation ($^1 22 - I_{OM1}$) is high in energy, it lies 26.3 kcal mol^{-1} above separated reactants and it presents Fe···N distances that have

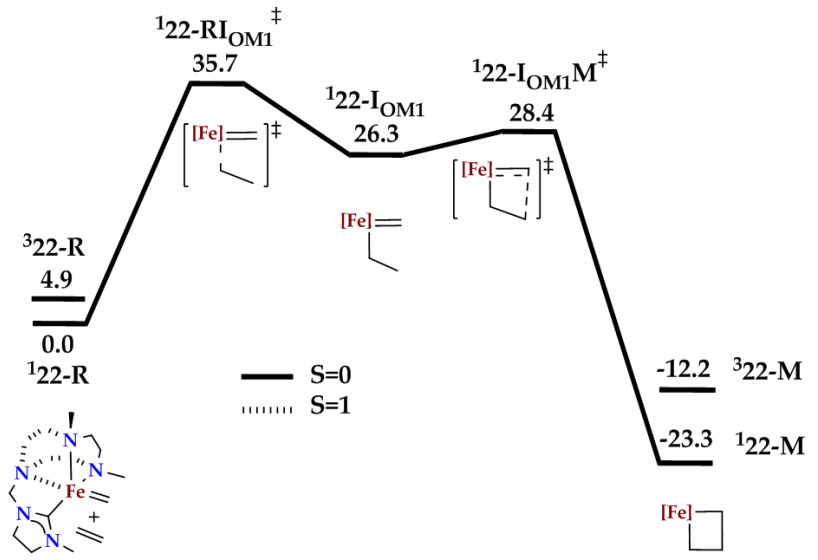

Figure 5.13: Gibbs energy profile (in kcal mol^{-1}) for metallacyclobutane formation, cycloaddition, involving **22** and ethene in singlet state.

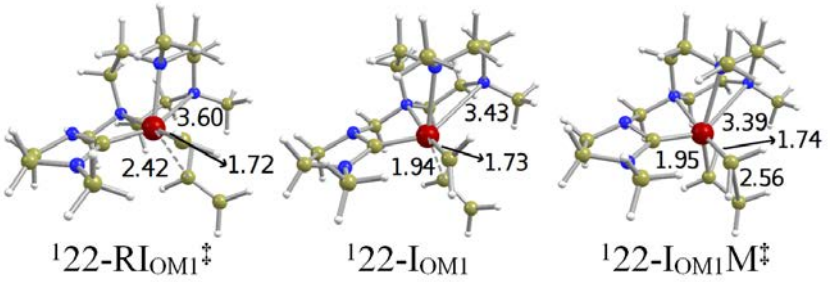

Figure 5.14: Optimized geometries of metallacyclobutane formation, cycloaddition, involving **22** and ethene in singlet state. Distances are in Å

been largely elongated. In particular, one of these Fe···N distance is so large ($>$ 3.4 Å) that indicates that the ligand decoordinates.

Cycloreversion takes place in similar steps to cycloaddition, although the geometries and energetics are slightly different, as the two processes occurs with two different ligands in *trans*. The energy profile of this process, as well as the competitive mechanism of cyclopropanation by reductive elimination are presented in Figure 5.15. The geometries of the two processes are depicted in Figure 5.16.

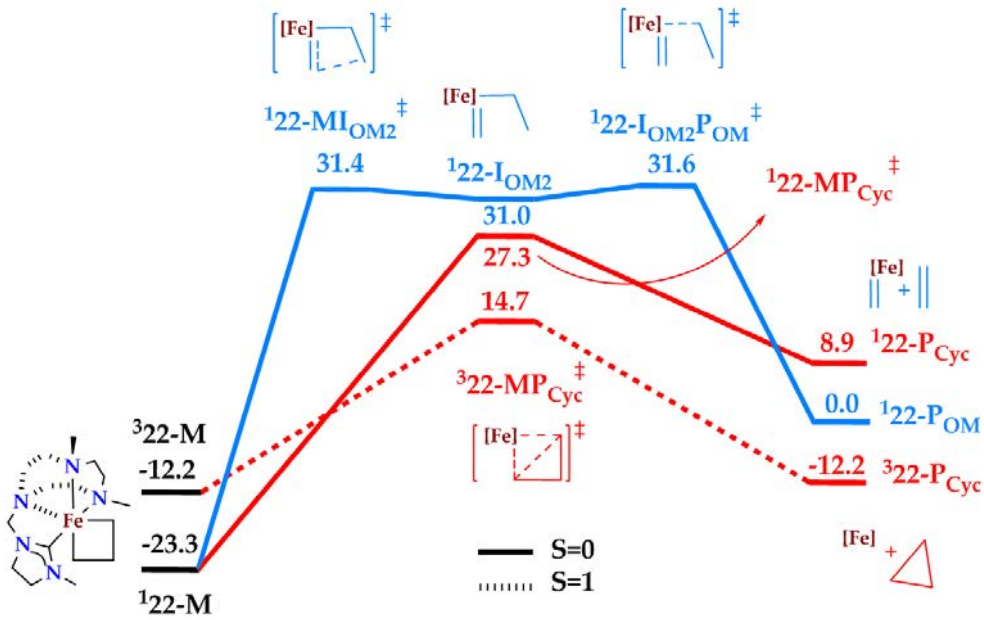

Figure 5.15: Gibbs energy profile (in kcal mol^{-1}) for cycloreversion and cyclopropanation by reductive elimination, involving **22** and ethene in singlet and triplet state.

The associated energetics suggest that alkene metathesis with **22** is kinetically unfavorable. The highest energy barrier associated to the cycloaddition is 35.7 kcal mol^{-1} ($^1 22 - RI^{\ddagger}_{OM1}$) above reactants and that of the cycloreversion 31.6 kcal mol^{-1} ($^1 22 - I_{OM2}P^{\ddagger}_{OM}$) with respect to the same asymptote. This implies that the energy barrier that has to be overcome from the metallacyclobutane is higher than 50 kcal mol^{-1}. At this point it is worth mentioning that any attempt to locate the cycloaddition and cycloreversion triplet state transition states lead to structures with energies close to those of the singlet state, which indicates that the reaction would not occur in the triplet state.

On the other hand, deactivation pathways show energy barriers that are significantly lower than those of the metathesis process, both for the singlet and triplet states. The transition states for alkene cyclopropanation are 27.3 ($^1 22 - MP^{\ddagger}_{Cyc}$) and 14.7 ($^3 22 - MP^{\ddagger}_{Cyc}$) kcal mol^{-1} above the separated reactants. This values are respectively 16.9 and 4.3 kcal mol^{-1} below those of metathesis.

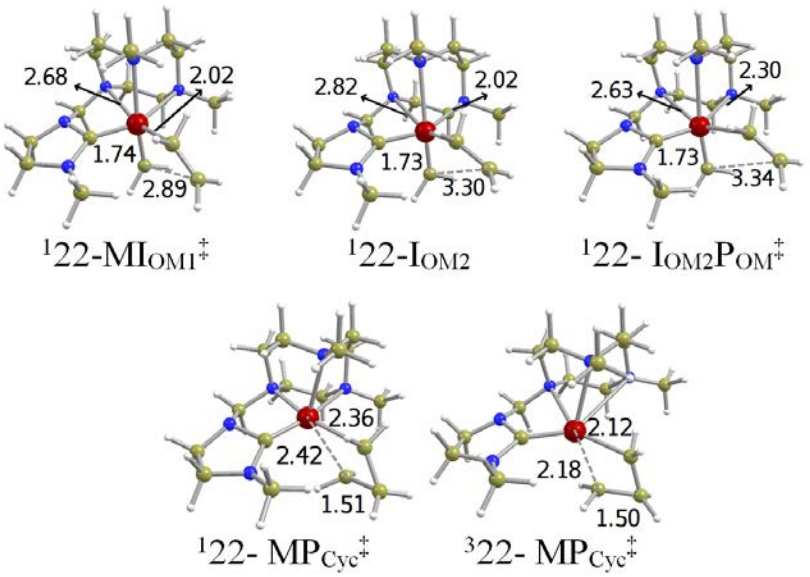

Figure 5.16: Optimized geometries for cycloreversion, in the singlet state, and cyclopropanation by reductive elimination, in singlet and triplet state, involving **22** and ethene. Distances are in Å

Moreover cyclopropanation by carbene transfer is even likely to happen. Figure 5.17 shows the energetic energy profile and Figure 5.18 the optimized structures for this pathway. The transition states lies 29.4 kcal mol^{-1} above separated reactant in the singlet state (^{1}22 − $RI_{Cyc}^{\ddagger}$) and 26.8 kcal mol^{-1} in the triplet (^{3}22 − $RI_{Cyc}^{\ddagger}$). IRC from the singlet transition state ^{1}22 − $RI_{Cyc}^{\ddagger}$ evolves spontaneously to the formation of an allyl hydride intermediate (^{1}22−I_{Cyc}) that has been associated to deactivation processes in olefin metathesis.[294,295] However in the triplet state this intermediate (^{1}22−I) is formed in a productive way to carry cyclopropanation through the subsequent transition state ^{1}22 − $I_{Cyc}I_{Cyc}^{\ddagger}$.

Although the main barriers for the carbene transfer (26.8 and 29.4 kcal mol^{-1}) path are larger than that for the reductive elimination in the triplet state (14.7 kcal mol^{-1}), the last does not take place, since the main barrier for cycloaddition step (35.7 kcal mol^{-1}) is larger than the barriers of the carbene transfer, in both spin states, thus the intermediate metallacyclebutane is not formed. Therefore, cyclopropanation by carbene transfer in the triplet state is expected to prevail in the reactivity of **22** with ethene.

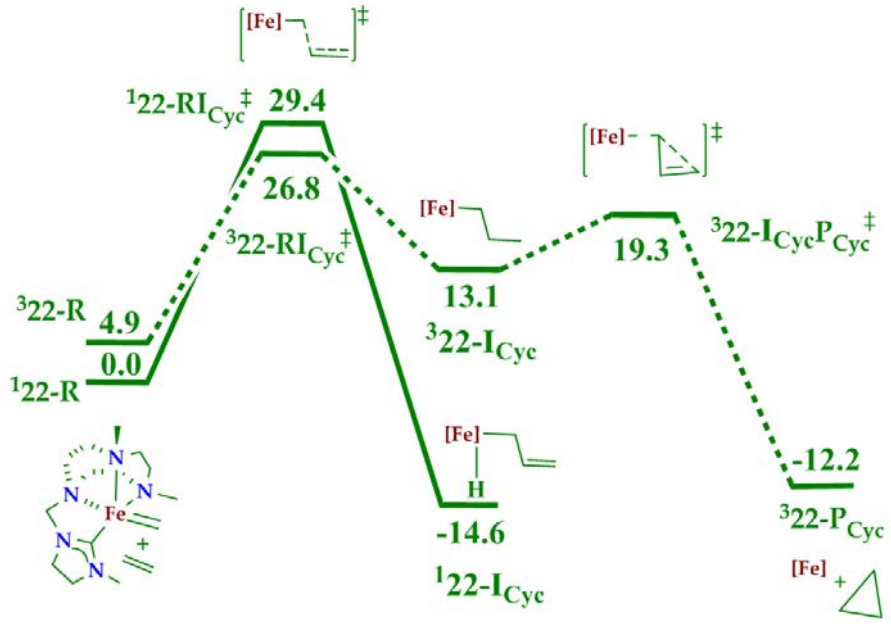

Figure 5.17: Gibbs energy profile (in kcal mol^{-1}) for carbene transfer involving **22** and ethene, in singlet and triplet state.

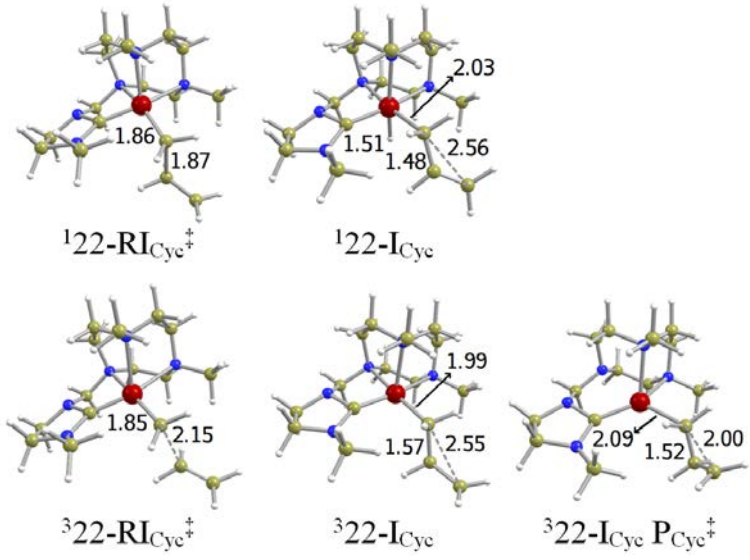

Figure 5.18: Optimized geometries for carbene transfer involving **22** and ethene, in singlet and triplet state. Distances are in Å

In summary, complex **22** does not appear to be a good candidate for olefin metathesis, despite its thermodynamics. Results suggest that its reaction with olefins would be unlikely, and if it comes to happen, would lead to cyclopropanation through carbene extraction mainly in the triplet state, with the highest energy barrier being 26.8 kcal mol^{-1} ($^{1}22 - RI^{\ddagger}_{Cyc}$).

This unlike reactivity can be explained by formal electron counting: **22** is an 18 electron complex and thus, it is not prone to accept the coordination of the incoming olefin, leading to very high energy barriers. This hypothesis is further confirmed when comparing the results of **22** with the reactivity of the analogous Fe^{2+} complex **18** with ethene. In the case of **18**, the initial carbene is 16 electrons and thus, the reaction pathway for metallacyclobutane formation shows the traditional cycloaddition transition states (se Figure 5.19) with energy barriers that are much lower than those of **22**. The triplet state is 21.8 mol^{-1} above the reactants. However, the singlet is only 13.1 mol^{-1}, being much smaller than the analogous one in of **22** ($^{1}22 - RI^{\ddagger}_{OM1}$) that is 35.7 kcal mol^{-1}.

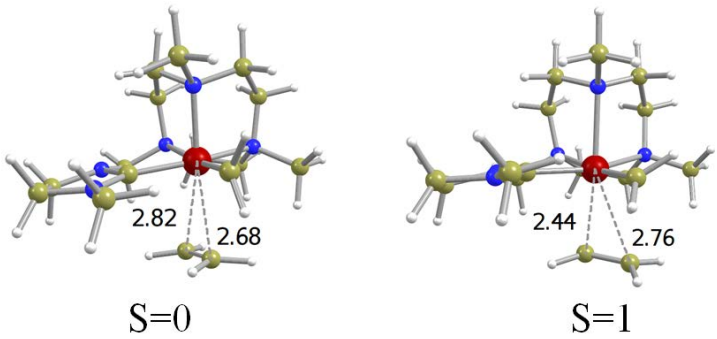

Figure 5.19: Optimized geometries for cycloaddition involving **18** and ethene, in singlet and triplet state. Distances are in Å

Overall, results show that addition of σ-donating ligands in formally Fe^{2+} $L_4Fe{=}CH_2$ complexes leads to carbene species with a singlet ground state. However, the presence of these ligands does not guarantee the formation of a singlet state metallacyclobutane intermediate by reaction with ethene. This arises from the fact that the resulting species presents only d^4 electrons in an octahedral environment, which preferentially leads to a triplet ground state, and only when the octahedral environment is distorted enough the singlet state can be favored.

In this view, metal reduction to Fe^0 leads to d^6 singlet state octahedral metallacycles and destabilized cyclopropanation products in the singlet state. These data are close to that computed for the efficient 2^{nd} Generation Grubbs Catalyst and appears as promising candidates. However, the energy barriers that have to be overcome to form the metallacyclobutane intermediate are very high suggesting that alkene metathesis with these complexes is kinetically inhibited. Indeed, the Fe^0 $L_4Fe{=}CH_2$ carbenes are formally 18 electron complexes and thus, olefin coordination appears to be strongly disfavored. In this view, the use of labile ligands, which would coordinate at the carbene and metallacyclobutane to stabilize the singlet state but discoordinate during the metallacyclobutane formation without a large energy cost could potentially be strategy when using $L_4Fe{=}CH_2$ complexes.

5.5 Radical Character of Triplet [M]=CR_2

Table 5.4 summarizes the spin density on the iron and on the carbon carbenic in the triplet state for complexes **14-24**.

Table 5.4: NPA spin densities over iron and the carbon atom of the carbene in the triplet state.

Complex	Fe	C	Complex	Fe	C
14	2.23	-0.49	20	1.70	0.18
15	2.27	-0.48	21	2.83	-0.54
16	1.93	-0.36	22	1.93	0.14
17	1.93	0.07	23	2.02	0.35
18	2.16	-0.36	24	1.14	0.50
19	1.36	0.59			

Complexes **14-16**, that do not have strong σ-donating groups show part of the β spin density on the carbenic carbon. This suggests a situation in between a [Fe]=CH_2 double bond formed with two unpaired electrons on the metal center and a situation in which the π-bond of [Fe]=CH_2 is not formed and thus three unpaired electrons are located over the metal center and one (with the opposite spin) on the carbene carbon. Figure 5.20 shows schematic representation of the two limit situation.

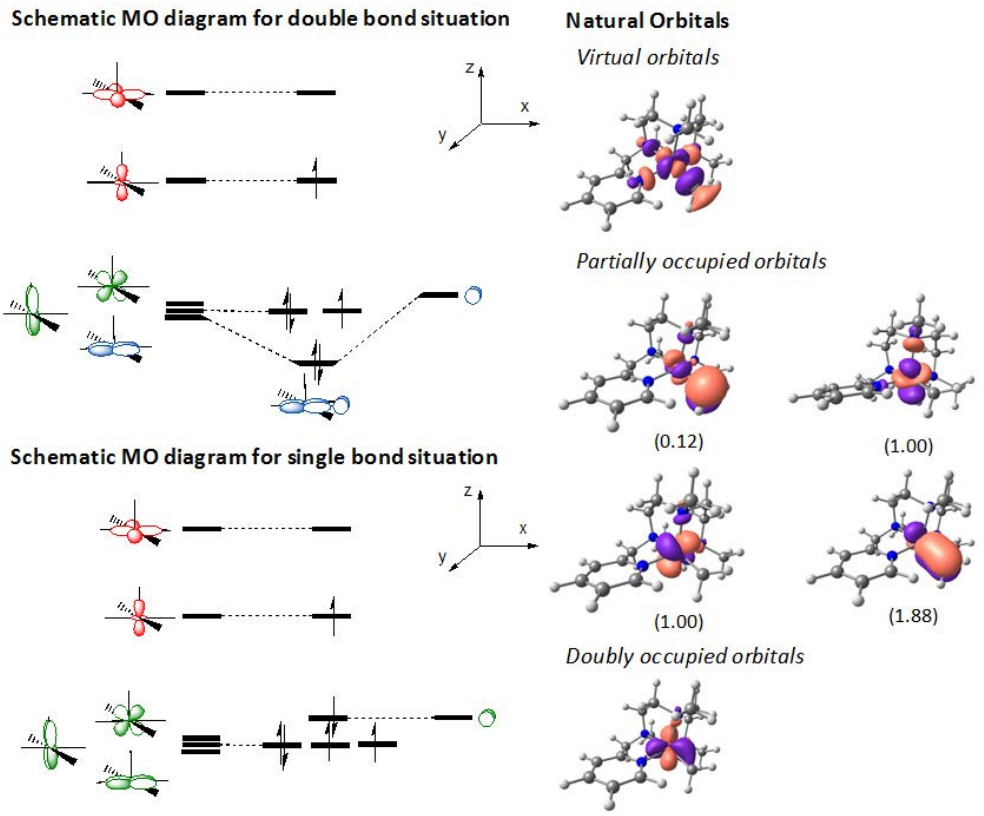

Figure 5.20: Schematic molecular orbitals diagram and Natural Orbitals of the triplet state of complex **14**.

Noteworthy, this situation with three unpaired electrons on the metal center and one on the carbene was already used to describe the electronic structure of (RPDI)Fe=CPh_2 (PDI = bis(imido)pyridine) complexes synthetized by Chirik and co-workers, which has a triplet ground state.[176] Similarly, we had discussed such behavior refering to the complex **2** in Section 3.1, which posses a non low-spin characteristics. Overall, the larger [Fe]=CH_2 distance and the spin density distribution are indicative of a significantly weaker π-bond in the triplet state.

Whereas complexes **14-16** present a SBP geometry around the metal, complexes **17-20** shows a TBP coordination, with **17** being the only exception, which is the only one that does not present strong σ-donating ligands. Interestingly, this geometrical change is associated with a change on the spin distribution, which suggest that the limit sit-

uation in which the [Fe]=CH_2 π-bond is formed (there are no unpaired electrons over the carbon of the carbene) becomes more important. This is consistent with a stronger [Fe]=CH_2 bond by the addition of σ-donor groups and appears to apply both for the singlet and triplet spin states.

Bridge Carbene

At this point it is worth mentioning that a part of the classical carbene discussed, can form another isomer is found to be a minimum in the potential energy surface. in this isomer, the carbene inserts in either the Fe-N bond involving the pyridine ligand or the Fe-C bond of the carbene N-heterocyclic. This species is a kind of bridged carbene and its structure resembles that recently reported as a masked carbene complex,[186] which we discussed in the introduction Chapter. The energies of these species are reported in Table 5.5 and the geometries in Appendix D.1.

Table 5.5: Relative Gibbs (G_{gp}+D2) energies of the bridged carbene isomers of complexes **14-24** with respect to the standard singlet carbene. Values in kcal mol^{-1}

	Standard Carbene			Bridged Carbene		
Carbene	S = 0	S = 1	S = 2	S = 0	S = 1	S = 2
14	0.0	-2.3	3.8	3.4	2.4	-17.6
15	0.0	-6.3	5.1	13.7	-19.1	-23.9
16	0.0	7.6	22.7	-11.3	-21.8	-26.5
17	0.0	3.2	16.1	18.1	11.8	10.9
18	0.0	-3.9	-[a]	-15.2	-23.9	-40.7
19	0.0	11.8	23.3	10.0	-1.3	9.3
20	0.0	5.3	20.1	-25.2	-20.6	-20.2
21	0.0	-0.4	0.2	27.6	13.0	11.4
22	0.0	4.9	7.6	0.2	-19.8	0.3
23	0.0	2.9	12.3	7.4	4.8	6.2
24	0.0	9.3	-[a]	-8.4	-7.6	16.4

[a] Optimization to the bridge carbene.

Most of these new species present an open-shell ground state, triplet or quintuplet, that usually lies lower in energy than the most carbene. Therefore, the formation of this species seems to be an im-

portant drawback that should be prevented during the synthesis and reactivity of $L_4Fe^{2+}{=}CR_2$ carbenes.

5.6 Bond strength *vs.* Cyclopropanation

The nature of the [Fe]=CH_2 may be an important factor for favoring or avoiding olefin metathesis over cyclopropanation, and we decided to access this relation regarding all the *in-silico* complexes we have studied in the previous and in this Chapters. Indeed, it seems that exists a dependence between [M]=CH_2 bond strength and the thermodynamics of cyclopropanation. Such strength can be measured by means of the bond dissociation energy (BDE). With the aim of determine the BDE, several asymptotes have been considered (see in Appendix D.2). Results show that the smaller BDE is that computed assuming a neutral carbene and a neutral metallic fragment, as in the equation 5.1. Therefore, the metal carbenes studied in this thesis are more likely to be Schrock type carbenes (see at Section 1.5).

$$L_n = CH_2(^1A) \rightarrow L_n(^3A) + CH_2(^3B_1) \tag{5.1}$$

Figure 5.21 plots the dependence between the [M]L_3=CH_2 strength, defined as the BDE, and the thermodynamics of cyclopropanation, in the most stable spin state for those complexes studied in Chapter 4 (**5-13**) and the studied in this Chapter (**14-24**). In Appendix XX we present the exact values.

Our computed BDE for complex **5**, which is an efficient catalyst for olefin metathesis, is 88.1 kcal.mol^{-1}. Complex **6**, arising from the substitution of Ru by Fe in complex **5**, has a BDE of only 53.1 kcal mol^{-1}. Nevertheless, the use of chelating ligands as well as strong donating groups increases the strength of the [M]L_3=CH_2 carbene bond. Complexes **9** and **10**, as well as the pincer complexes **10-13**, present BDE's between 72 and 83 kcal mol^{-1}, which are only slightly lower than those of complex **5**.

In the first set of pentacoordinate complexes (**14-16**), system **16** presents the least favorable cyclopropanation, which is consistent with the presence of stronger σ-donor ligands that made also the strongest [Fe]L_4=CH_2. With one exception, in the second set of complexes where N-containing ligands were replaced by C-containing ones (**17-20**) the BDE's were increased and cyclopropanation products became less sta-

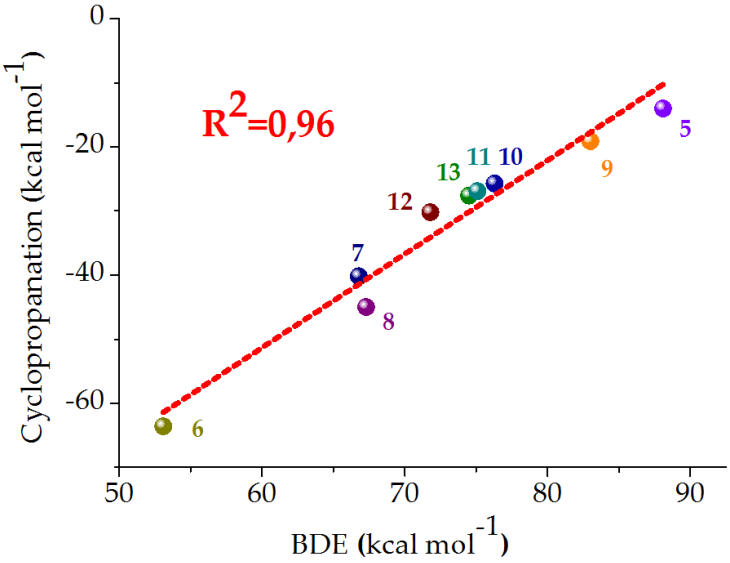

(a) Tetracoordinated (**5-13**)

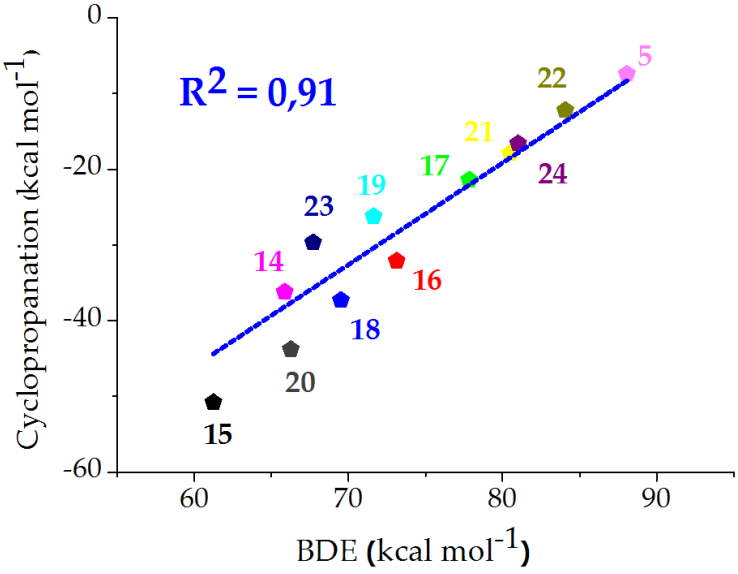

(b) Pentacoordinated (**14-24**)

Figure 5.21: Correlation between the thermodynamics for cyclopropanation and the $Fe{=}CH_2$ BDE. Grubbs 2^{nd} Generation ruthenium carbene (**5** is included.

ble. The last group of complexes are those with iron reduced by two electrons (**21-24**): these complexes formed a ensemble of species with the strongest [Fe]L_4=CH_2 and, consequently, with the less favorable cyclopropanation as well, among the pentacoordinate complexes.

These data indicate that the addition of strong tridentated donating ligands, with the strongest σ-donating group, and reduced the metallic center can show some beneficial effects:

(i) it favours the singlet states;

(ii) strengthens the M=CH_2 carbene bond;

(iii) disfavours cyclopropanation products.

5.7 Final Remarks

Here, in this Chapter, we used DFT (OPBE) calculations to analyze the influence of ancillary ligands, coordination around the metal center and iron formal oxidation state in the multiplicity of carbene ground state and its reactivity with olefins.

Addition of σ-donating ligands leads to a singlet ground state for the iron carbene. However, when the metal center is formally Fe^{2+} in the metal carbene (the carbene is counted as a neutral ligand) the addition of σ-donating ligands is not sufficient for achieving a singlet metallacyclobutane intermediate. This arise from the fact that the metal center (formally Fe^{4+} in the metallacyclobutane intermediate) has only 4d electrons and thus, the ground state in a high field ideal octahedron is the triplet. In this way, iron reduction to formally Fe^0 in the carbene leads to singlet ground state both for the carbene and metallacyclobutane intermediate and disfavors the alkene cyclopropanation at least in the singlet state. In fact, the resulting thermodynamics for methathesis and cyclopropanation of some of the here considered L_4Fe^0=CH_2 carbene species are close to those of the efficient Grubbs 2^{nd} Generation catalyst.

Regrettably, the energy barriers for metallacyclobutane formation are very high for the most promising candidates. This is attributed to the fact that the L_4Fe^0=CH_2 complexes are formally eighteen electron complexes and thus, the alkene coordination to them is strongly unfavorable. In this way, the potential use of labile ligands could be of interest since their coordination could stabilize the carbene and metallacyclobutane singlet state but also an easy decoordination of this

ligand could allow the cycloaddition process to occur.

Overall, the here reported data and that reported previously by us on tetracoordinated complexes suggest that there are no general rules to obtain an in-*silico* designed iron carbene complex with the appropriate preference for alkene metathesis with respect to cyclopropanation. In fact, the role of the ancillary ligands appears to be strongly related to the coordination number and the formal metal oxidation state.

The analysis of the strength of the metal-carbene bond and the spontaneity of cyclopropanation products show an inverse relationship for both tetracoordinate and pentacoordinate complexes, highlighting the importance of strengthening the metal–carbene. The use of strong σ-donating tridentate ligands can play this role reinforcing the [Fe]=CH_2 bond, which becomes only marginally lower than that of the Ru–based Grubbs catalyst. In this way, the use of such ligands in which the strongest σ-donating group stabilizes the singlet state for the carbene and metallacyclobutane intermediate, which becomes the ground state, and, as well as, strengthens the M=CH_2 bond, decreasing the thermodynamic preference for cyclopropanation. Similar achievements can be done by reducing the metallic center in the case of pentacoordinated [Fe]=CH_2. These two strategy emerges as a way to be pathed.

General Conclusions

This thesis is an extensive contribution to the efforts of carry out Olefin Metathesis based on iron catalysts, as a part of a more general emerging organometallic chemistry based on the earth-based metals. We have analyzed the reactivity of known iron and ruthenium carbenes with olefins, along with the nature of the ancillary ligands and geometry around the metal center that could favor the catalytic activity for olefin metathesis of a $L_3Fe{=}CH_2$ and $L_4Fe{=}CH_2$ iron carbenes. This work was addressed by through a computational procedure by DFT means, with OPBE functional.

Overall, electronic structure analysis of the triplet state of the different catalysts shows that whereas for the 2^{nd} Generation Grubbs catalyst, which is a ruthenium carbene, the two unpaired electrons lye on the metal cation, and for the case of iron carbene complexes there is an unpaired electron at the carbene, which may induce radical mechanisms.

In the case of ruthenium carbenes, olefin metathesis is, as expected, the preferred reaction through the Chauvin mechanism, reactivity of known iron-carbene complexes is very sensitive to the coordination around the metal center and the spin state of the metal-carbene complex.

Iron-carbene catalyst high-valent, however, face difficulties in the cycloaddition process, because they are high-coordinate and the coordination of the incoming olefin is hard to happen. This is the case iron carbenes belonging to the Piano-Stool (**3**) and Heme(4) kind that have 18 and 16 electrons respectively and are in the singlet state. For these complexes, the intermediate metallacyclebutane is not found, ergo olefin metathesis or reductive elimination does not take place. The cyclopropanation experimentally observed occurs through the concerted carbene transfer mechanism. Likewise, (18 e^-) **22** show high barriers in the cycloaddition step, and cyclopropnation by a stepwise carbene

transfer mechanism is more favourable. These are singlet state high-coordinated iron carbenes. Complex **10** is also in the singlet state, but because it is only a 16 e^- electrons, cycloaddition is allowed, although the subsequent step is cyclopropanation by reductive elimination.

Complexes **2** and **6**, on the other hand, are iron carbenes low-coordinated with a non-low-spin ground state with a radical character over the carbenic carbon, and induces cyclopropanation through the step-wise radical carbene transfer mechanism, which shows lower barriers than other possible reactivities.

Another significant part of this thesis is dedicated to analyzing how the nature of the ancillary ligands, coordination geometry around the metal center and the iron formal oxidation state influences the spin multiplicity of the metal carbene ground state, the [M=CR_2 bond strength and the reactivity regarding olefins. We focused on the factors favoring a singlet ground state for the active carbene and metallacyclobutane intermediate as well as those disfavoring the alkene cyclopropanation.

Results show that for the tetracoordinated iron-complexes, the addition of strong σ-donating ligands favors the carbene singlet state, although the intermediate does not show a singlet ground spin, which is only achieved, by using tricoordinated chelating ligands with the strongest σ-donor group in central position such as those of complex **10**–**13**. Fro the case of complex **10**, cyclopropanation is disfavoured facing olefin metathesis, unfortunately the kinetics is still favourable for cyclopropanation by reductive elimination from the intermediate metallacyclebutane.

Pentacoordinated complexes with σ-donating ligands leads to a singlet ground state for the iron carbenes, but, again, the intermediate metallacyclebutane is not in the singlet state. In this case, iron reduction to formally Fe^0 in the carbene leads to singlet ground state both for the carbene and metallacyclobutane intermediate and disfavors the alkene cyclopropanation at least in the singlet state, some of them resembling the efficient Grubbs 2^{nd} Generation catalyst. As this system are already 18 e^- the cycloaddition process is unlike. In this way, the potential use of labile ligands could be of interest to stabilize the metallacyclobutane and allow the cycloaddition process to occur.

The analysis metal-carbene bond strength and the of cyclopropanation products thermodynamics show an inverse relationship for both tetracoordinate and pentacoordinate complexes, highlighting the im-

portance of strengthening the metal–carbene. Strong σ-donating tridentate ligands reinforces the [Fe]=CH_2 bond for tetracoordinated complexes, which becomes only marginally lower than that of the Ru–based Grubbs catalyst. Similarly, pentacoordinated iron-carbenes achieves such goal also by reducing the metallic center. Therefore, these emerges as way to be followed.

Bibliography

[1] R. H. Grubbs (ed.), *Handbook of Metathesis*. Wiley-VCH Verlag GmbH & Co. KGaA, 2015.

[2] "The nobel prize in chemistry 2005." Available from `https://www.nobelprize.org/nobel_prizes/chemistry/laureates/2005/`. Retrieved: August 09, 2017.

[3] Y. Chauvin, "Olefin metathesis: The early days (nobel lecture)," *Angewandte Chemie International Edition*, vol. 45, pp. 3740–3747, 2006.

[4] R. R. Schrock, "Multiple metal-carbon bonds for catalytic metathesis reactions (nobel lecture)," *Angewandte Chemie - International Edition*, vol. 45, pp. 3748–3759, 2006.

[5] R. H. Grubbs, "Olefin-metathesis catalysts for the preparation of molecules and materials (nobel lecture)," *Angewandte Chemie International Edition*, vol. 45, pp. 3760–3765, 2006.

[6] "Preface," in *Catalysis without Precious Metals* (R. M. Bullock, ed.), pp. I–XVIII, Wiley-VCH Verlag GmbH & Co. KGaA, 2010.

[7] R. M. Bullock, "Abundant metals give precious hydrogenation performance," *Science*, vol. 342, pp. 1054–1055, 2013.

[8] S. Enthaler, K. Junge, and M. Beller, "Sustainable metal catalysis with iron: From rust to a rising star?," *Angewandte Chemie International Edition*, vol. 47, pp. 3317–3321, 2008.

[9] P. Gandeepan and C.-H. Cheng, "Cobalt catalysis involving π components in organic synthesis," *Accounts of Chemical Research*, vol. 48, pp. 1194–1206, 2015.

[10] P. J. Chirik, "Iron- and cobalt-catalyzed alkene hydrogenation: Catalysis with both redox-active and strong field ligands," *Accounts of Chemical Research*, vol. 48, pp. 1687–1695, 2015.

[11] P. L. Holland, "Distinctive reaction pathways at base metals in high-spin organometallic catalysts," *Accounts of Chemical Research*, vol. 48, pp. 1696–1702, 2015.

[12] C. C. C. Johansson Seechurn, M. O. Kitching, T. J. Colacot, and V. Snieckus, "Palladium-catalyzed cross-coupling: A historical contextual perspective to the 2010 nobel prize," *Angewandte Chemie International Edition*, vol. 51, pp. 5062–5085, 2012.

[13] A. Suzuki, "Cross-coupling reactions of organoboranes: An easy way to construct c-c bonds (nobel lecture)," *Angewandte Chemie International Edition*, vol. 50, pp. 6722–6737, 2011.

[14] E.-i. Negishi, "Magical power of transition metals: Past, present, and future (nobel lecture)," *Angewandte Chemie International Edition*, vol. 50, pp. 6738–6764, 2011.

[15] D. A. Colby, R. G. Bergman, and J. A. Ellman, "Rhodium-catalyzed C−C bond formation via heteroatom-directed C−H bond activation," *Chemical Reviews*, vol. 110, pp. 624–655, 2010.

[16] B. Marciniec (ed.), *Comprehensive Handbook on Hydrosilylation*. Pergamon, 1992.

[17] J. A. Osborn, G. Wilkinson, and J. J. Mrowca, *Tris(triphenylphosphine)halorhodium(I)*. John Wiley & Sons, Inc., 2007.

[18] W. S. Knowles, "Asymmetric hydrogenations (nobel lecture)," *Angewandte Chemie International Edition*, vol. 41, pp. 1998–2007, 2002.

[19] R. Noyori, "Asymmetric catalysis: Science and opportunities (nobel lecture 2001)," *Advanced Synthesis & Catalysis*, vol. 345, pp. 15–32, 2003.

[20] T. M. Trnka and R. H. Grubbs, "The development of $L_2X_2Ru{=}CHR$ olefin metathesis catalysts: An organometallic success story," *Accounts of Chemical Research*, vol. 34, pp. 18–29, 2001.

[21] I. Ojima, C.-Y. Tsai, M. Tzamarioudaki, and D. Bonafoux, *The Hydroformylation Reaction*. John Wiley & Sons, Inc., 2004.

[22] R. Jira, "Acetaldehyde from ethylene – A retrospective on the discovery of the wacker process," *Angewandte Chemie International Edition*, vol. 48, pp. 9034–9037, 2009.

[23] P. Chirik and R. Morris, "Getting down to earth: The renaissance of catalysis with abundant metals.," *Accounts of Chemical Research*, vol. 48, p. 2495, 2015.

[24] R. R. Schrock, "Recent advances in high oxidation state Mo and W imido alkylidene chemistry," *Chemical Reviews*, vol. 109, pp. 3211–3226, 2009.

[25] G. C. Vougioukalakis and R. H. Grubbs, "Ruthenium-based heterocyclic carbene-coordinated olefin metathesis catalysts," *Chemical Reviews*, vol. 110, pp. 1746–1787, 2010.

[26] K. Ivin and H. Mol, *Olefin Metathesis and Metathesis Polymerization*. London: Academic Press, 2 ed., 1997.

[27] R. R. Schrock, "Olefin metathesis by well-defined complexes of molybdenum and tungsten," in *Alkene Metathesis in Organic Synthesis* (A. Fürstner, ed.), pp. 1–36, Berlin, Heidelberg: Springer Berlin Heidelberg, 1998.

[28] V. Schneider and P. K. Frolich, "Mechanism of formation of aromatics from lower paraffins1,2," *Industrial & Engineering Chemistry*, vol. 23, pp. 1405–1410, 1931.

[29] D. Astruc, "The metathesis reactions: from a historical perspective to recent developments," *New Journal of Chemistry*, vol. 29, pp. 42–56, 2005.

[30] R. L. Banks and G. C. Bailey, "Olefin disproportionation. A new catalytic process," *I&EC Product Research and Development*, vol. 3, pp. 170–173, 1964.

[31] G. Natta, G. Dall'Asta, and G. Mazzanti, "Stereospecific homopolymerization of cyclopentene," *Angewandte Chemie International Edition in English*, vol. 3, pp. 723–729, 1964.

[32] N. Calderon, H. Y. Chen, and K. W. Scott, "Olefin metathesis - A novel reaction for skeletal transformations of unsaturated hydrocarbons," *Tetrahedron Letters*, vol. 8, pp. 3327 – 3329, 1967.

[33] K. Endo and R. H. Grubbs, "Chelated ruthenium catalysts for Z-selective olefin metathesis," *Journal of the American Chemical Society*, vol. 133, pp. 8525–8527, 2011.

[34] B. K. Keitz, K. Endo, P. R. Patel, M. B. Herbert, and R. H. Grubbs, "Improved ruthenium catalysts for Z-selective olefin metathesis," *Journal of the American Chemical Society*, vol. 134, pp. 693–699, 2012.

[35] S. J. Connon and S. Blechert, "Recent developments in olefin cross-metathesis," *Angewandte Chemie International Edition*, vol. 42, pp. 1900–1923, 2003.

[36] C. W. Bielawski and R. H. Grubbs, "Living ring-opening metathesis polymerization," *Progress in Polymer Science*, vol. 32, pp. 1 – 29, 2007.

[37] M. R. Buchmeiser, "Polymer-supported well-defined metathesis catalysts," *Chemical Reviews*, vol. 109, pp. 303–321, 2009.

[38] T. O. Schrader and M. L. Snapper, "Ring-opening cross-metatheses," in *Handbook of Metathesis* (R. H. Grubbs, ed.), pp. 205–237, Wiley-VCH Verlag GmbH, 2008.

[39] R. H. Grubbs, S. J. Miller, and G. C. Fu, "Ring-closing metathesis and related processes in organic synthesis," *Accounts of Chemical Research*, vol. 28, pp. 446–452, 1995.

[40] H. Mutlu, L. M. de Espinosa, and M. A. R. Meier, "Acyclic diene metathesis: a versatile tool for the construction of defined polymer architectures," *Chemical Society Reviews*, vol. 40, pp. 1404–1445, 2011.

[41] J. C. Mol, "Industrial applications of olefin metathesis," *Journal of Molecular Catalysis A*, vol. 213, pp. 39–45, 2004.

[42] A. H. Hoveyda and A. R. Zhugralin, "The remarkable metal-catalysed olefin metathesis reaction.," *Nature*, vol. 450, pp. 243–251, 2007.

[43] K. C. Nicolaou, P. G. Bulger, and D. Sarlah, "Metathesis reactions in total synthesis," *Angewandte Chemie International Edition*, vol. 44, pp. 4490–4527, 2005.

[44] A. Fürstner, "Metathesis in total synthesis.," *Chemical communications (Cambridge, England)*, vol. 47, pp. 6505–11, 2011.

[45] S. Kress and S. Blechert, "Asymmetric catalysts for stereocontrolled olefin metathesis reactions," *Chemical Society Reviews*, vol. 41, pp. 4389–4408, 2012.

[46] R. Pederson, I. Fellows, T. Ung, H. Ishihara, and S. Hajela, "Applications of olefin cross metathesis to commercial products," *Advanced Synthesis & Catalysis*, vol. 344, pp. 728–735, 2002.

[47] A. Fürstner and O. R. Thiel, "Formal total synthesis of (−)-balanol: concise approach to the hexahydroazepine segment based on rcm," *The Journal of Organic Chemistry*, vol. 65, pp. 1738–1742, 2000.

[48] K. C. Nicolaou, N. Winssinger, J. Pastor, S. Ninkovic, F. Sarabia, Y. He, D. Vourloumis, Z. Yang, T. Li, P. Giannakakou, and E. Hamel, "Synthesis of epothilones a and b in solid and solution phase," *Nature*, vol. 387, pp. 268–272, 1997.

[49] A. Fürstner, "Olefin metathesis and beyond," *Angewandte Chemie International Edition*, vol. 39, pp. 3012–3043, 2000.

[50] N. Calderon, "Olefin metathesis reaction," *Accounts of Chemical Research*, vol. 5, pp. 127–132, 1972.

[51] I. M. Baibich and J. R. Gregório, "Metátese catalítica de olefinas," *Química Nova*, vol. 16, pp. 120–129, 1993.

[52] P. Jean-Louis Hérisson and Y. Chauvin, "Catalyse de transformation des oléfines par les complexes du tungstène. ii. télomérisation des oléfines cycliques en présence d'oléfines acycliques," *Die Makromolekulare Chemie*, vol. 141, pp. 161–176, 1971.

[53] R. B. Woodward and R. Hoffmann, "Stereochemistry of electrocyclic reactions," *Journal of the American Chemical Society*, vol. 87, pp. 395–397, 1965.

[54] F. Bernardi, A. Bottoni, and G. P. Miscione, "DFT study of the olefin metathesis catalyzed by ruthenium complexes," *Organometallics*, vol. 22, pp. 940–947, 2003.

[55] T. J. Katz and J. McGinnis, "Mechanism of the olefin metathesis reaction," *Journal of the American Chemical Society*, vol. 97, pp. 1592–1594, 1975.

[56] A. M. Rouhi, "Olefin metathesis: The early days," *Chemical & Engineering News*, vol. 80, pp. 34–38, 2002.

[57] P. W. Jennings and L. L. Johnson, "Metallacyclobutane complexes of the group eight transition metals: Synthesis, characterizations, and chemistry," *Chemical Reviews*, vol. 94, pp. 2241–2290, 1994.

[58] A. F. Noels and A. Demonceau, "From olefin cyclopropanation to olefin metathesis through catalyst engineering: recent applications of olefin metathesis to fine organic synthesis and to polymer chemistry," *Journal of Physical Organic Chemistry*, vol. 11, 1998.

[59] E. O. Fischer and A. Maasböl, "On the existence of a tungsten carbonyl carbene complex," *Angewandte Chemie International Edition iToupetn English*, vol. 3, pp. 580–581, 1964.

[60] R. H. Crabtree, *The Organometallic Chemistry of the Transition Metals*. John Wiley & Sons, Inc., 2005.

[61] R. R. Schrock, "Alkylcarbene complex of tantalum by intramolecular α-hydrogen abstraction," *Journal of the American Chemical Society*, vol. 96, pp. 6796–6797, 1974.

[62] G. Occhipinti and V. R. Jensen, "Nature of the transition metal–carbene bond in grubbs olefin metathesis catalysts," *Organometallics*, vol. 30, pp. 3522–3529, 2011.

[63] H. Lu, W. I. Dzik, X. Xu, L. Wojtas, B. de Bruin, and X. P. Zhang, "Experimental evidence for cobalt(III)-carbene radicals: Key intermediates in cobalt(II)-based metalloradical cyclopropanation," *Journal of the American Chemical Society*, vol. 133, pp. 8518–8521, 2011.

[64] C. P. Casey and T. J. Burkhardt, "Reactions of (diphenylcarbene)pentacarbonyltungsten(0) with alkenes. role of metal-carbene complexes in cyclopropanation and olefin metathesis reactions," *Journal of the American Chemical Society*, vol. 96, pp. 7808–7809, 1974.

[65] Y. Chauvin, D. Commereuc, and D. Cruypelinck, "Catalysis of olefin transformation by tungsten complexes, 5. tungsten carbonyl carbenes activated by titanium tetrahalides as catalysts for the ring-opening polymerization of cyclopentene," *Die Makromolekulare Chemie*, vol. 177, 1976.

[66] R. Schrock, S. Rocklage, J. Wengrovius, G. Rupprecht, and J. Fellmann, "Preparation and characterization of active niobium, tantalum and tungsten metathesis catalysts," *Journal of Molecular Catalysis*, vol. 8, pp. 73 – 83, 1980.

[67] R. R. Schrock, J. S. Murdzek, G. C. Bazan, J. Robbins, M. DiMare, and M. O'Regan, "Synthesis of molybdenum imido alkylidene complexes and some reactions involving acyclic olefins," *Journal of the American Chemical Society*, vol. 112, pp. 3875–3886, 1990.

[68] R. R. Schrock and A. H. Hoveyda, "Molybdenum and tungsten imido alkylidene complexes as efficient olefin-metathesis catalysts," *Angewandte Chemie - International Edition*, vol. 42, pp. 4592–4633, 2003.

[69] A. Poater, X. Solans-Monfort, E. Clot, C. Copèret, and O. Eisenstein, "Understanding d0-olefin metathesis catalysts: Which metal, which ligands?," *Journal of the American Chemical Society*, vol. 129, pp. 8207–8216, 2007.

[70] S. J. Malcolmson, S. J. Meek, E. S. Sattely, R. R. Schrock, and A. H. Hoveyda, "Highly efficient molybdenum-based catalysts for enantioselective alkene metathesis," *Nature*, vol. 8, pp. 933 – 937, 2008.

[71] G. Natta, G. Dall'asta, and L. Porri, "Polymerization of cyclobutene and of 3-methylcyclobutene by $RuCl_3$ in polar protic solvents," *Die Makromolekulare Chemie*, vol. 81, pp. 253–257, 1965.

[72] S. T. Nguyen, L. K. Johnson, R. H. Grubbs, and J. W. Ziller, "Ring-opening metathesis polymerization (ROMP) of norbornene by a group VIII carbene complex in protic media," *Journal of the American Chemical Society*, vol. 114, pp. 3974–3975, 1992.

[73] P. Schwab, R. H. Grubbs, and J. W. Ziller, "Synthesis and applications of RuCl2(CHR')$(PR_3)_2$:the influence of the alkylidene moiety on metathesis activity," *Journal of the American Chemical Society*, vol. 118, pp. 100–110, 1996.

[74] M. S. Sandford, J. A. Love, and R. H. Grubbs, "Mechanism and activity of ruthenium olefin metathesis catalysts," *Journal of the American Chemical Society*, vol. 123, pp. 6543–6554, 2001.

[75] L. Ackermann, A. Fürstner, T. Weskamp, F. J. Kohl, and W. A. Herrmann, "Ruthenium carbene complexes with imidazolin-2-ylidene ligands allow the formation of tetrasubstituted cycloalkenes by rcm," *Tetrahedron Letters*, vol. 40, pp. 4787 – 4790, 1999.

[76] M. Scholl, T. M. Trnka, J. P. Morgan, and R. H. Grubbs, "Increased ring closing metathesis activity of ruthenium-based olefin metathesis catalysts coordinated with imidazolin-2-ylidene ligands," *Tetrahedron Letters*, vol. 40, pp. 2247 – 2250, 1999.

[77] M. Scholl, S. Ding, C. W. Lee, and R. H. Grubbs, "Synthesis and activity of a new generation of ruthenium-based olefin metathesis catalysts coordinated with 1,3-dimesityl-4,5-dihydroimidazol-2-ylidene ligands," *Organic Letters*, vol. 1, pp. 953–956, 1999.

[78] J. Huang, E. D. Stevens, S. P. Nolan, and J. L. Petersen, "Olefin metathesis-active ruthenium complexes bearing a nucleophilic carbene ligand," *Journal of the American Chemical Society*, vol. 121, pp. 2674–2678, 1999.

[79] J. S. Kingsbury, J. P. A. Harrity, P. J. Bonitatebus, and A. H. Hoveyda, "A recyclable ru-based metathesis catalyst," *Journal of the American Chemical Society*, vol. 121, pp. 791–799, 1999.

[80] S. B. Garber, J. S. Kingsbury, B. L. Gray, and A. H. Hoveyda, "Efficient and recyclable monomeric and dendritic Ru-based metathesis catalysts," *Journal of the American Chemical Society*, vol. 122, pp. 8168–8179, 2000.

[81] S. Gessler, S. Randl, and S. Blechert, "Synthesis and metathesis reactions of a phosphine-free dihydroimidazole carbene ruthenium complex," *Tetrahedron Letters*, vol. 41, pp. 9973 – 9976, 2000.

[82] B. Su, Z.-C. Cao, and Z.-J. Shi, "Exploration of earth-abundant transition metals (Fe, Co, and Ni) as catalysts in unreactive chemical bond activations," *Accounts of Chemical Research*, vol. 48, pp. 886–896, 2015.

[83] R. H. Morris, "Asymmetric hydrogenation, transfer hydrogenation and hydrosilylation of ketones catalyzed by iron complexes," *Chemical Society Reviews*, vol. 38, pp. 2282–2291, 2009.

[84] S. Chakraborty, P. Bhattacharya, H. Dai, and H. Guan, "Nickel and iron pincer complexes as catalysts for the reduction of carbonyl compounds," *Accounts of Chemical Research*, vol. 48, pp. 1995–2003, 2015.

[85] "Precious metals management - johnson matthey." Available from `http://www.platinum.matthey.com/prices`. Retrieved: August 08, 2017.

[86] E. Nakamura, "Managing the scarcity of chemical elements," *Nature Materials*, vol. 10, pp. 158–161, 2011.

[87] "Ferrous scrap price index." Available from `https://www.metalprices.com/metal/ferrous-scrap-price-index`. Retrieved: August 08, 2017.

[88] M. Tobisu and N. Chatani, "Cross-couplings using aryl ethers via C–O bond activation enabled by nickel catalysts," *Accounts of Chemical Research*, vol. 48, pp. 1717–1726, 2015.

[89] I. Bauer and H.-J. Knölker, "Iron catalysis in organic synthesis," *Chemical Reviews*, vol. 115, pp. 3170–3387, 2015.

[90] L. B. Hunt and F. M. Lever, "Availability of the platinum metals. survey of productive resources in relation to industrial uses," *Platinum Metals Review*, vol. 13, pp. 126–38, 1969.

[91] P. B. Kettler, "Platinum group metals in catalysis: fabrication of catalysts and catalyst precursors," *Organic Process Research & Development*, vol. 7, pp. 342–354, 2003.

[92] K. L. Haas and K. J. Franz, "Application of metal coordination chemistry to explore and manipulate cell biology," *Chemical Reviews*, vol. 109, pp. 4921–4960, 2009.

[93] P. Atkins, T. Overton, J. Rourke, M. Weller, and F. Armstrong, *Shriver and Atkins' Inorganic Chemistry*. Oxford University Press, 2010.

[94] A. Fürstner, "Iron catalysis in organic synthesis: A critical assessment of what it takes to make this base metal a multitasking champion," *ACS Central Science*, vol. 2, pp. 778–789, 2016.

[95] J. K. Kochi, "Electron-transfer mechanisms for organometallic intermediates in catalytic reactions," *Accounts of Chemical Research*, vol. 7, pp. 351–360, 1974.

[96] P. L. Holland, "Electronic structure and reactivity of three-coordinate iron complexes," *Accounts of Chemical Research*, vol. 41, pp. 905–914, 2008.

[97] D. Benito-Garagorri, I. Lagoja, L. F. Veiros, and K. A. Kirchner, "Reactivity of coordinatively unsaturated iron complexes towards carbon monoxide: to bind or not to bind?," *Dalton Transactions*, vol. 40, pp. 4778–4792, 2011.

[98] R. Poli, "Open shell organometallics: a general analysis of their electronic structure and reactivity," *Journal of Organometallic Chemistry*, vol. 689, pp. 4291 – 4304, 2004.

[99] J. N. Harvey, "Spin-forbidden reactions in transition-metal chemistry," in *Computational Organometallic Chemistry* (T. Cundari, ed.), pp. 291–320, Taylor & Francis, 2001.

[100] J. N. Harvey, R. Poli, and K. M. Smith, "Understanding the reactivity of transition metal complexes involving multiple spin states," *Coordination Chemistry Reviews*, vol. 238, pp. 347 – 361, 2003.

[101] F. Jia and Z. Li, "Iron-catalyzed/mediated oxidative transformation of C-H bonds," *Organic Chemistry Frontiers*, vol. 1, pp. 194–214, 2014.

[102] A. Gualandi, L. Mengozzi, and P. G. Cozzi, "Iron-promoted radical reactions: Current status and perspectives," *Asian Journal of Organic Chemistry*, pp. n/a–n/a, 2017.

[103] A. Guérinot and J. Cossy, "Iron-catalyzed C-C cross-couplings using organometallics," *Topics in Current Chemistry*, vol. 374, p. 49, 2016.

[104] J. C. Lo, D. Kim, C.-M. Pan, J. T. Edwards, Y. Yabe, J. Gui, T. Qin, S. Gutiérrez, J. Giacoboni, M. W. Smith, P. L. Holland, and P. S. Baran, "Fe-catalyzed C–C bond construction from olefins via radicals," *Journal of the American Chemical Society*, vol. 139, pp. 2484–2503, 2017.

[105] M. Costas, M. P. Mehn, M. P. Jensen, and L. Que, "Dioxygen activation at mononuclear nonheme iron active sites: Enzymes, models, and intermediates," *Chemical Reviews*, vol. 104, pp. 939–986, 2004.

[106] E. Bauer, ed., *Iron Catalysis II.* Springer International Publishing, 2015.

[107] C. Bolm, J. Legros, J. Le Paih, and L. Zani, "Iron-catalyzed reactions in organic synthesis," *Chemical Reviews*, vol. 104, pp. 6217–6254, 2004.

[108] I. Bauer and H.-J. Knölker, "Iron complexes in organic chemistry," in *Iron Catalysis in Organic Chemistry* (B. Plietker, ed.), pp. 1–27, Wiley-VCH Verlag GmbH & Co. KGaA, 2008.

[109] "Preface," in *Iron Catalysis in Organic Chemistry* (B. Plietker, ed.), pp. I–XV, Wiley-VCH Verlag GmbH & Co. KGaA, 2008.

[110] H. Shinokubo and K. Oshima, "Transition metal-catalyzed carbon–carbon bond formation with grignard reagents – novel reactions with a classic reagent," *European Journal of Organic Chemistry*, vol. 2004, pp. 2081–2091, 2004.

[111] F. Alois and M. Rubén, "Advances in iron catalyzed cross coupling reactions," *Chemistry Letters*, vol. 34, pp. 624–629, 2005.

[112] B. D. Sherry and A. Fürstner, "The promise and challenge of iron-catalyzed cross coupling," *Accounts of Chemical Research*, vol. 41, pp. 1500–1511, 2008.

[113] A. Fürstner, "From oblivion into the limelight: Iron (domino) catalysis," *Angewandte Chemie International Edition*, vol. 48, pp. 1364–1367, 2009.

[114] W. M. Czaplik, M. Mayer, J. Cvengroš, and A. J. von Wangelin, "Coming of age: Sustainable iron-catalyzed cross-coupling reactions," *ChemSusChem*, vol. 2, pp. 396–417, 2009.

[115] A. Rudolph and M. Lautens, "Secondary alkyl halides in transition-metal-catalyzed cross-coupling reactions," *Angewandte Chemie International Edition*, vol. 48, pp. 2656–2670, 2009.

[116] R. Jana, T. P. Pathak, and M. S. Sigman, "Advances in transition metal (Pd,Ni,Fe)-catalyzed cross-coupling reactions using alkyl-organometallics as reaction partners," *Chemical Reviews*, vol. 111, pp. 1417–1492, 2011.

[117] T. Mesganaw and N. K. Garg, "Ni- and Fe-catalyzed cross-coupling reactions of phenol derivatives," *Organic Process Research & Development*, vol. 17, pp. 29–39, 2013.

[118] A. A. O. Sarhan and C. Bolm, "Iron(III) chloride in oxidative C-C coupling reactions," *Chemical Society Reviews*, vol. 38, pp. 2730–2744, 2009.

[119] Z. Huang, L. Jin, Y. Feng, P. Peng, H. Yi, and A. Lei, "Iron-catalyzed oxidative radical cross-coupling/cyclization between phenols and olefins," *Angewandte Chemie International Edition*, vol. 52, pp. 7151–7155, 2013.

[120] Y. Hayashi, H. Shinokubo, and K. Oshima, "Intramolecular radical cyclization of 2-haloethanal allyl acetal and allyl 2-halophenyl ether with a grignard reagent in the presence of iron(II) chloride," *Tetrahedron Letters*, vol. 39, pp. 63 – 66, 1998.

[121] M. Guisán-Ceinos, F. Tato, E. Buñuel, P. Calle, and D. J. Cardenas, "Fe-catalysed kumada-type alkyl-alkyl cross-coupling. evidence for the intermediacy of Fe(I) complexes," *Chemical Science*, vol. 4, pp. 1098–1104, 2013.

[122] T. Hatakeyama, T. Hashimoto, Y. Kondo, Y. Fujiwara, H. Seike, H. Takaya, Y. Tamada, T. Ono, and M. Nakamura, "Iron-catalyzed suzuki−miyaura coupling of alkyl halides," *Journal of the American Chemical Society*, vol. 132, pp. 10674–10676, 2010.

[123] A. Leitner, "Iron-catalyzed cross-coupling reactions," in *Iron Catalysis in Organic Chemistry* (B. Plietker, ed.), pp. 147–176, Wiley-VCH Verlag GmbH & Co. KGaA, 2008.

[124] Z. Huang, L. Jin, Y. Feng, P. Peng, H. Yi, and A. Lei, "Iron-catalyzed oxidative radical cross-coupling/cyclization between phenols and olefins," *Angewandte Chemie International Edition*, vol. 52, pp. 7151–7155, 2013.

[125] M. Ouchi, T. Terashima, and M. Sawamoto, "Transition metal-catalyzed living radical polymerization: Toward perfection in catalysis and precision polymer synthesis," *Chemical Reviews*, vol. 109, pp. 4963–5050, 2009.

[126] T. Ando, M. Kamigaito, and M. Sawamoto, "Iron(II) chloride complex for living radical polymerization of methyl methacrylate," *Macromolecules*, vol. 30, pp. 4507–4510, 1997.

[127] C.-L. Sun, B.-J. Li, and Z.-J. Shi, "Direct C−H transformation via iron catalysis," *Chemical Reviews*, vol. 111, pp. 1293–1314, 2011.

[128] R. Shang, L. Ilies, and E. Nakamura, "Iron-catalyzed C–H bond activation," *Chemical Reviews*, vol. 117, pp. 9086–9139, 2017.

[129] D. L. Coward, B. R. M. Lake, and M. P. Shaver, "Understanding organometallic-mediated radical polymerization with an iron(II) amine–bis(phenolate)," *Organometallics*, vol. 0, p. null, 0.

[130] P. J. Chirik, "Modern alchemy: Replacing precious metals with iron in catalytic alkene and carbonyl hydrogenation reactions," in *Catalysis without Precious Metals* (R. M. Bullock, ed.), pp. 83–110, Wiley-VCH Verlag GmbH & Co. KGaA, 2010.

[131] B. A. F. Le Bailly and S. P. Thomas, "Iron-catalysed reduction of carbonyls and olefins," *RSC Advances*, vol. 1, pp. 1435–1445, 2011.

[132] S. C. E. Stieber, C. Milsmann, J. M. Hoyt, Z. R. Turner, K. D. Finkelstein, K. Wieghardt, S. DeBeer, and P. J. Chirik, "Bis(imino)pyridine iron dinitrogen compounds revisited: Differences in electronic structure between four- and five-coordinate derivatives.," *Inorganic Chemistry*, vol. 51, pp. 3770–3785, 2012.

[133] S. K. Russell, J. M. Darmon, E. Lobkovsky, and P. J. Chirik, "Synthesis of aryl-substituted bis(imino)pyridine iron dinitrogen complexes," *Inorganic Chemistry*, vol. 49, pp. 2782–2792, 2010.

[134] R. H. Morris, "Asymmetric hydrogenation, transfer hydrogenation and hydrosilylation of ketones catalyzed by iron complexes," *Chemical Society Reviews*, vol. 38, pp. 2282–2291, 2009.

[135] A. C. Mayer and C. Bolm, "Iron-catalyzed oxidation reactions," in *Iron Catalysis in Organic Chemistry* (B. Plietker, ed.), pp. 73–123, Wiley-VCH Verlag GmbH & Co. KGaA, 2008.

[136] M. S. Chen and M. C. White, "Combined effects on selectivity in fe-catalyzed methylene oxidation," *Science*, vol. 327, pp. 566–571, 2010.

[137] P. E. Gormisky and M. C. White, "Catalyst-controlled aliphatic C-H oxidations with a predictive model for site-selectivity," *Journal of the American Chemical Society*, vol. 135, pp. 14052–14055, 2013.

[138] G. Olivo, O. Cussó, and M. Costas, "Biologically inspired C−H and C=C oxidations with hydrogen peroxide catalyzed by iron coordination complexes," *Chemistry – An Asian Journal*, vol. 11, pp. 3148–3158, 2016.

[139] W. Wang, Q. Sun, D. Xu, C. Xia, and W. Sun, "Asymmetric epoxidation of olefins with h2o2 catalyzed by a bioinspired aminopyridine n4 iron complex," *ChemCatChem*, vol. 9, pp. 420–424, 2017.

[140] O. Cussó, M. Cianfanelli, X. Ribas, R. J. M. Klein Gebbink, and M. Costas, "Iron catalyzed highly enantioselective epoxidation of cyclic aliphatic enones with aqueous H_2O_2," *Journal of the American Chemical Society*, vol. 138, pp. 2732–2738, 2016.

[141] J. R. Ludwig, P. M. Zimmerman, J. B. Gianino, and C. S. Schindler, "Iron(III)-catalysed carbonyl-olefin metathesis," *Nature*, vol. 533, pp. 374–379, 2016.

[142] J. R. Ludwig, S. Phan, C. C. McAtee, P. M. Zimmerman, J. J. Devery, and C. S. Schindler, "Mechanistic investigations of the iron(III)-catalyzed carbonyl-olefin metathesis reaction," *Journal of the American Chemical Society*, vol. 139, pp. 10832–10842, 2017.

[143] M. M. Najafpour, R. Safdari, F. Ebrahimi, P. Rafighi, and R. Bagheri, "Water oxidation by a soluble iron(III)-cyclen complex: new findings," *Dalton Transactions*, vol. 45, pp. 2618–2623, 2016.

[144] Z. Codolà, L. Gómez, S. T. Kleespies, L. Que Jr, M. Costas, and J. Lloret-Fillol, "Evidence for an oxygen evolving iron–oxo–cerium intermediate in iron-catalysed water oxidation," *Nature Communications*, vol. 6, p. 5865, 2015.

[145] S. Kundu, E. Matito, S. Walleck, F. F. Pfaff, F. Heims, B. Rábay, J. M. Luis, A. Company, B. Braun, T. Glaser, and K. Ray, "O-O bond formation mediated by a hexanuclear iron complex supported on a stannoxane core," *Chemistry – A European Journal*, vol. 18, pp. 2787–2791, 2012.

[146] J. L. Fillol, Z. Codolà, I. Garcia-Bosch, L. Gómez, J. J. Pla, and M. Costas, "Efficient water oxidation catalysts based on readily available iron coordination complexes," *Nature Chemistry*, vol. 3, pp. 807–813, 2011.

[147] G. Hilt and J. Janikowski, "Iron-catalyzed cycloadditions and ring expansion reactions," in *Iron Catalysis in Organic Chemistry* (B. Plietker, ed.), pp. 245–269, Wiley-VCH Verlag GmbH & Co. KGaA, 2008.

[148] M. Brookhart and W. B. Studabaker, "Cyclopropanes from reactions of transition metal carbene complexes with olefins," *Chemical Reviews*, vol. 87, pp. 411–432, 1987.

[149] S.-F. Zhu and Q.-L. Zhou, "Iron-catalyzed transformations of diazo compounds," *National Science Review*, vol. 1, pp. 580–603, 2014.

[150] M. Brookhart and G. O. Nelson, "Isolation of stable secondary cationic iron carbene complexes dicarbonyl(η^5-cyclopentadienyl) phenylcarbene-iron hexafluorophosphate and carbonyl(η^5-cyclopentadienyl) triphenylphosphine(phenylcarbene)iron hexafluorophosphate," *Journal of the American Chemical Society*, vol. 99, pp. 6099–6101, 1977.

[151] S. Brandt and P. Helquist, "Cyclopropanation of olefins with a stable, iron-containing methylene transfer reagent," *Journal of the American Chemical Society*, vol. 101, pp. 6473–6475, 1979.

[152] M. Brookhart, J. R. Tucker, T. C. Flood, and J. Jensen, "Spectroscopic characterization of an electrophilic transition-metal-methylene complex, $\eta_5 - C_5H_5[(C_6H_5)_2\mathrm{PCH_2CH_2P(C_6H_5)_2}]\mathrm{Fe{=}CH_2^+}$," *Journal of the American Chemical Society*, vol. 102, pp. 1203–1205, 1980.

[153] M. Brookhart, M. B. Humphrey, H. J. Kratzer, and G. O. Nelson, "Reactions of η^5-$C_5H_5(CO)_2FeCHC_6H_5^+$ with alkenes and alkynes. observation of efficient benzylidene-transfer reactions," *Journal of the American Chemical Society*, vol. 102, pp. 7802–7803, 1980.

[154] K. A. M. Kremer, G. H. Kuo, E. J. O'Connor, P. Helquist, and R. C. Kerber, "Generation of (η^5-cyclopentadienyl)dicarbonyliron carbene complexes via protonation of the corresponding alkenyl complexes," *Journal of the American Chemical Society*, vol. 104, pp. 6119–6121, 1982.

[155] M. Brookhart, J. R. Tucker, and G. R. Husk, "Synthesis, spectral characterization and alkylidene-transfer reactions of electrophilic iron carbene complexes $Cp(CO)(L)Fe{=}CHR^+$(L=CO,PPh_3;R=Me,Et,$CHMe4_2$)," *Journal of the American Chemical Society*, vol. 105, pp. 258–264, 1983.

[156] M. Brookhart, W. B. Studabaker, and G. R. Husk, "Synthesis, spectral characterization, and carbene-transfer reactions of $CpFe(CO)_2{=}CH(C$-$C_3H_5)^+CF_3SO_3^-$. stabilization of cyclopropylmethylidene by an organometallic fragment," *Organometallics*, vol. 4, pp. 943–944, 1985.

[157] C. P. Casey, W. H. Miles, H. Tukada, and J. M. O. Connor, "Synthesis of electrophilic (dimethy1carbene)iron complexes," *Journal of the American Chemical Society*, vol. 104, pp. 3761–3762, 1982.

[158] C. P. Casey, W. H. Miles, and H. Tukada, "Synthesis, characterization and reactions of $(C_5H_5)(CO)_2Fe{=}C(CH_3)_2^+$ and $(C_5H_5)(CO_2Fe{=}CH$-$CH{=}C(CH_3)_2^+$," *Journal of the American Chemical Society*, vol. 107, pp. 2924–2931, 1985.

[159] C. Roger and C. Lapinte, "Synthesis and characterization of a stable iron-methylene complex; methylene activation by electron transfer catalysis (ETC)," *Journal of the Chemical Society, Chemical Communications*, pp. 1598–1600, 1989.

[160] C. Roger, L. Toupet, and C. Lapinte, "α-hydride abstraction via a three-step pathway: access to the electron rich iron methoxycarbene complex $[Fe(\eta^5$-$C_5Me_5)$(P,P'-$Ph_2PCH_2CH_2PPh_2)(=CHOMe)]^+PF_6^-$," *Journal of the Chemical Society, Chemical Communications*, pp. 713–715, 1988.

[161] W. J. Seitz, A. K. Saha, and M. M. Hossain, "Iron lewis acid catalyzed cyclopropanation reactions of ethyl diazoacetate and olefins," *Organometallics*, vol. 12, pp. 2604–2608, 1993.

[162] M. E. Dudley, M. M. Morshed, C. L. Brennan, M. S. Islam, M. S. Ahmad, M.-R. Atuu, B. Branstetter, and M. M. Hossain, "Acid-catalyzed reactions of aromatic aldehydes with ethyl diazoacetate - an investigation on the synthesis of 3-hydroxy-2-arylacrylic acid ethyl esters," *The Journal of Organic Chemistry*, vol. 69, pp. 7599–7608, 2004.

[163] S. J. Mahmood and M. M. Hossain, "Iron lewis acid catalyzed reactions of aromatic aldehydes with ethyl diazoacetate - unprecedented formation of 3-hydroxy-2-arylacrylic acid ethyl esters by a unique 1,2-aryl shift," *The Journal of Organic Chemistry*, vol. 63, pp. 3333–3336, 1998.

[164] C. Wang and B. Wan, "Recent advances in the iron-catalyzed cycloaddition reactions," *Chinese Science Bulletin*, vol. 57, pp. 2338–2351, 2012.

[165] D. Mansuy, M. Lange, J. C. Chottard, J. F. Bartoli, B. Chevrier, and R. Weiss, "Dichlorocarbene complexes of iron(II)-porphyrins–crystal and molecular structure of $Fe(TPP)(CCl_2)(H_2O)$," *Angewandte Chemie International Edition in English*, vol. 17, pp. 781–782, 1978.

[166] J. R. Wolf, C. G. Hamaker, J.-P. Djukic, T. Kodadek, and L. K. Woo, "Shape and stereoselective cyclopropanation of alkenes catalyzed by iron porphyrins.," *Journal of the American Chemical Society*, vol. 117, pp. 9194–9199, 1995.

[167] C. G. Hamaker, G. A. Mirafzal, and L. K. Woo, "Catalytic cyclopropanation with iron(II) complexes," *Organometallics*, vol. 20, pp. 5171–5176, 2001.

[168] G. Du, B. Andrioletti, E. Rose, and L. K. Woo, "Asymmetric cyclopropanation of styrene catalyzed by chiral macrocyclic iron(II) complexes," *Organometallics*, vol. 21, pp. 4490–4495, 2002.

[169] P. Tagliatesta and A. Pastorini, "Remarkable selectivity in the cyclopropanation reactions catalysed by an halogenated iron meso-tetraphenylporphyrin," *Journal of Molecular Catalysis A*, vol. 198, pp. 57 – 61, 2003.

[170] Y. Chen and X. P. Zhang, "Asymmetric cyclopropanation of styrenes catalyzed by metal complexes of D2-symmetrical chiral porphyrin: Superiority of cobalt over iron," *The Journal of Organic Chemistry*, vol. 72, pp. 5931–5934, 2007.

[171] T.-S. Lai, F.-Y. Chan, P.-K. So, D.-L. Ma, K.-Y. Wong, and C.-M. Che, "Alkene cyclopropanation catalyzed by halterman iron porphyrin: participation of organic bases as axial ligands," *Dalton Transactions*, pp. 4845–4851, 2006.

[172] B. Morandi, A. Dolva, and E. M. Carreira, "Iron-catalyzed cyclopropanation with glycine ethyl ester hydrochloride in water," *Organic Letters*, vol. 14, pp. 2162–2163, 2012.

[173] Y. Liu, W. Xu, J. Zhang, W. Fuller, C. E. Schulz, and J. Li, "Electronic configuration and ligand nature of five-coordinate iron porphyrin carbene complexes: An experimental study," *Journal of the American Chemical Society*, vol. 139, pp. 5023–5026, 2017.

[174] Y. Li, J.-S. Huang, Z.-Y. Zhou, C.-M. Che, and X.-Z. You, "Remarkably stable iron porphyrins bearing nonheteroatom-stabilized carbene or (alkoxycarbonyl)carbenes: Isolation, x-ray crystal structures, and carbon atom transfer reactions with hydrocarbons," *Journal of the American Chemical Society*, vol. 124, pp. 13185–13193, 2002.

[175] A. Klose, E. Solari, C. Floriani, N. Re, A. Chiesi-Villa, and C. Rizzoli, "Iron–carbene functionalities supported by a macrocyclic ligand: iron–carbon double bond stabilized by tetramethyldibenzotetraazaannulene," *Chemical Communications*, vol. 23, pp. 2297–2298, 1997.

[176] S. K. Russell, J. M. Hoyt, S. C. Bart, C. Milsmann, S. C. E. Stieber, S. P. Semproni, S. DeBeer, and P. J. Chirik, "Synthesis, electronic structure and reactivity of bis(imino)pyridine iron carbene complexes: evidence for a carbene radical," *Chemical Science*, vol. 5, pp. 1168–1174, 2014.

[177] V. Esposito, E. Solari, C. Floriani, N. Re, C. Rizzoli, and A. Chiesi-Villa, "Binding and redox properties of iron(II) bonded to an oxo surface modeled by calix[4]arene," *Inorganic Chemistry*, vol. 39, pp. 2604–2613, 2000.

[178] M. Giusti, E. Solari, L. Giannini, C. Floriani, A. Chiesi-Villa, and C. Rizzoli, "Iron-carbene bonded to a planar tetraoxo surface defined by dimethoxy-p-tert-butylcalix[4]arene dianion," *Organometallics*, vol. 16, pp. 5610–5612, 1997.

[179] S. K. Edulji and S. T. Nguyen, "Catalytic olefin cyclopropanation using μ-oxo−bis[(salen)iron(III)] complexes," *Organometallics*, vol. 22, pp. 3374–3381, 2003.

[180] S. K. Edulji and S. T. Nguyen, "Substrate scope in the olefin cyclopropanation reaction catalyzed by μ-oxo-bis[(salen)iron(III)] complexes," *Pure and Applied Chemistry*, vol. 76, pp. 645–649, 2009.

[181] C.-T. Yeung, K.-C. Sham, W.-S. Lee, W.-T. Wong, W.-Y. Wong, and H.-L. Kwong, "Cobalt and iron complexes of chiral C1- and C2-terpyridines: Synthesis, characterization and use in catalytic asymmetric cyclopropanation of styrenes," *Inorganica Chimica Acta*, vol. 362, pp. 3267 – 3273, 2009.

[182] G. Poignant, S. Nlate, V. Guerchais, A. J. Edwards, and P. R. Raithby, "Synthesis and properties of (η^2-C,X) chelate arylcarbene complexes [Fe(C_5Me_5)(L){η^2-C(OMe)C_6H_4-o-X}][OTf](L=CO,PMe_3;X=OMe,Cl), volume = 16, year = 1997," *Organometallics*, pp. 124–132.

[183] B. M. Lindley, A. Swidan, E. B. Lobkovsky, P. T. Wolczanski, M. Adelhardt, J. Sutter, and K. Meyer, "Fe(IV) alkylidenes via protonation of Fe(II) vinyl chelates and a comparative mössbauer spectroscopic study," *Chemical Science*, vol. 6, pp. 4730–4736, 2015.

[184] B. M. Lindley, B. P. Jacobs, S. N. MacMillan, and P. T. Wolczanski, "Neutral Fe(IV) alkylidenes, including some that bind dinitrogen," *Chem. Commun.*, vol. 2, pp. 7–10, 2016.

[185] B. P. Jacobs, R. G. Agarwal, P. T. Wolczanski, T. R. Cundari, and S. N. MacMillan, "Fe(IV) alkylidenes are actually Fe(II), and a related octahedral Fe(II) alkylidene is a conjugated vinyl complex," *Polyhedron*, vol. 116, pp. 47 – 56, 2016.

[186] J. Liu, L. Hu, L. Wang, H. Chen, and L. Deng, "An iron(II) ylide complex as a masked open-shell iron alkylidene species in its alkylidene-transfer reactions with alkenes," *Journal of the American Chemical Society*, vol. 139, pp. 3876–3888, 2017.

[187] D. Gillingham and N. Fei, "Catalytic X-H insertion reactions based on carbenoids," *Chemical Society Review*, vol. 42, pp. 4918–4931, 2013.

[188] V. Tyagi, R. B. Bonn, and R. Fasan, "Intermolecular carbene s-h insertion catalysed by engineered myoglobin-based catalysts," *Chemical Science*, vol. 6, pp. 2488–2494, 2015.

[189] G. Sreenilayam and R. Fasan, "Myoglobin-catalyzed intermolecular carbene n-h insertion with arylamine substrates," *Chemical Communication*, vol. 51, pp. 1532–1534, 2015.

[190] L. K. Baumann, H. M. Mbuvi, G. Du, and L. K. Woo, "Iron porphyrin catalyzed N-H insertion reactions with ethyl diazoacetate," *Organometallics*, vol. 26, pp. 3995–4002, 2007.

[191] D. A. Sharon, D. Mallick, B. Wang, and S. Shaik, "Computation sheds insight into iron porphyrin carbenes electronic structure, formation, and n-h insertion reactivity," *Journal of the American Chemical Society*, vol. 138, pp. 9597–9610, 2016.

[192] A. Conde, G. Sabenya, M. Rodríguez, V. Postils, J. M. Luis, M. M. Díaz-Requejo, M. Costas, and P. J. Pérez, "Iron and manganese catalysts for the selective functionalization of arene c(sp^2)−h bonds by carbene insertion," *Angewandte Chemie*, vol. 128, pp. 6640–6644, 2016.

[193] A. Varela-Alvarez and D. G. Musaev, "Can bis(imino)pyridine iron, (PDI)FeL_1L_2, complexes catalyze C-H bond functionalization?," *Chemical Science*, vol. 4, pp. 3758–3764, 2013.

[194] J. L. Belof, C. R. Cioce, X. Xu, X. P. Zhang, B. Space, and H. L. Woodcock, "Characterization of tunable radical metal-carbenes: Key intermediates in catalytic cyclopropanation," *Organometallics*, vol. 30, pp. 2739–2746, 2011.

[195] H. Jiang, K. Lang, H. Lu, L. Wojtas, and X. P. Zhang, "Asymmetric radical bicyclization of allyl azidoformates via cobalt(II)-based metalloradical catalysis," *Journal of the American Chemical Society*, vol. 139, pp. 9164–9167, 2017.

[196] W. I. Dzik, X. P. Zhang, and B. De Bruin, "Redox noninnocence of carbene ligands: Carbene radicals in (catalytic) C-C bond formation," *Inorganic Chemistry*, vol. 50, pp. 9896–9903, 2011.

[197] W. I. Dzik, X. Xu, X. P. Zhang, J. N. H. Reek, and B. de Bruin, "'Carbene radicals' in Co^{II}(por)-catalyzed olefin cyclopropanation," *Journal of the American Chemical Society*, vol. 132, pp. 10891–10902, 2010.

[198] F. Wang, Q. Meng, and M. Li, "Density functional computations of the cyclopropanation of ethene catalyzed by iron(II) carbene complexes Cp(CO)(L)Fe=CHR,L=CO,PMe_3,R=Me,OMe,Ph,CO_2Me," *International Journal of Quantum Chemistry*, vol. 108, pp. 945–953, 2008.

[199] G. Dazinger and K. Kirchner, "Competitive alkylidene transfer to olefins and alkylidene-to-olefin interconversion of the electrophilic iron carbene complexes $[FeCp(CO)(L)(CHR)]^+$(L=CO,PH_3;R=Me,Et): a theoretical study," *Organometallics*, vol. 23, pp. 6281–6287, 2004.

[200] F. N. Tebbe, G. W. Parshall, and D. W. Ovenall, "Titanium-catalyzed olefin metathesis," *Journal of the American Chemical Society*, vol. 101, pp. 5074–5075, 1979.

[201] X. Hou and K. Nomura, "(Arylimido)vanadium(V)alkylidene complexes containing fluorinated aryloxo and alkoxo ligands for fast living ring-opening metathesis polymerization (romp) and highly *cis*-specific romp," *Journal of the American Chemical Society*, vol. 137, pp. 4662–4665, 2015.

[202] X. Hou and K. Nomura, "Ring-opening metathesis polymerization of cyclic olefins by (arylimido)vanadium(V)-alkylidenes: Highly active, thermally robust *cis* specific polymerization," *Journal of the American Chemical Society*, vol. 138, pp. 11840–11849, 2016.

[203] J. Louie and R. H. Grubbs, "Reaction of diazoalkanes with iron phosphine complexes affords novel phosphazine complexes," *Organometallics*, vol. 20, pp. 481–484, 2001.

[204] M. Vasiliu, A. J. Arduengo, and D. A. Dixon, "Role of electronegative substituents on the bond energies in the grubbs metathesis catalysts for M = Fe, Ru, Os," *The Journal of Physical Chemistry C*, vol. 118, pp. 13563–13577, 2014.

[205] O. Eisenstein, R. Hoffmann, and A. R. Rossi, "Some geometrical and electronic features of the intermediate stages of olefin metathesis," *Journal of the American Chemical Society*, vol. 103, pp. 5582–5584, 1981.

[206] A. Poater, E. Pump, S. V. C. Vummaleti, and L. Cavallo, "The activation mechanism of fe-based olefin metathesis catalysts," *Chemical Physics Letters*, vol. 610-611, pp. 29–32, 2014.

[207] A. Poater and L. Cavallo, "A comprehensive study of olefin metathesis catalyzed by Ru-based catalysts," *Beilstein Journal of Organic Chemistry*, vol. 11, pp. 1767–1780, 2015.

[208] M. Mauksch and S. B. Tsogoeva, "Iron-catalyzed olefin metathesis with low-valent iron alkylidenes," *Chemistry – A European Journal*, vol. 23, pp. 10264–10269, 2017.

[209] I. N. Levine, *Quantum Chemistry*. Prentice Hall, 5th ed., 1999.

[210] W. Koch and M. C. Holthausen, *A Chemist's Guide to Density Functional Theory*. Weinheim - New York: Wiley-VCH, 2nd ed., 2001.

[211] F. Jensen, *Introduction to Computational Chemistry*. John Wiley & Sons, 2006.

[212] A. Leach, *Molecular Modelling: Principles and Applications*. Prentice Hall, 2nd ed., 2001.

[213] P. W. Atkins, *Molecular Quantum Mechanics*. Oxford: Oxford University Press, second ed., 2005.

[214] P. Hohenberg and W. Kohn, "Inhomogeneous electron gas," *Physical Review*, vol. 136, pp. B864–B871, 1964.

[215] C. J. Cramer, *Essentials of Computational Chemistry: Theories and Models*. West Sussex, England: John Wiley & Sons, second ed., 2004.

[216] W. Kohn and L. J. Sham, "Self-consistent equations including exchange and correlation effects," *Physical Review*, vol. 140, pp. A1133–A1138, 1965.

[217] J. P. Perdew and K. Schmidt, "Jacob's ladder of density functional approximations for the exchange-correlation energy," *AIP Conference Proceedings*, vol. 577, pp. 1–20, 2001.

[218] J. P. Perdew, A. Ruzsinszky, L. A. Constantin, J. Sun, and G. I. Csonka, "Some fundamental issues in ground-state density functional theory: A guide for the perplexed," *Journal of Chemical Theory and Computation*, vol. 5, pp. 902–908, 2009.

[219] S. H. Vosko, L. Wilk, and M. Nusair, "Accurate spin-dependent electron liquid correlation energies for local spin density calculations: a critical analysis," *Canadian Journal of Physics*, vol. 58, pp. 1200–1211, 1980.

[220] A. D. Becke, "Density-functional exchange-energy approximation with correct asymptotic behavior," *Physical Review A*, vol. 38, pp. 3098–3100, 1988.

[221] A. J. Cohen and N. C. Handy, "Dynamic correlation," *Molecular Physics*, vol. 99, pp. 607–615, 2001.

[222] N. C. Handy and A. J. Cohen, "Left-right correlation energy," *Molecular Physics*, vol. 99, pp. 403–412, 2001.

[223] C. Lee, W. Yang, and R. G. Parr, "Development of the colle-salvetti correlation-energy formula into a functional of the electron density," *Physical Review B*, vol. 37, pp. 785–789, 1988.

[224] J. P. Perdew, K. Burke, and M. Ernzerhof, "Generalized gradient approximation made simple," *Physical Review Letters*, vol. 77, pp. 3865–3868, 1996.

[225] M. Swart, M. Solà, and F. M. Bickelhaupt, "A new all-round density functional based on spin states and S_N2 barriers," *The Journal of Chemical Physics*, vol. 131, p. 094103, 2009.

[226] M. Swart, A. R. Groenhof, A. W. Ehlers, and K. Lammertsma, "Validation of exchange–correlation functionals for spin states of iron complexes," *The Journal of Physical Chemistry A*, vol. 108, pp. 5479–5483, 2004.

[227] J. Tao, J. P. Perdew, V. N. Staroverov, and G. E. Scuseria, "Climbing the density functional ladder: Nonempirical meta-generalized gradient approximation designed for molecules and solids," *Physical Review Letters*, vol. 91, p. 146401, 2003.

[228] A. D. Becke, "Density-functional thermochemistry.III. the role of exact exchange," *The Journal of Chemical Physics*, vol. 98, pp. 5648–5652, 1993.

[229] P. J. Stephens, F. J. Devlin, C. F. Chabalowski, and M. J. Frisch, "Ab initio calculation of vibrational absorption and circular dichroism spectra using density functional force fields," *The Journal of Physical Chemistry*, vol. 98, pp. 11623–11627, 1994.

[230] V. N. Staroverov, G. E. Scuseria, J. Tao, and J. P. Perdew, "Comparative assessment of a new nonempirical density functional: Molecules and hydrogen-bonded complexes," *The Journal of Chemical Physics*, vol. 119, pp. 12129–12137, 2003.

[231] S. Grimme, "Density functional theory with london dispersion corrections," *Wiley Interdisciplinary Reviews: Computational Molecular Science*, vol. 1, pp. 211–228, 2011.

[232] S. Grimme, "Semiempirical GGA-type density functional constructed with a long-range dispersion correction.," *Journal of computational chemistry*, vol. 27, pp. 1787–99, 2006.

[233] D. Schröder, S. Shaik, and H. Schwarz, "Two-state reactivity as a new concept in organometallic chemistry," *Accounts of Chemical Research*, vol. 33, pp. 139–145, 2000.

[234] R. Poli and J. N. Harvey, "Spin forbidden chemical reactions of transition metal compounds. new ideas and new computational challenges," *Chemical Society Review*, vol. 32, pp. 1–8, 2003.

[235] C. A. Gaggioli, L. Belpassi, F. Tarantelli, J. N. Harvey, and P. Belanzoni, "Spin-forbidden reactions: Adiabatic transition states using spin–orbit coupled density functional theory," *Chemistry – A European Journal*, p. n/a, 2013.

[236] J. N. Harvey, M. Aschi, H. Schwarz, and W. Koch, "The singlet and triplet states of phenyl cation. a hybrid approach for locating minimum energy crossing points between non-interacting potential energy surfaces," *Theoretical Chemistry Accounts*, vol. 99, pp. 95–99, 1998.

[237] M. M. Francl, W. J. Pietro, W. J. Hehre, J. S. Binkley, M. S. Gordon, D. J. DeFrees, and J. A. Pople, "Self-consistent molecular orbital methods. 23. a polarization-type basis set for 2nd-row elements," *Journal of Chemical Physics*, vol. 77, pp. 3654–3665, 1982.

[238] P. C. Hariharan and J. A. Pople, "The influence of polarization functions on molecular orbital hydrogenation energies," *Theoretica Chimica Acta*, vol. 28, pp. 213–222, 1973.

[239] M. J. Frisch, J. A. Pople, and J. S. Binkley, "Self-consistent molecular-orbital methods. 25. supplementary functions for gaussian-basis sets," *Journal of Chemical Physics*, vol. 80, pp. 3265–3269, 1984.

[240] A. Ehlers, M. Böhme, S. Dapprich, A. Gobbi, A. Höllwarth, V. Jonas, K. Köhler, R. Stegmann, A. Veldkamp, and G. Frenking, "A set of f-polarization functions for pseudo-potential basis sets of the transition metals Sc-Cu, Y-Ag and La-Au," *Chemical Physics Letters*, vol. 208, pp. 111–114, 1993.

[241] R. Krishnan, J. S. Binkley, R. Seeger, and J. A. Pople, "Self-consistent molecular-orbital methods. XX. basis set for correlated wave-functions," *Journal of Chemical Physics*, vol. 72, pp. 650–654, 1980.

[242] M. J. Frisch, G. W. Trucks, H. B. Schlegel, G. E. Scuseria, M. A. Robb, J. R. Cheeseman, G. Scalmani, V. Barone, B. Mennucci, G. A. Petersson, H. Nakatsuji, M. Caricato, X. Li, H. P. Hratchian, A. F. Izmaylov, J. Bloino, G. Zheng, J. L. Sonnenberg, M. Hada, M. Ehara, K. Toyota, R. Fukuda, J. Hasegawa, M. Ishida, T. Nakajima, Y. Honda, O. Kitao, H. Nakai, T. Vreven, J. A. Montgomery Jr., J. E. Peralta, F. Ogliaro, M. Bearpark, J. J. Heyd, E. Brothers, K. N. Kudin, V. N. Staroverov, R. Kobayashi, J. Normand, K. Raghavachari, A. Rendell, J. C. Burant, S. S. Iyengar, J. Tomasi, M. Cossi, N. Rega, J. M. Millam, M. Klene, J. E. Knox, J. B. Cross, V. Bakken, C. Adamo, J. Jaramillo, R. Gomperts, R. E. Stratmann, O. Yazyev, A. J. Austin, R. Cammi, C. Pomelli, J. W. Ochterski, R. L. Martin, K. Morokuma, V. G. Zakrzewski, G. A. Voth, P. Salvador, J. J. Dannenberg, S. Dapprich, A. D. Daniels, Ö. Farkas, J. B. Foresman, J. V. Ortiz, J. Cioslowski, and D. J. Fox, "Gaussian 09, Revision D.01." Gaussian, Inc., Wallingford CT, 2009.

[243] L. Maestre, R. Dorel, O. Pablo, I. Escofet, W. M. C. Sameera, E. Alvarez, F. Maseras, M. M. Díaz-Requejo, A. M. Echavarren, and P. J. Pérez, "Functional-group-tolerant, silver-catalyzed N–N bond formation by nitrene transfer to amines," *Journal of the American Chemical Society*, vol. 139, pp. 2216–2223, 2017.

[244] G. Berghold, C. J. Mundy, A. H. Romero, J. Hutter, and M. Parrinello, "General and efficient algorithms for obtaining maximally localized wannier functions," *Physical Review B*, vol. 61, pp. 10040–10048, 2000.

[245] N. Marzari, A. A. Mostofi, J. R. Yates, I. Souza, and D. Vanderbilt, "Maximally localized wannier functions: Theory and applications," *Reviews of Modern Physics*, vol. 84, pp. 1419–1475, 2012.

[246] J. VandeVondele, M. Krack, F. Mohamed, M. Parrinello, T. Chassaing, and J. Hutter, "Quickstep: Fast and accurate density functional calculations using a mixed gaussian and plane waves approach," *Computer Physics Communications*, vol. 167, pp. 103 – 128, 2005.

[247] "Cp2k code." Available from `https://www.cp2k.org/`. Retrieved: Octubre 09, 2017.

[248] S. Goedecker, M. Teter, and J. Hutter, "Separable dual-space gaussian pseudopotentials," *Physical Review B*, vol. 54, pp. 1703–1710, 1996.

[249] C. Hartwigsen, S. Goedecker, and J. Hutter, "Relativistic separable dual-space gaussian pseudopotentials from h to rn," *Physical Review B*, vol. 58, pp. 3641–3662, 1998.

[250] J. VandeVondele and J. Hutter, "An efficient orbital transformation method for electronic structure calculations," *The Journal of Chemical Physics*, vol. 118, pp. 4365–4369, 2003.

[251] P. Vidossich and A. Lledós, "The use of localised orbitals for the bonding and mechanistic analysis of organometallic compounds," *Dalton Transactions*, vol. 43, pp. 11145–11151, 2014.

[252] M. Swart, "Accurate spin-state energies for iron complexes," *Journal of Chemical Theory and Computation*, vol. 4, pp. 2057–2066, 2008.

[253] J. Conradie and A. Ghosh, "DFT calculations on the spin-crossover complex Fe(salen)(NO): A quest for the best functional," *Journal of Physical Chemistry B*, vol. 111, pp. 12621–12624, 2007.

[254] Z. Varga, P. Verma, and D. G. Truhlar, "Hyper open-shell states: The lowest excited spin states of o atom, Fe^{2+} ion, and FeF_2," *Journal of the American Chemical Society*, vol. 139, pp. 12569–12578, 2017.

[255] M. Glatz, C. Schröder-Holzhacker, B. Bichler, B. Stöger, K. Mereiter, L. F. Veiros, and K. Kirchner, "Synthesis and characterization of cationic dicarbonyl Fe(II) pnp pincer complexes," *Monatshefte für Chemie - Chemical Monthly*, vol. 147, pp. 1713–1719, 2016.

[256] C. Schröder-Holzhacker, B. Stöger, E. Pittenauer, G. Allmaier, L. F. Veiros, and K. Kirchner, "High-spin iron(II) complexes with mono-phosphorylated 2,6-diaminopyridine ligands," *Monatshefte für Chemie - Chemical Monthly*, vol. 147, pp. 1539–1545, 2016.

[257] B. Heggen and W. Thiel, "Theoretical investigation on the mechanism of iron catalyzed cross coupling reactions via ferrate intermediates," *Journal of Organometallic Chemistry*, vol. 804, pp. 42 – 47, 2016.

[258] M. Swart, M. Guell, and M. Sola, "A multi-scale approach to spin crossover in Fe(II) compounds," *Phys. Chem. Chem. Phys.*, vol. 13, pp. 10449–10456, 2011.

[259] S. F. Vyboishchikov, M. Bühl, and W. Thiel, "Mechanism of olefin metathesis with catalysis by ruthenium carbene complexes: Density functional studies on model systems," *Chemistry - A European Journal*, vol. 8, pp. 3962–3975, 2002.

[260] L. Cavallo, "Mechanism of ruthenium-catalyzed olefin metathesis reactions from a theoretical perspective," *Journal of the American Chemical Society*, vol. 124, pp. 8965–8973, 2002.

[261] C. Adlhart and P. Chen, "Mechanism and activity of ruthenium olefin metathesis catalysts: The role of ligands and substrates from a theoretical perspective," *Journal of the American Chemical Society*, vol. 126, pp. 3496–3510, 2004.

[262] B. F. Straub, "Origin of the high activity of second-generation grubbs catalysts," *Angewandte Chemie International Edition*, vol. 44, pp. 5974–5978, 2005.

[263] G. Occhipinti, H.-R. Bjorsvik, and V. R. Jensen, "Quantitative structure−activity relationships of ruthenium catalysts for olefin metathesis," *Journal of the American Chemical Society*, vol. 128, pp. 6952–6964, 2006.

[264] D. Benitez, E. Tkatchouk, and W. A. Goddard III, "Relevance of *cis*- and *trans*-dichloride ru intermediates in grubbs-II olefin metathesis catalysis ($H_2IMesCl_2Ru{=}CHR$)," *Chemical Communications*, vol. 450, pp. 6194–6196, 2008.

[265] X. Solans-Monfort, R. Pleixats, and M. Sodupe, "DFT mechanistic study on diene metathesis catalyzed by Ru-based grubbs–hoveyda-type carbenes: The key role of π-electron density delocalization in the hoveyda ligand," *Chemistry – A European Journal*, vol. 16, pp. 7331–7343, 2010.

[266] H.-C. Yang, Y.-C. Huang, Y.-K. Lan, T.-Y. Luh, Y. Zhao, and D. G. Truhlar, "Carbene rotamer switching explains the reverse trans effect in forming the grubbs second-generation olefin metathesis catalyst," *Organometallics*, vol. 30, pp. 4196–4200, 2011.

[267] P. Liu, X. Xu, X. Dong, B. K. Keitz, M. B. Herbert, R. H. Grubbs, and K. N. Houk, "Z-selectivity in olefin metathesis with chelated Ru catalysts: Computational studies of mechanism and selectivity," *Journal of the American Chemical Society*, vol. 134, pp. 1464–1467, 2012.

[268] Y. Dang, Z.-X. Wang, and X. Wang, "A thorough DFT study of the mechanism of homodimerization of terminal olefins through metathesis with a chelated ruthenium catalyst: From initiation to Z-selectivity to regeneration," *Organometallics*, vol. 31, pp. 7222–7234, 2012.

[269] Y. Dang, Z.-X. Wang, and X. Wang, "Does the ruthenium nitrato catalyst work differently in Z-selective olefin metathesis? A DFT study," *Organometallics*, vol. 31, pp. 8654–8657, 2012.

[270] A. K. Rappe and W. A. Goddard, "Olefin metathesis - a mechanistic study of high-valent group vi catalysts," *Journal of the American Chemical Society*, vol. 104, pp. 448–456, 1982.

[271] F. Nuñez-Zarur, J. Poater, L. Rodríguez-Santiago, X. Solans-Monfort, M. Solà, and M. Sodupe, "On the electronic structure of second generation hoveyda–grubbs alkene metathesis precursors," *Computational and Theoretical Chemistry*, vol. 996, pp. 57–67, 2012.

[272] A. G. Wenzel and R. H. Grubbs, "Ruthenium metallacycles derived from 14-electron complexes. new insights into olefin metathesis intermediates," *Journal of the American Chemical Society*, vol. 128, pp. 16048–16049, 2006.

[273] P. E. Romero and W. E. Piers, "Direct observation of a 14-electron ruthenacyclobutane relevant to olefin metathesis," *Journal of the American Chemical Society*, vol. 127, pp. 5032–5033, 2005.

[274] K. Paredes-Gil, X. Solans-Monfort, L. Rodriguez-Santiago, M. Sodupe, and P. Jaque, "DFT study on the relative stabilities of substituted ruthenacyclobutane intermediates involved in olefin cross-metathesis reactions and their interconversion pathways," *Organometallics*, vol. 33, pp. 6065–6075, 2014.

[275] C. H. Suresh and N. Koga, "Orbital interactions in the ruthenium olefin metathesis catalysts," *Organometallics*, vol. 23, pp. 76–80, 2004.

[276] X. Solans-Monfort, C. Copèret, and O. Eisenstein, "Metallacyclobutanes from schrock-type d0 metal alkylidene catalysts: Structural preferences and consequences in alkene metathesis," *Organometallics*, vol. 34, pp. 1668–1680, 2015.

[277] A. A. Danopoulos, P. Braunstein, M. Wesolek, K. Y. Monakhov, P. Rabu, and V. Robert, "Three-coordinate iron(II) N-heterocyclic carbene alkyl complexes," *Organometallics*, vol. 31, pp. 4102–4105, 2012.

[278] Y. Liu, L. Wang, and L. Deng, "Three-coordinate iron(II) dialkenyl compound with NHC ligation: Synthesis, structure, and reactivity," *Organometallics*, vol. 34, pp. 4401–4407, 2015.

[279] J. A. Przyojski, K. P. Veggeberg, H. D. Arman, and Z. J. Tonzetich, "Mechanistic studies of catalytic carbon–carbon cross-coupling by well-defined iron NHC complexes," *ACS Catalysis*, vol. 5, pp. 5938–5946, 2015.

[280] A. J. Arduengo, R. L. Harlow, and M. Kline, "A stable crystalline carbene," *Journal of the American Chemical Society*, vol. 113, pp. 361–363, 1991.

[281] J. B. Alexander, D. S. La, D. R. Cefalo, A. H. Hoveyda, and R. R. Schrock, "Catalytic enantioselective ring-closing metathesis by a chiral biphen−Mo complex," *Journal of the American Chemical Society*, vol. 120, pp. 4041–4042, 1998.

[282] J. J. Van Veldhuizen, S. B. Garber, J. S. Kingsbury, and A. H. Hoveyda, "A recyclable chiral Ru catalyst for enantioselective olefin metathesis. efficient catalytic asymmetric ring-opening/cross metathesis in air," *Journal of the American Chemical Society*, vol. 124, pp. 4954–4955, 2002.

[283] R. K. M. Khan, S. Torker, and A. H. Hoveyda, "Readily accessible and easily modifiable Ru-based catalysts for efficient and Z-selective ring-opening metathesis polymerization and ring-opening/cross-metathesis," *Journal of the American Chemical Society*, vol. 135, pp. 10258–10261, 2013.

[284] P. E. Sues, J. M. John, R. R. Schrock, and P. Müller, "Molybdenum and tungsten alkylidene and metallacyclobutane complexes that contain a dianionic biphenolate pincer ligand," *Organometallics*, vol. 35, pp. 758–761, 2016.

[285] M. E. O'Reilly, I. Ghiviriga, K. A. Abboud, and A. S. Veige, "Unusually stable tungstenacyclobutadienes featuring an ono trianionic pincer-type ligand," *Dalton Transactions*, vol. 42, pp. 3326–3336, 2013.

[286] R. Schowner, W. Frey, and M. R. Buchmeiser, "Cationic tungsten-oxo-alkylidene-n-heterocyclic carbene complexes: Highly active olefin metathesis catalysts," *Journal of the American Chemical Society*, vol. 137, pp. 6188–6191, 2015.

[287] R. E. Andrew, L. Gonzalez-Sebastian, and A. B. Chaplin, "NHC-based pincer ligands: carbenes with a bite," *Dalton Transactions*, vol. 45, pp. 1299–1305, 2016.

[288] A. Company, L. Gómez, M. Güell, X. Ribas, J. M. Luis, L. Que, and M. Costas, "Alkane hydroxylation by a nonheme iron catalyst that challenges the heme paradigm for oxygenase action," *Journal of the American Chemical Society*, vol. 129, pp. 15766–15767, 2007.

[289] D. Font, M. Canta, M. Milan, O. Cussó, X. Ribas, R. J. M. Klein Gebbink, and M. Costas, "Readily accessible bulky iron catalysts exhibiting site selectivity in the oxidation of steroidal substrates," *Angewandte Chemie International Edition*, vol. 55, pp. 5776–5779, 2016.

[290] U. Kernbach, M. Ramm, P. Luger, and W. P. Fehlhammer, "A chelating triscarbene ligand and its hexacarbene iron complex," *Angewandte Chemie International Edition in English*, vol. 35, pp. 310–312, 1996.

[291] C. Vogel, F. Heinemann, J. Sutter, C. Anthon, and K. Meyer, "An iron nitride complex," *Angewandte Chemie International Edition*, vol. 47, pp. 2681–2684, 2008.

[292] K. Riener, S. Haslinger, A. Raba, M. P. Högerl, M. Cokoja, W. A. Herrmann, and F. E. Kühn, "Chemistry of iron N-heterocyclic carbene complexes: Syntheses, structures, reactivities, and catalytic applications," *Chemical Reviews*, vol. 114, pp. 5215–5272, 2014.

[293] K. Paredes-Gil, X. Solans-Monfort, L. Rodriguez-Santiago, M. Sodupe, and P. Jaque, "DFT study on the relative stabilities of substituted ruthenacyclobutane intermediates involved in olefin cross-metathesis reactions and their interconversion pathways," *Organometallics*, vol. 33, pp. 6065–6075, 2014.

[294] W. Janse van Rensburg, P. J. Steynberg, W. H. Meyer, M. M. Kirk, and G. S. Forman, "DFT prediction and experimental observation of substrate-induced catalyst decomposition in ruthenium-catalyzed olefin metathesis," *Journal of the American Chemical Society*, vol. 126, pp. 14332–14333, 2004.

[295] A.-M. Leduc, A. Salameh, D. Soulivong, M. Chabanas, J.-M. Basset, C. Copéret, X. Solans-Monfort, E. Clot, O. Eisenstein, V. P. W. Böhm, and M. Röper, "β-h transfer from the metallacyclobutane: A key step in the deactivation and byproduct formation for the well-defined silica-supported rhenium alkylidene alkene metathesis catalyst," *Journal of the American Chemical Society*, vol. 130, pp. 6288–6297, 2008.

Appendices

A

Additional data to Chapter 2

A.1 Geometries of Known Carbenes

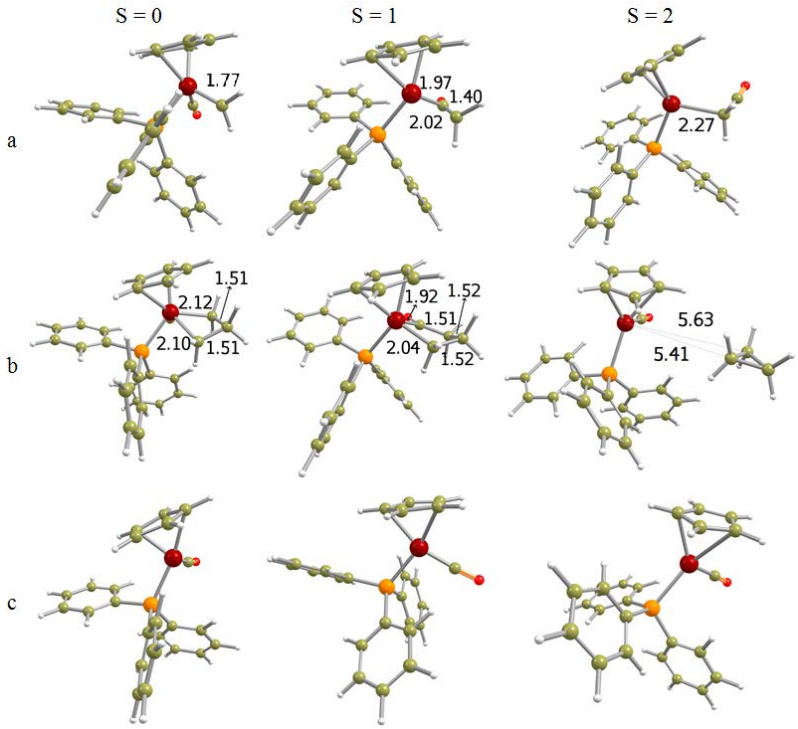

Figure A.1: Optimized geometries of different spin states of the metal carbene, metallacyclobutane intermediate and cyclopropanation products for complexes **I**. Distances are in Å

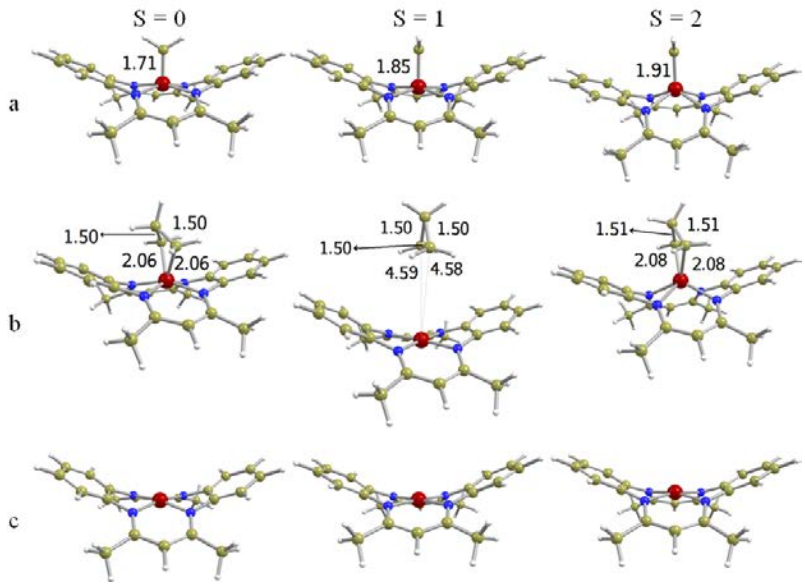

Figure A.2: Optimized geometries of different spin states of the metal carbene, metallacyclobutane intermediate and cyclopropanation products for complexes **II**. Distances are in Å

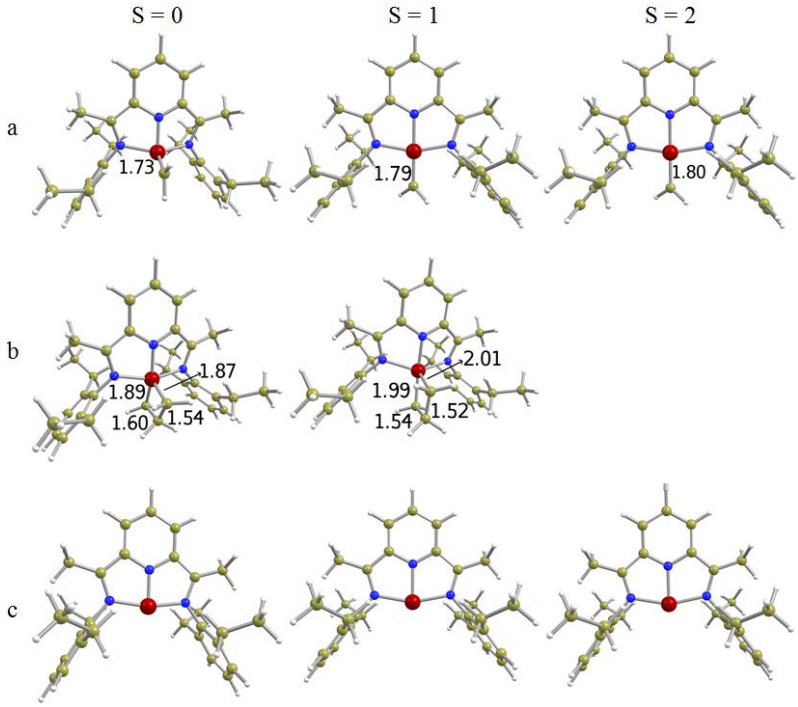

Figure A.3: Optimized geometries of different spin states of the metal carbene, metallacyclobutane intermediate and cyclopropanation products for complexes **III**. Distances are in Å

B

Additional data to Chapter 3

B.1 Stability of the metallacyclobutanes

In the intermediate metallacyclobutane two substituents can be in the carbons α (metallacycle-I) or in a carbon α and other in carbon-β (metallacycle-II), according to Scheme B.1. Any of these possibilities can be either *cis* or *trans* isomers.

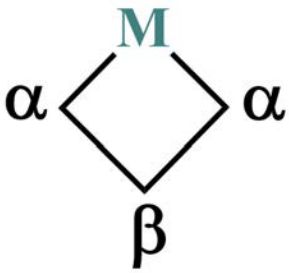

Scheme B.1

We have analyzed the relative stability of these two possibilities, regarding the *trans* configuration. In the case of Complex **1**, metallacycle-I is 1.4 kcal mol^{-1} more stable than the metallacycle-II. The same is true for the Complex **2** where the metallacycle-I is 1.0 kcal mol^{-1} more stable than metallacycle-II. On the other hand, for the Complexes **3** and **4**, the opposite is observed: metallacycle-II is more stable in both cases: 9.4 kcal mol^{-1} more stable Catalyst **3**, and 7.0 energies in kcal mol^{-1} for the Catalyst **4**. See the optimized geometries in Figure B.1.

Because high steric hindrance around the metallic center in Catalyst **3** and **4** avoids large groups near to ancillary ligands, then metallacycle-II implies in a more stable intermediate. On the other hand for Catalyst **1** and **2** the steric hindrance is smaller, allowing metallacycle-I configuration.

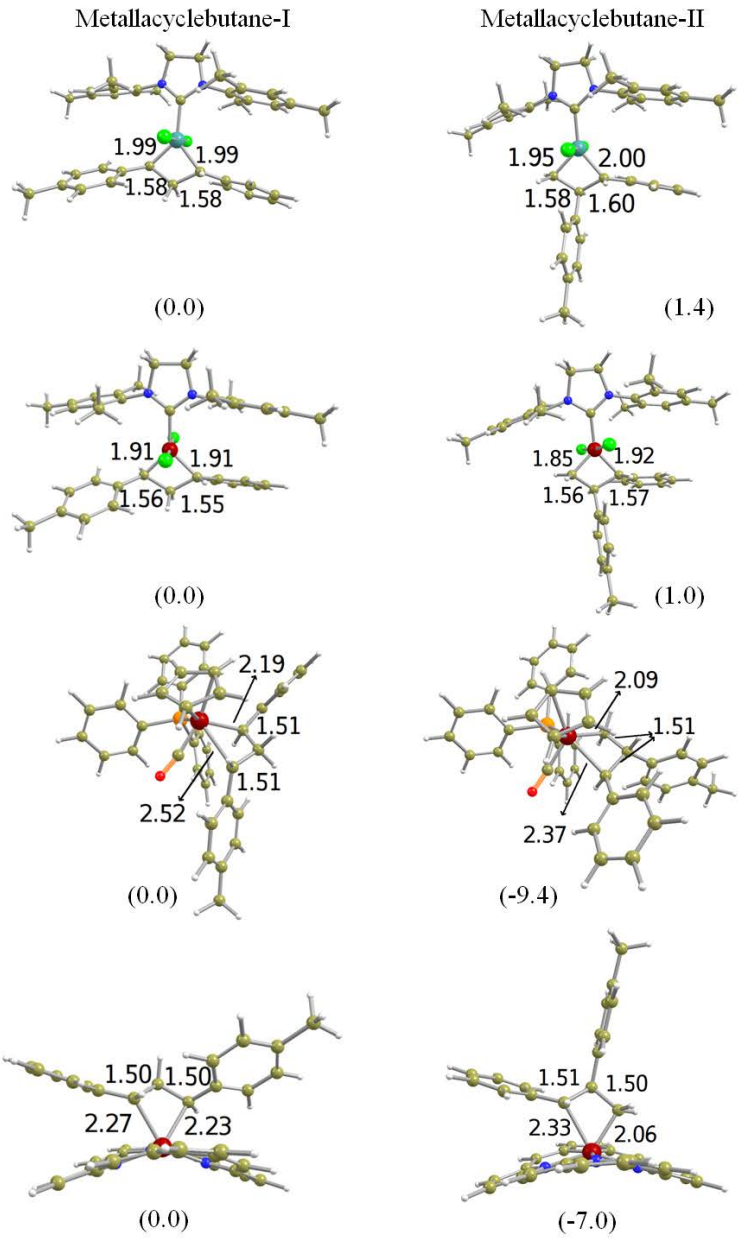

Figure B.1: Optimized geometry of isomers of metallacyclobutane for the Complex **1-4**. Relative Gibbs Free energies in kcal mol^{-1}. Distances in Å

B.2 Scans

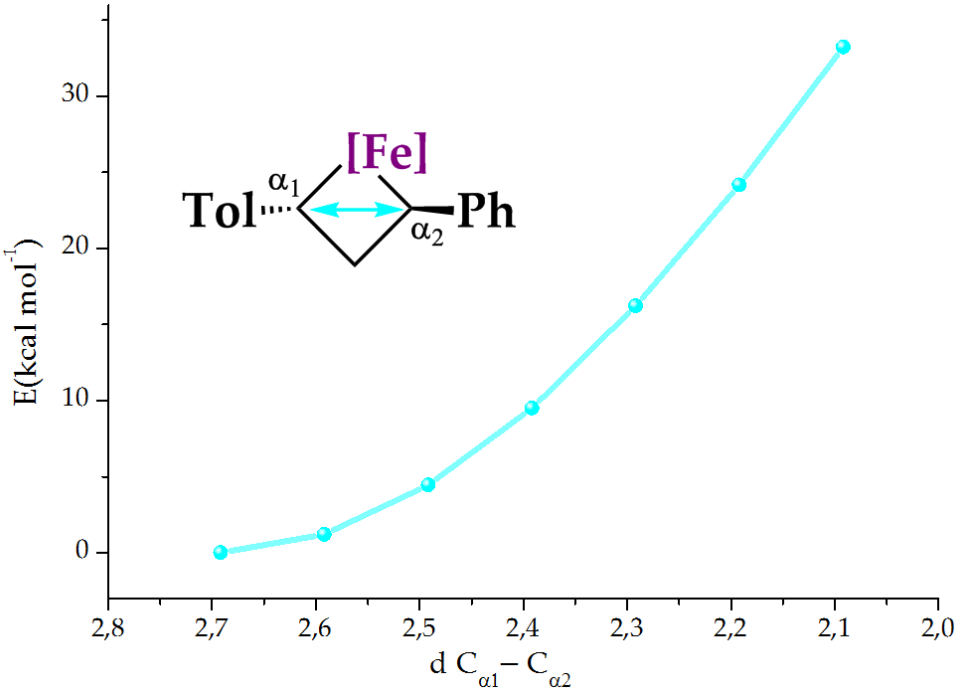

Figure B.2: Scan for the approaching of $C_\alpha - C_\alpha$ in $^1 2 - M$. Distances in Å

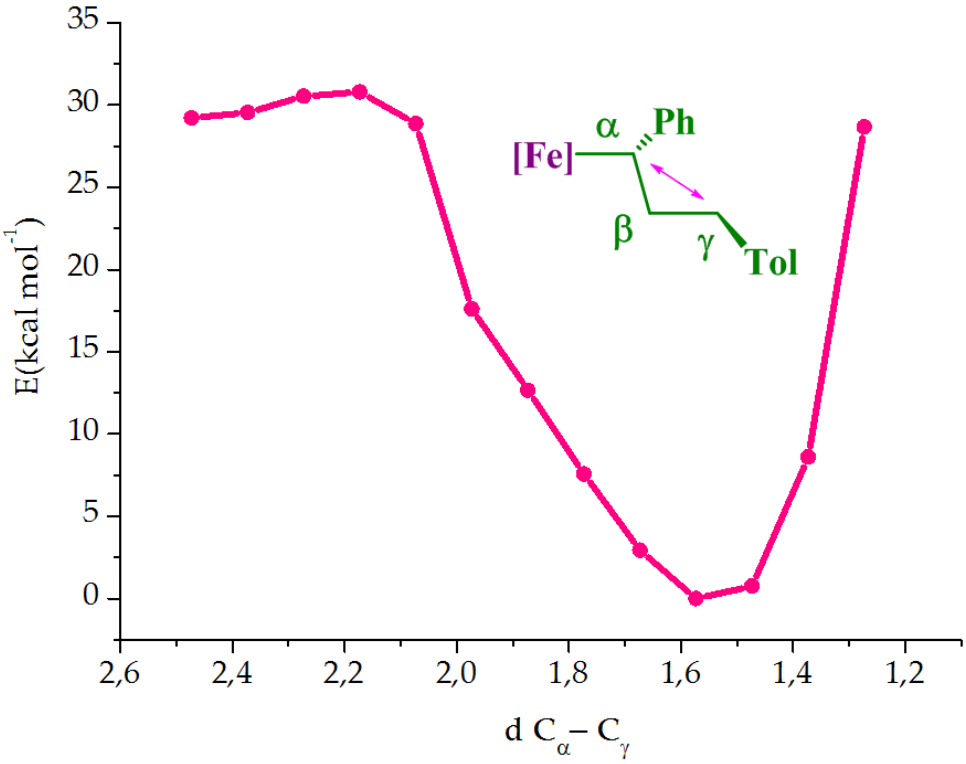

Figure B.3: Scan of the approaching of $C_\alpha - C_\gamma$ in $^1 2 - I$. Distances in Å

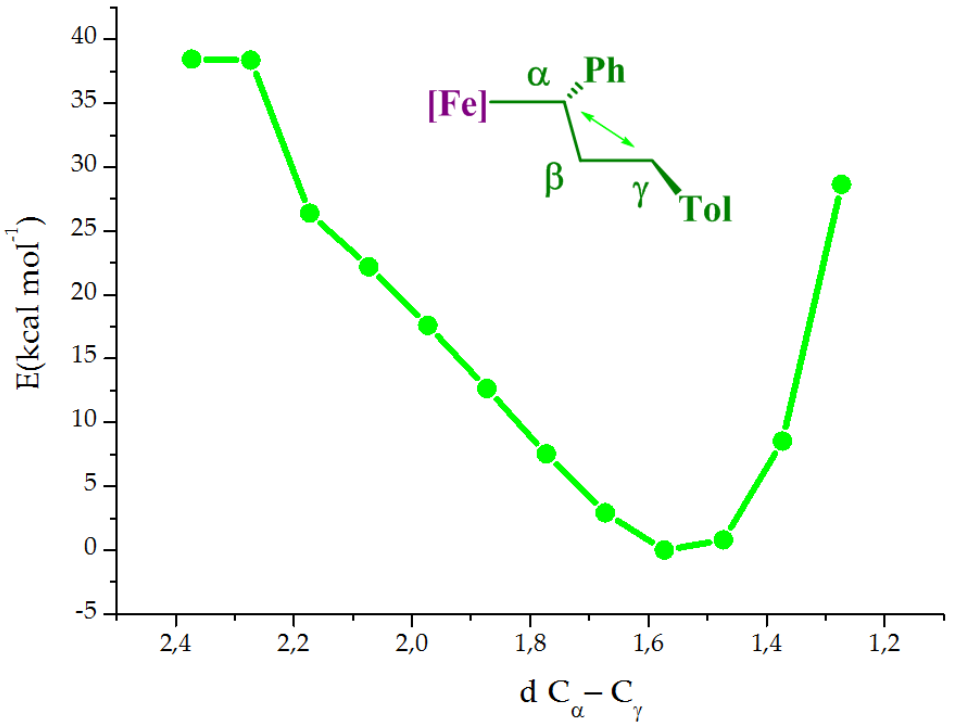

Figure B.4: Scan of the approaching of $C_\alpha - C_\alpha$ in ${}^3\mathbf{4} - \mathbf{I}$. Distances in Å

C

Additional data to Chapter 4

C.1 Geometries of Transition States

C.2 Catalyst 5

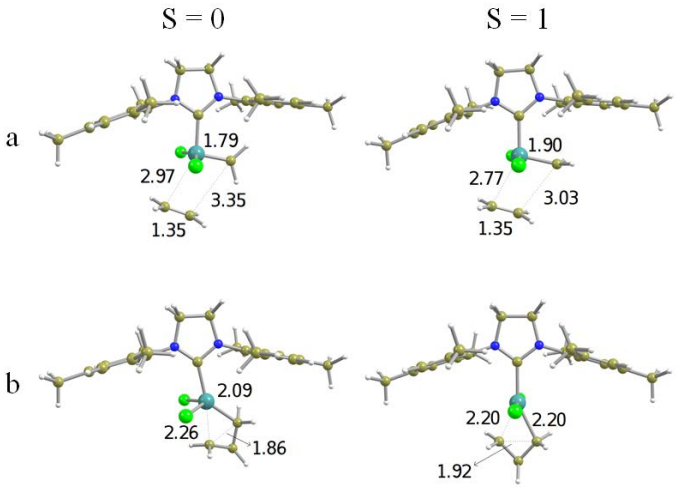

Figure C.1: Optimized geometries of singlet and triplet states of (a) transition states for *cycloaddition/cycloreversion*, and (b) cyclopropanation by reductive elimination of Complex **5** with ethene.

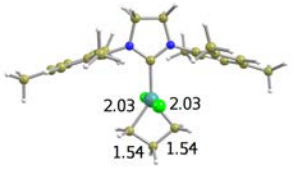

Figure C.2: **MECP 5.1**. Distances in Å

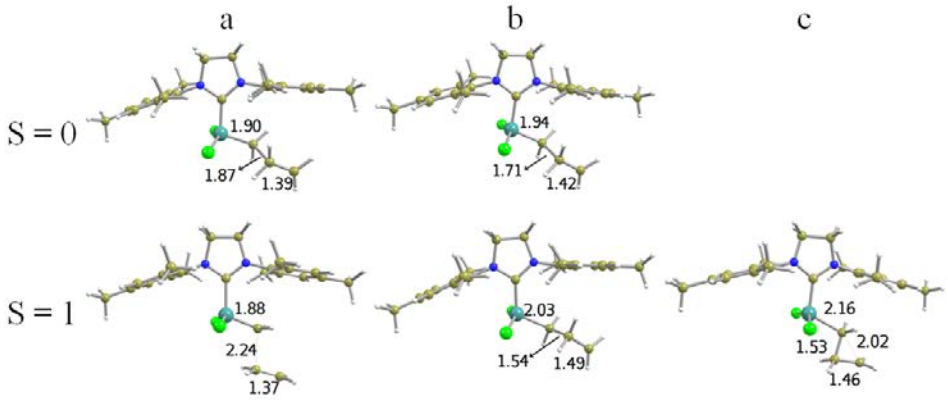

Figure C.3: Optimized geometries of singlet (if exists) and triplet states of (a) transition states of the attack to the carbene by the olefin, (b) minimum intermediate, and (c) transition state of cyclization, for carbene transfer of Complex **5** with ethene.

C.3 Catalyst 6

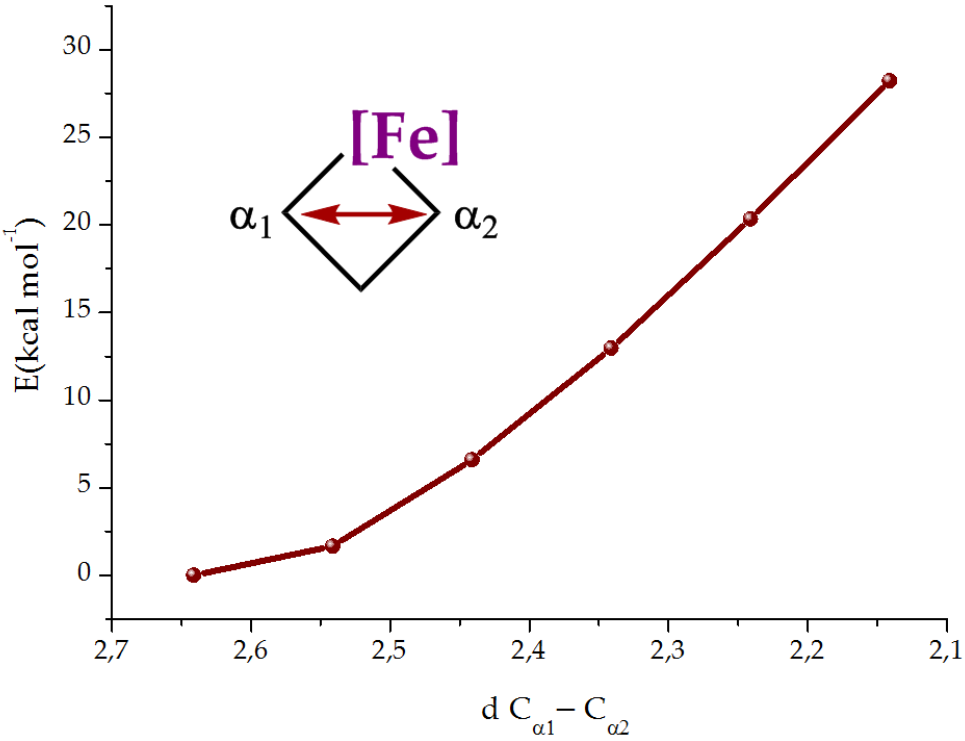

Figure C.4: Scan for the approaching of $C_\alpha - C_\alpha$ in the metallacyclebutane singlet of Complex **6**. Distances in Å

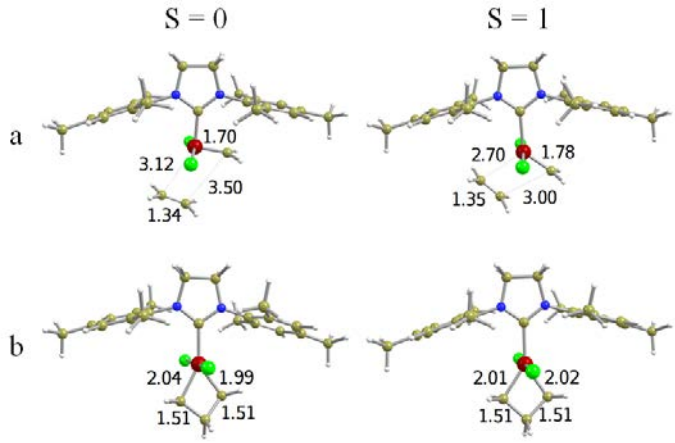

Figure C.5: Optimized geometries of singlet and triplet states of (a) transition states for cycloaddition/cycloreversion, and (b) cyclopropanation by reductive elimination of Complex **6** with ethene. All distances are in Å

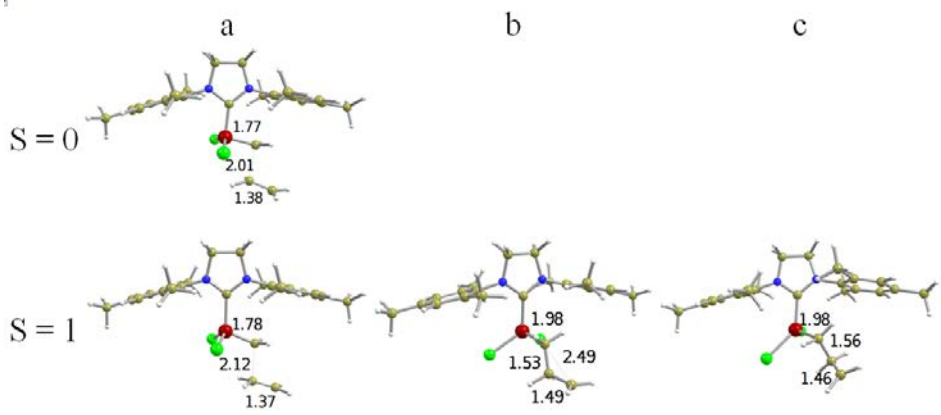

Figure C.6: Optimized geometries of singlet and triplet states of (a) transition states of the attack to the carbene by the olefin, (b) minimum intermediate, and (c) transition state of cyclization, for carbene transfer of Complex **6** with ethene. All distances are in Å

D

Additional data to Chapter 5

D.1 Bridge Carbenes Geometry

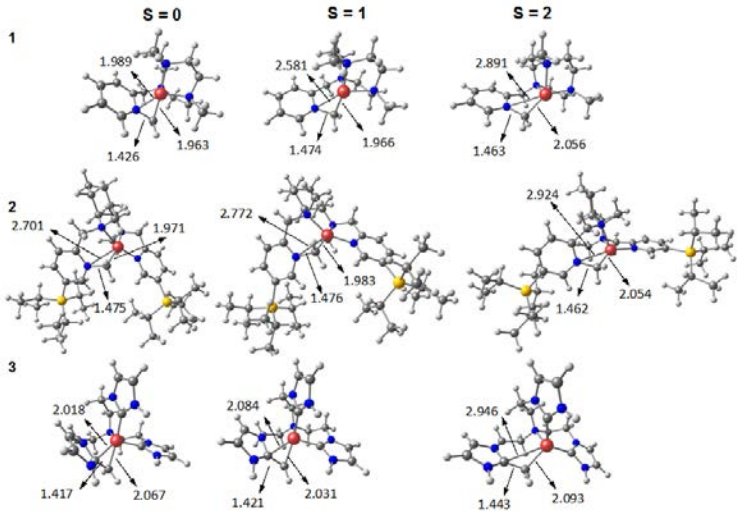

Figure D.1: Optimized structures for the bridged carbene isomers of complexes **14** to **16**. Distances are in Å

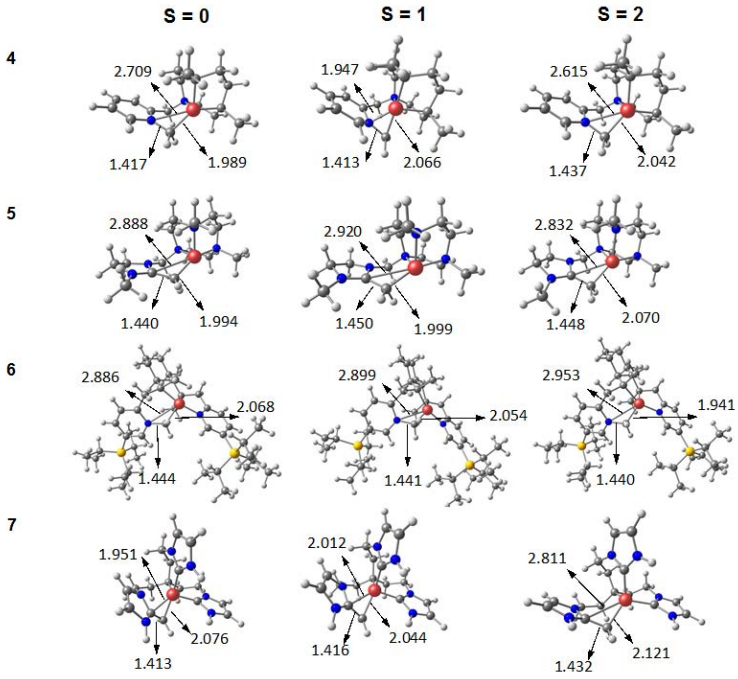

Figure D.2: Optimized structures for the bridged carbene isomers of complexes **17** to **20**. Distances are in Å

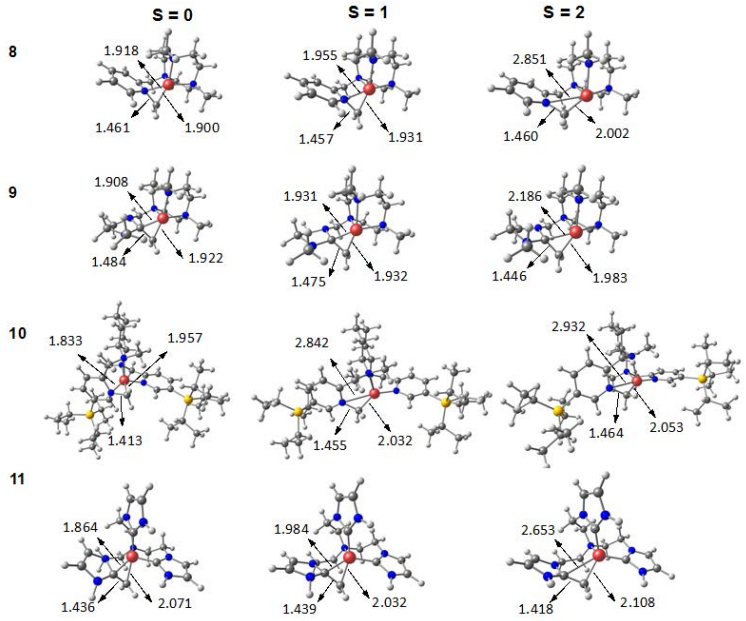

Figure D.3: Optimized structures for the bridged carbene isomers of complexes **21** to **24**. Distances are in Å

D.2 Bond Dissociation Energy Asymptotes

With the aim of determining the Bond dissociation Energy of the $Fe{=}CH_2$ carbene bonds, it is mandatory to determine the most favourable asymptote for the separated fragments, regarding the charge and spin multiplicity.

For such goal we calculated the adiabatic BDE of the catalyst **I** and **II** (as defined in Scheme 2.1), and **5** (as defined in Section 4.2), in the singlet state, since for these systems is the most stable spin state. For the products of the BDE we combined three possible charges for the carbene fragment (0, -1 and -2) and the corresponding same charge for the metal fragment, in order to reproduce the global charge of the system. Moreover, for each charge of the metal we considered three spin states, whereas for the carbene fragment we considered either one or two different multiplicities. The computed BDEs for Complex **I** are shown in Table D.1, those of Complex **II** in Table D.2, and those for Complex **5** in Table D.3.

Table D.1: $Fe{=}CH_2$ bond dissociation energies (BDE) in kcal mol^{-1} of Complex **I**, considering all possible combinations of charge and multiplicity of the resulting fragments.

complex		fragment		carbene		BDE
charge	multiplicity	charge	multiplicity	charge	multiplicity	
+1	singlet	+1	singlet	0	singlet	105.4
+1	singlet	+1	singlet	0	triplet	83.8
+1	singlet	+1	triplet	0	singlet	99.8
+1	singlet	+1	triplet	0	triplet	78.2
+1	singlet	+1	quintet	0	singlet	126.9
+1	singlet	+1	quintet	0	triplet	105.2
+1	singlet	+2	doublet	-1	doublet	317.2
+1	singlet	+2	quartet	-1	doublet	335.0
+1	singlet	+2	sextet	-1	doublet	362.0
+1	singlet	+3	singlet	-2	doublet	883.4
+1	singlet	+3	triplet	-2	doublet	883.6
+1	singlet	+3	quintet	-2	doublet	902.8

Table D.2: $Fe{=}CH_2$ bond dissociation energies (BDE) in kcal mol^{-1} of Complex **II**, considering all possible combinations of charge and multiplicity of the resulting fragments.

complex		fragment		carbene		BDE
charge	multiplicity	charge	multiplicity	charge	multiplicity	
+1	singlet	+1	singlet	0	singlet	117.4
+1	singlet	+1	singlet	0	triplet	95.7
+1	singlet	+1	triplet	0	singlet	82.2
+1	singlet	+1	triplet	0	triplet	60.5
+1	singlet	+1	quintet	0	singlet	95.6
+1	singlet	+1	quintet	0	triplet	73.9
+1	singlet	+2	doublet	-1	doublet	204.0
+1	singlet	+2	quartet	-1	doublet	195.6
+1	singlet	+2	sextet	-1	doublet	213.8
+1	singlet	+3	singlet	-2	doublet	669.0
+1	singlet	+3	triplet	-2	doublet	653.4
+1	singlet	+3	quintet	-2	doublet	655.3

Table D.3: $Fe{=}CH_2$ bond dissociation energies (BDE) in kcal mol^{-1} of Complex **5**, considering all possible combinations of charge and multiplicity of the resulting fragments.

complex		fragment		carbene		BDE
charge	multiplicity	charge	multiplicity	charge	multiplicity	
+1	singlet	+1	singlet	0	singlet	127.6
+1	singlet	+1	singlet	0	triplet	106.0
+1	singlet	+1	triplet	0	singlet	111.4
+1	singlet	+1	triplet	0	triplet	89.8
+1	singlet	+1	quintet	0	singlet	131.5
+1	singlet	+1	quintet	0	triplet	109.8
+1	singlet	+2	doublet	-1	doublet	262.5
+1	singlet	+2	quartet	-1	doublet	252.1
+1	singlet	+2	sextet	-1	doublet	276.0
+1	singlet	+3	singlet	-2	doublet	725.7
+1	singlet	+3	triplet	-2	doublet	736.0
+1	singlet	+3	quintet	-2	doublet	735.4

D.3 BDE *vs.* Cyclopropanation

As expected, the splitting in a neutral triplet carbene and the corresponding triplet metal fragment with the appropriate charge leads to the lowest BDE. Based on these results we further assumed that for all others studied species the same behaviour must apply.

Table D.4: Bond dissocation energies and thermodynamics for alkene cyclopropanation (both in kcal mol^{-1}) for complexes **5-13**. Cyclopropanation values are for the most stable spin state.

complex	BDE	cyclopropanation	complex	BDE	cyclopropanation
5	88.1	-14.0	10	76.3	-25.7
6	53.1	-63.6	11	75.1	-26.9
7	66.8	-40.2	12	71.8	-30.2
8	67.3	-45.0	13	74.5	-27.6
9	83.0	-19.1	-	-	-

Table D.5: Bond dissocation energies and thermodynamics for alkene cyclopropanation (both in kcal mol^{-1}) for complexes **14-24**. The cyclopropanation values are for the most stable spin state.

complex	BDE	cyclopropanation	Complex	BDE	cyclopropanation
5	88.1	-7.4	19	71.6	-26.2
14	66.3	-43.8	20	65.9	-36.2
15	61.2	-50.8	21	80.5	-17.9
16	73.1	-32.1	22	84.1	-12.2
17	77.9	-21.4	23	67.7	-29.7
18	69.5	-37.3	24	81.0	-16.6